Accelerated cementitious matrices: hydration, microstructure and mechanical strength

Doctoral Thesis

Doctoral thesis written by:

Renan Pícolo Salvador

Thesis directors:

Sergio Henrique Pialarissi Cavalaro

Antonio Domingues de Figueiredo

Barcelona, November 2016

Universitat Politècnica de Catalunya

Departament d´Enginyeria Civil i Ambiental

Acta de calificación de tesis doctoral

Nombre y apellidos	RENAN PÍCOLO SALVADOR
Programa de doctorado	INGENIERÍA DE LA CONSTRUCCIÓN
Unidad estructural responsable del programa	DEPARTAMENTO DE INGENIERÍA CIVIL Y AMBIENTAL

Resolución del Tribunal

Reunido el Tribunal designado a tal efecto, el doctorando / la doctoranda expone el tema de su tesis doctoral titulada "*Accelerated cementitious matrices: hydration, microstructure and mechanical strength*".

Acabada la lectura y después de dar respuesta a las cuestiones formuladas por los miembros titulares del tribunal, éste otorga la calificación:

☐ NO APTO   ☐ APROBADO   ☐ NOTABLE   ☐ SOBRESALIENTE

| (Nombre, apellidos y firma)

Presidente/a | (Nombre, apellidos y firma)

Secretario/a |
|---|---|
| (Nombre, apellidos y firma)

Vocal | (Nombre, apellidos y firma)

Vocal | (Nombre, apellidos y firma)

Vocal |

_____, _____ de _____ de _____.

El resultado del escrutinio de los votos emitidos por los miembros titulares del tribunal, efectuado por la Escuela de Doctorado, a instancia de la Comisión de Doctorado de la UPC, otorga la MENCIÓN CUM LAUDE:

☐ SÍ   ☐ NO

| (Nombre, apellidos y firma)

Presidente de la Comisión Permanente de la Escuela de Doctorado | (Nombre, apellidos y firma)

Secretario de la Comisión Permanente de la Escuela de Doctorado |
|---|---|

Barcelona a _____ de _____ de _____.

To my beloved parents, José and Vanda, whose efforts and support made me person I am.

ACKNOWLEDGEMENTS

Thanks for all the friends that I met in Barcelona and had the opportunity to share great moments with: Amin, Amir, Ana, Anna, Carlos, Cézar, Débora, Diego, Edu, Francesco, Fran, Isaac, Janill, Jordi, Júlia, Liao, Lidiane, Martha, Pau, Rubén, Sandra, Tai and Tina. I especially thank my dear friends Andressa, Helen, Luis, Maria, Mylene, Razmik and Ricardo, with whom life outside the university was a pleasure.

I would also like to thank my parents, José and Vanda, and my sisters, Raquel and Angélica, for their unconditional support during my stay in Barcelona and for always being there for me whenever I needed.

I really thank Talita for being my dear partner in this journey and staying by my side during all the experiences I was able to have. It wouldn't have been the same without you!

SUMMARY

Sprayed concrete is widely used as structural support for the stabilization of tunnel walls and underground constructions. The performance of sprayed cementitious matrices containing accelerators is strongly related to their mechanical properties at early and late ages. In practice, this is the main parameter that governs their mix design and applicability.

Mechanical strength development results from the combination of several factors associated with mix composition, application method and microstructure of the matrix. The compatibility between cement and accelerator is one of the most important parameters that control kinetics of hydration and the rate of mechanical strength gain. The spraying process also needs to be taken into account, since it leads to faster reaction rates and directly affects the porosity of the matrix.

Although the sprayed concrete technology advanced considerably over the past years, questions continue to arise regarding its performance, efficient use and optimized mix design. One of the main subjects that requires further research is the characterization of the early age hydration behavior of accelerated cementitious matrices. The influence of accelerator reactions on the mechanical properties of the matrix at short and long term and the influence of spraying on kinetics of hydration also need to be evaluated.

In this context, a study covering these demands is proposed in this doctoral thesis. The first subject contemplates the characterization of the kinetics and mechanisms of hydration and the microstructure development of accelerated cement pastes. The early age hydration behavior of different mix composition was analyzed and compared. Results obtained allowed the elucidation of the main chemical processes occurring during accelerator reaction and further cement hydration and their influence on the microstructure of the matrix.

The second subject comprises the parametrization of the early age hydration behavior of cement pastes containing accelerators. The main chemical properties of cements and accelerators were evaluated, explaining their influence on accelerator reactivity and on cement hydration. By doing so, the mix design of accelerated cementitious matrices may be optimized and unpredictable hydration reactions and their consequences may be avoided.

The third subject deals with the characterization of the setting and hardening processes of accelerated cementitious matrices by ultrasound measurements. This subject was proposed because the current standard methods to characterize early strength evolution are discontinuous and have a limited application range. By using the ultrasound technique, a more complete characterization of the evolution of mechanical properties of the matrix was assessed.

The fourth subject aims at evaluating how spraying affects accelerator reactivity and further cement hydration. A small-scale spraying equipment was used to simulate real life applications of sprayed concrete. A significant influence of the mixing process on reaction rates and on microstructure of the matrix was observed.

The last subject of this thesis focuses on the evaluation of how accelerated hydration reactions influence the mechanical strength development of the matrix. The main chemical processes influencing the mechanical properties at early and late ages were determined. Results provided the characterization of the mechanical performance of sprayed materials based on their chemical composition, in order to improve their mix design and quality control.

RESUMEN

El hormigón proyectado es ampliamente utilizado como soporte estructural para la estabilización de túneles y construcciones subterráneas. El desempeño de mezclas cementicias que contienen acelerantes está fuertemente relacionado con sus propiedades mecánicas a cortas y largas edades. En la práctica, este es el principal parámetro que gobierna su diseño y aplicabilidad.

El desarrollo de resistencia mecánica resulta de la combinación de diversos factores asociados al diseño de la mezcla, método de aplicación y microestructura de la matriz. La compatibilidad entre cemento y acelerante es uno de los parámetros más importantes que controla la cinética de hidratación y la velocidad de ganancia de resistencia mecánica. El proceso de proyección también debe de ser considerado, puesto que la velocidad de mezcla influye en la cinética de reacción y afecta la porosidad de la matriz.

A pesar de que la tecnología del hormigón proyectado haya avanzado considerablemente durante los años pasados, cuestiones relacionadas a su desempeño, uso eficiente y diseño optimizado siguen surgiendo. Uno de los temas que requiere investigación es la caracterización de la hidratación a cortas edades de mezclas cementicias aceleradas. La influencia de las reacciones causadas por el acelerante en las propiedades mecánicas de la matriz a corto y largo plazo y la influencia de la proyección en la cinética de hidratación también necesitan ser evaluados.

En este contexto, un estudio que engloba estas demandas es propuesto en esta tesis doctoral. El primer tema planteado es la caracterización de la cinética, de los mecanismos de hidratación y de la microestructura de pastas de cemento aceleradas. La hidratación a cortas edades de diferentes mezclas cementicias fue analizada y comparada. Los resultados obtenidos permitieron la elucidación de los procesos químicos que ocurren durante la reacción del acelerante y en la posterior hidratación del cemento, analizando su influencia en la microestructura de la matriz.

El segundo tema comprende la parametrización de la hidratación a cortas edades de pastas de cemento con acelerantes. Las principales propiedades químicas de los cementos y acelerantes fueron evaluadas, justificando su influencia en la reactividad del acelerante y en la

hidratación del cemento. Por lo tanto, el diseño de mezclas aceleradas puede ser optimizado y reacciones de hidratación imprevistas y sus consecuencias pueden ser evitadas.

El tercer tema trata de la caracterización de los procesos de fraguado y endurecimiento de mezclas cementicias aceleradas por medidas de ultrasonido. Este tema fue propuesto porque los métodos actuales para caracterizar la evolución de resistencia a corta edad son discontinuos y tienen un rango limitado para su realización. Utilizando la técnica de ultrasonidos, se puede obtener una caracterización más completa del desarrollo de propiedades mecánicas de la matriz.

El cuarto tema tiene como objetivo evaluar como el proceso de proyección afecta la reactividad del acelerante y la posterior hidratación del cemento. Un equipo de proyección de pequeña escala fue utilizado para simular aplicaciones de hormigón proyectado en escala real. Una influencia significativa del método de mezcla en las velocidades de reacción y en la microestructura de la matriz fue observada.

El último tema de esta tesis enfoca la evaluación de como reacciones de hidratación aceleradas influyen en el desarrollo de resistencia mecánica de la matriz. Los procesos químicos principales que afectan las propiedades mecánicas a cortas y largas edades fueron determinados. Los resultados obtenidos proporcionan la caracterización del desempeño mecánico de materiales proyectados basado en su composición química, con el objetivo de optimizar su diseño y control.

CONTENTS

4. Parameters controlling early age hydration of accelerated cement pastes 75

LIST OF FIGURES

Chapter 1

Chapter 2

Chapter 3

Chapter 4

Chapter 6

Chapter 7

Appendix B

Appendix C

LIST OF TABLES

Chapter 1

Chapter 2

Chapter 3

Chapter 4

Chapter 5

Chapter 6

Chapter 7

Appendix A

Appendix B

NOMENCLATURE

The nomenclature of mixes used in this thesis follows the pattern *'production process'_'matrix type'_'cement type'_'accelerator type and dosage'*. Each item used in the nomenclature is described in table N.1. Examples of the nomenclature used are presented in table N.2.

Table N.1 - Description of items used in the nomenclature of mixes.

Item	Type	Nomenclature / Abbreviation
Production process	Hand-mixing	HM
	Mechanical mixing	MM
	Spraying	SP
Matrix	Suspension	S
	Paste	P
	Mortar	M
Cement	CEM I (commercial)	I
	CEM II/A-L (commercial)	II
	Formulated[a]	Clinker type and content_setting regulator type and content_addition
Accelerator	Reference (no accelerator)	REF
	Alkali-free	AKF Al_2O_3/SO_4^{2-} molar ratio
	Alkaline	ALK

[a] Used exclusively in chapter 4.

Table N.2 - Nomenclature of mixes used in this thesis.

Example	Nomenclature
Mechanically mixed suspension produced with cement type I and accelerator AKF 0.61 at 7.0 % bcw	MM_S_I_AKF 0.61 7%.
Hand-mixed paste produced with cement type I and no accelerator	HM_P_I_REF
Mechanically mixed paste produced with cement type II/A-L and accelerator AKF 0.42 at 11 % bcw	MM_P_II_AKF 0.42 11%
Sprayed mortar produced with cement type II/A-L and accelerator ALK at 3.0 % bcw	SP_M_II_ALK 3%

1. Introduction

1.1. Prologue

This doctoral thesis was accomplished at the Department of Civil and Environmental Engineering (BarcelonaTech) from the Polytechnic University of Catalonia in Barcelona, Spain. The work was directed by Professor Sergio Henrique Pialarissi Cavalaro, member of this university, and codirected by Professor Antonio Domingues de Figueiredo, member of the Polytechnic School of University of São Paulo from São Paulo, Brazil. This thesis comprehends a part of a research project with the collaboration from Industrias Químicas del Ebro from Zaragoza, Spain.

The experimental program was majorly conducted at the Laboratory of Technology of Structures Luis Agulló from the Polytechnic University of Catalonia (UPC). X-ray diffraction and scanning electron microscopy were performed at the Scientific and Technological Center from the University of Barcelona (CCIT-UB). Software development and data analysis for ultrasound measurements were executed at the Institute of Physical and Information Technologies Leonardo Torres Quevedo from the Spanish National Research Council (CSIC).

The research focuses on the hydration behavior, microstructure development and mechanical strength evolution of accelerated cementitious matrices, directing its application to sprayed concrete technology. Firstly, the study focuses on cement pastes to evaluate the chemical processes and microstructural changes occurring during hydration. Then, the

investigation is extended to mortars, in order to analyze the influence of accelerated hydration and phase formation on their mechanical properties at early and late ages.

The subject proposed intersects both academic and practical interests. From an academic point of view, the characterization of chemical and microstructural phenomena occurring during hydration is quite complex, because they are interdependent processes. Therefore, studying hydration of cementitious systems containing accelerators offers significant scientific challenges, requiring a substantial effort in developing experimental techniques and test methods for its evaluation.

In practice, understanding kinetics and mechanisms of accelerated cement reactions and correlating them with the evolution of mechanical properties is necessary to select cements and accelerators with proper compatibility to enhance concrete performance. Such approach would optimize mix design of sprayed matrices without numerous and extensive field spray trials, which are a common practice nowadays. Besides, this evaluation would be an important reference to accelerator manufacturers for the development of formulations with enhanced performance with cements from different sources. As a result, an improvement in sprayed concrete technology could be achieved, making it more efficient, durable and sustainable.

1.2.   Background and context

Sprayed concrete is a construction technique used worldwide in underground constructions due to technical and economic advantages over conventional concrete [1]. Approximately 22.8 million cubic meters of sprayed concrete are expected to be used in the year 2020 and Europe will consume around 37 % of that amount due to tunneling and mining projects [2]. The value of the sprayed concrete market is projected to reach USD 7.6 billion by 2020, which means an annual growth of 8.0 % between 2015 and 2020 [2]. The high demand of sprayed concrete is promising and, therefore, research and development on this subject are a current need.

The performance of sprayed cementitious matrices containing accelerators is strongly related to their mechanical properties at short and long term. Mechanical strength development is the result of the combination of several factors related to mix composition, application method and microstructure of the matrix. In practice, this is the main parameter that governs their mix design and applicability.

The main classes of accelerators employed in sprayed concrete are either alkali-free or alkaline. Alkali-free accelerators are mostly composed by an aluminum sulfate solution stabilized by an organic acid [3], while the main component in alkaline formulations is sodium aluminate [4]. Accelerators increase the rate of early strength development due to the formation of calcium sulfoaluminate hydrates, which cause a rapid increase in stiffness of the matrix [5,6]. Due to this process, the use of accelerators enables the build-up of concrete layers with proper thickness [7,8].

The compatibility between cement and admixtures plays a major role in hydration kinetics and mechanical strength evolution [9]. Regarding accelerators, formulations based on sodium aluminate rapidly deplete sulfate ions from the liquid phase and lead to accelerated undersulfated C_3A reactions, which inhibit further alite hydration [4,10,11]. As a consequence, compressive strength from 7 days on in alkaline accelerated sprayed concrete may be up to 20 % lower in comparison with concrete produced with alkali-free accelerators [1].

Regarding the application method, high shearing conditions achieved during spraying accelerate C_3A reactions and cement matrices may hydrate as undersulfated, even in systems with proper sulfate balance [12,13]. The elevated temperature reached during application increases the hydration rate, resulting in an inhomogeneous precipitation of hydrated phases and coarser porosity [13,14]. The increase in temperature affects the morphology and nature of hydrates, forming denser C-S-H, smaller ettringite crystals [13,15] and larger amounts of monosulfoaluminate [16].

Despite the remarkable advances in the field of sprayed concrete over the past years, questions continue to arise regarding its applicability and performance. Indeed, several subjects need to be addressed to provide an efficient use of sprayed concrete, with an optimized mix design. Some of these subjects, which are contemplated in this doctoral thesis, are described subsequently:

- It is still necessary to understand the basic chemical principles that govern accelerator reactivity and further cement hydration and their influence on the microstructure of the matrix. Furthermore, a study combining the main variables affecting hydration kinetics of accelerated matrices is essential to parametrize the chemical interaction between cements and accelerators. Consequently, the performance of sprayed concrete could be optimized and an unpredictable hydration behavior and its consequences could be avoided.

- The current standard methods to characterize early strength evolution (Vicat, needle and pin penetration tests) are discontinuous and have a limited application range [1]. In addition, studies regarding sprayed concrete are restricted due to the difficulty in following accelerated hydration reactions. Since the determination of initial stiffness and early age strength in sprayed concrete is crucial for its proper application and for safety reasons, efforts towards the definition of test methods to provide a continuous monitoring of the setting and hardening processes in accelerated matrices are necessary. By doing so, a more complete characterization of the evolution of mechanical properties of the matrix may be assessed.

- The vast majority of studies that evaluate the compatibility between cements and accelerators deals with accelerated cement pastes produced by hand or mechanical mixing [4,10,17–20]. Since these mixing processes differ considerably from the method for placing sprayed concrete, accelerated matrices should also be produced by spraying. Consequently, the matrix would be more similar to that obtained in real life applications and the comparison between microstructural properties and macro-scale performance would be more reasonable.

- Research conducted in the field focuses either on the chemical or on the mechanical properties, without addressing the relation between them. Although some chemical processes are known empirically to influence the mechanical strength of the matrix, it is not clear how, why and to what extent they are significant. The influence of accelerated hydration reactions on the mechanical strength evolution still needs to be evaluated to characterize the performance of sprayed materials and to improve its design and quality control.

- For the characterization of mechanical properties, tests are usually performed in sprayed concrete. This requires the use of large amounts of materials and expensive equipment, which are not common in laboratories from universities. Therefore, a small-scale version of sprayed concrete testing that resembles real-life applications needs to be developed. By doing so, the evaluation of sprayed matrices may be performed more easily, with a more sustainable and less labor-intensive procedure.

1.3. Objectives

Five general objectives corresponding to the main subjects addressed in this doctoral thesis are defined as follows:

- Characterize kinetics and mechanisms of hydration and the microstructure of accelerated cement pastes.

- Parametrize the early age hydration behavior of accelerated cement pastes in terms of the chemical composition of cement and accelerators.

- Characterize the early age properties (setting and hardening processes) of accelerated cementitious matrices by ultrasound propagation velocity.

- Analyze how spraying influences hydration and microstructure of accelerated cement pastes.

- Evaluate how the chemical processes occurring during hydration influence the mechanical strength development of accelerated cementitious matrices at early and late ages.

In order to fulfill these main goals, the specific objectives presented in table 1.1 are proposed.

Table 1.1 - Specific objectives of the research.

General objectives	Specific objectives
Characterization of accelerated cement pastes	- Elucidate the main chemical processes occurring during hydration
	- Characterize the kinetics and mechanisms of hydration
	- Evaluate different types of cements and accelerators, comparing their behavior
	- Analyze the microstructure development of accelerated cement pastes
	- Elaborate a conceptual hydration model of cement pastes containing accelerators
Parametrization of hydration behavior	- Parametrize the kinetics and mechanisms of hydration of cement pastes based on the chemical composition of cements and accelerators
	- Identify the main properties and characteristics that govern accelerator reactivity and further cement hydration
	- Specify combinations of materials for optimal compatibility between cement and accelerator
Characterization of early age properties by ultrasound measurements	- Characterize the setting and hardening processes in accelerated cement pastes and mortars by ultrasound propagation velocity
	- Identify the main properties and parameters that govern the propagation of ultrasound waves
	- Correlate chemical properties and phase composition with ultrasound propagation velocity
Influence of spraying on hydration	- Analyze how spraying influences accelerator reactivity and further cement hydration
	- Evaluate the microstructure and morphology of precipitated hydrates in pastes produced by spraying
	- Compare spraying with hand-mixing, highlighting the main properties affected by the mixing process
Characterization of mechanical properties	- Analyze how accelerated hydration reactions influence the evolution of mechanical strength at early and late ages
	- Correlate chemical properties and phase composition with mechanical strength development
	- Specify combinations of materials to provide proper mechanical properties
	- Develop and adapt a small-scale testing for the characterization of sprayed matrices

1.4. Experimental program

Figure 1.1 represents a general overview of the experimental program conducted, showing the main subjects analyzed in each step. The description of each chapter from the experimental campaign is presented subsequently.
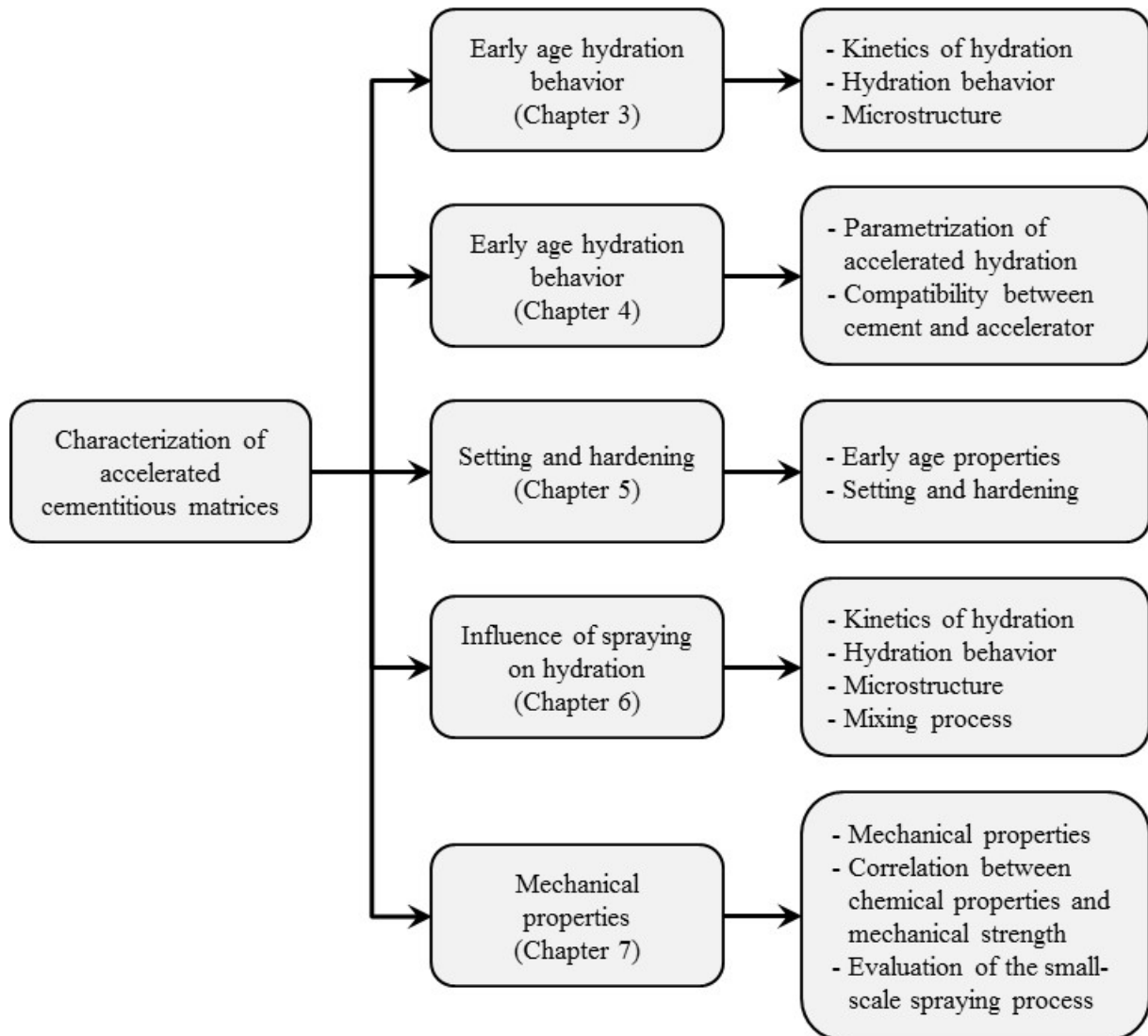
Figure 1.1 - Overview of the experimental program for the characterization of accelerated cementitious matrices.

Chapter 3 deals with the characterization of kinetics and mechanisms of hydration and the microstructure of accelerated cement pastes. Mixes were composed by 2 types of cement and 4 types of accelerator. Results presented the chemical processes occurring during hydration and the behavior of pastes with different mix composition was compared. Based on the results obtained, a conceptual hydration model was developed.

In chapter 4, the early age hydration behavior of accelerated cement pastes is parametrized in terms of the chemical composition of cements and accelerators. The evaluation comprised a total of 56 different accelerated pastes, produced by the combination of 8 types of cement, 3 alkali-free accelerators employed at 2 dosages and 1 alkaline accelerator used at 1 dosage. Results explained the principles governing accelerator reactivity and further cement

hydration. Combinations of compatible materials were recommended to enhance the hydration behavior of the matrix.

Chapter 5 covers the characterization of setting and hardening of accelerated cement pastes and mortars by ultrasound propagation velocity. Pastes and mortars were prepared using materials and dosages employed in chapter 3. Results obtained indicated the main processes that influence microstructure development and ultrasound propagation velocity, explaining their origin.

Chapter 6 presents the influence of spraying on hydration kinetics and on the microstructure of cement pastes containing accelerators. The composition of cement pastes was the same as in chapter 3. This evaluation explains important differences in hydration behavior caused by the mixing process, highlighting the main properties affected.

In Chapter 7, the influence of the hydration behavior on the mechanical strength development at early and late ages was analyzed. Sprayed mortars were produced using the same materials and dosages as in chapter 3. Results showed how the accelerated hydration and the evolution of phase composition affect the development of mechanical properties of the matrices.

To complete the document, the state of the art, conclusions and future perspectives and the bibliography are presented in chapters 2, 8 and 9, respectively. In addition to these chapters, the thesis contains 4 appendices (Appendix A, Appendix B, Appendix C and Publication).

2. State of the art

2.1. Introduction

In recent years, sprayed concrete has been widely employed in underground constructions. Continuous research and advances in materials and equipment have broadened the range for its application. The development of different test methods for its characterization and quality control has also contributed to the growth of the technology.

Considering the significant potential of this construction technique, some further work is still needed to reliably comprehend its chemical and mechanical properties. A science-based approach in hydration chemistry of cementitious matrices containing accelerators is the key to better comprehend the macro mechanical behavior of sprayed concrete. By doing so, improvements in mix design could be assessed and the performance of sprayed concrete could be optimized.

Taking this into account, this chapter presents a brief review on the topics related to this doctoral thesis. Firstly, section 2.2 deals with the composition and reactivity of Portland cement. Then, section 2.3 presents the principles of hydration processes of cement and its individual phases, focusing on kinetics, thermodynamics and microstructure development. Finally, section 2.4 corresponds to sprayed concrete and the chemistry of accelerators and accelerated hydration.

2.2. Chemistry of Portland cement

2.2.1. Definition

Portland cement is a finely ground inorganic material that reacts with water, forming a paste that sets, hardens and develops mechanical strength [21]. It is known as a hydraulic binder because the products formed by the chemical reactions have water-resisting properties and are capable of binding several particles, such as aggregates [22]. It is the main material used in construction engineering to produce structural concrete.

2.2.2. Composition

The main constituents of Portland cement are described in table 2.1. It is a polycrystalline compound composed by a clinker and a calcium sulfate source. Since raw materials are in incipient fusion during the clinkering process, phases formed are not pure and contain certain amounts of substituent elements in their structure, altering their composition. Alite and belite are the denomination of tricalcium and dicalcium silicates with substituent oxides, respectively [21,22].

Table 2.1 - Main phases present in ordinary Portland cements [21,22].

Phase	Oxide composition	Notation[a]	Substituent oxides	Solubility	Mass percentage (%)
Alite	$3CaO \cdot SiO_2$	α-C_3S	A, F, M	High	50 - 70
Belite	$2CaO \cdot SiO_2$	β-C_2S	A, F, M, $\bar{S}$, K	Low	15 - 30
Tricalcium aluminate	$3CaO \cdot Al_2O_3$	C_3A	K, N, F, S	High (increase with Na^+ and K^+ contents)	5 - 10
Calcium alumino-ferrite	$Ca_2(Al_xFe_{1-x})_2O_5$	C_4AF (x = 0.5)	M, S, T	Increase with Al/Fe ratio	5 - 15
Periclase	MgO	M	-	Low	0 - 2
Lime	CaO	C	-	Low, due to supercalcination	0 - 1
Arcanite	$K_2O \cdot SO_3$	$K\bar{S}$	-	High	0 - 1
Thenardite	$Na_2O \cdot SO_3$	$N\bar{S}$	-	High	0 - 1
Syngenite	$K_2O \cdot CaO \cdot 2SO_3$	$KC\bar{S}_2$	-	High	0 - 1
Langbeinite	$K_2O \cdot 2CaO \cdot 3SO_3$	$KC_2\bar{S}_3$	-	High	0 - 1
Aphtitalite	$3K_2O \cdot Na_2O \cdot 4SO_3$	$K_3N\bar{S}_4$	-	High	0 - 1
Gypsum	$CaO \cdot SO_3 \cdot 2H_2O$	$C\bar{S}H_2$	-	High	2 - 5
Hemihydrate	$CaO \cdot SO_3 \cdot 0.5H_2O$	$C\bar{S}H_{0.5}$	-	High	2 - 5
Anhydrite	$CaO \cdot SO_3$	$C\bar{S}$	-	High	1 - 2

[a] Simplified notation adopted in cement chemistry: S: SiO_2; C: CaO; A: Al_2O_3; F: Fe_2O_3; M: MgO; N: Na_2O; K: K_2O; $\bar{S}$: SO_3; T: TiO_2; H: H_2O.

The most common sulfate source (expressed as SO_3) in ordinary Portland cements is gypsum ($CaSO_4.2H_2O$), which is added to the clinker during grinding. Due to the elevated temperature in this operation, gypsum may dehydrate, forming hemihydrate ($CaSO_4.0.5H_2O$) and anhydrite ($CaSO_4$) [21]. Hemihydrate is the most soluble sulfate form, whereas anhydrite is the least soluble. Calcium sulfate acts as a set regulator, retarding the quick-setting tendency attributed to the highly reactive C_3A phase [23].

The contents of free calcium oxide and magnesium oxide are limited to 5 and 2 % by mass because these compounds may participate in deleterious expansive reactions at late ages, originating pathologies due to cracking. [21,24]. Alkali content, expressed as sodium oxide equivalent, is limited to 0.60 - 1.0 %, in order to avoid possible reactions with reactive aggregates [25].

The use of Portland cement type I has been decreasing over the past years due to its replacement by composite cements. Additions, such as limestone filler, pozzolans (fly ash, silica fume and rice husk ash) and ground blast-furnace slag are some examples of inorganic compounds that present a great potential as supplementary cementitious materials [26–29]. These compounds started to be used in concrete in an attempt to provide a destination for residues or by-products generated by several industrial activities [26]. However, they improve several concrete properties (durability, strength, permeability and tendency to crack, for example [27,28]) and help decrease the overall energy consumption and CO_2 emissions by cement manufacturing. Therefore, cements containing these additions are fairly common nowadays [30,31].

2.2.3. Reactivity of clinker phases

Reactivity is one of the most important chemical properties of cement and is directly related to the solubility of cement compounds. As mentioned in section 2.2.2, the major constituents of Portland cement contain impurities, due to the incorporation of aluminum, iron, magnesium, sodium, potassium and sulfur into their structure. Depending on the quantity of an impurity in the solid solution with a clinker compound, its crystal structure, solubility and reactivity may be significantly altered. Structural holes and imperfections caused by the incorporation of large amounts of foreign ions increase the reactivity of cement compounds with water [19,23]. However, some ions may lead to the precipitation of insoluble compounds on the surface of cement grains, reducing their solubility [32].

In industrial cements, alite may be present mainly in three crystalline forms: triclinic, monoclinic and trigonal. These forms are a slight distortion of an ideal C_3S pseudostructure built from SiO_4 tetrahedra, calcium and oxygen ions. The coordination of oxygen ions around calcium is irregular, being concentrated on one side of each calcium ion. This spatial arrangement leaves large structural voids, which account for the high reactivity of alite [33].

Similarly, belite also presents an irregular structure in industrial cements, being mainly detected in β-C_2S crystalline form. However, interstitial holes formed in its crystal structure are much smaller, making belite significantly less reactive than alite. The γ-C_2S has a regularly packed and coordinated structure, and, therefore, is nonreactive [33]. Another reason why C_2S is less reactive than C_3S may be attributed to the presence of O_2^- ions in C_3S structure, which are strong Bronsted bases [34].

Calcium aluminates are mainly found in cubic and orthorhombic forms, being mostly influenced by alkali contents. Cubic C_3A contains around 1.0 % Na_2O and 0.70 % K_2O substituting calcium oxide, whereas in orthorhombic C_3A, Na_2O and K_2O are present in 0.60 % and 4.0 %, respectively [21]. Due to the higher alkali content, orthorhombic C_3A has a very complex crystal structure, characterized by large structural voids, making it more soluble and reactive than cubic C_3A. Therefore, orthorhombic C_3A content must be limited in cements for special applications, such as in sulfate-resistant cements [35].

Calcium alumino-ferrite phases belong to the $Ca_2(Al_xFe_{1-x})_2O_5$ solid solution series, where $0 < x < 0.7$. The equimolecular composition, C_4AF, is the most common compound detected in cements. Due to similarities in cell parameters, an intergrowth in ferrite and aluminate phases may occur. The higher the Fe_2O_3/Al_2O_3 ratio, the less soluble this compound will be. Therefore, C_4AF is less reactive than C_3A [21].

Both MgO and CaO form cubic structures, where each magnesium or calcium ion is surrounded by six oxygen ions in a regular octahedron. Due to the small ionic radius of Mg^{2+}, oxygen ions are in close contact and the magnesium ions are well packed in the interstices of MgO structure. However, in CaO structure, oxygen ions are forced apart and calcium ions are not well packed, due to the larger Ca^{2+} ionic radius. For this reason, crystalline CaO is more reactive than MgO. CaO itself presents a low solubility and reactivity when compared to other clinker phases due to its supercalcination caused by the high temperature in the clinkering kiln [23].

Alkali sulfates are the most soluble compounds present in cement. However, they do not present significant hydration reactions. As mentioned before, alkalis play an important role on C_3A structure, and, therefore, on its reactivity [23].

Since reactions with water occur typically at the cement-water interface, understanding surface reactivity is of crucial importance. The fluid-solid interaction alters both the surface layers of the solid and the boundary layer of the fluid surrounding it. Then, it is critical to recognize that, at this interface, neither the crystal nor the fluid is equivalent to its bulk counterpart [36].

Surface reactivity of a cement phase depends ultimately on its chemical composition, atomic structure and morphology. These properties present several inhomogeneities and can be modified by sorption, desorption or exchange reactions that happen, rarely uniformly, across

the surface. The vast majority of cement reactions starts on reactive sites, micro-cracks or surface defects, such as vacancies or dislocations, present on the mineral crystal [19].

2.3.   Cement hydration

Hydration is absolutely central to cementitious materials. It is the process by which a fluid suspension is transformed into a rigid solid, at room temperature, without the need for heat or other external processing agents. It happens with minimal bulk volume change and leads to the development of mechanical strength. The chemistry of concrete is essentially the chemistry underlying in the reaction between Portland cement and water. For those reasons, understanding the mechanisms that govern hydration may provide the means to develop cheaper, more efficient and more sustainable cementitious materials and processes [37,38].

As Portland cement is a complex polyphasic material, many studies have been performed on pure phases, with the aim of elucidating their hydration chemistry before continuing studies on real cements. Since alite is the major component in cement and dominates the early strength evolution, pure C_3S and alite itself have been extensively used in research [12,39,40]. Tricalcium aluminate has also been employed in studies regarding its interaction with calcium sulfates [41–43]. Belite and calcium alumino-ferrite are not common subjects for investigation on early age hydration due to their lower reactivity.

Since hydration is an exothermic process, one of the most common methods to follow its early progress is isothermal calorimetry of cement pastes [34,38]. Using this technique, the heat transfer generated during physical and chemical processes is monitored and a heat flow curve by time is obtained. The kinetics and mechanisms of hydration may be analyzed and the influence of different additions and admixtures may be evaluated [12,44,45]. Due to this reason, the following sections (2.3.1 to 2.3.3) will be based on calorimetry results.

2.3.1. Hydration of silicate phases

2.3.1.1. Hydration of C$_3$S

Figure 2.1 presents the heat flow monitored by isothermal calorimetry and the evolution of calcium concentration in the liquid phase during the early hydration of alite. Typically, this process may be divided in five stages, which are described as follows [34,37,38].
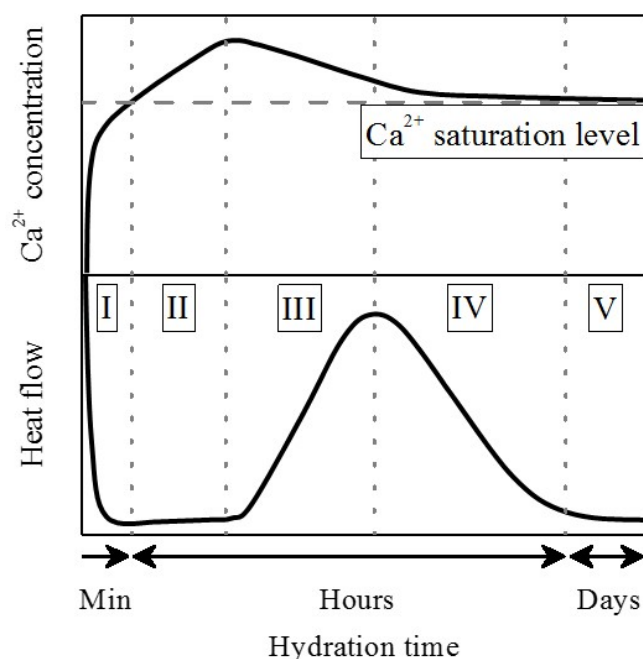
Figure 2.1 - Heat flow curve monitored by isothermal calorimetry coupled with liquid phase analysis of a pure C$_3$S paste, with water/cement ratio lower than 1.0 (adapted from [34]).

Stage I - pre-induction period

The pre-induction period is characterized by a large exothermic signal, due to the heat generated by wetting of particles, C$_3$S dissolution and initial hydration. The dissolution of tricalcium silicate is controlled by the formation of etch pits on the surface of particles [19,46]. This process releases Ca^{2+}, H$_2$SiO$_4^{2-}$ and OH$^-$ into solution, according to chemical equation 2.1 [47]. It also reacts with water, leading to the precipitation of C-S-H and portlandite, according to chemical equation 2.2 [34]. C-S-H is a calcium silicate hydrated phase of variable composition, whose CaO/SiO$_2$ ratio in this stage is approximately 2.5 [22].

$$C_3S + 3H_2O \rightleftharpoons 3Ca^{2+} + H_2SiO_4^{2-} + 4OH^-$$ Ch. equation 2.1

$$C_3S + (3 - x + n)H \rightarrow C_xSH_n + (3 - x)CH$$ Ch. equation 2.2

Stage II - induction period

The induction period is characterized by very low reaction rates. The solubility of C_3S decreases to a minor extent, but it continues to dissolve and release Ca^{2+} into the liquid phase, until the solution is supersaturated. The dissolution process is controlled by the step retreat of the surface pits generated in the former stage [46]. Nucleation of C-S-H initiates, but C_3S hydration is still negligible [37,47].

Stage III - acceleration period

The acceleration period is characterized by a large heat release due to the increase in the rate of alite hydration. During this stage, small particles (< 5 µm) hydrate preferentially. Calcium concentration in the liquid phase decreases, favoring alite dissolution and the consequent precipitation of C-S-H and portlandite. Nucleation and growth of C-S-H are the rate-controlling steps during this stage and hydration rate is proportional to the number of active growth sites for C-S-H. The main physical phenomena occurring during the acceleration period are the stiffening and setting of the paste, reduction in porosity and development of initial mechanical strength [22,38,47].

Stage IV - deceleration period

Hydration proceeds at lower rates because only large unhydrated particles (> 5 µm) are left to react, voids have been filled by C-S-H, the quantity of water available has decreased and its contact with anhydrous phases is difficult. The rate determining step during this stage is the densification process of the initially loosely packed C-S-H particles [48]. Formerly, diffusion across a dense layer of C-S-H formed around anhydrous grains was the mechanism accepted to control reaction rates during the deceleration period [49].

Stage V - hydration at late ages

A gradual densification of the microstructure occurs and the heat flow becomes low. Calcium concentration remains at calcium hydroxide saturation [37]. After the hydration process has been completed, an ageing of the hydrated C-S-H may occur. It is characterized by the polycondensation of the SiO_4 tetrahedra, increasing the chain length in the C-S-H structure [33]. For pure saturated C_3S pastes, the CaO/SiO_2 ratio of C-S-H varies between 1.7 and 1.8 [21].

2.3.1.2. Hydration of β-C_2S

Dicalcium silicate is less extensively studied than C_3S because its hydration contributes mostly to long term properties of cementitious matrices. Belite hydration becomes significant only after 10 days, approximately [37]. However, there has been a continued interest in belite cements, due to lower heat of hydration and improved durability. The β polymorph is the most extensively studied because it is the most commonly found in Portland cements [50,51].

Hydration of dicalcium silicate is similar to tricalcium silicate and is represented in chemical equation 2.3. The composition of C-S-H is similar to that formed by C_3S, although the development of microstructure proceeds considerably slower. The evaluation of this process by conduction calorimetry is more difficult due to its lower enthalpy and slower kinetics of hydration [34].
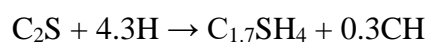
$C_2S + 4.3H \rightarrow C_{1.7}SH_4 + 0.3CH$ 　　　　　　　　　　　Ch. equation 2.3

2.3.2. Hydration of aluminate phases

Tricalcium aluminate is the most reactive phase in Portland cement and influences early hydration and rheology significantly. It reacts immediately and completely with water, but the products formed do not give rise to mechanical strength and volume stability. However, calcium sulfate additions alter the mechanisms of C_3A hydration considerably and allow its use as a hydraulic compound [21]. Therefore, C_3A hydration in the presence of calcium sulfate is of major interest for practical purposes. Details about C_3A hydration with and without calcium sulfate additions are presented subsequently.

2.3.2.1. Hydration of C₃A in the absence of calcium sulfate

C_3A hydration in the absence of gypsum may lead to flash-set. Irregular flakes of poorly crystalline AFm phases are initially formed and, then, converted into a permeable network of metastable hexagonal hydrates composed by C_4AH_{19} and C_2AH_8. Below relative humidity of 88 %, C_4AH_{19} loses part of its interlayer water and forms C_4AH_{13} [34]. Hydrogarnet, a thermodynamically stable phase composed by C_3AH_6, is formed as hydration proceeds [21]. These processes are represented by chemical equations 2.4 and 2.5, respectively.

$$2C_3A + 27H \rightarrow C_4AH_{19} \ (or \ C_4AH_{13}) + C_2AH_8 \qquad\qquad \text{Ch. equation 2.4}$$

$$C_4AH_{19} + C_2AH_8 \rightarrow 2C_3AH_6 \qquad\qquad \text{Ch. equation 2.5}$$
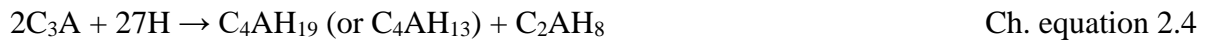
2.3.2.2. Hydration of C₃A in the presence of calcium sulfate

When calcium sulfate is present in the system, C_3A hydration occurs in two steps. The first one consumes calcium sulfate and forms ettringite (AFt) as the main hydration product. The second step starts when the sulfate source has been depleted and corresponds to the reaction of C_3A with ettringite, forming AFm phases. Depending on the initial calcium sulfate content, monosulfoaluminate and hydroxyl-AFm are the main phases formed. These processes are represented by chemical equations 2.6 and 2.7, respectively [41,42,52].

$$C_3A + 3C\bar{S}H_2 + 26H \rightarrow C_6A\bar{S}_3H_{32} \qquad\qquad \text{Ch. equation 2.6}$$

$$2C_3A + C_6A\bar{S}_3H_{32} + 4H \rightarrow 3C_4A\bar{S}H_{12} \qquad\qquad \text{Ch. equation 2.7}$$

C_3A hydration with gypsum can be followed by isothermal calorimetry, as represented in figure 2.2. Typically, this process can be divided in four stages, which are described as follows [41,42,52].
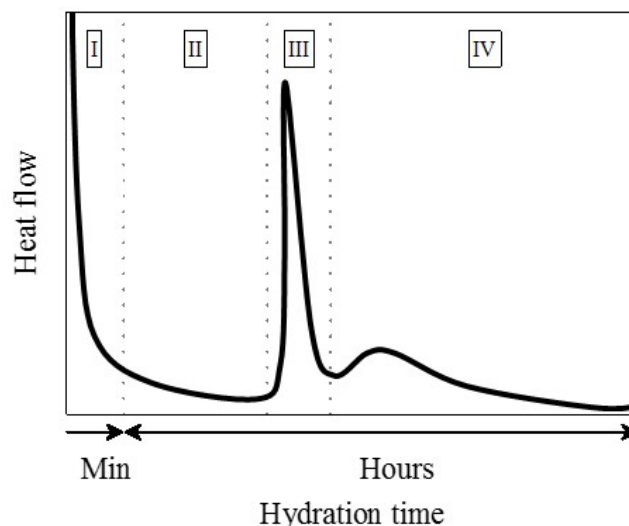
Figure 2.2 - Heat flow curve of a C_3A paste with gypsum, monitored by isothermal calorimetry [41,42,52].

Stage I - pre-induction period

Gypsum dissolves and releases Ca^{2+} and SO_4^{2-} ions into the liquid phase. C_3A dissolves and reacts rapidly with calcium and sulfate ions present in solution. Ettringite is the main hydrate formed, but monosulfoaluminate and hydroxy-AFm may also precipitate. Due to the adsorption of sulfate ions on reactive dissolution sites of C_3A particles, their surface becomes rich in calcium sulfoaluminate hydrates. Since these hydrates are thermodynamically more stable and less soluble than anhydrous calcium aluminate [16], the rate of C_3A dissolution and further hydration reduces significantly [41,47].

Stage II - induction period

The induction period is characterized by low rates of C_3A dissolution and hydration. Ettringite is constantly formed, consuming calcium and sulfate ions from de liquid phase [42]. According to tests performed in diluted suspensions [41], the concentration of SO_4^{2-} is constant up to the middle of the induction period, decreasing linearly after that, until complete disappearance. Calcium concentration follows the same tendency, but increases or levels up just before the onset of stage III. The length of the induction period is directly proportional to gypsum content and depends on C_3A particle size.

Stage III - C₃A dissolution

Sulfate concentration in the liquid phase is very low, leading to sulfate desorption from C_3A surface to reestablish the thermodynamic equilibrium. The sharp exothermic signal is attributed to C_3A dissolution and further reaction with SO_4^{2-} ions to form ettringite [41].

Stage IV - formation of AFm phases

Sulfate ions deplete and C_3A reacts with ettringite to form monosulfoaluminate (chemical equation 2.7). In the heat flow curve, this process is identified as a broad shoulder in the deceleration period [22,41,47]. Depending on C_3A reactivity and on sulfate content, this shoulder may be overlapped with the peak from C_3A dissolution, which makes stages III and IV not clearly distinguishable.

2.3.2.3. Influence of calcium sulfate content and structure on C₃A hydration

The influence of calcium sulfate content on C_3A hydration was evaluated in diluted suspensions by [42]. Increasing sulfate contents lead to longer induction periods because it takes more time to reach sulfate depletion. In addition, the rate and extent of C_3A dissolution are reduced when larger amounts of calcium sulfate are employed.

C_3A hydration with different calcium sulfate sources (gypsum and hemihydrate) was also analyzed in the same research paper [42]. Since hemihydrate is more soluble than gypsum ($CaSO_4 \cdot 2H_2O$: 0.255 g/100 g H_2O at 20 ºC; $CaSO_4 \cdot 0.5H_2O$: 0.32 g/100 g H_2O at 20 ºC [53]), the liquid phase becomes saturated in Ca^{2+} and SO_4^{2-} ions faster when hemihydrate is used. Therefore, the rate of ettringite formation increases. In addition to that, hemihydrate avoids the precipitation of AFm phases, which usually happens on the initial contact of C_3A and water.

2.3.2.4. Hydration of C₄AF

The course of C_4AF hydration is very similar to that of C_3A. In the absence of calcium sulfate, metastable iron-substituted AFm phases $C_4(A,F)H_{19}$ and $C_2(A,F)H_8$ form initially and then convert into $C_3(A,F)H_6$. The latter compound is unstable at high temperatures and

decomposes to C_3AH_6 and $Fe(OH)_3$. The crystalline phases have a higher A/F ratio than the unhydrated material and, hence, an iron-rich hydroxide must form in order to maintain stoichiometry. These processes are represented by chemical equation 2.8 [34].

$$3C_4AF + 60H \rightarrow 2C_4(A,F)H_{19} + 2C_2(A,F)H_8 + 4(F,A)H_3 \rightarrow$$
$$\rightarrow 2C_3(A,F)H_6 + 2(F,A)H_3 + 24H$$

Ch. equation 2.8
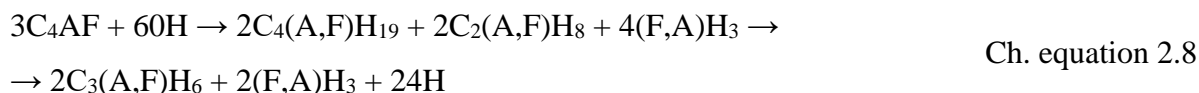
C_4AF hydrates with gypsum following the same sequence as C_3A. An iron substituted AFt phase forms and then converts into AFm when gypsum depletes. Amorphous aluminum-substituted $Fe(OH)_3$ also forms. Since hydration is similar, C_3A and C_4AF compete for gypsum during hydration, although most of it is consumed by C_3A due to its higher reactivity [34].

2.3.3. Hydration of Portland cement

On the contact of cement with water, hydration starts and several phenomena occur during the whole process. It is a sequence of overlapping chemical reactions among clinker components, calcium sulfate and water, with correspondent kinetics and enthalpies, which lead to setting and hardening. The main steps that govern hydration are the dissolution of clinker phases, nucleation of hydrated phases, diffusion of species to active sites and growth of crystals.

Figure 2.3 shows a general heat flow curve monitored by isothermal calorimetry of a CEM I paste. The main hydration stages observed are described subsequently [22,34,47].
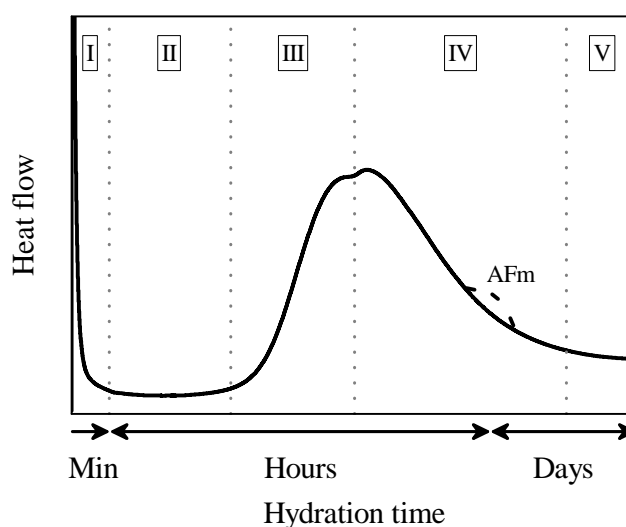
Figure 2.3 - Heat flow curve of a CEM I paste with w/c ratio of 0.45 [22,34,47].

Stage I - pre-induction period

Rapid dissolution of alkali sulfates, gypsum, alite and aluminate phases, which increases the pH of the liquid phase to 12 and releases heat. Initial formation of ettringite occurs. The rapid formation of aluminate hydrates influences rheology and subsequent microstructure.

Stage II - induction period

Period of low activity, with consequent low heat evolution. C-S-H nucleates, the liquid phase becomes supersaturated with Ca^{2+} and the concentrations of SO_4^{2-}, $H_2SiO_4^{2-}$ and $[Al(OH)_4]^-$ decrease. Continued formation of AFm and AFt phases influences workability, but it is the formation of C-S-H that usually leads to setting.

Stage III - acceleration period

Alite hydration accelerates, forming CH and C-S-H, with consequent large heat release. The paste changes from plastic to rigid consistency (initial and final set occur), early strength develops and porosity reduces. The concentration of Ca^{2+} decreases to saturation level and the concentration of SO_4^{2-} constantly reduces.

Stage IV - deceleration period

The rate of alite hydration decreases and the heat released during this stage is low. Sulfate ions desorb from C-S-H and renewed C_3A hydration occurs, with consequent secondary formation of ettringite. Then, C_3A reacts with ettringite, forming monosulfoaluminate.

Stage V - hydration at late ages

Hydration completes if enough water and space are available. Polycondensation of SiO_4 tetrahedra occurs, increasing C-S-H chain length. Mechanical strength increases continuously at very low rates due to decreasing porosity. Particle-to-particle and paste-to-aggregate bond formation occurs and the matrix shrinks due to drying.

Hydration products identified in hardened pastes are presented in table 2.2 [21,22]. Typically, an ordinary Portland cement is approximately 30 to 50 % hydrated at 1 day. The degree of hydration increases up to 80 % until 28 days and the matrix reaches around 75 % of the design strength. After this period, most of the unhydrated material left is the slow reacting belite phase [37].

Table 2.2 - Hydrated phases in hardened cement pastes [21,22].

Hydrated phase	Oxide composition	Notation	Remarks
Calcium silicate hydrate	$xCaO \cdot SiO_2 \cdot yH_2O$	C-S-H	Contains Al^{3+} and SO_4^{2-} as substituents ions. CaO/SiO_2 ratio varies according to cement composition and hydration conditions.
Portlandite	$CaO \cdot H_2O$	CH	Small contents formed by lime hydration.
Hydrogarnet	$3CaO \cdot Al_2O_3 \cdot 6H_2O$	C_3AH_6	Thermodynamically stable product from C_3A hydration. Fe^{3+} replaces Al^{3+} when formed by C_4AF.
Tetracalcium aluminate tetrahydrate	$4CaO \cdot Al_2O_3 \cdot 19H_2O$	C_4AH_{19}	Metastable products from C_3A hydration, which transform into C_3AH_6. Fe^{3+} replaces Al^{3+} when formed by C_4AF.
Dicalcium aluminate octahydrate	$2CaO \cdot Al_2O_3 \cdot 8H_2O$	C_2AH_8	
Ettringite	$6CaO \cdot Al_2O_3 \cdot 3SO_3 \cdot 32H_2O$	$C_6A\bar{S}_3H_{32}$	Product from the reaction between C_3A and gypsum at early ages. Fe^{3+} replaces Al^{3+} when formed by C_4AF.
Calcium monosulfoaluminate	$4CaO \cdot Al_2O_3 \cdot SO_3 \cdot 12H_2O$	$C_4A\bar{S}H_{12}$	Formed from the reaction between C_3A and ettringite when sulfate depletes. Fe^{3+} replaces Al^{3+} when formed by C_4AF.
Calcium hemicarboaluminate	$4CaO \cdot Al_2O_3 \cdot 0.5CO_2 \cdot 12H_2O$	$C_4A\bar{C}_{0.5}H_{12}$	Formed when the content of limestone filler in cement is below 4 %.
Calcium monocarboaluminate	$4CaO \cdot Al_2O_3 \cdot CO_2 \cdot 11H_2O$	$C_4A\bar{C}H_{11}$	Formed when the content of limestone filler in cement is above 4 %.
Brucite[a]	$MgO \cdot H_2O$	MH	Formed by MgO hydration at early ages. Then, it transforms into hydrotalcite.
Hydrotalcite[a]	$2MgO \cdot 0.5Al_2O_3 \cdot 0.5CO_3 \cdot 4H_2O$	$M_2A_{0.5}\bar{C}_{0.5}H_4$	Al^{3+} and Fe^{3+} replace Mg^{2+}. H_2O molecules occupy interlamellar spaces.

[a] Brucite and hydrotalcite are mentioned although the hydration mechanism of periclase has not been dealt with in the former sections due to its low solubility [33].

2.3.3.1. Influence of calcium sulfate on cement hydration

In Portland cements, calcium sulfate should be dosed correctly in order to achieve an optimal hydration behavior. High gypsum contents lead to the excessive formation of ettringite after paste sets, which can cause disruption of the paste microstructure, cracking and may lead to durability issues at later ages. Low gypsum contents accelerate C_3A reactions and the consequent formation of AFm phases, which may occur before the onset of alite hydration. This process fills up the pores of the matrix quickly and suppresses alite hydration, retarding strength development [34,54].

The hydration behavior of three cement pastes containing different amounts of gypsum is illustrated in figure 2.4 (adapted from [54]). In properly and enough sulfated systems, the renewed C_3A hydration occurs after the acceleration period of alite hydration. This is observed by a shoulder after the maximum heat flow of alite hydration is reached. However, C_3A hydration is accelerated in undersulfated systems. The first exothermic signal in the heat flow curve corresponds to undersulfated C_3A reactions and the second one is the alite hydration peak. It is possible to notice that the rate and extent of alite hydration are significantly reduced, leading to lower degrees of hydration until 24 h.
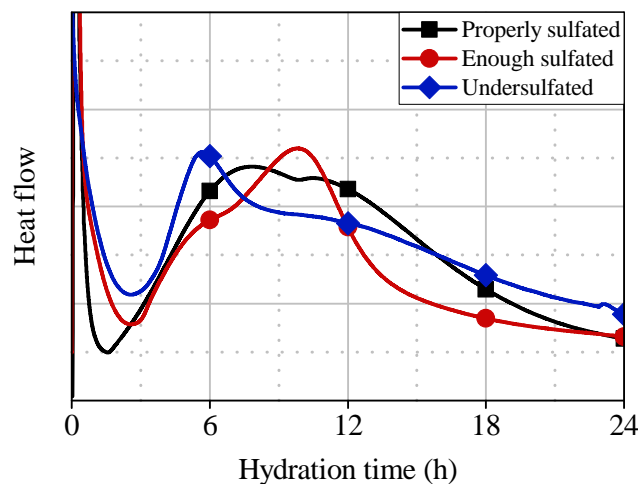
Figure 2.4 - Heat flow curves of properly, enough and undersulfated systems (adapted from [54]).

2.3.3.2. Influence of aluminum on cement hydration

As presented in table 2.1, cement compounds contain foreign ions in their crystal lattice. Al^{3+} is one of the most important ions that replace Si^{4+} in the structure of siliceous compounds

[21], generating different polymorphs with modified crystallinity, solubility and intrinsic reactivity [55–57]. Calcium silicate phases doped with small amounts of aluminum usually have lower solubility than pure compounds, even in solutions with high pH [58,59].

Alite containing aluminum presents a different hydration behavior from pure tricalcium silicate. In the presence of gypsum, aluminum reacts with sulfate ions, leading to the formation of calcium sulfoaluminate hydrates. This reaction does not affect silicate hydration negatively, which proceeds normally [54,60]. However, when the liquid phase does not contain sulfate ions, aluminum incorporated in alite structure tend to form hydroxy-AFm phases, which precipitate on the surface of alite particles. This process blocks the reactive sites present on alite surface, reducing its solubility and reactivity.

Furthermore, as soon as alite is in contact with water, aluminum ions pass into solution in the form of $[Al(OH)_4]^-$. When their concentration in solution is above 0.005 mmol/L, aluminate ions adsorb on reactive sites of C-S-H nuclei and may even substitute silicon in the C-S-H crystal lattice, forming a calcium alumino-silicate hydrate [32,61–63]. In this case, aluminum poisons the first C-S-H nuclei and prevents them from growing. In addition to that, C-A-S-H does not act as a nucleation site for C-S-H growth [32,61].

The results of these processes are a delay on the onset of the acceleration period and a reduction in the rate of mechanical strength development at early ages. These processes are important when accelerators are used in sprayed concrete, because they are based either on sodium aluminate or on aluminum sulfate solutions. The chemistry of accelerators will be discussed in section 2.4.1.

2.3.3.3. Influence of limestone filler on cement hydration

Limestone filler influences cement hydration physically and chemically. The physical effect is cement dilution, which increases the space for the precipitation of hydrates. In addition, due to its elevated fineness, it favors nucleation and growth of C-S-H crystals and their densification as hydration progresses. Therefore, higher degrees of hydration are obtained in comparison with cements that do not contain this addition [64].

Chemically, limestone filler participates in cement hydration reactions from their beginning, competing with gypsum to retard C_3A hydration [65,66]. It avoids accelerated undersulfated C_3A reactions, leading to proper alite hydration and to higher degrees of

hydration in cements containing low gypsum amounts. In addition, it reacts with monosulfoaluminate, yielding ettringite and calcium hemicarboaluminate (chemical equation 2.9), which then converts into calcium monocarboaluminate. By this reaction, ettringite is indirectly stabilized, consequently increasing the volume of hydrates and decreasing the porosity of the paste [45].

$$3C_4A\bar{S}H_{12} + Ca^{2+} + CO_3^{2-} + 2OH^- + 19H_2O \rightarrow C_6A\bar{S}_3H_{32} + 2C_4A\bar{C}_{0.5}H_{12}$$ Ch. equation 2.9
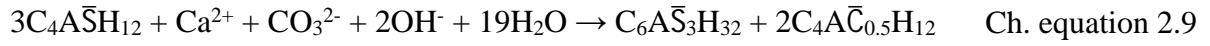
2.3.4. Principles of thermodynamic and kinetics of hydration

Hydration is fundamentally a dissolution-precipitation process [40,67]. For hydration to proceed, the solubility of hydration products must be lower than the solubility of anhydrous phases. Table 2.3 presents the dissolution reactions and the solubility coefficients of some hydrated phases present in hardened pastes [16,53,68]. Solubility values of anhydrous phases were not available. Calcium concentration (the common ion in all the phases) in thermodynamic equilibrium ($[Ca^{2+}]_{eq}$) was determined in order to facilitate the comparison of the solubility of each compound.

Table 2.3 - Thermodynamic data of hydrated phases in hardened pastes at 25 °C and 1 bar [16,53,68].

Phase	Dissolution reaction	pK_{S0}	$[Ca^{2+}]_{eq}$ (mmol/L)[a]
C-S-H (jennite)	$C_{1.67}SH_{2.1} \rightleftharpoons 1.67Ca^{2+} + HSiO_3^- + 2.33OH^- + 0.5H_2O$	13.17	2.2
C-S-H (tobermorite)	$C_{0.83}SH_{1.3} \rightleftharpoons 0.83Ca^{2+} + HSiO_3^- + 0.67OH^- + 0.43H_2O$	8.0	0.62
CH	$CH \rightleftharpoons Ca^{2+} + 2OH^-$	5.26	11.1
C_3AH_6	$C_3AH_6 \rightleftharpoons 3Ca^{2+} + 2[Al(OH)_4]^- + 4OH^-$	20.84	4.6
C_4AH_{13}	$C_4AH_{13} \rightleftharpoons 4Ca^{2+} + 2[Al(OH)_4]^- + 6OH^- + 6H_2O$	25.40	7.0
C_2AH_8	$C_2AH_8 \rightleftharpoons 2Ca^{2+} + 2[Al(OH)_4]^- + 2OH^- + 3H_2O$	13.56	5.5
$C_6A\bar{S}_3H_{32}$	$C_6A\bar{S}_3H_{32} \rightleftharpoons 6Ca^{2+} + 2[Al(OH)_4]^- + 4OH^- + 3SO_4^{2-} + 26H_2O$	44.9	1.5
$C_4A\bar{S}H_{12}$	$C_4A\bar{S}H_{12} \rightleftharpoons 4Ca^{2+} + 2[Al(OH)_4]^- + 4OH^- + SO_4^{2-} + 6H_2O$	29.26	2.8
$C_4A\bar{C}_{0.5}H_{12}$	$C_4A\bar{C}_{0.5}H_{12} \rightleftharpoons 4Ca^{2+} + 2[Al(OH)_4]^- + 5OH^- + 0.5CO_3^{2-} + 5.5H_2O$	29.13	3.3
$C_4A\bar{C}H_{11}$	$C_4A\bar{C}H_{11} \rightleftharpoons 4Ca^{2+} + 2[Al(OH)_4]^- + 4OH^- + CO_3^{2-} + 5H_2O$	31.47	1.8

[a] Calculated from pK_{S0}, considering the phase dissolution in pure water at 25 °C, until saturation.

Considering the system CaO-SiO_2-H_2O, alite always hydrates when the concentration of calcium hydroxide is between 0 and 36 mmol/L (maximum supersaturation of portlandite), because C-S-H is less soluble than C_3S in these conditions. However, belite is less soluble than C-S-H when the concentration of calcium hydroxide is above 30 mmol/L, indicating that C_2S should not dissolve to precipitate C-S-H. Since C_3S and C_2S coexist in Portland cements, belite cannot dissolve as long as alite hydrates, because the ionic concentration in the liquid phase during alite hydration is higher than the solubility of belite [37,69].

Regarding the system CaO-Al_2O_3-H_2O, several hydrates are less soluble than anhydrous phases. The least soluble and most thermodynamically stable hydrate is C_3AH_6, but its formation is not kinetically favored when compared to C_4AH_{13} and C_2AH_8. Therefore, C_4AH_{13} and C_2AH_8 precipitate initially and then convert into hydrogarnet (section 2.3.2.1) [21,70].

A different behavior is observed in the system CaO-Al_2O_3-$CaSO_4$-H_2O. Ettringite formation is kinetically and thermodynamically favored and this hydrate precipitates at the beginning of the hydration process. When dissolved sulfates are completely consumed and C_3A reactions are still ongoing, ettringite dissolves to restore sulfate concentration in the liquid phase and monosulfoaluminate is formed. Although this phase is more soluble than ettringite, monosulfoaluminate is the resulting phase from C_3A and C_4AF hydrations due to the limited sulfate content present in cements [68].

In cements containing limestone filler (system CaO-Al_2O_3-$CaSO_4$-$CaCO_3$-H_2O), hemicarboaluminate is the initial AFm phase formed [68]. If calcium carbonate content is above 4 %, hemicarboaluminate converts into the less soluble and thermodynamically stable monocarboaluminate (table 2.3). Carbonate ions displace sulfate ions (chemical equation 2.9), which are then consumed for ettringite formation [71]. Therefore, in CEM II/A-L pastes, monocarboaluminate and ettringite are the main hydrates formed by C_3A hydration [45].

Regarding a simplified evaluation of kinetics of hydration, a hydrating cement paste is composed by two solid phases (anhydrous and hydrated) and one liquid phase. The anhydrous phase dissolves at a dissolution rate R_{diss} and the hydrated phase precipitates at a precipitation rate R_{prec}. Since hydration occurs due to interfacial reactions, dissolution and precipitation rates depend on the interface area between the solid and the solution. In addition, these processes are time dependent because the surface area of anhydrous phases decreases and the surface of the precipitating material increases as hydration progresses. When thermodynamic equilibrium is reached, the dissolution rate is approximately equal to the precipitation rate ($R_{prec} \sim R_{diss}$) [37].

Figure 2.5 presents the hydration progress of an ordinary Portland cement paste determined by X-ray diffraction and Rietveld refinement (adapted from [72]). Alite and C_3A are the most reactive phases, reaching degrees of hydration between 40 and 60 % and 20 and 80 % at 1 day, respectively. On the contrary, around 20 % of belite react until 10 days of hydration, which makes it the least reactive phase in Portland cements.
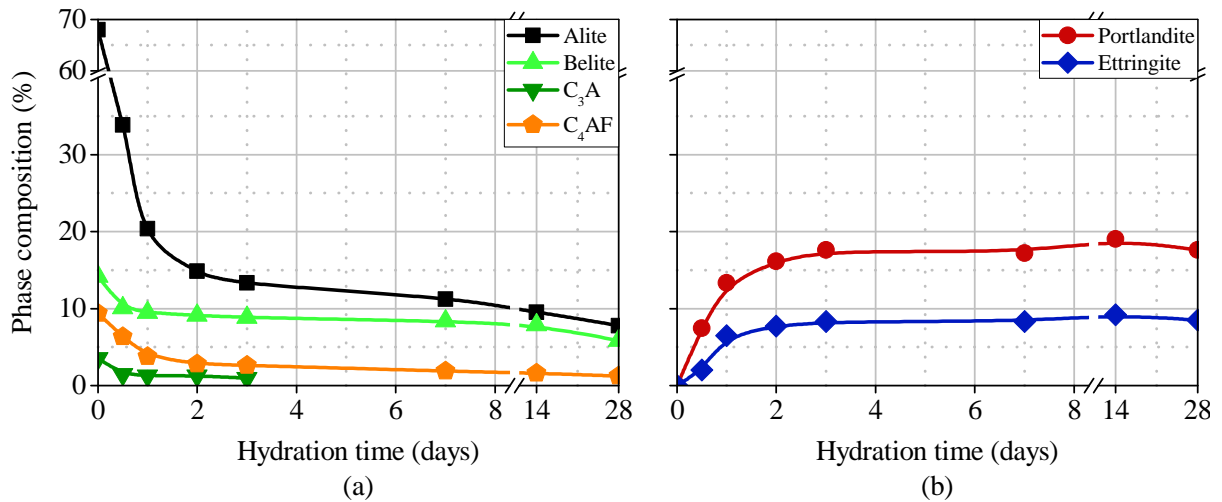
Figure 2.5 - Evolution of anhydrous (a) and hydrated (b) phases of an ordinary Portland cement paste during hydration, determined by X-ray diffraction and Rietveld refinement (adapted from [72]).

2.3.5. Microstructure development and its relation to the properties of the matrix

Figure 2.6 presents a schematic microstructural development of a polymineralic cement grain [73]. The processes occurring during hydration are explained subsequently [21,34,38,73].
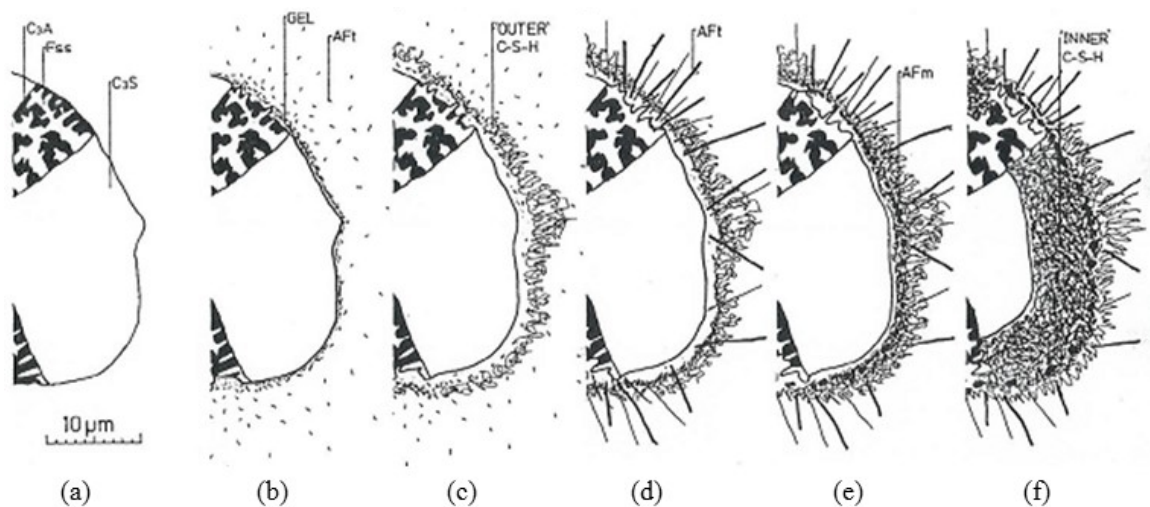
Figure 2.6 - Development of microstructure during hydration of a Portland cement from 0 to 3 h (a and b), 3 to 24 h (c and d) and from 24 h on (e and f) [73].

The early period of hydration (0 - 3 h)

Early hydration is dominated by C_3A and C_3S reactions (figures 2.6.a and 2.6.b). Within a few minutes, an aluminate-rich amorphous layer forms on the surface of the grain and short AFt rods nucleate at edge of gel and in solution.

The middle period of hydration (3 - 24 h)

After induction period finishes, C-S-H precipitates on a network of AFt needles and grows outwards into the water-filled space (figures 2.6.c and 2.6.d). At the end of the acceleration period, C-S-H densifies close to the surface of the particle and secondary formation of ettringite occurs, forming large prismatic needles (length of 10 µm and thickness of 1 µm). Hexagonal plates of portlandite, with mean diameter between 10 and 100 µm, precipitate. During this period, around 30 to 50 % of the cement reacts.

The late period of hydration (from 24 h on)

Thin hexagonal plates of AFm (length of 1 µm and width of 0.1 µm) are formed by the reaction of C_3A with AFt phases occurring inside the shell (figures 2.6.e and 2.6.f). Continuous growth of C-S-H reduces the space between anhydrous grain and hydrated shell. C-S-H formed outside of the shell becomes more fibrous. The approximate composition of a hardened paste, in volume percentage, is C-S-H (50 %), portlandite (12 %), AFm phases (13 %), capillary pores (20 %) and unhydrated cement (5 %).

The microstructural properties of a cementitious matrix influence its engineering properties, such as workability, setting times and strength. The stiffening of the paste is the first process that occurs and is associated with slump loss in concrete. The gradual loss of free water from the system as a result of the formation of hydration products, surface adsorption by poorly crystalline products and evaporation leads to stiffening [23].

The setting process of a cement paste comprehends the coagulation of cement grains and the stiffening of the coagulated structure. The first process occurs during the first minutes after mixing and the structure formed is mechanically reversible. The second step arises

simultaneously with the acceleration period of hydration and the cohesion of the paste is proportional to the amount of hydrates precipitated. Hydrates formed interact with each other, forming a structure of a network of agglomerated solid particles, which is mechanically irreversible [74]. In general terms, normal set is controlled by alite hydration, although recrystallization of ettringite may also influence setting [34].

The main source of strength in the solid products is the existence of van der Waals forces of attraction in the hydrated cement paste. The cohesion of the paste and strength of concrete depend on the degree of adhesive action and on the extent and nature of the surfaces involved. Hydration products tend to adhere strongly to each other and to other solids, such as anhydrous clinker grains and aggregate particles [23].

Although porosity is an important factor that controls strength, the morphology, density, volume and binding capacities of hydration products also participate on the strength evolution process. Cement pastes with large, well-developed crystals with distinct grain boundaries present higher strength than pastes containing ill-crystallized hydrates. This occurs due to the stronger interaction among hydrated products and the denser microstructure obtained when proper mix designs and curing methods are used [21].

2.4. Sprayed concrete

Sprayed concrete has grown into an important and widely used construction technique, with technical and economic interests. Due to continued research and development in materials, equipment and construction procedures, several improvements in the efficiency and in the range of application of this construction process have been achieved. When properly installed, it is a structural and durable material, with excellent bonding properties to different types of substrates [75,76].

One of the central advantages of sprayed concrete is that two stages of concrete laying (pouring and compacting) are merged. It is particularly convenient when the use of formwork is not feasible or when normal casting procedures cannot be employed. Therefore, the main applications of sprayed concrete are rock support, stabilization of underground constructions, such as tunnel linings, and the repair and reinforcement of varied elements [1].

The basic constituent materials of sprayed concrete (cement, aggregates, water and superplasticizer) are similar to those used in conventional concrete. The main difference is the use of accelerators, which are added at the nozzle when the mix is pneumatically sprayed. The mix design should be such that the fresh mix presents adequate workability and flowability for pumping and the in-place concrete develops acceptable mechanical and physical properties, considering the effects associated with the placement process (air-entrapment, porosity, rebound and velocity of spraying) [77–80].

Due to safety issues, the main properties of interest in sprayed concrete are the consistency and the rate of setting, hardening and early age strength development. The matrix must have an adequate consistency to enable the build-up of layers with proper thickness for rapid progression of construction operations [7,8]. Rapid set and high early strength are crucial to prevent dangerous and costly fallouts of large masses of fresh material from walls and overhead areas. These properties are achieved by the incorporation of accelerators, which are described in the following subsection (2.4.1).

2.4.1. Accelerators

Accelerators comprise a range of chemicals that influence the rate of cement hydration, thereby shortening setting times and increasing the rate of early strength development [33]. Several types of compounds have been used as accelerators in sprayed concrete. Table 2.4 presents their basic chemical composition, mode of action and usual dosages [1,7,81].

Table 2.4 - Accelerators used in sprayed concrete [1,7,81].

Chemical composition	Mode of action	Dosage (% bcw)
Alkaline carbonate	Acceleration of alite hydration	2.5 - 6.0
Alkaline silicate	Precipitation of calcium silicate	> 10.0
Alkaline aluminate	Formation of calcium sulfoaluminate hydrates	2.0 - 4.0
Aluminum sulfate (alkali-free)	Formation of calcium sulfoaluminate hydrates	3.0 - 10.0

Nowadays, accelerators commonly found in practice are aqueous solutions based either on alkali aluminate or alkali-free aluminum sulfate. Sodium aluminate is widely used in several countries because, when compared to aluminum sulfate, lower dosages are required, it presents a broader range of application and is cheaper. However, this type of admixture has major

drawbacks, such as safety issues in handling and spraying operations and reductions in ultimate strength of around 20 % [1,18]. Due to these limitations, alkaline aluminate accelerators have been frequently replaced by alkali-free formulations, which are mandatorily specified in some guidelines because their alkali content is lower than 1.0 % (expressed as Na_2O equivalent content) [82].

Both types of accelerators are sources of dissolved aluminum to the cement matrix. Alkaline accelerators provide $[Al(OH)_4]^-$ ions, while alkali-free accelerators provide Al^{3+} ions, which convert into $[Al(OH)_4]^-$ due to elevated pH in the matrix. The most probable reactions that occur in a cementitious matrix when $[Al(OH)_4]^-$ ions are added are represented in table 2.5 [4,21,83]. The standard Gibbs free energy of formation of each hydrated phase was obtained from [16].

Table 2.5 - Possible reactions of $[Al(OH)_4]^-$ ions in cementitious matrices at room temperature and the standard Gibbs free energy of formation of each hydrated phase [4,16,21,83].

Ch. equation	Reaction	$\Delta_f G^0$ (kJ/mol)
2.10	$Al^{3+} + 3OH^- \rightleftharpoons Al(OH)_3 + OH^- \rightleftharpoons [Al(OH)_4]^-$	-
2.11	$2[Al(OH)_4]^- + 6Ca^{2+} + 4OH^- + 3SO_4^{2-} + 26H_2O \rightleftharpoons C_6A\bar{S}_3H_{32}$	- 15207.0
2.12	$2[Al(OH)_4]^- + 4Ca^{2+} + 4OH^- + SO_4^{2-} + 6H_2O \rightleftharpoons C_4A\bar{S}H_{12}$	- 7739.6
2.13	$2[Al(OH)_4]^- + 4Ca^{2+} + 6OH^- + 6H_2O \rightleftharpoons C_4AH_{13}$	- 7326.6
2.14	$2[Al(OH)_4]^- + 2Ca^{2+} + 2OH^- + 3H_2O \rightleftharpoons C_2AH_8$	- 4812.8
2.15	$2[Al(OH)_4]^- + 4Ca^{2+} + 5OH^- + 0.5CO_3^{2-} + 5.5H_2O \rightleftharpoons C_4A\bar{C}_{0.5}H_{12}$	- 7339.5
2.16	$1.8[Al(OH)_4]^- + 4Ca^{2+} + 5OH^- + 1.1SO_4^{2-} + Na^+ + 9.9H_2O \rightleftharpoons$ $C_4A_{0.9}\bar{S}_{1.1}N_{0.5}H_{16}$	-

As observed in table 2.5, reactions of $[Al(OH)_4]^-$ ions depend mainly on the availability of Ca^{2+} and SO_4^{2-} ions in the liquid phase. When enough sulfate is available, ettringite (chemical equation 2.11) is the main hydrate formed by accelerator reaction since it is the most thermodynamically stable and least soluble phase (table 2.3). However, if sulfate concentration is low, monosulfoaluminate or C-A-H phases may also precipitate (chemical equations 2.12, 2.13 and 2.14). In the presence of any carbonate in the system, hemicarboaluminate might also be formed (chemical equation 2.15). When Na^+ concentration in the liquid phase is above 0.40 mol/L, the formation of U-phases (sodium calcium alumino-silicate hydrate, represented by chemical equation 2.16) has already been reported [83].

The precipitation of these hydrates by accelerator reaction increase the solid/liquid ratio of the matrix, leading to a rapid increase in stiffness. Formation and growth of ettringite nanocrystals are the main processes that reduce setting times and increase the rate of early strength development [84]. Accelerated cement pastes may present setting times 150 to 250 times faster than pastes without accelerator, depending on accelerator type and dosage [1,5].

The consumption of Ca^{2+} and SO_4^{2-} ions from the liquid phase favors alite and gypsum dissolution to balance the ionic concentration in the chemical equilibria, initially disturbed by accelerators. This accelerates alite hydration and, therefore, advances the hardening and strength development processes. When the resulting accelerated matrix has a proper sulfate balance (C_3A/SO_3 ratio between 0.67 and 0.90), degrees of hydration at 24 h may be up to 20 % higher than in systems that do not contain accelerators [1,11].

The chemical composition of accelerators plays an important role in hydration kinetics and mechanical strength evolution. Accelerators based on sodium aluminate solutions rapidly deplete sulfate ions from the liquid phase. Consequently, undersulfated C_3A reactions occur, suppressing alite hydration [4,10,11]. Compressive strengths in alkaline accelerated sprayed concrete at 12 h and 7 days are respectively 70 and 20 % lower when compared to concrete produced with accelerators based on aluminum sulfate [1]. Ultimate strengths are optimized when the Al_2O_3/SO_4^{2-} ratio of alkali-free accelerators ranges between 0.38 and 0.60 [1].

Alite dissolution is also affected by the acid usually used as a stabilizing agent in alkali-free accelerators [3]. Phosphoric acid strongly decreases the rate and extension of alite hydration [3,19]. When compared to formulations containing formic acid, final setting is retarded and compressive strength at 12 h is reduced by 50 % [1]. Ultimate strength gain and modulus of elasticity are also negatively affected and reductions around 20 % at 28 days have been reported [18].

Cement composition is also a key factor that influences accelerator reactivity. CEM II/A-L has a better compatibility with accelerators based on aluminum sulfate than CEM I, due to the addition of limestone filler [5,11,18]. The solubility of calcium sulfate used as a setting regulator in cement influences accelerator reactivity and setting times are reduced when hemihydrate is only the sulfate source [11,85,86].

The performance of sprayed cementitious matrices containing accelerators depends strongly on the application method. High shearing conditions achieved during spraying

increases the rate of accelerator reaction [13] and causes a rapid stiffening of the matrix, which leads to air entraining and to an improper consolidation. In addition, C_3A reactions are advanced and the cement may hydrate as undersulfated, even in systems with proper sulfate balance [12]. Finally, the elevated temperature reached during application increases hydration rate, resulting in an inhomogeneous precipitation of hydrated phases and coarser porosity [14]. As a result, reductions of around 20 % in compressive strength and modulus of elasticity at 28 days have been reported in sprayed concrete when compared to conventional concrete [1,18].

In general, processes that accelerate early hydration and strength gain tend to decrease strength at late ages. The microstructure of the mature matrix is significantly influenced by the use of accelerators and by the mixing process [13,87]. Therefore, tests should be performed in accelerated sprayed pastes. By using this procedure, which is similar to real life applications, the characterization of properties of the matrix may provide more reasonable results for the evaluation of the behavior of sprayed concrete.

2.4.2. Chemical and mechanical characterization of accelerated matrices

Several standards are available for the definition, execution and mechanical characterization of sprayed concrete [88–93]. However, no standardized tests have been defined for the chemical characterization of accelerated cementitious matrices. From a detailed review of the literature regarding the subjects of this research, the tests presented in table 2.6 may be employed to evaluate the chemical and mechanical properties of cementitious matrices produced with accelerators. These are the main tests that will be performed in the experimental program of this thesis.

Table 2.6 - Tests for the characterization of accelerated cementitious matrices.

Objective	Test	Age	Reference
Chemical characterization	*In situ* X-ray diffraction (XRD)	0 - 48 h	[19]
	Isothermal calorimetry	0 - 48 h	[19,94]
	Evolution of temperature	0 - 48 h	[1,95]
	Powder XRD	-	[96]
	Thermogravimetry (TGA)	-	[97]
	Scanning electron microscopy (SEM)	-	[98]
Mechanical characterization	Determination of setting times	Until final setting	[99]
	Needle penetration test	Until 2 h	[91,100]
	Pin penetration test	From 4 h on	[91]
	Determination of ultrasonic wave propagation velocity	0 - 24 h	[101,102]
	Compression	From 1 day on	[103]
	Water accessible porosity	From 7 days on	[104]

The evaluation of chemical and mechanical properties at early ages in cementitious matrices containing accelerators is rather complex due to the difficulty in following accelerated hydration reactions. Efforts must be concentrated in this subject because the characterization of hydration processes may provide valuable information about the mechanical behavior of the matrix at early and late ages. Moreover, the determination of initial stiffness and early age strength in these mixes is crucial for their proper application and for safety reasons. This evaluation may help improve the sprayed concrete technology, regarding its mix design and applicability.

3. Hydration and microstructure of accelerated cement pastes[1]

3.1. Introduction

As discussed in section 2.4, accelerators alter the kinetics of hydration of cementitious materials, reducing setting times and increasing the rate of early strength development. These chemicals lead to the precipitation of calcium sulfoaluminate hydrates, which increase the solid/liquid ratio of the matrix. This property enables the build-up of concrete layers with proper thickness, providing an adequate support to the unstable ground in underground constructions.

Although some researches have been done on the chemistry of accelerated hydration reactions [4,20,84], it is still necessary to elucidate the main mechanisms involved when alkali-free and alkaline accelerators are used. The characterization of the hydration behavior and the microstructure development of cementitious matrices containing these types of accelerators is crucial for sprayed concrete technology. This evaluation may provide valuable information for the comprehension of the macrostructural behavior of sprayed concrete.

The objectives of the experimental campaign conducted in this chapter are:

- Characterize the kinetics and mechanisms of hydration of cement pastes produced with alkali-free and alkaline accelerators.

- Elucidate the main chemical processes occurring in accelerated cement pastes.

- Analyze how these chemicals influence the microstructure development of cement pastes.

- Establish a conceptual model regarding the hydration behavior of cement pastes containing different types of accelerator.

In this part of the experimental program, tests were performed with cement suspensions and pastes produced by hand-mixing. Pastes were composed by the combination of 2 types of cement and 4 types of accelerator, either alkali-free or alkaline. Liquid phase analysis, conductimetry, determination of pH, *in situ* and powder XRD, isothermal calorimetry, TGA and SEM imaging were performed to characterize kinetics and mechanisms of hydration. According to the results, variations in reaction kinetics caused by different accelerator formulations are explained and the main mechanisms governing accelerator reactivity and further cement hydration are highlighted.

3.2. Experimental methodology

3.2.1. Materials

3.2.1.1. Cements

Two types of Portland cement (CEM I 52.5R and CEM II/A-L 42.5R) were used in this study. These cements were selected among the commonly used in sprayed concrete applications. CEM II/A-L is widely used in countries from northern Europe, while CEM I is common in Spain and countries from Asia and America. Table 3.1 and 3.2 show their mineralogical composition determined by XRD and Rietveld refinement (structure models presented in Appendix A) and their chemical composition determined by X-ray fluorescence (XRF) spectrometry, respectively. Besides, table 3.3 summarizes their chemical and physical properties and figure 3.1 their particle size distribution.

Table 3.1 - Mineralogical composition of cements determined by XRD and Rietveld refinement.

Compound	CEM I (%)	CEM II/A-L (%)	Compound	CEM I (%)	CEM II/A-L (%)
C_3S	58.3	51.7	$CaCO_3$	1.9	11.3
C_2S	11.2	6.7	$CaSO_4.2H_2O$	2.1	0.7
C_3A_c	4.1	2.9	$CaSO_4.0.5H_2O$	4.4	5.3
C_3A_o	0.6	0.7	K_2SO_4	-	0.5
C_4AF	13.4	14.8	$K_2Ca(SO_4)_2.H_2O$	1.1	-
CaO	1.1	1.2	MgO	-	0.6
$Ca(OH)_2$	1.7	0.7	$MgCO_3$	-	3.1

Table 3.2 - Chemical composition of cements determined by XRF spectrometry.

Compound	CEM I (%)	CEM II/A-L (%)	Compound	CEM I (%)	CEM II/A-L (%)
LOI	2.88	6.42	SO_3	3.53	3.21
CaO	62.62	62.48	MgO	1.95	1.69
SiO_2	19.89	17.61	K_2O	0.99 (0.98)[a]	0.83 (0.62)[a]
Al_2O_3	4.74	4.04	Na_2O	0.13 (0.011)[a]	0.13 (0.035)[a]
Fe_2O_3	3.26	3.53	Minor components	0.11	0.09

[a] K_2O and Na_2O readily soluble, determined by ion chromatography from a solution extracted from a cement suspension with w/c equal to 9, 5 min after mixing cement and water [45].

Table 3.3 - Chemical and physical properties of cements.

Property	CEM I	CEM II/A-L
Total heat of hydration[a] (J/g)	433.0	381.0
C_3A/SO_3 molar ratio	0.39	0.33
Insoluble residue (%)	2.74	2.90
Specific surface BET (m^2/g)	2.96	1.88
d_{10} (µm)	2.04	2.39
d_{50} (µm)	11.4	15.7
d_{90} (µm)	34.8	48.0

[a] The total heat of hydration was estimated from the mineralogical composition of the cement, determined by XRD, as the relative sum of the heats of hydration of the individual phases (C_3S: 510 J/g; C_2S: 260 J/g; C_3A: 1100 J/g; C_4AF: 410 J/g [21]).
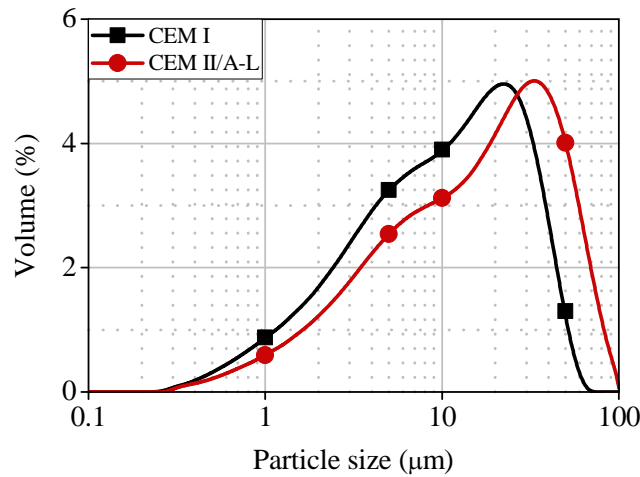
Figure 3.1 - Particle size distribution of cements.

3.2.1.2. Water and superplasticizer

For the preparation of cement suspensions and pastes, deionized water (Milli-Q, 18 ohm.s) and a superplasticizer based on a polycarboxylate solution (34 % of solid content) were employed.

3.2.1.3. Accelerators

Table 3.4 presents the composition and characteristics of the accelerators employed. Three alkali-free accelerators composed by aluminum hydroxysulfate solutions were selected to cover the types commonly found in practice. They consist in aluminum sulfate solutions with additions of different amounts of aluminum hydroxide. Formic acid is used to keep the pH around 3.0 to avoid aluminum hydrolysis and the consequent precipitation of aluminum hydroxide. Their nomenclature corresponds to *'AKF Al_2O_3/SO_4^{2-} molar ratio'*.

Table 3.4 - Composition and characteristics of accelerators.

Characteristic	AKF 0.38	AKF 0.42	AKF 0.61	ALK
Solid content (%)	40.0	34.5	47.6	43.0
Al_2O_3 content (%)[a]	11.2	10.1	13.5	24.0
SO_4^{2-} content (%)	27.6	22.5	21.0	-
Na_2O content (%)	-		-	19.0
pH at 20 °C	2.6	2.4	3.0	12.0[b]
Al_2O_3/SO_4^{2-} molar ratio	0.38	0.42	0.61	-
Stabilizing agent	Colloidal silica	Formic acid	Formic acid	-

[a] Al_2O_3 corresponds to Al^{3+} and $[Al(OH)_4]^-$ in alkali-free and alkaline accelerators, respectively.

[b] Solution at 1.0 %.

An alkaline accelerator composed by an aqueous solution of aluminum and sodium hydroxides was used. NaOH is used to dissolve $Al(OH)_3$, producing stable and soluble $[Al(OH)_4]^-$ ions. This accelerator does not contain sulfate ions and is identified by *'ALK'*.

3.2.2. Composition and preparation of cement suspensions and pastes

3.2.2.1. Cement suspensions

Reference cement suspensions (without accelerator) were composed by cement and a water/cement (w/c) ratio equal to 9. Due to the high w/c ratio, superplasticizer was not used for this test to avoid retarding effects on cement hydration. Accelerated suspensions contained either accelerators AKF 0.61 at 7.0 % or ALK at 3.0 % by cement weight (% bcw). AKF-61 at 7.0 % bcw provides an increase of 19.77 mmol/L, 16.32 mmol/L and 17.41 mmol/L in the concentrations of Al^{3+}, SO_4^{2-} and H^+ ions, respectively. When ALK is used at 3.0 % bcw, the amounts of 15.11 mmol/L of $[Al(OH)_4]^-$, 19.68 mmol/L of Na^+ and 4.57 mmol/L of OH^- are provided to the suspension.

Suspensions were prepared by adding water to cement, followed by 5 min of mixing using a magnetic stirrer. In accelerated suspensions, accelerator was added 5 min after cement and water had been mixed. A total of 1000 g of suspension was prepared, so that all the samples for ion chromatography could be extracted from the same batch. During the whole test,

suspensions were maintained under constant stirring, under controlled conditions, at 20 °C and 50 % relative humidity.

3.2.2.2. Cement pastes

Reference cement pastes (without accelerator) were composed by cement, a w/c ratio equal to 0.45 and superplasticizer at 1.0 % bcw. In accelerated pastes, accelerators dosages varied according to the type used. AKF 0.38 was used at 7.0 %, AKF 0.42 at 11.0 %, AKF 0.61 at 5.0 and 7.0 % and ALK at 3.0 % bcw. Accelerators dosages were determined according to the procedure described by [1] to assure equivalent mechanical performance in pastes and fall within the dosages usually applied in tunnels executed with sprayed material. Water contents of superplasticizer and accelerators were deducted from the total amount of mixing water in order to keep the final w/c ratio equal to 0.45.

The composition of each paste in terms of ions and compounds present is described in table 3.5. An information of interest is the $Al_2O_3/SO_4^{2-}{}_{(dissolved)}$ ratio of the paste right after accelerator addition. In all the pastes produced with alkali-free accelerators, this ratio is below 0.33 (the molar ratio from ettringite). However, the pastes containing the alkaline accelerator present ratios above 0.33, which means that the amount of dissolved sulfate available to react with all the aluminate ions from accelerator is not enough to form ettringite. Therefore, ettringite is the only hydrate formed when alkali-free accelerators are employed, whereas monosulfoaluminate and hydroxy-AFm may also be produced in pastes admixed with the alkaline formulation.

Table 3.5 - Composition of ions and compounds in accelerated cement pastes.

n (mmol/g cement)	I_0.38 7% / II_0.38 7%	I_0.42 11% / II_0.42 11%	I_0.61 5% / II_0.61 5%	I_0.61 7% / II_0.61 7%	I_ALK 3% / II_ALK 3%
Total SO_4^{2-} in cement[a]	0.441 / 0.401	0.441 / 0.401	0.441 / 0.401	0.441 / 0.401	0.441 / 0.401
SO_4^{2-} dissolved in paste before accelerator addition[b]	0.163 / 0.181	0.163 / 0.181	0.163 / 0.181	0.163 / 0.181	0.163 / 0.181
Al_2O_3 in accelerator	0.077	0.109	0.066	0.093	0.071
SO_4^{2-} in accelerator	0.201	0.258	0.109	0.153	-
H^+ in accelerator	-	0.046	0.117	0.163	-
Na^+ in accelerator	-	-	-	-	0.184
SO_4^{2-} necessary for ettringite formation	0.231	0.327	0.199	0.278	0.212
$Al_2O_3/SO_4^{2-}{}_{(dissolved)}$ ratio of paste right after accelerator addition	0.21 / 0.20	0.26 / 0.25	0.23 / 0.24	0.29 / 0.28	0.44 / 0.39
SO_4^{2-} remaining after accelerator reaction[c]	0.411	0.371	0.351	0.316	0.229
Final C_3A/SO_3 molar ratio	0.42 / 0.36	0.47 / 0.40	0.50 / 0.42	0.55 / 0.48	0.76 / 0.70

[a] Determined by ion chromatography with a solution obtained from the dissolution of 1.00 g of cement in 10.0 mL of concentrated nitric acid, according to [105].

[b] Determined by ion chromatography with a solution extracted from a cement paste containing a w/c ratio equal to 0.45, 1 h after mixing cement and water.

[c] Considering ettringite as the hydrate formed by accelerator reaction.

Moreover, as accelerator formulations contain different Al_2O_3/SO_4^{2-} ratios, the initial sulfate balance from cement changes. The final C_3A/SO_3 molar ratio of the paste was calculated considering the sulfate amount remaining after accelerator reaction and the initial C_3A content of cements (C_3A_{cement}), according to equation 3.1 (all units in mol). Sulfate remaining after accelerator addition corresponds to the sum of sulfate contents from cement ($SO_4^{2-}{}_{cement}$) and accelerator ($SO_4^{2-}{}_{accelerator}$) minus the sulfate content consumed by aluminum ions from accelerator to form ettringite ($SO_4^{2-}{}_{consumed\ by\ accelerator}$). The final C_3A/SO_3 ratio is an important parameter to verify if cement pastes will behave as either properly or undersulfated, since high C_3A/SO_3 ratios may be detrimental for alite hydration [60], causing retardations in setting and strength evolution [34,106].

$$\text{Final } C_3A/SO_3 \text{ ratio} \quad = \quad \frac{C_3A_{cement}}{SO_4^{2-}{}_{cement} + SO_4^{2-}{}_{accelerator} - SO_4^{2-}{}_{consumed\ by\ accelerator}} \qquad \text{Equation 3.1}$$

Pastes were prepared under controlled conditions, at 20 °C and 50 % relative humidity. Reference pastes were obtained by pre-mixing water and superplasticizer and homogenizing the resulting solution with cement by means of a vortex external mixer during 60 s. In accelerated pastes, accelerators were added 1 h after cement and water had been homogenized. The resulting paste was vigorously hand-mixed for 15 s with a spatula (for future reference, all the pastes used in this chapter will be referred to as *'hand-mixed pastes'*). Samples were destined to the tests right after accelerator homogenization. During the period between the mixing of cement and water and accelerator addition, the paste was kept inside a calorimeter at 20 °C in order to avoid the influence of variations in temperature.

The procedure for accelerator mixing intends to reproduce the condition usually found in practice, since accelerator addition occurs almost 1 h after the mixing of the other components. Moreover, this also allows a clearer evaluation of the heat flow attributed to accelerator reaction in calorimetry tests. Otherwise, the heat flow from accelerator reaction would overlap with the initial heat released generated by the mixing of cement and water.

3.2.3. Test methods

Tests conducted with cement pastes and suspensions are shown in table 3.6. Their descriptions are presented subsequently. Liquid phase analysis, conductimetry, determination of pH, TGA and SEM were performed with mixes I_REF, I_AKF 0.61 7% and I_ALK 3%. Isothermal calorimetry was performed with a total of 12 different pastes (reference and accelerated pastes containing AKF 0.38 7%, AKF 0.42 11%, AKF 0.61 5%, AKF 0.61 7% and ALK 3% with CEM I and CEM II/A-L). *In situ* XRD was conducted with the same pastes as isothermal calorimetry, with the exception of II_REF.

Table 3.6 - Tests conducted with cement pastes and suspensions.

Test	Sample	Age / period of time
Liquid phase analysis	Solution extracted from cement suspension	Before accelerator addition and 15 min, 1, 3, 6 and 9 h after accelerator addition
Conductimetry	Suspension	Before accelerator addition, 15 min and every hour after accelerator addition (until 9 h)
Determination of pH	Suspension	Before accelerator addition, 15 min and every hour after accelerator addition (until 9 h)
In situ XRD	Fresh paste	0 - 48 h
Powder XRD	Ground hardened paste	7, 28 and 98 days
Isothermal calorimetry	Fresh paste	0 - 48 h
TGA	Freeze-dried and ground paste	15 min, 3, 12 and 48 h after accelerator addition
SEM	Freeze-dried paste	15 min, 3 and 12 h after accelerator addition

3.2.3.1. Liquid phase analysis

Liquid phase analysis was conducted to quantify the concentrations of Ca^{2+}, SO_4^{2-} and $[Al(OH)_4]^-$ ions in diluted cement suspensions (w/c equal to 9). The objective is to determine the influence of each accelerator on the ionic equilibria in the liquid phase, which may be associated with key changes in kinetics and mechanisms of hydration. This procedure is an adaptation of the method used in [41].

Tests were performed in solutions extracted from the cement suspension before accelerator addition (5 min after mixing cement and water) and 15 min, 1, 3, 6 and 9 h after accelerator addition. The concentrations of calcium and sulfate ions were determined by ion chromatography using a Dionex ICS-3000 chromatographer, while aluminum was quantified by atomic absorption spectrometry in an AnalytiK Jena ContrAA 700 spectrometer.

3.2.3.2. Conductimetry and pH

Conductivity and pH were employed to monitor the progress of the ionic concentration in cement suspensions. They were measured before accelerator addition and 15 min and every hour after accelerator addition (until 9 h of hydration). Conductivity was measured in a Crison

GLP 31 conductimeter and pH was determined in Crison Basic 20 pH-meter. These tests were performed to complement the liquid phase analysis.

3.2.3.3. *In situ* and powder XRD

In situ XRD was performed to obtain a time resolved determination of the phase composition of accelerated cement pastes during hydration. A PANalytical X'Pert PRO MPD θ/θ powder diffractometer in reflection Bragg-Brentano geometry, with Ni filtered $CuK\alpha_1$ radiation ($\lambda = 1.5418$ Å) and a PIXcel detector (active length of 3.347 °), operating at 45 kV and 40 mA, was used. Sample holders were cylindrical, with a diameter of 32 mm and a depth of 3 mm, containing approximately 3.7 g of paste. In order to avoid water evaporation and the contact of the paste with atmospheric CO_2, sample holders were covered with Kapton® film (thickness of 7.5 µm). During this test, the temperature of the sample was kept at 26 ºC and sample holders were spun at 2 revolutions per second.

X-ray patterns were obtained from 5 º2θ to 55 º2θ, using a step width of 0.026 º2θ and 20.9 s per step, with a fixed divergence slit of 0.5 °. Under these data acquisition conditions, it is possible to record a diagram in approximately 200 s. For each sample, the first diagram was obtained 5 min after accelerator addition and, then, every 15 min, for 48 h. X-ray patterns were analyzed quantitatively by Rietveld refinement using the software X'Pert High Score Plus and the structure models and the strategy for analysis presented in Appendix A. Amorphous content was determined by the internal standard method (described in detail in [107]) to provide an indirect assessment of the C-S-H amount present in the paste. Alumina powder (SRM 676a, from NIST) was employed as an internal standard reference material.

At the ages of 7, 28 and 98 days, the samples used for *in situ* XRD were crushed and ground to a maximum size of 63 µm. After that, a powder diagram was recorded using the same test configuration as *in situ* XRD and was analyzed by Rietveld refinement with the structure models presented in table A.1. Pastes were not lyophilized because the stability and crystallinity of ettringite and monosulfoaluminate could be compromised, leading to errors in their quantification [108].

Based on the calculated volumes of cement before hydration ($V_{cement, t = 0}$), water (V_w), accelerators solid content (V_a), unhydrated cement at time t ($V_{cement, t}$) and hydrates at time t ($V_{hydrates, t}$), the porosity at time t (P_t) can be calculated according to equation 3.2 [16,109]. In

these calculations, shrinkage and the porosity created by air voids or cracks are not considered. The change in volume is expressed entirely in terms of porosity.

$$P_t = \frac{V_{cement,\ t=0} + V_w + V_a - V_{cement,\ t} - V_{hydrates,\ t}}{V_{cement,\ t=0} + V_w + V_a} \qquad \text{Equation 3.2}$$

3.2.3.4. Isothermal calorimetry

Isothermal calorimetry was performed to determine how accelerators influence kinetics of cement hydration. Tests were executed at 20 °C during 48 h in a commercial I-cal 4000 isothermal calorimeter, using 15.0 g of cement paste. Heat flow curves were also obtained at 26 °C with cement pastes employed in *in situ* XRD.

3.2.3.5. TGA

Thermal analysis was performed in hydrated pastes to quantify the contents of portlandite and chemically bound water. Tests were executed from 30 to 1000 °C at a heating rate of 10 °C/min with N_2 flow of 50 mL/min employing a SDT Q-600 thermobalance. Cement pastes were analyzed at 15 min, 3, 12 and 48 h after accelerator addition. These ages correspond to points I, II, III and IV in figure 3.2 and represent the times after accelerator reaction, at the onset of the main hydration process, after the acceleration period and after the deceleration period, respectively.
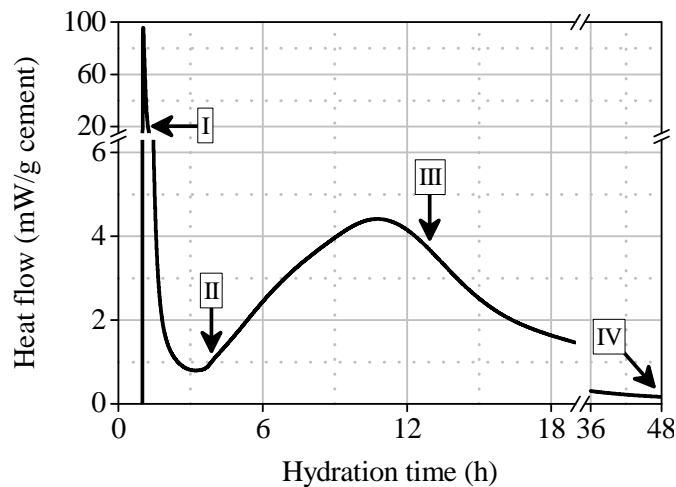
Figure 3.2 - Heat flow curve of an accelerated paste. Points I, II, III and IV represent the ages when hydration was stopped to prepare samples for TGA analyses.

Hydration was stopped by freezing the paste in liquid nitrogen for 15 min and drying in vacuum during 24 h. Then, they were crushed and ground to a maximum diameter of 63 µm using a manual agate mortar. In each analysis, approximately 25 mg of paste were tested in 90 µL alumina crucibles.

Portlandite was quantified by its dehydration, calculating the mass loss in the temperature range from 350 to 500 ℃. Chemically bound water was calculated from 40 to 1000 ℃, correcting the value obtained by the mass loss corresponding to the decarbonation of anhydrous cement, according to [110]. This temperature range was adopted because only the non-evaporable water remains in freeze-dried pastes [108].

3.2.3.6. SEM

Scanning electron microscopy was used to evaluate how accelerators influence the microstructure of cement pastes. Tests were executed in a JEOL JSM 7100F microscope at the voltage of 20 kV. Cement pastes were analyzed at 15 min, 3 and 12 h after accelerator addition and hydration was stopped by freeze-drying, similarly to TGA analyses. Samples were coated with carbon. Morphology of the precipitated hydrates was evaluated by secondary electron imaging of fracture surfaces and their chemical composition was assessed by energy dispersive X-ray analysis.

3.3. Results and discussion

3.3.1. Liquid phase analysis

The evolution of the concentration of Ca^{2+} and SO_4^{2-} ions during hydration in suspensions I_REF, I_AKF 0.61 7% and I_ALK 3% are represented in figures 3.3.a and 3.3.b, respectively. Initial calcium concentration (from 0 to 15 min of hydration) in the reference paste is the highest. During the period between 1 and 6 h, calcium concentration increases steadily, mainly due to gypsum and alite continuous dissolutions. From 6 h on, calcium is consumed due to the precipitation of hydrated phases.
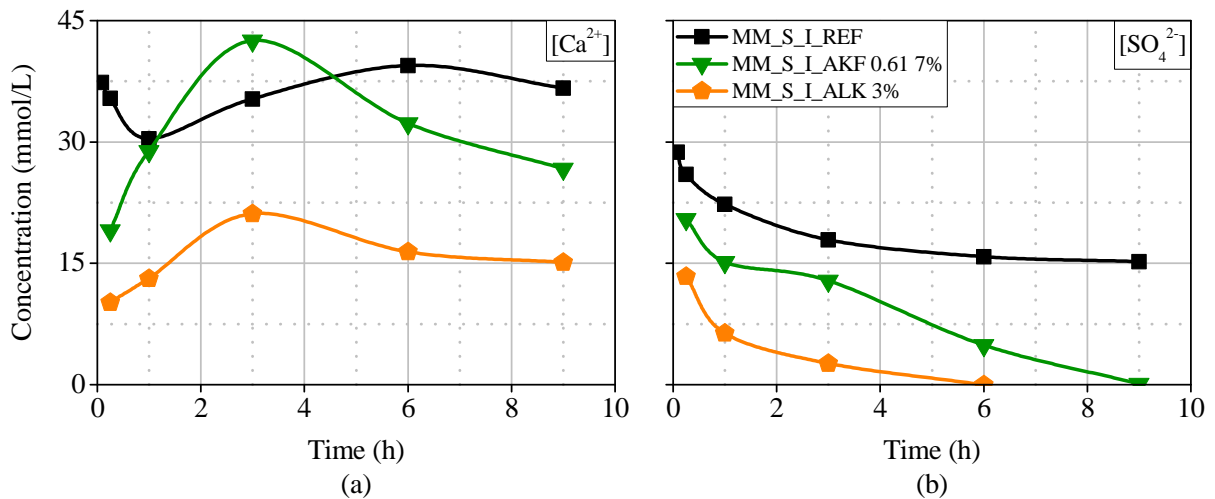
Figure 3.3 - Concentration of calcium (a) and sulfate (b) ions of solutions extracted from cement suspensions I_REF, I_AKF 0.61 7% and I_ALK 3%.

In accelerated suspensions, accelerators consume calcium ions from the liquid phase, resulting in lower Ca^{2+} concentrations than in the reference suspension at 15 min. From 15 min to 3 h, Ca^{2+} concentration increases steadily. Such effect is more pronounced in the suspension I_AKF 0.61 7% because this admixture contains 24 % more aluminum than ALK 3%. As a consequence, Ca^{2+} consumption is higher, favoring alite and gypsum dissolutions in order to balance the chemical equilibria in the liquid phase. The acid contained in AKF 0.61 also favors alite dissolution [19]. From 3 h on, calcium starts to be consumed due to the precipitation of calcium-containing hydrated phases.

Sulfate concentration in the suspension I_REF decreases throughout the whole experiment and is always higher than in accelerated suspensions. In the suspension I_ AKF 0.61 7%, sulfate concentration is lower than in I_REF at 15 min, indicating that a fast reaction occurs right after accelerator addition with the consequent consumption of sulfate ions. Sulfates contained in the alkali-free accelerator help balance gypsum dissolution and sulfates deplete between 6 and 9 h.

A similar trend is observed in suspension I_ALK 3%, although a higher rate of sulfate consumption is observed during the first minutes. As the accelerator ALK does not contain any sulfates, gypsum is the only sulfate source to control accelerator reaction for the formation of AFt and AFm phases. Sulfate depletion is the fastest and occurs between 3 and 6 h.

Aluminate ($[Al(OH)_4]^-$) concentrations in all the solutions were in the range between (0.020 ± 0.005) mmol/L, which corresponds to 0.10 and 0.13 % of the amount added by AKF

0.61 7% and ALK 3%, respectively. Such low concentrations indicate that all aluminate ions are rapidly consumed as soon as accelerators are added, consuming Ca^{2+} and SO_4^{2-} from the liquid phase, according to chemical equations 2.11 and 2.12, from table 2.5. In this context, aluminate ions act as the limiting reactant in the process.

3.3.2. Conductivity and pH

Conductivity and pH measurements during hydration in suspensions I_REF, I_AKF 0.61 7% and I_ALK 3% are represented in figure 3.4. Initial conductivity (at 5 min) is the result of a rapid formation of Ca^{2+}, Na^+, K^+, SO_4^{2-} and OH^- ions by the dissolution of alite, gypsum and soluble alkali sulfates. In the reference suspension, conductivity and pH increase constantly until 6 h as a result of the continuous dissolutions of gypsum and alite. At 6 h, conductivity starts to drop due to the precipitation of calcium-containing hydrated phases.
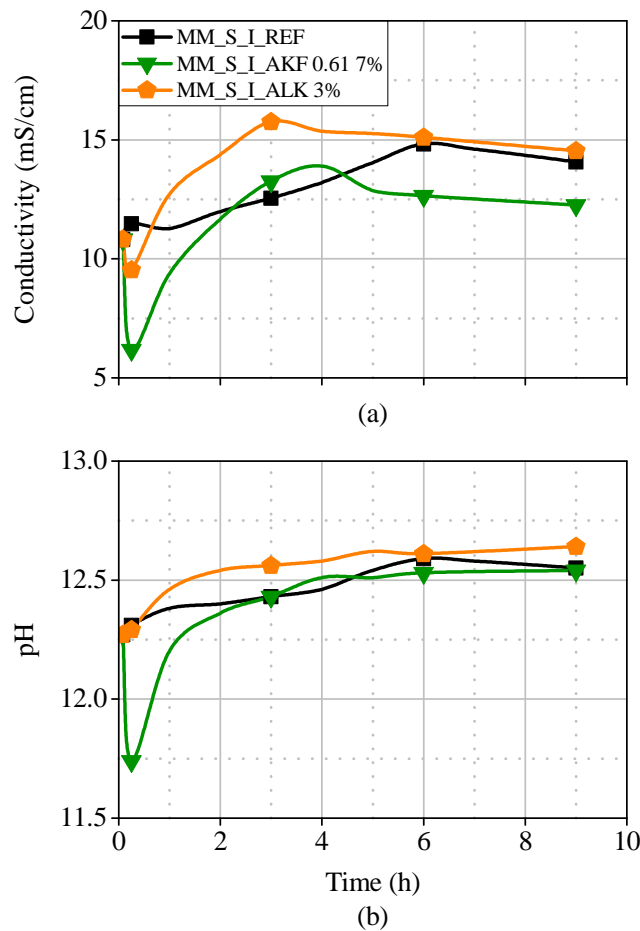
Figure 3.4 - Conductivity (a) and pH (b) of cement suspensions I_REF, I_AKF 0.61 7% and I_ALK 3%.

In the suspension I_AKF 0.61 7%, a sudden drop in conductivity occurs after accelerator addition due to the precipitation of insoluble compounds and the consequent decrease in the ionic content in solution. The initial decrease in conductivity is followed by a drop in pH caused by the acid contained in this accelerator. Hydroxide concentration also decreases to the conversion from Al^{3+} to $[Al(OH)_4]^-$, according to chemical equation 2.10, from table 2.5. From 15 min to 4 h, conductivity and pH increase continually due to the dissolution of cement compounds. Conductivity starts to drop after that as a result of the precipitation of hydrated phases.

The suspension I_ALK 3% presents a similar behavior. However, the drop in conductivity is less pronounced than in the suspension I_AKF 0.61 7% because the alkaline accelerator contains NaOH. This strong electrolyte increases the ionic concentration in the liquid phase and maintains an elevated pH during the whole test. The highest conductivity value is observed at 3 h. After that, conductivity starts to decrease again and may be associated calcium and sulfate consumptions in figure 3.3.

3.3.3. *In situ* and powder XRD

Firstly, results from *in situ* XRD and isothermal calorimetry of pastes I_REF, I_AKF 0.61 7% and I_ALK 3% from 0 to 48 h at 26 ºC are evaluated simultaneously. By doing so, the main chemical processes occurring during hydration may be associated with the heat flow signals in the calorimetric curves. After that, the evolution of phase composition of all accelerated pastes tested is characterized from the beginning of hydration until 98 days to evaluate the influence of different accelerator formulations on cement hydration.

3.3.3.1. *In situ* XRD associated with isothermal calorimetry

The quantitative evolution of phase composition of pastes I_REF, I_AKF 0.61 7% and I_ALK 3% and their associated heat flow curves obtained at 26 ºC are presented altogether in figure 3.5. In order to simplify the interpretation of the graphs, only the reacting phases (alite, C_3A, gypsum, portlandite, ettringite and AFm) are presented. Slow reacting phases (belite and ferrite) were not plotted. C-S-H has a low degree of crystallinity and can only be quantified indirectly by the content of amorphous phases.
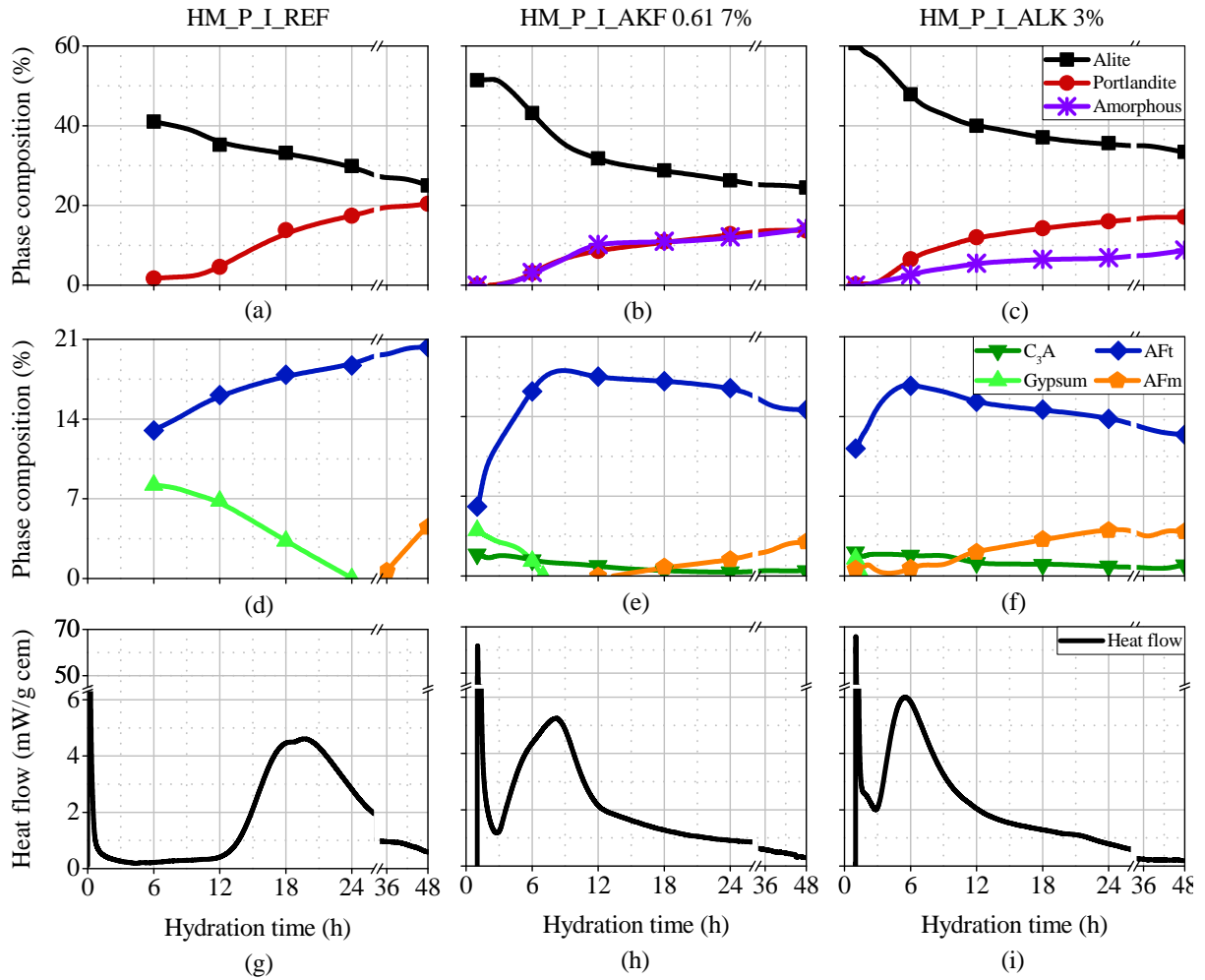
Figure 3.5 - Evolution of alite, portlandite and amorphous contents (a, b, c), C_3A, gypsum, ettringite and AFm phases (d, e, f) and heat flow curves (g, h, i) obtained with hand-mixed pastes I_REF (left), I_AKF 0.61 7% (medium) and I_ALK 3% (right) at 26 ºC.

Paste I_REF has an elevated content of free water in the period between water addition and 6 h of hydration. Therefore, this period was not considered in the analysis, given the uncertainties in the refinements. In addition, C_3A and amorphous contents could not be determined properly in this paste because the background adjustment was affected by a water layer generated between the surface of the paste and the Kapton® film. Due to these reasons, the refinements obtained with paste I_REF are semi-quantitative.

The main changes occurring in phase composition during hydration of pastes I_REF, I_AKF 0.61 7% and I_ALK 3% are summarized in table 3.7.

Table 3.7 - Main changes occurring in phase composition during hydration of hand-mixed pastes I_REF, I_AKF 0.61 7% and I_ALK 3%.

Period (h)	I_REF	I_AKF 0.61 7%	I_ALK 3%
0 - 1	Initial dissolution of alkali sulfates, gypsum and alite.	Initial dissolution of alkali sulfates, gypsum and alite.	Initial dissolution of alkali sulfates, gypsum and alite.
1 - 1.5	Induction period. Low activity during this stage due to the retarding effect of the superplasticizer.	Massive precipitation of ettringite due to accelerator reaction. This process corresponds to the sharp peak in the heat flow curve at 1 h (named accelerator peak hereinafter). Alite is partially dissolved by the acid contained in accelerator.	Massive precipitation of ettringite due to accelerator reaction (sharp exothermic signal in the heat flow curve at 1 h - accelerator peak). Monosulfoaluminate is also formed. Gypsum is detected in small amounts (< 1 %).
1.5 - 3	Induction period.	Short induction period.	Short induction period. Gypsum depletes. Formation of AFm phases continues (related to a bump in the heat flow curve between 1.5 - 3 h).
3 - 12	Induction period. Gypsum dissolves at a constant rate. Alite starts to be consumed at 10 h, with consequent formation of CH.	Gypsum depletes at around 4 h. C_3A hydration with sulfates forms ettringite continuously until 5 h. From 5 to 7 h, the rate of ettringite formation decreases because C_3A hydration is controlled by sulfates desorbed from C-S-H. This process coincides with a change in slope in the main peak at 5 h. Alite hydrates at a faster rate (38 % consumed until 12 h), forming CH and C-S-H.	Ettringite reaches its maximum content at 5 h and, then, starts to be consumed by C_3A, forming AFm phases. Alite hydrates at a faster rate, forming CH and C-S-H. At 12 h, 34 % of alite were consumed. As a consequence, C-S-H formation proceeds at a lower extent than in I_AKF 0.61 7%. CH precipitation is favored due to NaOH contained in accelerator.
12 - 30	Alite hydrates between 12 - 18 h. CH and ettringite precipitate during the acceleration period. Gypsum depletes at 20 h and secondary ettringite formation occurs by C_3A hydration with sulfates desorbed from C-S-H (related to a shoulder in the main peak at 20 h).	Alite continues to hydrate and CH is constantly formed, but at slower rates. At 24 h, 49 % of alite were consumed. C_3A hydration consumes ettringite, forming monosulfoaluminate. This process corresponds to a change in slope in the heat flow curve at 12 h.	The rates of alite consumption and CH formation decrease and are lower than in paste I_AKF 0.61 7%. At 24 h, 41 % of alite were consumed. Ettringite content starts to drop, with consequent formation of monosulfoaluminate (mainly from 20 h on, as observed by a bump in the heat flow curve).
30 - 48	Alite hydration rate is low and CH content is maintained approximately constant. Ettringite starts to be consumed by C_3A after 30 h, forming AFm phases.	Alite continues to hydrate, forming CH constantly. Ettringite continues to be consumed for the formation of monosulfoaluminate.	Alite hydrates constantly at low rates, forming CH and C-S-H. Ettringite is consumed and AFm phases continue to be formed.

Regarding the accelerated pastes, the rapid increase in ettringite content from 1 to 5 h does not occur only due to C_3A hydration during this period (C_3A consumption is low and is not in agreement with the high ettringite contents formed). A possible explanation to this fact is that ettringite is formed too rapidly due to the incorporation of dissolved Al^{3+} ions in the paste. This suggests that some amorphous alumina containing phase may form first and ettringite progressively crystallizes from this phase prior to the renewed C_3A hydration. This process increases the intensity of X-ray diffracted beams, leading to the quantification of larger amounts of this phase. A similar behavior was reported by [111], which describes a gel-like structure in ettringite precipitated at very early ages.

Based on the results obtained in this section and on previous researches regarding accelerated hydration [4,5,10,20], the chemical processes occurring during hydration were associated with the heat flow curves. Figure 3.6 identifies 5 general hydration stages, whose main chemical processes are described subsequently (different chemical processes may occur depending on the composition of cements and accelerators). Their description will be used to interpret further analyses by isothermal calorimetry.
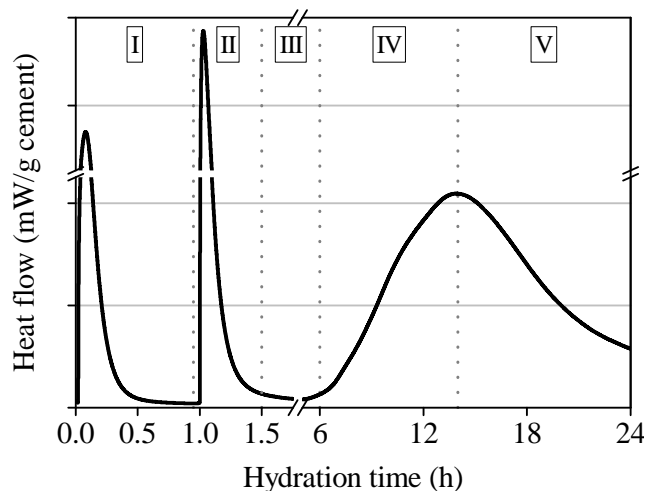
Figure 3.6 - Designation of 5 stages during hydration of an accelerated cement paste (Y-axis does not correspond to a real scale).

Stage I - pre-induction period

Dissolution of alkali sulfates, gypsum, alite and aluminate phases and initial ettringite formation, with consequent large heat release.

Stage II - accelerator reaction

$[Al(OH)_4]^-$ ions from accelerator consume Ca^{2+} and SO_4^{2-} ions from the liquid phase to form ettringite (chemical equation 2.11), which precipitates massively, releases heat and stiffens the paste. This process is named accelerator peak in the text. Depending on accelerator reactivity, initial and final setting may occur. Alite may be partially dissolved if accelerator is acidic.

Stage III - induction period

Period of low reaction rates with low heat evolution. Alite and gypsum dissolve to balance the concentration of Ca^{2+} in the chemical equilibria, previously disturbed by accelerators. Gypsum may deplete, depending on the amount of sulfate consumed by accelerator, and undersulfated C_3A reactions may occur. If they happen, a large heat release is observed during the induction period.

Stage IV - acceleration period

The rate of alite hydration increases, with consequent formation of CH and C-S-H. C_3A hydration continues (forming either ettringite, if sulfates are present, or monosulfoaluminate, in the absence of dissolved sulfates).

Stage V - deceleration period

The rate of alite hydration decreases and C_3A hydration consumes ettringite, forming monosulfoaluminate.

3.3.3.2. Evolution of phase composition of accelerated pastes

Figure 3.7 presents the evolution of phase composition in accelerated cement pastes measured by *in situ* and powder XRD. Only the reacting phases (alite, portlandite and ettringite) are shown in order to simplify the interpretation of the graphs. Figure 3.8 shows the evolution

of amorphous phases and porosity. Results obtained with CEM I pastes are grouped on the left and with CEM II/A-L pastes are grouped on the right.
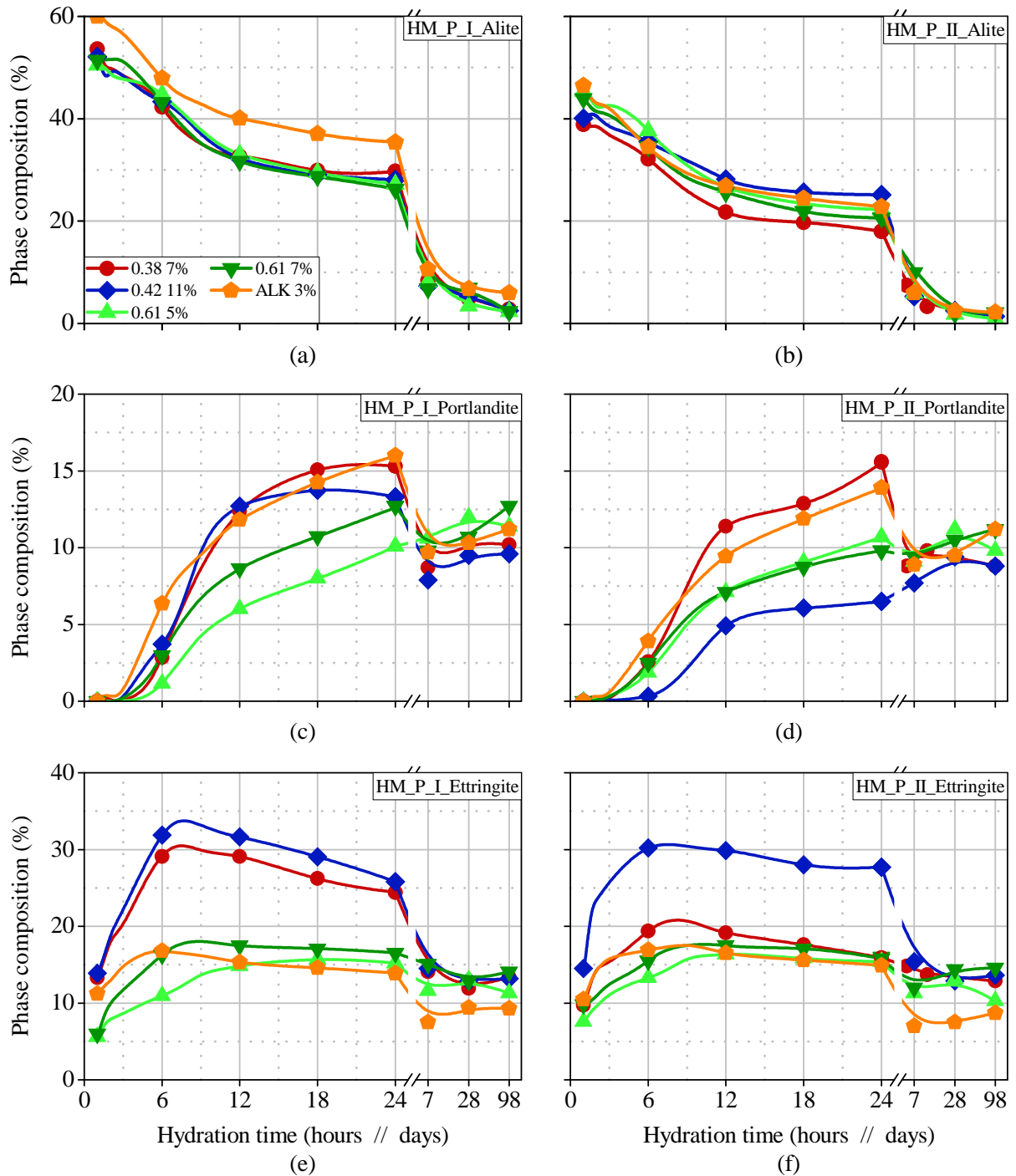
Figure 3.7 - Evolution of the contents of alite (a and b), portlandite (c and d) and ettringite (e and f) in CEM I and CEM II/A-L hand-mixed pastes from accelerator addition until 98 days.
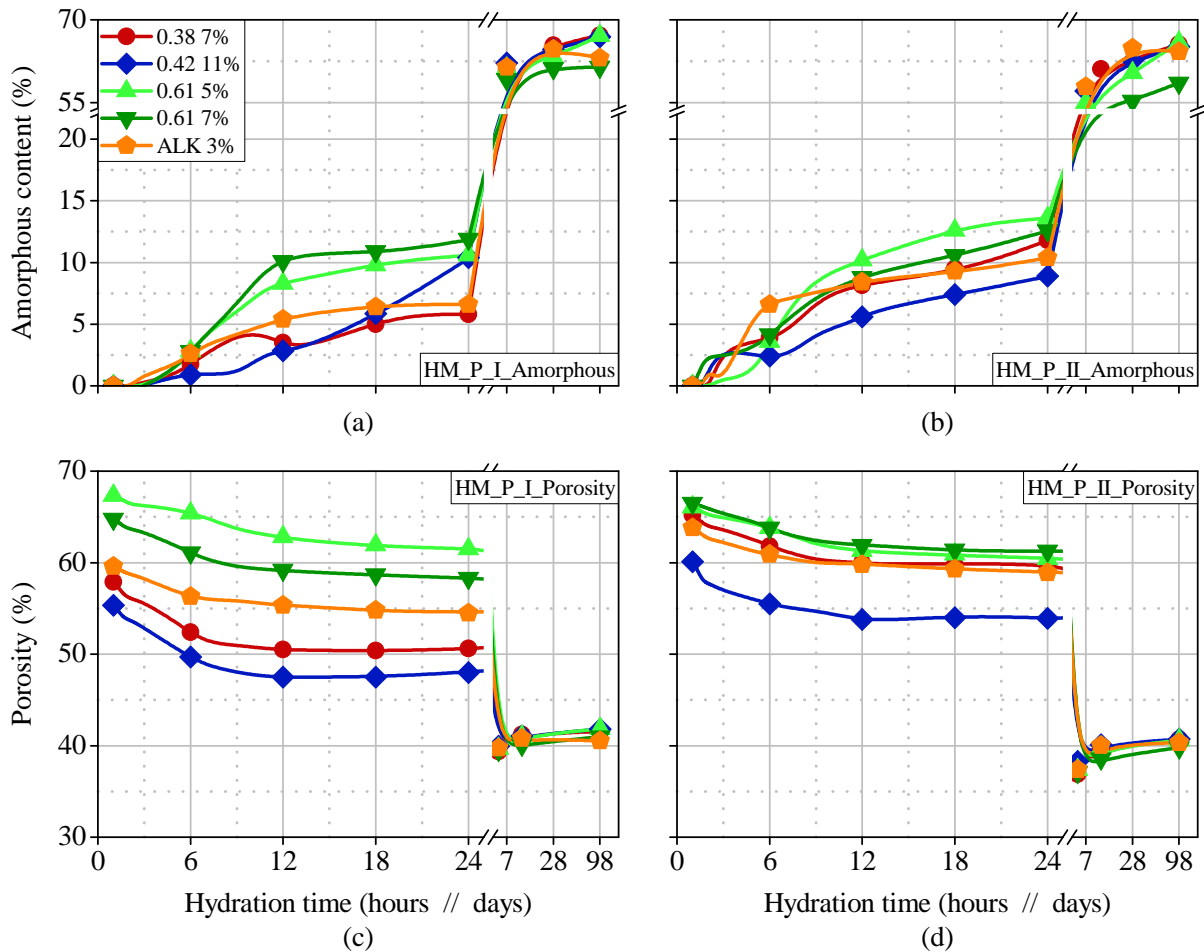
Figure 3.8 - Evolution of amorphous phases (a and b) and porosity (c and d) in CEM I and CEM II/A-L hand-mixed pastes from accelerator addition until 98 days.

All pastes present a significant precipitation of ettringite due to accelerator reaction (initial value in the graphs from figures 3.7.e and 3.7.f). Ettringite formation increases the solid/liquid ratio of the matrix [84], leads to reduction in porosities (figures 3.8.a and 3.8.b) and interconnects the solid phase. The amount of ettringite formed follows the ascending order of the Al^{3+} content in accelerators (AKF 0.61 5% < AKF 0.61 7% < AKF 0.38 7% < AKF 0.42 11%). Therefore, shorter setting times and faster rates of early strength development may be obtained with accelerators containing larger Al^{3+} amounts.

Ettringite is formed continuously until 7 h of hydration, approximately, due to C_3A hydration in presence of sulfates. The crystallization of ettringite during this period also contribute to increase its amount quantified by XRD. Ettringite contents in I_AKF 0.38 7% were larger than expected, as this accelerator contains an average Al^{3+} concentration, between AKF 0.61 5% and AKF 0.61 7%. This occurs due to the high sulfate concentration in AKF 0.38, which displaces the chemical equilibria into the formation of ettringite.

Alite is slowly consumed until approximately 3 h in all pastes to balance the concentration of Ca^{2+} in the liquid phase, initially disturbed by accelerators. From 3 h on, the rate of alite hydration increases, with consequent formation of portlandite and amorphous phases. The rate of alite consumption in the main hydration process in CEM I pastes is inversely proportional to the final C_3A/SO_3 ratio of the paste shown in table 3.5 (AKF 0.38 7% > AKF 0.42 11% > AKF 0.61 7% > AKF 0.61 5%). Reductions in porosity follow the same order as alite consumption, because the precipitation of portlandite and C-S-H fill up the pores of the matrix.

Pastes containing AKF 0.38 7% and AKF 0.42 11% are properly sulfated, because the amount of sulfate remaining after accelerator reaction postpones C_3A hydration, which occurs after the acceleration period of silicate hydration. Therefore, aluminate hydrates formed have little influence on alite hydration, which occurs at faster rates. On the contrary, as accelerator AKF 0.61 provides the lowest sulfate content to the matrices, the paste becomes undersulfated. Hence, C_3A hydration is accelerated and the matrix is filled with aluminate hydrated products before the onset of the main hydration peak. Consequently, the rate and extent of alite hydration is reduced [41,42].

Although paste II_AKF 0.42 11% is properly sulfated, the rate and extent of alite hydration and portlandite precipitation are lower than in other matrices. This occurs because CEM II/A-L contains around 23 % less C_3A than CEM I and limestone filler also controls C_3A hydration [65,66], resulting in a lower consumption of ettringite to form monosulfoaluminate. Therefore, the large amount of ettringite produced (above 30 % by mass) is maintained approximately constant until 12 h of hydration, filling up the space available and inhibiting silicate hydration.

The initial amount of ettringite precipitated in pastes containing the alkaline accelerator is higher than in pastes produced with AKF 0.61 5% and lower than in the other pastes. This is directly related to aluminum concentration in accelerator ALK (table 3.4). Besides, the rate of ettringite formation until 6 h in pastes I_ALK 3% and II_ALK 3% is the lowest because gypsum present in cement is the only sulfate source for the reaction to occur. Therefore, accelerator reactivity is limited by gypsum dissolution and AFm phases are formed at the moment accelerator ALK is added [10]. The maximum ettringite content is reached at 5 and 9 h in pastes I_ALK 3% and II_ALK 3%, respectively. As paste II_ALK 3% has a lower final C_3A/SO_3 ratio than the equivalent CEM I paste and contains limestone filler, C_3A hydration is postponed and ettringite consumption is retarded.

Initial alite dissolution in alkaline accelerated pastes is favored because this accelerator contains NaOH, which leads to a faster portlandite precipitation [112]. However, the high final C_3A/SO_3 ratio of these matrices promotes an undersulfated accelerated C_3A hydration that takes place before or during the silicate acceleration period, with the consequent formation of AFm phases. This process delays alite hydration from 10 h on due to the space filling caused by the early formation of aluminate hydrates and to the precipitation of these phases on the surface of alite, reducing its solubility. At 98 days, pastes I_ALK 3% and II_ALK 3% contain the highest alite content, indicating the decrease in the extension of silicate hydration.

The observations derived from *in situ* and powder XRD suggest a competition between silicate and aluminate hydrations. C_3A hydration is significantly affected by the addition of accelerators, especially by the ones containing high Al^{3+} concentrations. The large amount of aluminate hydrates formed by accelerator reaction and accelerated undersulfated C_3A reactions inhibit alite hydration, lowering its extent and intensity.

3.3.4. Isothermal calorimetry

Heat flow curves of all cement pastes analyzed are shown in figure 3.9. Results obtained with CEM I pastes are presented on the left, whereas results from CEM II/A-L pastes are on the right. Figures 3.9.a and 3.9.b represent the curve from 0 to 24 h, while figures 3.9.c and 3.9.d show a zoom of the heat flow curve from 1.0 to 1.5 h. The second period covers the heat flow peak generated by accelerator reaction (accelerator peak).
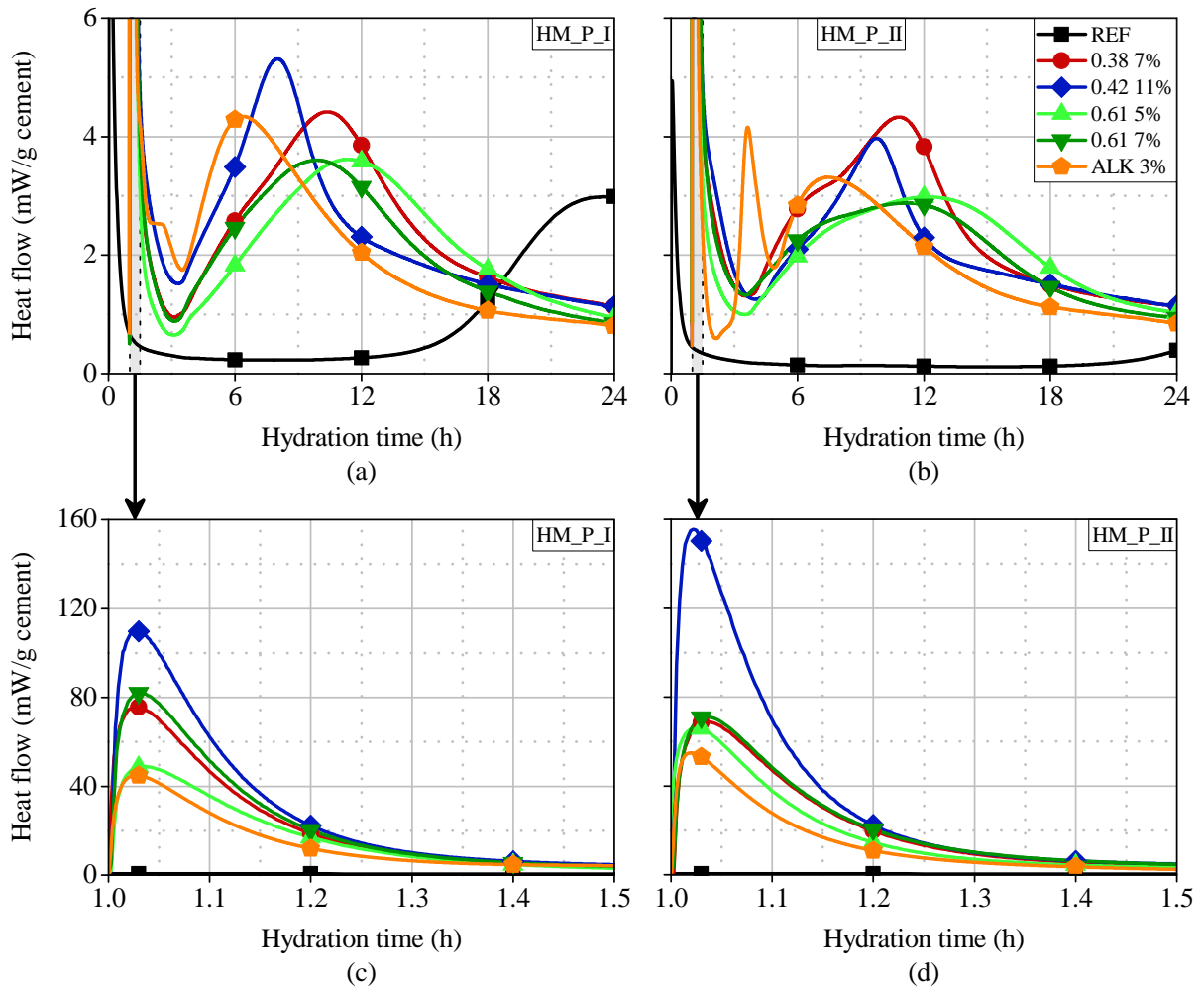
Figure 3.9 - Heat flow curves obtained with CEM I and CEM II/A-L hand-mixed pastes from 0 to 24 h (a and b) and from 1.0 to 1.5 h (c and d).

To analyze the influence of different mix composition on hydration, the parameters described in table 3.8 were used to analyze heat of hydration curves. Results obtained by their calculation are summarized in table 3.9 and the conclusions derived from this analysis are presented subsequently.

Table 3.8 - Parameters employed to analyze the hydration behavior of different mixes.

Process	Parameter	Method for calculation
Accelerator reactivity	Accelerator reaction rate	Slope of the ascending part of the accelerator peak
	Energy released in accelerator reaction	Area under the accelerator peak from 1 to 1.5 h
	Maximum heat flow in accelerator peak	Directly taken from heat flow curve
Cement hydration	Length of induction period	Period between 1.5 h (end of the accelerator peak) and the onset of the main hydration peak
	Cement hydration rate	Slope of the ascending part of the acceleration period
	Energy released during the main hydration peak	Area under the curve between the end of the induction period and the time when the heat flow reaches 1.0 mW/g cement in the deceleration period
	Maximum heat flow from main hydration peak	Directly taken from heat flow curve
	Energy released until 24 h	Total energy released until 24 h minus the energy released by accelerator reaction

Table 3.9 - Analysis of the heat flow curves obtained with hand-mixed pastes.

Paste	Slope - accel. peak (mW/g.h)	Energy released - accel. peak[a] (J/g)	Maximum heat flow - accel. peak (mW/g)	Induction period (h)	Slope acceleration - main peak (mW/g.h)	Energy released - main peak (J/g)	Maximum heat flow - main peak (mW/g)	Energy released until 24 h (J/g)
I_REF	-	-	-	15.8	0.42	164.8	3.08	74.8
I_AKF 0.38 7%	2421	29.76	75.8	1.98	0.63	187.6	4.42	202.9
I_AKF 0.42 11%	3495	42.72	110.0	2.01	0.77	184.6	5.31	210.8
I_AKF 0.61 5%	1044	19.61	48.9	1.85	0.44	159.6	3.62	182.4
I_AKF 0.61 7%	2231	32.79	82.0	1.81	0.58	147.8	3.60	178.1
I_ALK 3%	1187	14.25	45.0	2.17	1.34	133.3	4.34	174.8
II_REF	-	-	-	23.0	0.17	138.1	1.63	14.1
II_AKF 0.38 7%	1542	28.70	68.9	2.44	0.75	183.3	4.33	200.6
II_AKF 0.42 11%	6677	53.29	155.6	2.84	0.58	186.2	3.97	197.6
II_AKF 0.61 5%	2129	23.03	66.2	2.21	0.42	154.5	2.98	177.1
II_AKF 0.61 7%	1554	30.38	71.0	2.17	0.40	140.0	2.88	173.9
II_ALK 3%	2207	14.50	54.9	2.41	1.20	135.3	3.31	161.2

[a] The energy corresponding to the accelerator peak was corrected using the variation of heat generated by the removal of the sample from the calorimeter for accelerator addition.

The heat flow in the accelerator peak is a consequence of ettringite formation. The main hydration peak is a result of alite and C_3A hydrations, with consequent formation of portlandite, C-S-H, ettringite and AFm phases. As CEM I contains 58.3 % of alite and 4.7 % of C_3A, while these compounds are present in 51.7 % and 3.6 % in CEM II/A-L (table 3.1), shorter induction periods and higher intensities in the main hydration peak are observed in CEM I pastes. These parameters are also influenced by cement fineness (CEM I is finer than CEM II/A-L, table 3.3).

Hydration behavior with both cement types depends on accelerator type and dosage. The rate of reaction, the energy released and the maximum heat flow calculated from the accelerator peak in alkali-free accelerated pastes are directly proportional to the Al^{3+} content in accelerators (AKF 0.42 11% > AKF 0.61 7% > AKF 0.38 7% > AKF 0.61 5%). The higher the Al^{3+} content incorporated in the matrix, the larger the amount of sulfoaluminate hydrates formed and, therefore, the higher is the exothermal signal generated by accelerator reaction. Pastes I_AKF 0.42 11% and II_AKF 0.42 11% present the highest values of these variables, whereas the lowest values are found in pastes I_AKF 0.61 5% and II_AKF 0.61 5%.

All accelerated pastes present shorter induction periods than the respective reference pastes and this reduction is a function of accelerator dosage, as expected. The consumption of calcium and sulfate ions from the liquid phase caused by the accelerators favors alite and gypsum dissolution in order to balance the ionic concentration in the chemical equilibria. Then, silicate ion concentration also increases, leading to an enhancement in nucleation and growth of hydrates and accelerating the onset of the main hydration peak. It is important to note that pastes I_REF and II_REF have a retarding effect of the superplasticizer, which increases induction periods and broadens the main hydration peak.

Reaction rate in the main hydration peak follows the inverse order of the final C_3A/SO_3 ratio of the paste (table 3.5). Since accelerators AKF 0.38 and AKF 0.42 contain Al_2O_3/SO_4^{2-} molar ratios similar to that of ettringite, the larger amounts of sulfate left decrease the rate of gypsum dissolution and retard further C_3A hydration. Pastes I_AKF 0.38 7% and I_AKF 0.42 11% present the highest rate and maximum heat flow in the main hydration peak (table 3.9) and the highest degrees of hydration at 24 h, as illustrated in figure 3.10. The energy associated with the main hydration peak in these pastes is higher than in the reference pastes, indicating that cement hydration is not negatively affected by accelerator reaction.
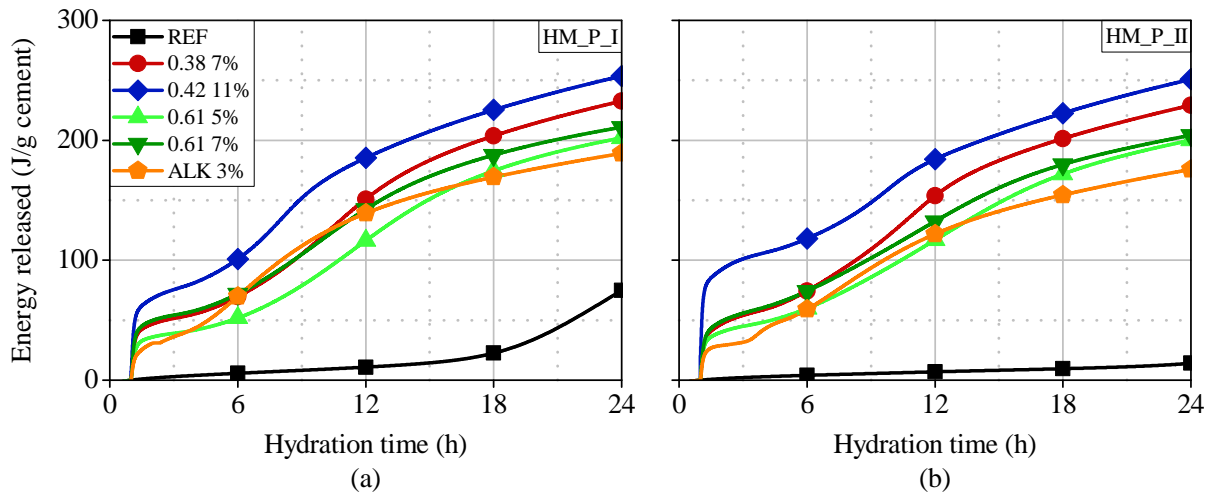
Figure 3.10 - Energy release curves obtained with CEM I (a) and CEM II/A-L (b) hand-mixed pastes from accelerator addition to 24 h.

Pastes containing AKF 0.38 7% and AKF 0.42 11% behave as properly sulfated and the main hydration peak in these systems is separated in two exothermal events. The onset of the main hydration process occurs with the beginning of alite hydration. Then, a shoulder representing C_3A hydration with sulfates desorbed from C-S-H surface [113] is observed. The changes in slope occur approximately at 6.2, 7.4, 7.5 and 8.1 h in pastes I_AKF 0.42 11%, I_AKF 0.38 7%, II_AKF 0.42 11% and II_AKF 0.38 7%, respectively. The retardation caused in the secondary ettringite formation is inversely proportional to the final C_3A/SO_3 ratio of each paste.

On the contrary, pastes produced with AKF 0.61 5% and AKF 0.61 7% present higher final C_3A/SO_3 ratios than pastes containing AKF 0.38 7% and AKF 0.42 11%. Consequently, C_3A hydration is accelerated and the early formed AFm phases fill up the space in the matrix quickly, suppressing alite hydration. This is observed by the lower values of slope, energy released and maximum heat flow in the main hydration peak obtained in pastes produced with AKF 0.61 5% and AKF 0.61 7% with both types of cement. This process is more aggravated by the use of higher dosages of this accelerator, since more dissolved aluminum is added to the matrix.

With respect to the alkaline accelerator, the rate of ettringite formation is the lowest, due to the limited sulfate content in these pastes. Considering that the alkaline accelerator consumes approximately 50 % of the sulfate available in the paste and part of the sulfates left are adsorbed onto C-S-H surface, further C_3A hydration proceeds as in undersulfated systems (high C_3A/SO_3 ratio in table 3.5). In the heat flow curves, a separation of the main hydration peak in two

thermal events occurs. It can be observed by a bump around 2.5 h in paste I_ALK 3% in figure 3.9.a and by a sharp peak occurring around 3.6 h in paste II_ALK 3% in figure 3.9.b, due to the formation of AFm phases. Monosulfoaluminate is preferentially formed when limestone is not present [41,54], while hemicarboaluminate and monocarboaluminate are formed when cements contain additions of limestone filler [45].

Furthermore, degrees of hydration at 24 h in alkaline accelerated pastes are the lowest among all the samples analyzed (figure 3.10). This occurs due to the high final C_3A/SO_3 ratio of these pastes and consequent decrease in the extension of silicate hydration from 10 h on, as described in section 3.3.3. These processes may result in lower mechanical strengths at later ages.

3.3.5. TGA

Results corresponding to the quantification of portlandite and chemically bound water by TGA in pastes I_REF, I_AKF 0.61 7% and I_ALK 3% are shown in table 3.10.

Table 3.10 - Portlandite and chemically bound water quantified by thermogravimetry in hand-mixed pastes I_REF, I_AKF 0.61 7% and I_ALK 3%.

Compound	Age	I_REF	I_AKF 0.61 7%	I_ALK 3%
Portlandite (%)	15 min	1.79	2.41	1.93
	3 h	1.89	3.00	3.14
	12 h	2.64	10.79	14.00
	48 h	17.70	17.37	18.00
Chemically bound water (%)	15 min	2.17	3.82	3.39
	3 h	2.08	4.69	4.43
	12 h	2.54	10.18	10.83
	48 h	14.76	17.79	14.73

A clear influence of accelerators on hydration is observed. Both accelerated pastes contain more portlandite and chemically bound water than the reference paste until 12 h of hydration. As the superplasticizer retards hydration in paste I_REF, that difference at the earliest ages is expected. However, as hydration proceeds, portlandite and chemically bound

water contents in the reference paste tend to overcome the amount contained in accelerated pastes. Since the formation of aluminate hydrates in paste I_REF is not accelerated, enough space remains for alite hydration to proceed normally and a higher degree of hydration may be achieved.

Analyzing the influence of accelerator type, portlandite contents in paste I_ALK 3% are higher than in I_AKF 0.61 7%. As ALK contains NaOH, it increases the concentration of OH⁻ ions in the liquid phase, which leads to portlandite precipitation [112]. An exception is the portlandite amount at 15 min, which is larger in I_AKF 0.61 7%. Since AKF 0.61 contains formic acid, it favors initial alite dissolution with consequent portlandite formation [19].

Chemically bound water contents in accelerated pastes depend on the hydration period. At 15 min and 3 h, paste I_AKF 0.61 7% contains more chemically bound water than I_ALK 3% because ettringite amounts are larger when alkali-free accelerators are employed (figure 3.7). As paste I_ALK 3% presents a faster hydration until 12 h (figure 3.9), it contains more chemically bound water than I_AKF 0.61 7%. At 48 h, the opposite behavior is observed, since the degree of hydration in paste I_AKF 0.61 7% is higher than in I_ALK 3% (figure 3.10). These data corroborate the results obtained in *in situ* XRD and isothermal calorimetry.

3.3.6. SEM and EDS microanalysis

SEM images obtained with hand-mixed pastes I_REF, I_AKF 0.61 7% and I_ALK 3% are presented in figures 3.11, 3.12 and 3.13, respectively. All the figures contain two images of each paste freeze-dried at 15 min, 3 and 12 h of hydration. Regions analyzed by EDS are indicated by a number in the corresponding image. Results obtained in the EDS spectra are represented as the relative intensities of each element, placed above each image. The peaks considered to measure the intensity of Ca, Si, Al, S and Na are correspondent to the energies of 3.73, 1.78, 1.52, 2.33 and 1.1 keV, respectively.
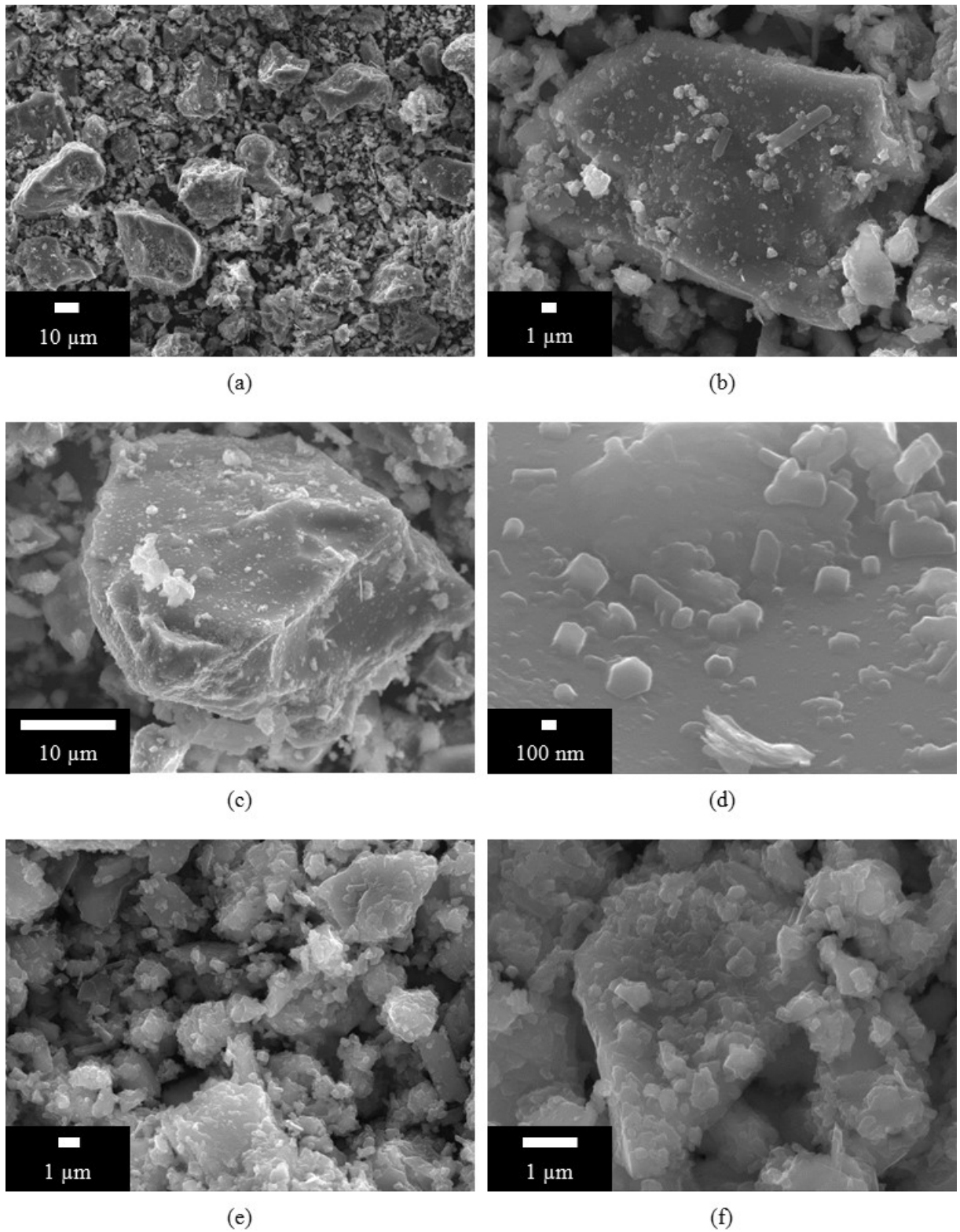
Figure 3.11 - SEM images of paste HM_I_REF at 15 min (a and b), 3 h (c and d) and 12 h (e and f).

[1] $Ca:Si:Al:S:Na = 100:22.7:8.5:17.8:1.4$ [2] $Ca:Si:Al:S:Na = 100:30.5:27.6:41.4:3.9$

(a)

(b)

[3] $Ca:Si:Al:S:Na = 100:36.5:16.3:24.3:3.2$

(c)

(d)

(e)

(f)
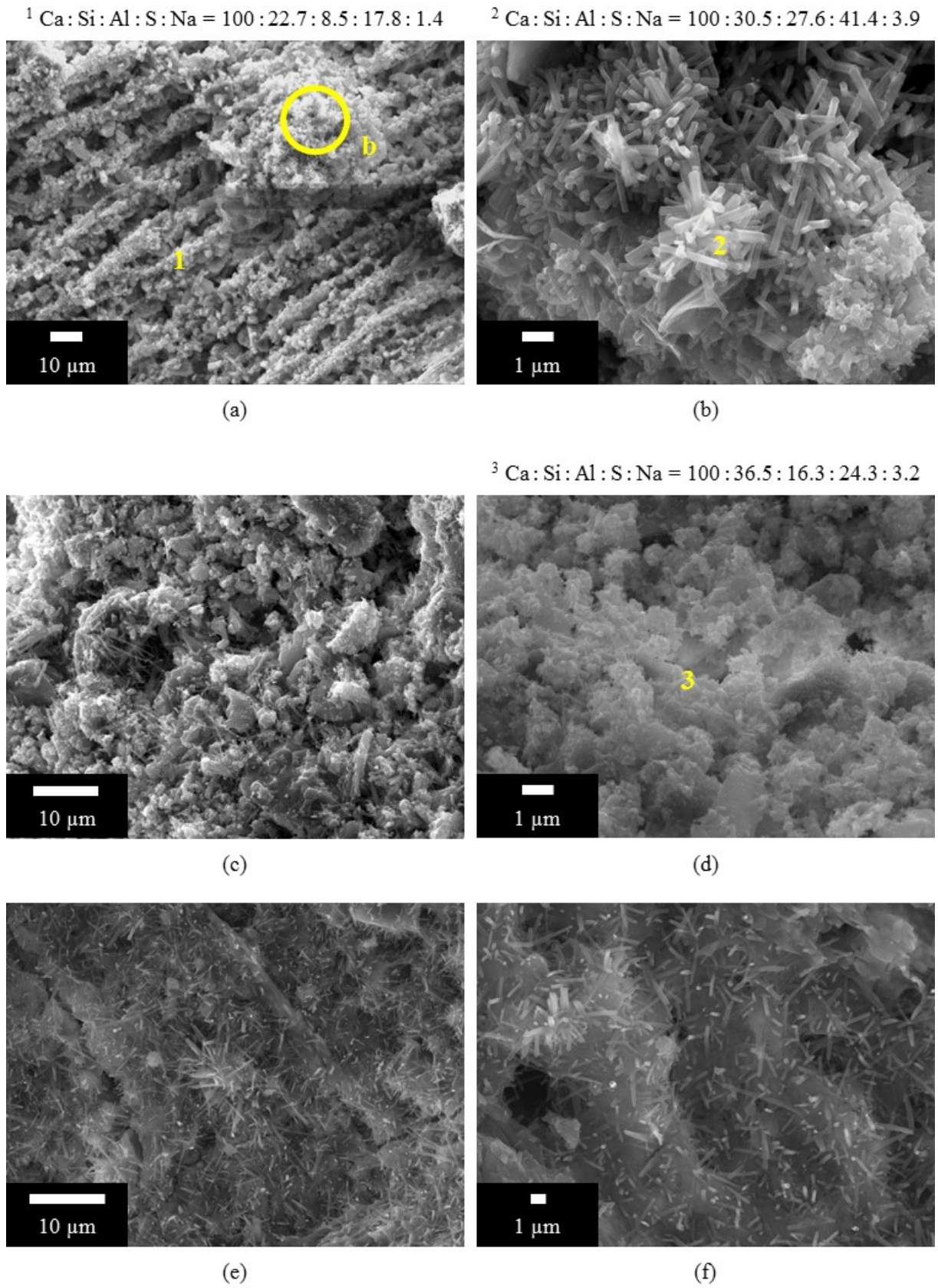
Figure 3.12 - SEM images of paste HM_I_AKF 0.61 7% at 15 min (a and b), 3 h (c and d) and 12 h (e and f).

[1] Ca : Si : Al : S : Na = 100 : 16.8 : 62.1 : 9.3 : 3.5

[2] Ca : Si : Al : S : Na = 100 : 16.5 : 14.8 : 6.6 : 4.5

(a)

(b)

[3] Ca : Si : Al : S : Na = 100 : 14.2 : 6.7 : 4.4 : 4.4

[4] Ca : Si : Al : S : Na = 100 : 38.8 : 16.0 : 14.5 : 4.5
[5] Ca : Si : Al : S : Na = 100 : 43.7 : 25.3 : 12.6 : 6.6

(a)

(b)

(e)

(f)
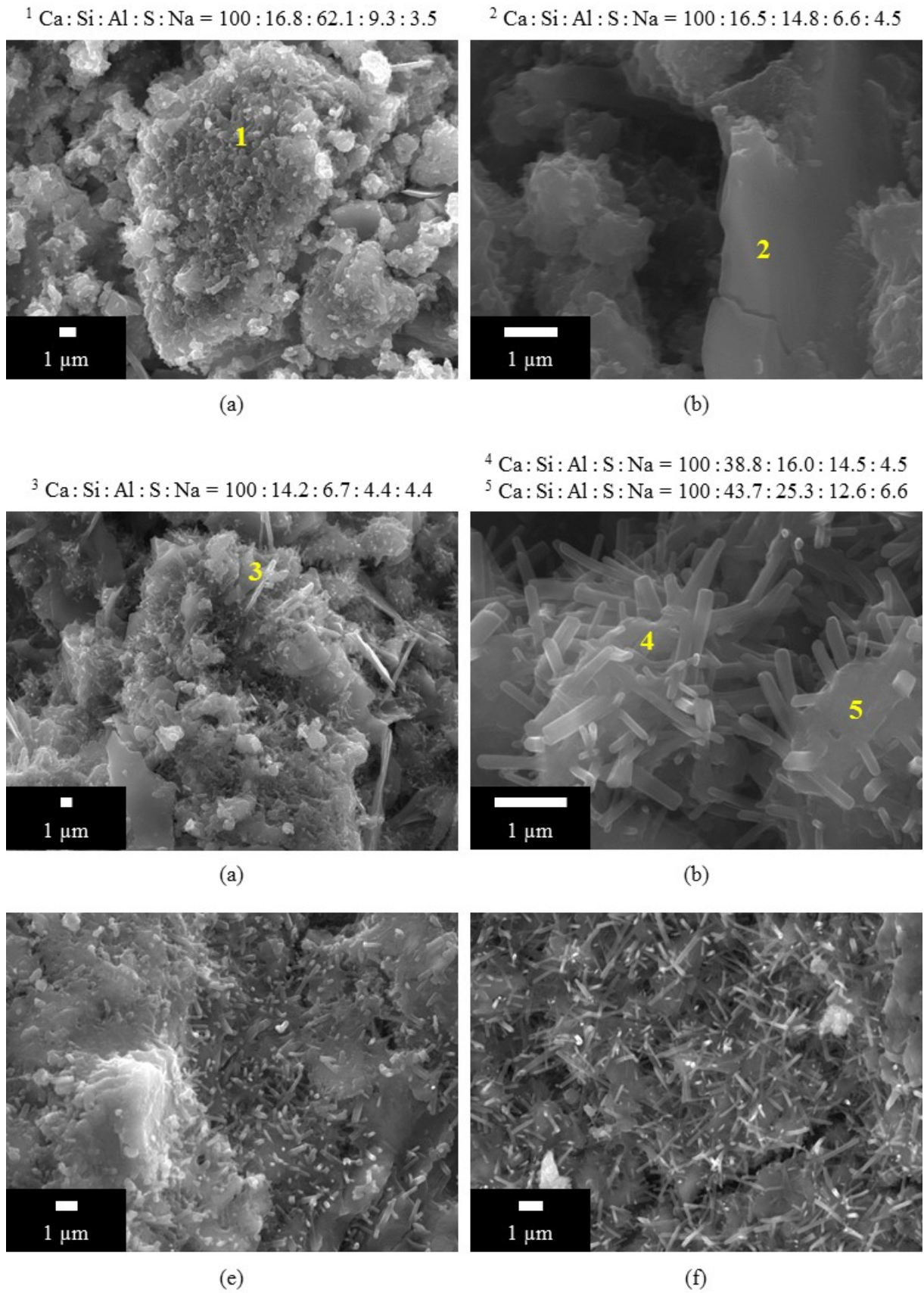
Figure 3.13 - SEM images of paste HM_I_ALK 3% at 15 min (a and b), 3 h (c and d) and 12 h (e and f).

In paste I_REF at 15 min, cement grains are completely apart and no connection among them is observed (figures 3.11.a and 3.11.b). A few deposits of hydrated phases on the surface of a cement particle may be seen. At 3 h, the borders of a cement grain start to present pitches caused by the dissolution of alite and a higher density of hydration products is observed (figures 3.11.c and 3.11.d). Microstructure has not developed considerably until 12 h, but a larger area of cement particles are covered by hydration products (figures 3.11.e and 3.11.f).

Paste I_AKF 0.61 7% at 15 min presents a significant microstructure development (figure 3.12.a). Extensive alite dissolution and surface pitching are observed, as indicated by the regular and step nature of the matrix, which may be compared to results presented in [46]. The tridimensional pore structure and connections formed are similar to the ones observed by [114]. In this paste, alite dissolution is favored by the acid contained in AKF 0.61, enriching the solution close to the grains with calcium and silicate ions. Therefore, hydrates preferentially precipitate in those regions, due to their elevated calcium concentration. As indicated by the EDS results, the region analyzed is composed mainly by C-S-H (Si/Ca equal to 0.227 and Al/Ca equal to 0.085). Sulfoaluminate hydrates (Al/S ratio equal to 0.48) are also present.

Figure 3.12.b represents a magnification of the region indicated by 'b' in figures 3.12.a. The precipitation of a large amount of ettringite crystals measuring approximately 2 µm in length on the region with extensive alite dissolution is observed. This hydrate nucleates and precipitates as hexagonal needle-like crystals with flat terminations in an ordered structure. The Al/S ratio found in that zone is equal to 0.667, which is the exact value found in pure ettringite. These crystals bond cement grains together and are responsible for the reduction of setting times and the increase in early age strength of the matrix (as observed in [84]).

At 3 h of hydration, microstructure is denser and a larger area is covered by hydration products (figure 3.12.c). The space surrounding cement grains is filled by ettringite crystals. Figure 3.12.d and the corresponding EDS results indicate that C-S-H (Si/Ca equal to 0.365) and ettringite (Al/S equal to 0.67) are the main hydrates formed. AFm phases were not found in this paste at 3 h, which is in agreement with the fact that gypsum depletion does not occur until 3 h in this paste. Then, further C_3A hydration occurs in the presence of enough sulfate to form ettringite.

At 12 h, paste I_AKF 0.61 7% presents a large amount of ettringite crystals (figures 3.12.e and 3.12.f). This hydrate is distributed throughout the whole matrix, although crystals

are not uniformly dispersed. Some ettringite needles tend to nucleate and grow at specific regions in the matrix. AFm phases could not be observed in this paste at 12 h either.

Paste I_ALK 3% at 15 min contains a large amount of hydrated phases precipitated on the surface of a cement particle (figure 3.13.a). According to the EDS results, hydrates present Al/Ca, Si/Ca and Al/S ratios equal to 0.62, 0.168 and 6.7, respectively, indicating they might be composed by hydroxy and sulfated AFm phases, with low content of C-S-H. They are formed by the fast reaction of $[Al(OH)_4]^-$ ions from the accelerator with Ca^{2+} ions from the liquid phase, as well as by C_3A hydration in a medium with limited sulfate content. This corroborates the results obtained by liquid phase analysis and *in situ* XRD, which show a fast sulfate depletion when the alkaline accelerator is employed (figures 3.3 and 3.5).

Figure 3.13.b shows a hydrated phase in the form of a plate, presenting an Al/S ratio equal to 2.2 and an elevated sodium content. This aluminate hydrate may be an AFm phase denominated U-phase, which was also reported by [83,115,116] in cement systems containing sodium concentrations above 0.40 mol/L. Accelerator ALK provides a propitious sodium content for U-phase formation (0.41 mol/L, table 3.5).

At 3 h of hydration, microstructure is fairly heterogeneous (figure 3.13.c). Aluminate hydrates (Al/S ratio equal to 1.5) in the form of needles and plates are deposited on the surface of a cement particle. Silicon is also present and may be in the form of C-S-H or substituting Al^{3+} in the lattice of aluminate hydrates, as also observed by [81,117]. As presented in figure 3.13.d, AFm and AFt phases coexist on the surface of a cement grain, confirming the hypothesis derived from the *in situ* XRD analysis. In this context, since AFm phases are more thermodynamically stable and less soluble than alite [16] and they fill up the space available in the paste quickly, C_3S dissolution may be inhibited due to the hydrated aluminate layer formed over its surface and to the lack of space. This explains why pastes with alkaline accelerator present a lower degree of hydration at 24 h when compared to the other pastes.

At 12 h, the microstructure of the paste is not as homogeneous as the paste produced with AKF 0.61 7%, as observed in figures 3.13.e and 3.13.f. Ettringite is not dispersed uniformly throughout the whole matrix. Some regions are characterized by fairly smooth surfaces, where AFm phases may be deposited. The precipitation of these phases on the surface of a cement particle limits it hydration.

The characterization of microstructure by SEM imaging is in line with the results obtained by *in situ* XRD and isothermal calorimetry. Hence, these observations confirm the kinetics and mechanisms of hydration proposed for pastes with both accelerator types and help understand the differences between accelerated and reference pastes.

3.4.   Conceptual model of mechanisms of hydration

Figures 3.14.a, 3.14.b and 3.14.c present a conceptual model for the hydration of an ordinary Portland cement without accelerator, with an alkali-free and an alkaline accelerator, respectively. They represent the evolution of phase composition, the microstructure and the main processes occurring during hydration of these pastes. It was developed based on the literature [21,41,42,46,73,114], updated with the results obtained in this chapter.
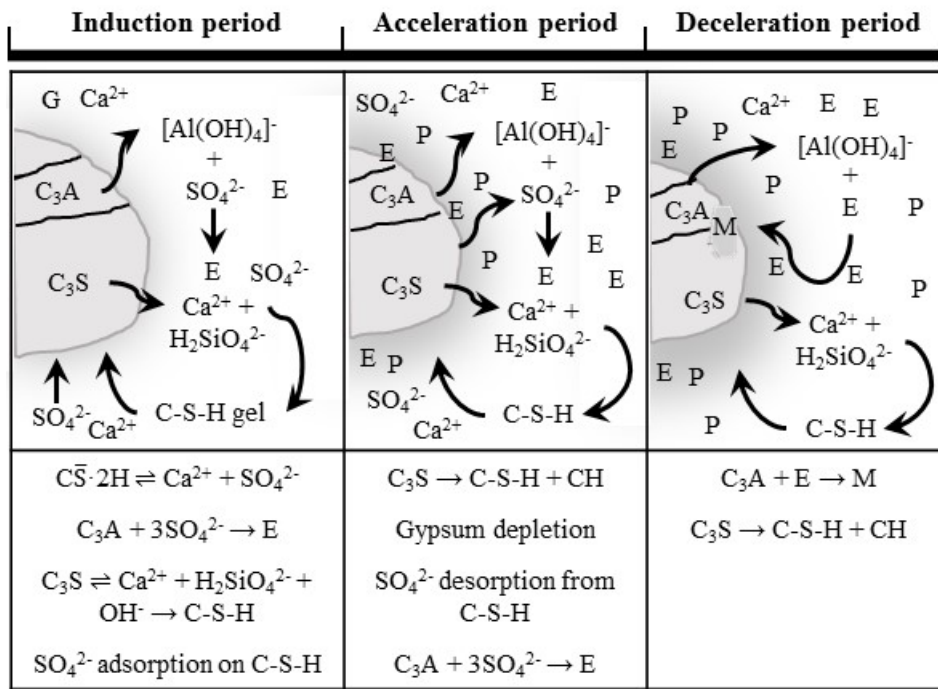
(a)
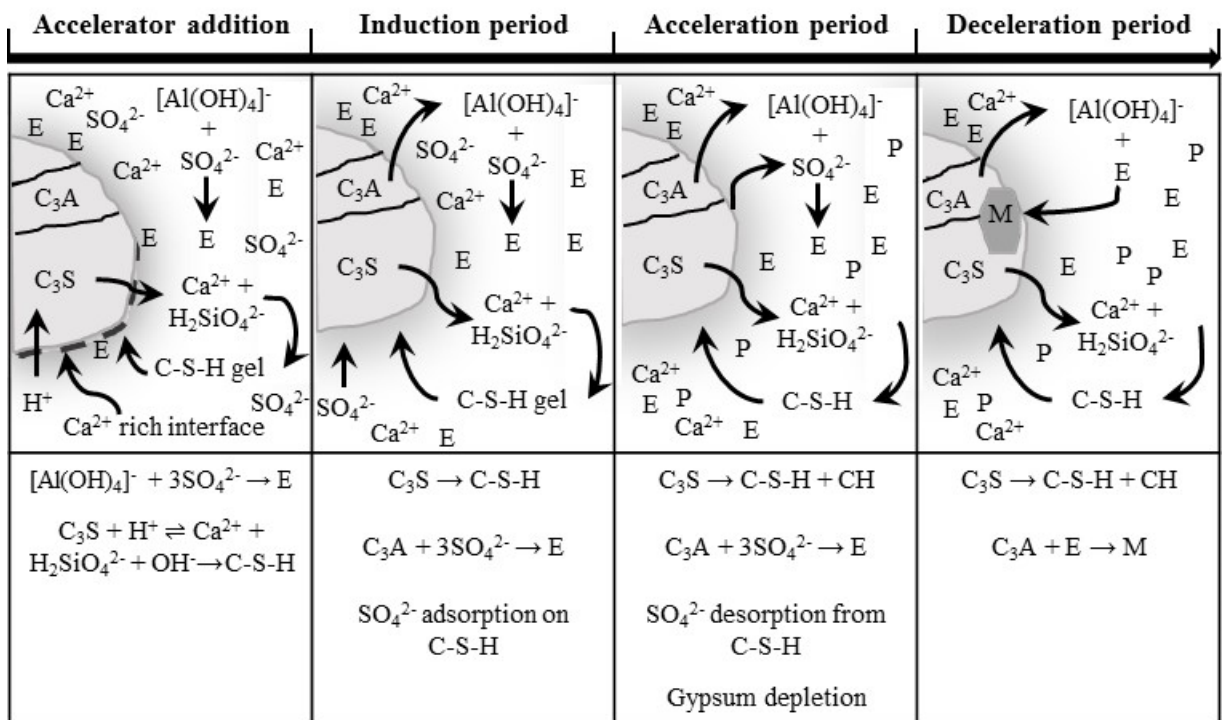
(b)
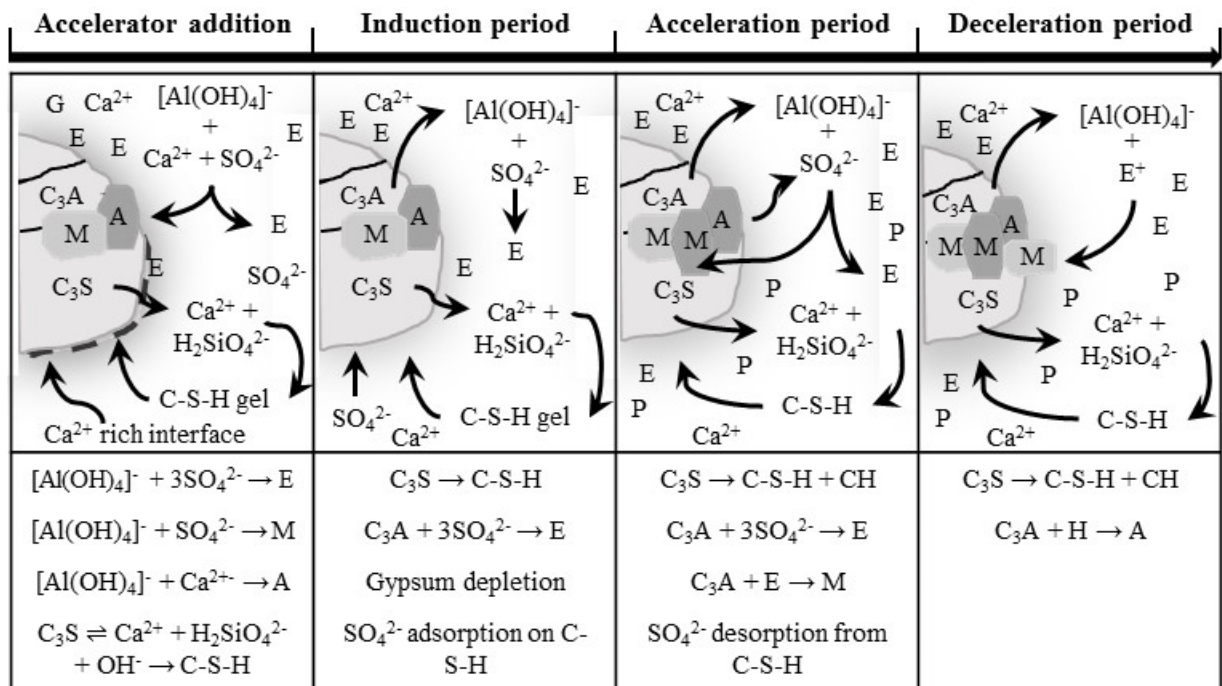
(c)

Figure 3.14 - Conceptual model for the hydration of an ordinary Portland cement in a reference paste (a), in a paste with an alkali-free accelerator (b) and in a paste with an alkaline accelerator (c), considering a polyphase cement grain with gypsum. Subtitles: G: gypsum; P: portlandite; E: ettringite; M: monosulfoaluminate; A: hydroxy-AFm.

In pastes containing alkali-free accelerators, ettringite is the main hydrate formed by accelerator reaction. The formation of a calcium rich interface is favored due to the acid contained in their formulation. As this accelerator also contains sulfate ions, undersulfated C_3A reactions are avoided and cement particles are not covered by AFm phases before the acceleration period. Therefore, alite hydration is not suppressed and proceeds normally. However, the early formation of hydrated aluminate phases by accelerator reaction fill up the space in the matrix quickly and reduce the degree of hydration at later ages.

Aluminate accelerators lead to the formation of ettringite and AFm phases at the moment of their addition. They rapidly consume Ca^{2+} ions and deplete sulfate from the liquid phase. This favors C_3S dissolution, thus increasing calcium concentration on the interface alite-water. Given the absence of sulfates in solution, C_3A hydration leads to the formation of AFm phases. These phases precipitate preferentially where calcium concentration is higher, which is found at the alite-water interface. As AFm phases are thermodynamically more stable and less soluble than C_3S, inner alite is less susceptible to dissolving and hydrating because its reactive sites are blocked. Consequently, the degree of hydration reached in alkaline accelerated pastes should be smaller than in pastes without accelerators and in pastes produced with alkali-free accelerators.

The chemical and physical aspects of cement hydration in the presence of accelerators present major influences on the evolution of mechanical strength in accelerated matrices. Since mechanical strength is directly proportional to the degree of hydration of cement, the precipitation of AFm phases on alite surface and the space filling caused by the early formation of sulfoaluminate hydrated phases decrease the rate of strength gain at late ages. As observed by [1,18], mortars and concrete containing alkali-free accelerators present higher ultimate strengths than matrices produced with alkaline accelerators. The fast sulfate depletion caused by sodium aluminate leads to undersulfated C_3A reactions [54], which are absolutely detrimental for strength development.

3.5. Concluding remarks

Chapter 3 presented the characterization of the early age hydration behavior of cement pastes containing alkali-free and alkaline accelerators. The following conclusions may be drawn from the experimental results:

- Accelerator reactions lead to a fast formation of sulfoaluminate hydrates, mainly ettringite. The higher the Al^{3+} content incorporated in the paste by accelerators, the larger the amount of sulfoaluminate hydrates precipitated.

- Induction periods are significantly shortened in accelerated pastes. The consumption of calcium and sulfate ions from the liquid phase caused by accelerators favors alite and gypsum dissolution in order to balance their concentration in the liquid phase. Then, the concentration of silicate ions also increases, leading to an enhancement in nucleation and growth of hydrates and accelerating the onset of the main hydration peak.

- The amount of sulfate remaining after accelerator reaction is important to control further C_3A hydration. In properly sulfated systems (low final C_3A/SO_3 ratios), sulfate depletion occurs shortly after the acceleration period of alite hydration. Therefore, uncontrolled C_3A reactions do not occur and the rate of alite hydration increases, leading to higher degrees of hydration at 24 h. However, in undersulfated systems (high final C_3A/SO_3 ratios), C_3A hydration is accelerated, with consequent formation of AFm phases. These hydrates precipitate on the surface of a cement particle, decreasing its solubility. As a result, the rate and extension of alite hydration are reduced.

- The large amounts of aluminate hydrates formed by accelerator reaction fill up the matrix before the onset of the main hydration process and reduce the extent of alite hydration from 12 h on. This process is intensified when high dosages of accelerators are employed, since a larger amount of Al^{3+} is added to the matrix.

- The microstructure of alkali-free accelerated pastes, regarding aluminate hydrates, is composed mainly by ettringite. This hydrate nucleates and precipitates as hexagonal needle-like crystals with flat terminations in an ordered structure. On the contrary, pastes produced with alkaline accelerators also contain AFm phases, which are plate-like crystals. Since this accelerator contains NaOH, U-phase formation was also observed.

4. Parameters controlling early age hydration of accelerated cement pastes[2]

4.1. Introduction

As discussed in section 2.4.1, several factors influence the chemical processes occurring in accelerated matrices, such as the mix design and the application method. The interaction between cement and accelerator plays a major role in hydration kinetics and mechanical strength evolution. The use of incompatible materials affects cement hydration negatively and the accelerated cement matrix obtained may not present the expected mechanical properties.

In previous studies regarding this subject [3–5,10,18,19,85,86], the influence of the chemical composition of cements and accelerators on hydration was analyzed based on particular variations in the mix composition of cement pastes. These studies did not consider changes in more than one variable at once, which commonly happens in practice. In addition, discussion of results was majorly qualitative and the compatibility between cements and accelerators could not be parametrized. Therefore, a study combining the main variables

---

affecting hydration kinetics of accelerated matrices is still necessary to parametrize their early age hydration behavior.

The objectives of the experimental campaign conducted in this chapter are:

- Parametrize the early age hydration behavior of accelerated cement pastes based on the chemical composition of cements and accelerators.

- Identify the main properties and characteristics that govern accelerator reactivity and further cement hydration.

- Specify combinations of cements and accelerators with proper compatibility to obtain an optimal performance.

In this chapter, tests were performed with cement pastes produced by hand-mixing. Cement pastes were produced by the combination of 8 cements, 3 alkali-free accelerators used at 5.0 and 7.0 % bcw and 1 alkaline accelerator added at 3.0 % bcw, resulting in 56 different mixes. Cements and accelerators were designed specifically for this part of the experimental program and do not correspond to commercial formulations.

In situ XRD, isothermal calorimetry and SEM analysis were performed to characterize the kinetics and mechanisms of hydration of accelerated pastes. Since sprayed concrete requires an adequate mechanical strength development until 24 h of hydration to guarantee its proper applicability, the progress of the construction work and for safety issues, the analysis conducted in this chapter is restricted to ages until 24 h. The evolution of hydration and mechanical strength at later ages is the subject dealt with in chapters 3 and 7.

Results obtained provide a better comprehension of how the hydration process of cement pastes is influenced by the chemical composition of their starting materials. Moreover, results may have a significant repercussion on how to select compatible cements and accelerators to provide a proper mechanical strength development. This chapter may be a reference to accelerator manufacturers for the development of formulations with enhanced performance with cements from different sources.

4.2. Experimental methodology

4.2.1. Materials

Water and superplasticizer employed in this section are the same as the ones used in chapter 3 (described in section 3.2.1). Cements and accelerators were formulated specifically for this experimental program and are described as follows.

4.2.1.1. Cements

Two types of clinker, two types of setting regulator, limestone filler and silica sand were used to prepare cements. Table 4.1 shows the nomenclature of the materials employed. Their descriptions and characterization are presented subsequently.

Table 4.1 - Materials used to prepare cements.

Material	Type and description	Abbreviation
Clinker	Ordinary	OPC
	Sulfate-resisting	SRC
Setting regulator	Gypsum	G
	Calcium sulfate hemihydrate	H
Addition	Limestone filler	F
	Silica sand	-

A total of 8 different types of cement were produced by manually homogenizing clinker, setting regulator and additions in an agate mortar for 5 min. Table 4.2 presents the composition of cements. Their nomenclature follows the pattern '*clinker type and content*'_'*setting regulator type and content*'_'*addition*'.

Table 4.2 - Composition of cements, in mass percentages.

Nomenclature	Clinker type and content	Setting regulator type and content	Silica sand content	Limestone filler content	C_3A/SO_3 molar ratio
OPC 98_G 2	OPC, 98.0 %	G, 2.0 %	-	-	0.866
OPC 96_G 4	OPC, 96.0 %	G, 4.0 %	-	-	0.586
OPC 94_G 6	OPC, 94.0 %	G, 6.0 %	-	-	0.443
OPC 96_H 3.38	OPC, 96.0 %	H, 3.38 %	0.62 %	-	0.586
OPC 96_G 4_F	OPC, 83.52 %	G, 3.48 %	-	13.0 %	0.586
OPC 94_G 6_F	OPC, 81.78 %	G, 5.22 %	-	13.0 %	0.443
OPC 96_H 3.38_F	OPC, 83.52 %	H, 2.94 %	0.54 %	13.0 %	0.586
SRC 96_G 4	SRC, 96.0 %	G, 4.0 %	-	-	0.182

Clinkers

Ordinary and sulfate-resisting clinkers (OPC and SRC) were selected due to their different C_3A content, which plays a significant role on the overall hydration kinetics and on the evolution of alite hydration [19,54]. Table 4.3 shows their mineralogical composition determined by XRD and Rietveld refinement (structure models presented in Appendix A) and their chemical composition determined by XRF spectrometry. Besides, table 4.4 summarizes their physical properties and figure 4.1 shows that clinkers present an analogous particle size distribution, which is important to control hydration kinetics and the rate of strength gain [118].

Table 4.3 - Mineralogical and chemical composition of clinkers.

Mineralogical composition			Chemical composition		
Compound	OPC (%)	SRC (%)	Compound	OPC (%)	SRC (%)
C_3S	71.0	67.3	LOI	0.20	0.13
C_2S	7.4	11.9	CaO	65.6	65.8
C_3A_c	2.4	0.9	SiO_2	21.1	21.6
C_3A_o	3.2	0.7	Al_2O_3	5.1	4.2
C_4AF	12.8	15.9	Fe_2O_3	3.4	4.9
CaO	0.2	0.5	SO_3	1.2	1.0
$Ca(OH)_2$	0.3	0.3	MgO	1.8	1.3
$CaCO_3$	1.1	1.0	K_2O	0.94	0.57
MgO	0.5	0.4	Na_2O	0.13	0.10
K_2SO_4	0.3	0.1	TiO_2	0.22	0.20
Na_2SO_4	0.8	1.0	Minor phases	0.31	0.20

Table 4.4 - Physical properties of clinkers.

Property	OPC	SRC
Specific surface BET (m^2/g)	1.52	1.10
d_{10} (µm)	1.81	2.37
d_{50} (µm)	11.2	13.1
d_{90} (µm)	29.9	33.4
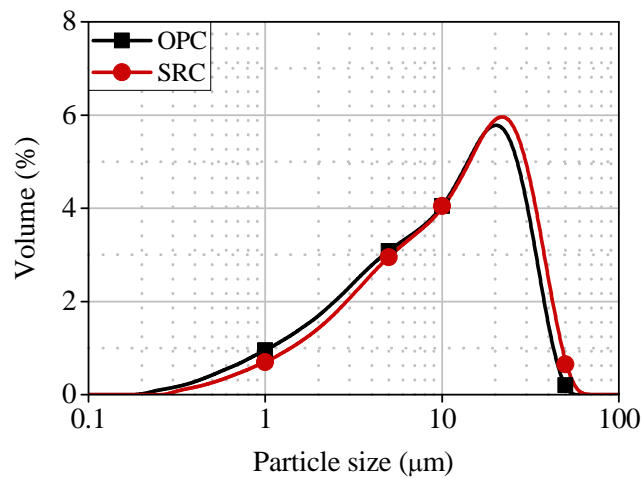
Figure 4.1 - Particle size distribution of clinkers.

Setting regulators

Gypsum (99.5 %, Sigma Aldrich) and calcium sulfate hemihydrate (99.5 %, Sigma Aldrich) were selected as setting regulators. These types of calcium sulfate are commonly found in cements. Gypsum is added to clinkers before grinding and may dehydrate partially, forming hemihydrate, due to the elevated temperature reached during this process [21]. As these compounds present different solubility, as discussed in section 2.3.2.3, it is important to analyze how they affect the rate of accelerator reaction.

OPC cements were prepared with gypsum contents of 2.0, 4.0 and 6.0 % to obtain total SO_3 contents of 2.1, 3.0 and 4.0 %, respectively. Although the standard UNE EN 197-1:2011 [24] prescribes a minimum clinker content of 95.0 % in a cement type I, cement OPC 94_G 6 (94.0 % of clinker and 6.0 % of gypsum) was produced for exploratory tests. Only one cement was produced with the SRC clinker, using 4.0 % of gypsum to maintain the same sulfate amount as in cement OPC 96_G 4.

Hemihydrate was added at 3.38 % to produce OPC cements with the same molar amount of sulfate as 4.0 % of gypsum. This difference is related to the lower water content in hemihydrate. Therefore, 0.62 % of silica sand (calculated over the total mass of cement) was added with hemihydrate to maintain the same proportion of clinker and calcium sulfate.

Additions

Limestone filler (98 % $CaCO_3$, d_{50} = 8.3 µm) was used at the content of 13.0 % in substitution of cement to reproduce CEM II/A-L used in former studies [5,18]. Silica sand (98.5 % SiO_2, d_{50} = 25.5 µm) was added to counterbalance the lower water content in calcium sulfate hemihydrate, as mentioned in the former subsection.

4.2.1.2. Accelerators

The composition and characteristics of the accelerators employed are summarized in table 4.5. It is important to mention that these formulations do not contain any additives as stabilizing agents.

Table 4.5 - Composition and characteristics of accelerators.

Characteristic	AKF 0.33	AKF 0.60	AKF 0.74	ALK
Solid content (%)	40.16	45.99	49.11	43.00
Al_2O_3 content (%)	7.44	13.47	16.59	24.00
SO_4^{2-} content (%)	21.04	21.04	21.04	-
Formic acid content (%)	11.48	11.48	11.48	-
Na_2O content (%)	-	-	-	19.00
pH at 20 ºC	2.8	3.0	2.9	12.0[a]
Al_2O_3/SO_4^{2-} molar ratio	0.33	0.60	0.74	-

[a] Solution at 1.0 %.

The formulations of alkali-free accelerators are similar to the accelerators used in chapter 3 (table 3.4). These formulations contain the same sulfate and formic acid contents and the aluminum concentration was the only factor varying in their composition. Therefore, different Al_2O_3/SO_4^{2-} molar ratios were obtained, varying from 0.33 (the same ratio as in ettringite) to 0.74. Their nomenclature is determined by *'AKF Al_2O_3/SO_4^{2-} molar ratio'*. The alkaline accelerator is based on a sodium aluminate solution, does not contain sulfate ions and is identified by *'ALK'*.

4.2.2. Composition and preparation of cement pastes

Reference pastes (without accelerator) are composed by cement, a water/cement (w/c) ratio equal to 0.45 and superplasticizer at 1.0 % bcw. In accelerated pastes, alkali-free accelerators were added at the dosages of 5.0 and 7.0 % bcw, while the alkaline accelerator was used at the dosage of 3.0 % bcw. All pastes were prepared by hand-mixing, according to the procedures described in section 3.2.2, and were destined to the tests right after accelerator homogenization. Accelerated pastes are named *'cement type'_'accelerator name and dosage'*.

4.2.3. Test methods

Tests conducted with cement pastes are shown in table 4.6. *In situ* XRD, isothermal calorimetry and SEM were performed with cements pastes following the procedures described in sections 3.2.3.3, 3.2.3.4 and 3.2.3.6, respectively.

Table 4.6 - Tests conducted with cement pastes.

Test	Sample	Age / period of time
In situ XRD	Fresh paste	0 - 48 h
Isothermal calorimetry	Fresh paste	0 - 24 h
SEM	Freeze-dried paste	15 min, 3 and 12 h after accelerator addition

In situ XRD was conducted with pastes OPC 96_G 4_AKF 0.60 7%, OPC 96_G 4_AKF 0.74 7% and SRC 96_G 4_AKF 0.74 7%. These pastes were selected to evaluate how Al^{3+} concentration in accelerators and C_3A content in cements containing 4.0 % of gypsum (resulting in different final C_3A/SO_3 ratios) influence the mechanisms and kinetics of hydration. Isothermal calorimetry was performed with a total of 56 accelerated pastes, produced by the combination of 8 types of cement (table 4.2), 3 alkali-free accelerators employed at 5.0 and 7.0 % bcw and 1 alkaline accelerator used at 3.0 % bcw (table 4.5). SEM was performed with pastes OPC 96_G 4_F_AKF 0.60 7% and OPC 96_G 4_F_ALK 3% with the aim to analyze how the presence of limestone filler influences the microstructure after accelerator reaction.

4.3. Results and discussion

4.3.1. Evolution of phase composition during hydration and its relation to the heat flow curves

The quantitative evolution of phase composition and the associated heat flow curves obtained at 26 ºC are presented altogether in figure 4.2. In order to simplify the interpretation of the graphs, only the reacting phases (alite, C_3A, gypsum, portlandite, ettringite, AFm and amorphous) are presented. Slow reacting phases (belite and ferrite) were not plotted.
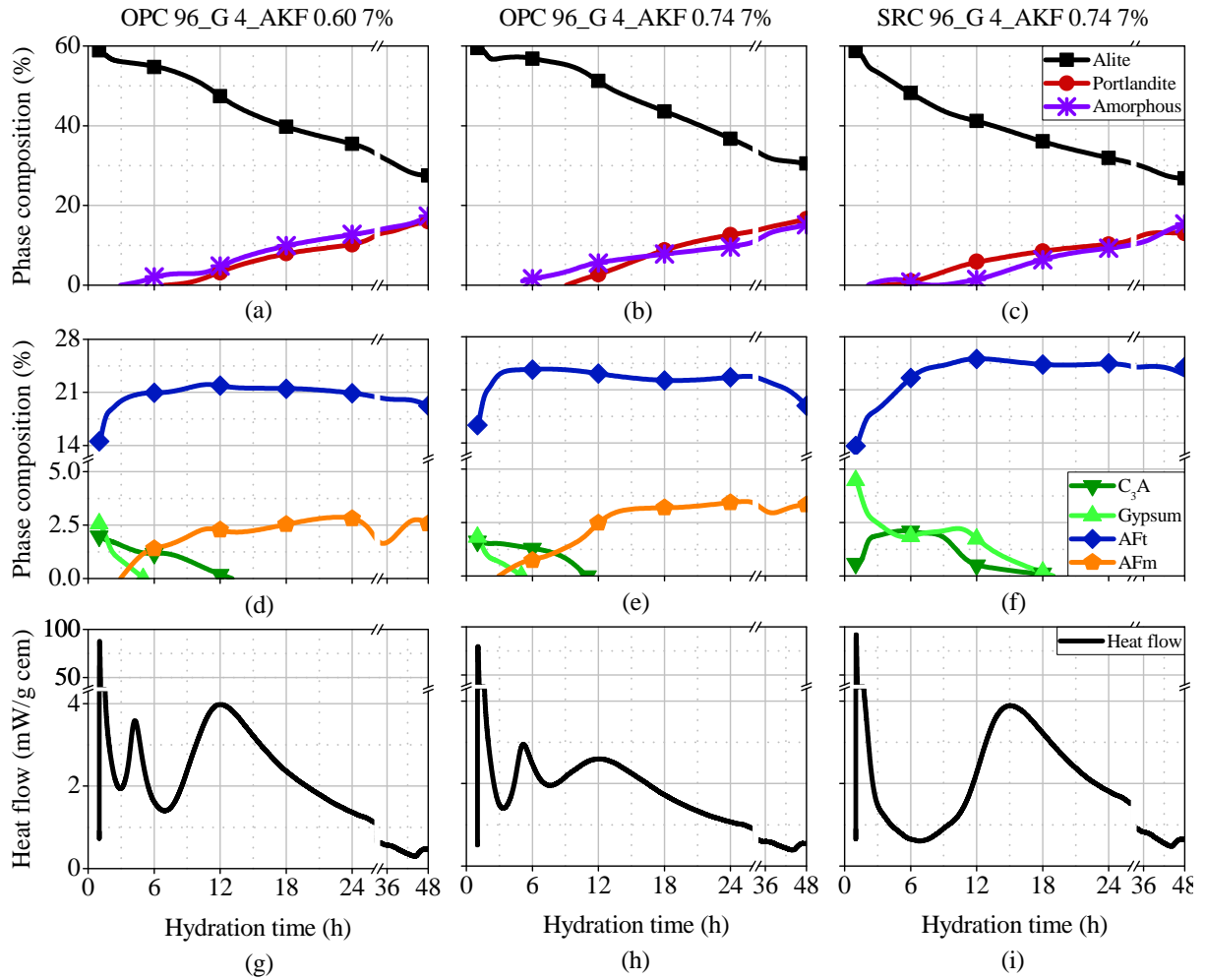
Figure 4.2 - Evolution of the contents of alite, portlandite and amorphous (a, b, c), C_3A, gypsum, ettringite and AFm phases (d, e, f) and heat flow curves (g, h, i) obtained with pastes OPC 96_G 4_AKF 0.60 7% (left), OPC 96_G 4_AKF 0.74 7% (medium) and SRC 96_G 4_AKF 0.74 7% (right) at 26 ºC.

All the pastes present a massive precipitation of ettringite due to accelerator reaction, according to chemical equation 2.11, from table 2.5. This process is associated with the sharp exothermic signal in the heat flow curve at 1 h (accelerator peak). Initial C_3A hydration with gypsum also produces ettringite, but at a minor extent. The amount of ettringite precipitated initially is directly proportional to Al^{3+} concentration in accelerators and to C_3A content in cement (OPC 96 G 4_AKF 0.74 7% > OPC 96 G 4_AKF 0.60 7% > SRC 96 G 4_AKF 0.74 7%). The amount of gypsum left after accelerator addition follows the reverse order of the quantity of ettringite formed, as expected.

In paste OPC 96_G 4_AKF 0.60 7%, gypsum remaining after accelerator reaction (2.6 % by mass) dissolves to balance Ca^{2+} and SO_4^{2-} concentrations in the liquid phase. In addition, it is constantly consumed by C_3A, with consequent ettringite formation until 3 h. At this time,

gypsum depletes and C_3A starts to react with ettringite, forming monosulfoaluminate. This process corresponds to the exothermic peak between 3 and 7 h in the heat flow curve. This paste is undersulfated because C_3A hydrates before the onset of silicate hydration [54,60].

Alite is consumed slowly until 7 h, increasing the concentration of calcium and silicate ions in the liquid phase. At 7 h, the onset of the main hydration peak occurs, increasing the rate of alite consumption and portlandite and amorphous phases precipitation. C_3A continues reacting with ettringite, forming AFm phases, during the acceleration period until 13 h. Finally, the deceleration period starts and hydration proceeds at a slow rate from 24 h on. 53.3 % of alite were consumed until 48 h of hydration.

Paste OPC 96_G 4_AKF 0.74 7% presents the same hydration behavior as OPC 96_G 4_AKF 0.60 7%. However, as accelerator AKF 0.74 contains 23 % more Al^{3+} than AKF 0.60 (table 4.5), less gypsum remains after accelerator reaction (1.8 % by mass). In addition, faster rates of ettringite precipitation and gypsum consumption are observed. The maximum ettringite content is achieved at 3 h, coinciding with gypsum depletion, the onset of the accelerated C_3A hydration and the beginning of AFm phases formation. Due to lower gypsum amounts left after accelerator reaction, the peak related to C_3A hydration is wider and less intense than in paste OPC 96_G 4_AKF 0.60 7% (similarly to results from [42]).

The larger amount of aluminate hydrated phases precipitated until 3 h when accelerator AKF 0.74 is employed contributes to a larger space filling in the matrix. In addition, aluminum in solution may be adsorbed on C-S-H nuclei or even substitute silicon in calcium silicate hydrate, forming C-A-S-H [61]. This phase does not act as a nucleation site and, therefore, induction periods are increased, as discussed in section 2.3.3.2. Furthermore, the incorporation of aluminum on the surface of silicate-containing phases decreases their solubility and reactivity, as indicated by [59].

The combination of these processes is detrimental for alite hydration and for mechanical strength development. In paste OPC 96_G 4_AKF 0.74 7%, alite dissolution is inhibited, the onset of the main hydration peak is retarded (it starts at around 7.8 h) and reaction rates during the acceleration peak are slower. In this paste, 48.7 % of alite hydrated until 48 h (9.4 % less than in paste OPC 96_G 4_AKF 0.60 7%).

The hydration behavior of paste SRC 96_G 4_AKF 0.74 7% differs from the other pastes analyzed. Initial ettringite amount in this paste is the lowest because the SRC clinker

contains 3 times less C_3A than the OPC clinker (table 4.3). As a result, the amount of gypsum left after accelerator addition is the highest (4.5 % by mass). Furthermore, as this paste presents the lowest final C_3A/SO_3 ratio (0.41, table B.1), the rate of C_3A hydration is slower and gypsum depletes after the acceleration period of alite hydration. The maximum ettringite content is achieved around 12 h and is maintained constant after that. AFm phases were not detected until the end of this test.

Paste SRC 96_G 4_AKF 0.74 7% is properly sulfated, because C_3A hydration occurs after the onset of the main hydration peak [54,60]. Since the early space filling caused by accelerated undersulfated C_3A reactions is avoided, alite hydration is not negatively affected. In fact, alite is constantly consumed during the induction period to balance the chemical equilibria disturbed by the accelerator. The rate of reaction during the acceleration period is 3.8 times higher than in OPC 96_G 4_AKF 0.74 7%. Until 48 h, 54.5 % of alite were consumed (12 % more than in the equivalent OPC paste).

4.3.2. Influence of cement and accelerator composition on the kinetics and mechanisms of hydration of accelerated pastes

Results obtained by isothermal calorimetry performed at 20 ºC with all the pastes analyzed are presented from figure B.1 to B.8, in Appendix B. To analyze the influence of different mix composition on hydration, the parameters described in table 3.8 were used to analyze heat of hydration curves. Results from this analysis are shown in table B.1, also in Appendix B. Discussion of results is presented subsequently, separated by each parameter analyzed.

4.3.2.1. Al^{3+} content in accelerator and accelerator dosage

As the quantity of Al^{3+} introduced in the paste depends on accelerator dosage, these parameters are analyzed simultaneously. Considering ettringite as the only sulfoaluminate hydrate immediately formed by accelerator reaction, the theoretical ettringite amounts produced by each accelerator are presented in table 4.7. The higher the Al^{3+} content incorporated in the paste, the larger the amount of ettringite produced.

Table 4.7 - Theoretical amounts of ettringite formed by accelerator reaction.

Accelerator	Dosage (% bcw)	Al³⁺ introduced in the paste (mmol/g cement)	Ettringite formed (mmol/g cement)
AKF 0.33	5.0	0.0730	0.0365
	7.0	0.102	0.0510
AKF 0.60	5.0	0.132	0.0660
	7.0	0.185	0.0925
AKF 0.74	5.0	0.163	0.0815
	7.0	0.228	0.114
ALK	3.0	0.141[a]	0.0706

[a] As $[Al(OH)_4]^-$.

Figure 4.3 shows the influence of Al^{3+} content on the accelerator peak in pastes OPC 98_G 2, OPC 96_G 4 and OPC 94_G 6. The energy released follows the ascending order of the amount of ettringite precipitated, according to each accelerator and dosage. However, accelerator reaction rate presents a saturation point at 0.185 mmol of Al^{3+} / g cement in all cements analyzed. Accelerator efficiency decreases above this limit probably due to a lack of sulfates dissolved in the medium, because the rate of gypsum dissolution is lower than the rate of accelerator reaction. As a result, AFm phases may be formed at the moment of accelerator addition [10].
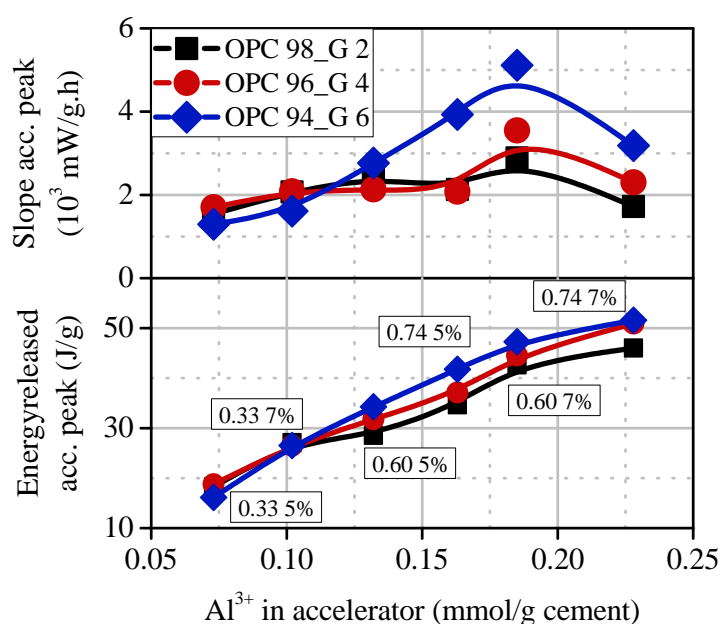
Figure 4.3 - Influence of Al^{3+} content introduced in the paste on the accelerator peak.

4.3.2.2. Al₂O₃/SO₄²⁻ molar ratio of accelerator

The influence of the Al_2O_3/SO_4^{2-} ratio of accelerators on the overall hydration behavior is presented in figure 4.4. Since AKF 0.33 provides the lowest amount of sulfoaluminate hydrates at the moment of its addition, early space filling is not prejudicial for alite hydration to proceed normally. The shape of the main hydration peak (figures B.1, B.2 and B.3) indicates that cement hydration mechanisms are not negatively affected by this admixture. Since no sulfates from cement are required for accelerator reaction, C_3A hydrates in a properly sulfated medium and AFm phases are formed after the acceleration period of silicate hydration. Due to these reasons, the energy released during the main hydration peak in all the pastes containing AKF 0.33 is the highest when compared to equivalent pastes with the other alkali-free accelerators at the same dosage.
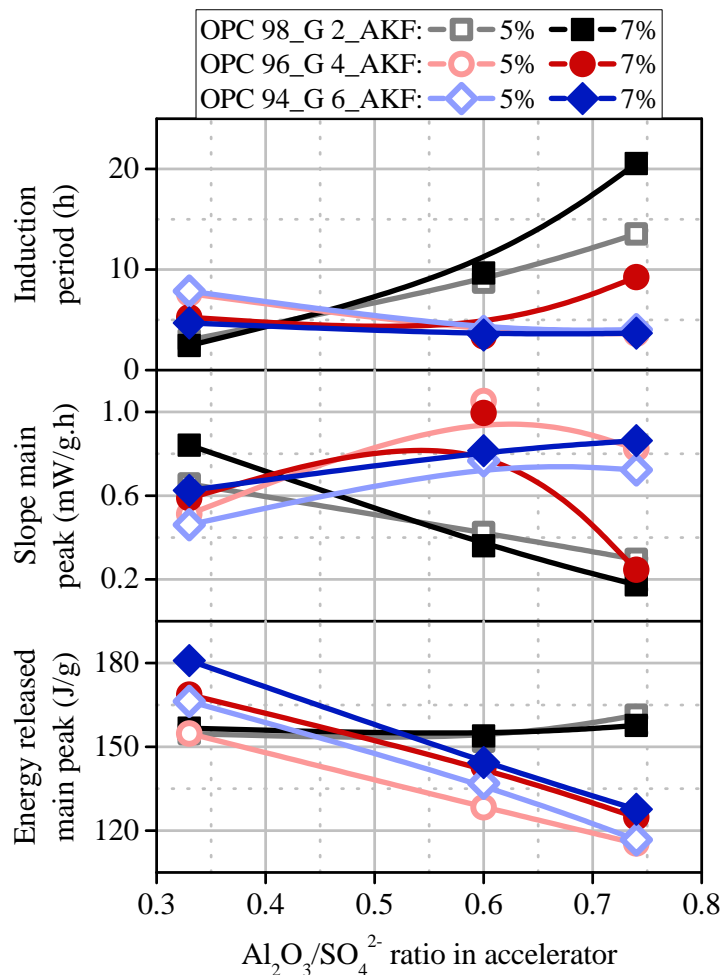
Figure 4.4 - Influence of Al_2O_3/SO_4^{2-} ratio on the main hydration peak.

Accelerator AKF 0.60 promotes shorter induction periods, faster hydration rates and higher intensities in the main hydration peak than AKF 0.33 in all the pastes. Since AKF 0.60 contains 81 % more Al^{3+} than AKF 0.33, the imbalance in the chemical equilibria caused by accelerator reaction favors gypsum and alite dissolutions. In addition, C_3A reactions are accelerated and the resulting hydration rate in the main peak corresponds to the sum of silicate and aluminate hydrations.

The tendencies observed for AKF 0.74 depend on accelerator dosage and gypsum amount in cement. In pastes OPC 98_G 2_AKF 0.74 5%, OPC 98_G 2_AKF 0.74 7% and OPC 96_G 4_AKF 0.74 7%, induction periods are significantly increased and the reaction rate during the main hydration peak are reduced. As this accelerator contains the highest Al^{3+} concentration and Al_2O_3/SO_4^{2-} ratio, the large amount of sulfoaluminate hydrates formed fills up the space available in the paste. The elevated consumption of sulfate ions from the liquid phase promotes undersulfated C_3A reactions, with the consequent formation of AFm phases before the onset of the main hydration peak. The result of these processes is a great suppress in alite dissolution and further hydration. Pastes OPC 94_G 6 are not negatively affected by AKF 0.74 at 5.0 and 7.0 % bcw, because the high Al_2O_3/SO_4^{2-} ratio of accelerator is counterbalanced by the larger gypsum content in cement.

4.3.2.3. Gypsum amount in cement and final C_3A/SO_3 ratio of the paste

The influence of gypsum amount on the accelerator peak in pastes containing alkali-free accelerators may also be analyzed in figure 4.3. Reaction rate and the energy released in the accelerator peak are proportional to gypsum amount in cement, mainly for AKF 0.60 and AKF 0.74 in both dosages. An addition of 2 % of gypsum increases the energy released by 10 % and reaction rate by a minimum of 30 %. AKF 0.33 does not follow this tendency because it does not require sulfates from the liquid phase.

Kinetics of cement hydration after accelerator reaction is very sensitive to gypsum amount and the final C_3A/SO_3 ratio of the paste. Figure 4.5 presents heat flow curves of pastes OPC 98_G 2, OPC 96_G 4 and OPC 94_G 6 containing AKF 0.74 (highest Al_2O_3/SO_4^{2-} ratio) at 7.0 % bcw. In cements containing lower gypsum amounts, C_3A hydration is advanced due to a fast sulfate depletion [41,42]. In other words, as the final C_3A/SO_3 ratio increases, aluminate reaction takes place earlier, as indicated by the arrows.
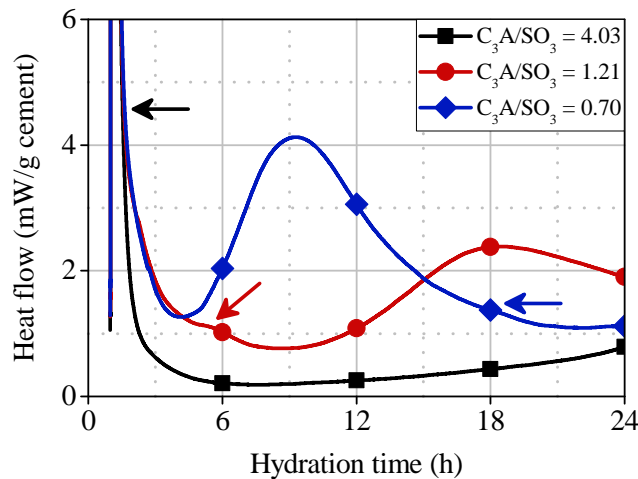
Figure 4.5 - Heat flow curves of pastes OPC 98_G 2, OPC 96_G 4 and OPC 94_G 6 produced with AKF 0.74 at 7.0 % bcw. Arrows represent C_3A hydration in the absence of dissolved sulfates, forming AFm phases.

Paste OPC 94_G 6_AKF 0.74 7% presents a proper sulfate balance and C_3A hydration occurs after the acceleration period of alite hydration. Therefore, higher degrees of hydration are obtained at 24 h (table B.1). However, as paste OPC 96_G 4_AKF 0.74 7% is poorly sulfated, C_3A hydration is accelerated and takes place at 6 h approximately, retarding the onset of the main hydration peak and reducing its intensity.

Paste OPC 98_G 2_AKF 0.74 7% is the most unfavorable case because only 0.05 mmol of SO_4^{2-}/g cement remains after accelerator reaction (final C_3A/SO_3 ratio equal to 4.03, table B.1). The limited sulfate content left leads to undersulfated C_3A reactions, generating hydroxyl-AFm and monosulfoaluminate [42] during the accelerator peak. The precipitation of these phases on alite and C_3A surfaces decreases their solubility and delays their hydration, increasing induction periods, lowering reaction rates and broadening the main hydration peak. A small signal of silicate reaction can only be observed after 18 h, compromising the evolution of mechanical strength of the matrix.

Figure 4.6 shows the influence of the final C_3A/SO_3 ratio on the main hydration peak in pastes OPC 98_G 2, OPC 96_G 4 and OPC 94_G 6 containing AKF 0.60 and AKF 0.74 at 5.0 and 7.0 % bcw. Accelerator AKF 0.33 was not used in this evaluation because it does not change the initial C_3A/SO_3 ratio of cements. Increasing C_3A/SO_3 ratios retard the onset of the main hydration peak and decrease reaction rates. Therefore, lower degrees of hydration are obtained at 24 h.
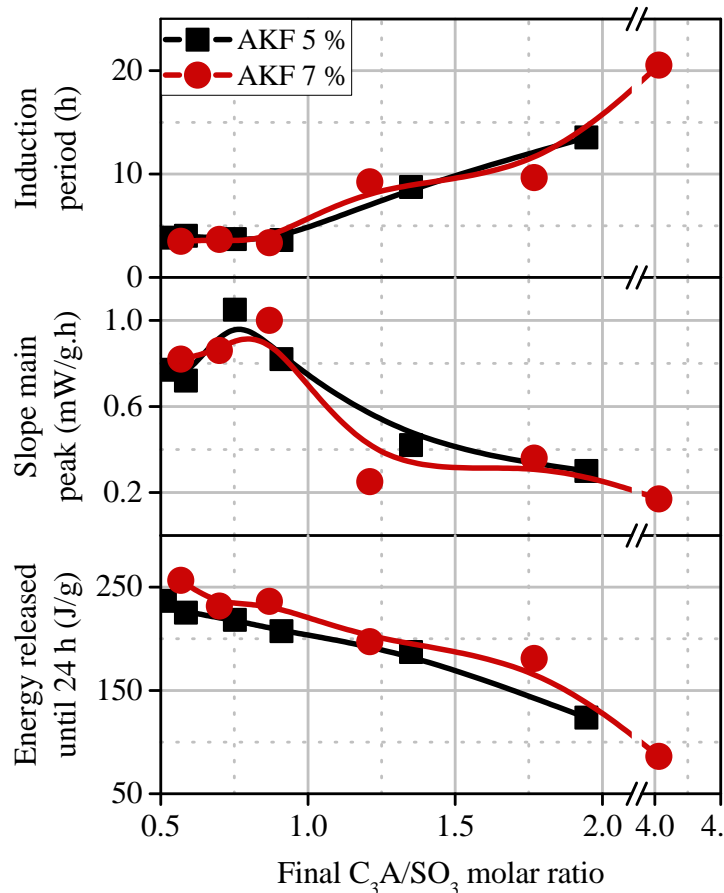
Figure 4.6 - Influence of the final C_3A/SO_3 ratio on the main hydration peak in pastes OPC 98_G 2, OPC 96_G 4 and OPC 94_G 6 containing accelerators AKF 0.60 and AKF 0.74 at 5.0 and 7.0 % bcw.

In the mixes evaluated, the optimal C_3A/SO_3 ratio for proper cement hydration is between 0.67 and 0.90. Within this range, induction periods and degrees of hydration are not negatively affected and, more importantly, the main hydration peak presents the highest intensities and reaction rates. Values below 0.67 provide higher degrees of hydration in the main peak, although reaction rates and intensities are not optimal. On the contrary, values above 0.90 are absolutely detrimental for cement hydration. Induction periods are significantly longer, retarding the hardening of the paste and the development of mechanical strength.

The reactivity of the alkaline accelerator is also enhanced by larger gypsum amounts, as observed in figure 4.7. Since this accelerator is based on sodium aluminate, gypsum is the only sulfate source for the formation of sulfoaluminate hydrated phases. Therefore, paste OPC 94_G 6_ALK 3%, which contains the largest gypsum amount, presents the fastest and most extensive accelerator reactions.
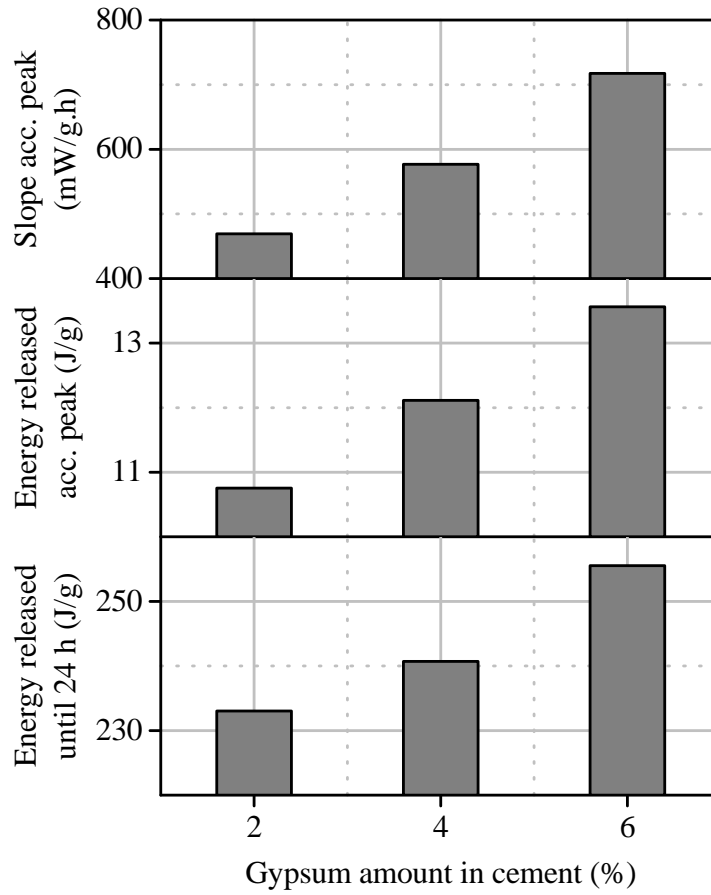
Figure 4.7 - Influence of gypsum amount on the reactivity of the alkaline accelerator and on the degree of hydration of the cement paste.

Pastes OPC 98_G 2_ALK 3%, OPC 96_G 4_ALK 3% and OPC 94_G 6_ ALK 3% present a sharp peak during the induction period related to the renewed C_3A hydration (figures B.1, B.2 and B.3). The dissolution of C_3A and the formation of AFm phases are accelerated in pastes containing lower gypsum amounts. As this process occurs before the onset of the main hydration peak, alite hydration is suppressed. Paste OPC 98_G 2_ALK 3% presents the lowest energy released until 24 h because it is undersulfated (C_3A/SO_3 ratio equal to 7.57, table B.1).

4.3.2.4. Calcium sulfate type in cement

The influence of the setting regulator type on the hydration of pastes OPC 96_G 4 and OPC 96_H 3.38 (equivalent amounts of calcium sulfate in mol) is analyzed. Accelerator reaction rates are more than 20 % higher in pastes containing hemihydrate (66 and 55 % higher when AKF 0.74 7% and ALK 3% are employed, respectively), as presented in figure 4.8. Since calcium sulfate hemihydrate is more soluble than gypsum, it provides a faster increase in the

concentration of sulfate ions in the liquid phase. The use of hemihydrate is particularly important when sulfate from cement is substantially necessary to control accelerator reaction (accelerators dosages of 7.0 % bcw and for accelerators with Al_2O_3/SO_4^{2-} ratios equal to 0.74).
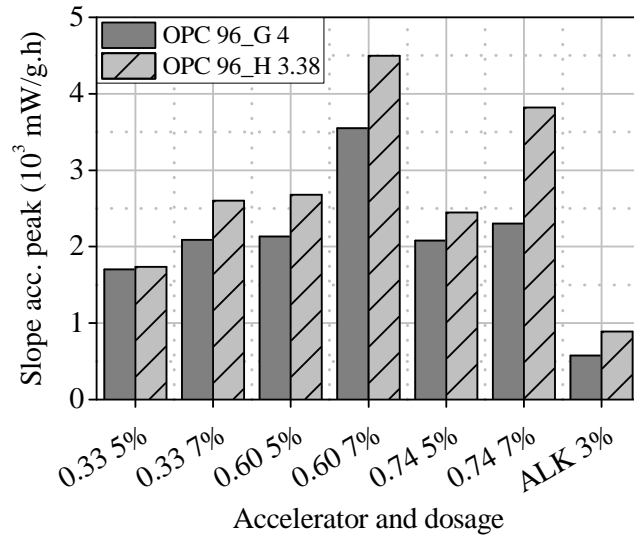
Figure 4.8 - Accelerator reaction rates in pastes OPC 96_G 4 and OPC 96_H 3.38.

Figure 4.9 correlates the energy released in the accelerator peak and the Al^{3+} content from alkali-free accelerators in pastes OPC 96_G 4 and OPC 96_H 3.38. A linear regression properly fits those parameters, providing R^2 values higher than 0.985 in all the cases. Values of linear and angular coefficients of the regressions obtained are presented in table 4.8. The angular coefficient represents the rate of ettringite formation [42], confirming that hemihydrate improves accelerator reactivity.
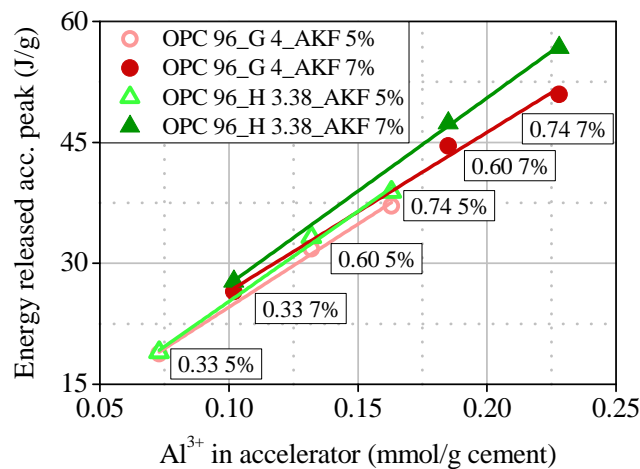
Figure 4.9 - Correlations between the energy released in the accelerator peak and Al^{3+} content in accelerator in pastes OPC 96_G 4 and OPC 96_H 3.38 containing alkali-free accelerators.

Table 4.8 - Coefficients a and b for the linear regressions obtained (y = a + bx).

Paste	a	b
OPC 96_G 4_AKF 5%	3.97	205.9
OPC 96_G 4_AKF 7%	6.81	197.2
OPC 96_H 3.38_AKF 5%	2.90	223.7
OPC 96_H 3.38_AKF 7%	4.27	231.2

Linear coefficients should be close to zero considering ettringite as the only hydrate formed by accelerator reaction. However, linear coefficients are not zero, indicating that other exothermic processes occur when accelerators are added. They might be corresponded to alite dissolution caused by formic acid contained in accelerators [10] and to the formation of hydroxyl-AFm by C_3A hydration in the absence of sulfates [41,42]. Since formic acid concentration is identical in all formulations, the heat generated by the acid dissolution must be equal in pastes containing accelerator dosages of either 5.0 or 7.0 % bcw. Therefore, as the y-intercepts are lower in pastes OPC 96_H 3.38, the formation of hydroxyl-AFm during the accelerator peak is reduced if hemihydrate is the setting regulator, due to the higher concentration of sulfate ions available in the liquid phase.

The fast consumption of sulfate ions in pastes OPC 96_H 3.38 by accelerator reaction advances further C_3A hydration, as also observed in [42]. Consequently, a shoulder related to the formation of AFm phases in pastes containing Al^{3+} additions above 0.163 mmol/g cement (AKF 0.60 at 7.0 % bcw and AKF 0.74 at 5.0 and 7.0 % bcw) may be observed around 5 and 6 h of hydration in figure B.4. The accelerated formation of AFm phases reduces reaction rates during the acceleration period and degrees of hydration until 24 h [19], as observed in figure 4.10. A similar behavior is observed in the paste containing the alkaline accelerator.
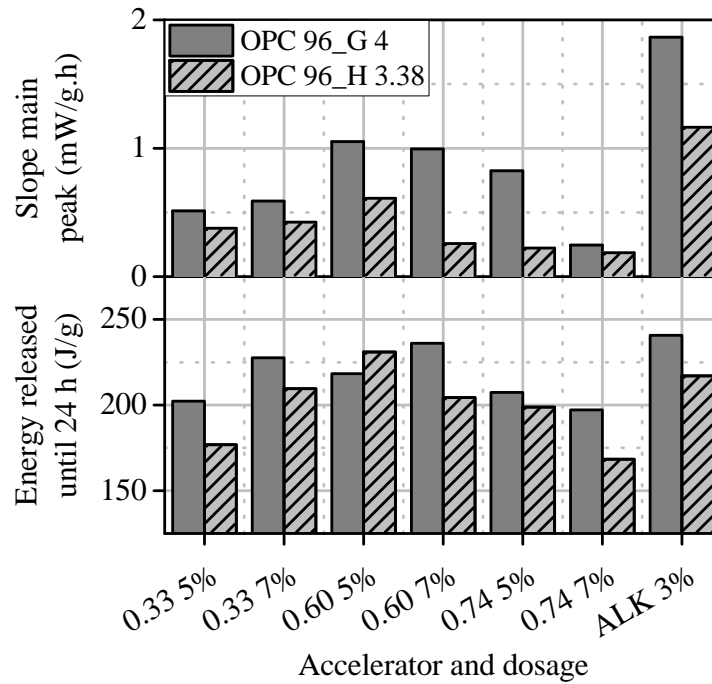
Figure 4.10 - Slope of the main hydration peak and energy released until 24 h in pastes OPC 96_G 4 and OPC 96_H 3.38.

4.3.2.5. C₃A content in cement

The influence of C_3A content on the hydration behavior of pastes OPC 96_G 4 and SRC 96_G 4 is analyzed in figure 4.11. Accelerator reactivity is enhanced in pastes SRC 96_G 4. Since this cement contains only 1.6 % of C_3A (approximately 28 % of the amount in OPC 96_G 4), initial sulfate consumption proceeds at a minor extent and more sulfate ions are available for accelerator reaction. Therefore, accelerator reaction rates and the energies released during this process are around 15 % and 10 % higher in SRC pastes, respectively.
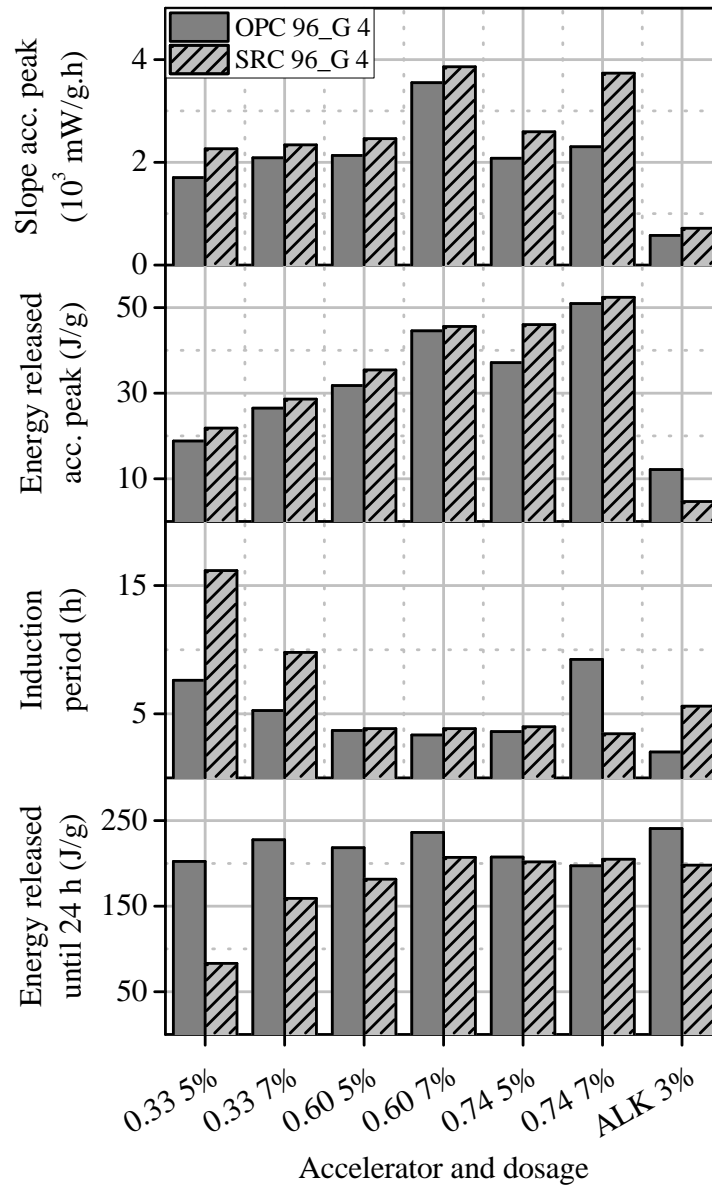
Figure 4.11 - Reaction rates and energies associated with the accelerator peak, induction periods and energies released until 24 h of hydration of pastes produced with OPC 96_G 4 and SRC 96_G 4.

The SRC clinker is coarser than the OPC clinker and induction periods are extended in SRC 96_G 4 pastes. Accelerator AKF 0.33 leads to the longest retardation on the onset of the main hydration peak because it consumes the lowest amount of Ca^{2+} ions from de liquid phase, resulting in low rates of alite dissolution. Furthermore, C_3A hydration in pastes SRC 96_G 4_AKF 0.33 5% and SRC 96_G 4_AKF 0.33 7% is retarded due to their low final C_3A/SO_3 ratios. Consequently, their degrees of hydration at 24 h are considerably reduced.

Accelerators AKF 0.60 and AKF 0.74 consume more calcium and sulfate ions than AKF 0.33. This favors alite and gypsum dissolutions, increases the rates of nucleation and growth of

hydrates and reduces induction periods in SRC 96_G 4 pastes. Besides, the retardation in C_3A hydration is not so severe because these accelerators lead to higher final C_3A/SO_3 ratios than AKF 0.33. The most synergistic effect occurs in paste SRC 96_G 4_AKF 0.74 7%, with a final C_3A/SO_3 ratio equal to 0.41 (while the equivalent OPC paste has a final C_3A/SO_3 ratio equal to 1.21, which is not adequate for strength development). The accelerated undersulfated C_3A hydration is avoided in pastes SRC 96_G 4 due to their proper sulfate balance.

Paste SRC 96_G 4_ALK 3% presents the same overall hydration behavior as OPC 96_G 4_ALK 3%. The accelerated C_3A hydration in SRC 96_G 4_ALK 3% occurs between 3.2 and 5 h and the energy associated with this process corresponds to 11.2 J/g cement (figure B.8). However, C_3A hydration takes place between 1.8 and 3.4 h in the equivalent OPC paste and releases an energy equal to 23.0 J/g cement (figure B.2). The lower C_3A content and the resulting lower C_3A/SO_3 ratio in SRC 96_G 4_ALK 3% are responsible for the retardation and the lower intensity of undersulfated C_3A reactions.

4.3.2.6. Limestone filler in cement

Figure 4.12 shows the energy released by accelerator reaction in pastes OPC 96_G 4, OPC 94_G 6 and OPC 96_H 3.38 with and without limestone filler. Results of pastes containing limestone filler are presented as determined and normalized by the content of clinker plus calcium sulfate (87 % by mass).
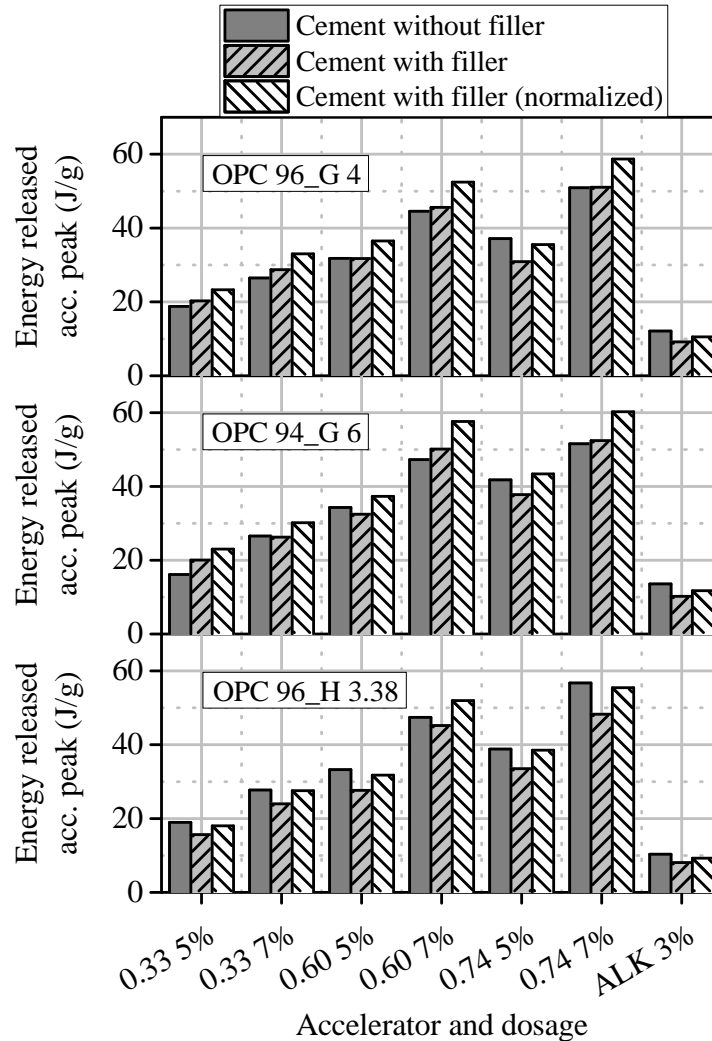
Figure 4.12 - Energy released during the accelerator peak in pastes OPC 96_G 4, OPC 94_G 6 and OPC 96_H 3.38 with and without limestone filler.

Analyzing the results as determined, the energy released by accelerator reaction in pastes OPC 96_G 4_F and OPC 94_G 6_F is not significantly different from the equivalent pastes without limestone filler (the difference falls within the ± 8 % interval). However, considering the normalized results, it is clear that accelerator reactivity is enhanced by this addition. Increments of 20 % in the energy released in the accelerator peak in pastes containing limestone filler and accelerators AKF 0.60 and 0.74 are observed. Normalized results in pastes OPC 96_H 3.38_F present the same tendency, although the influence of limestone filler is minor when hemihydrate is the calcium sulfate source.

Limestone filler competes with gypsum to retard C_3A hydration [65,66] and may also control the reaction of Al^{3+} from the accelerator, forming hemi and monocarboaluminate [10]. These phases are more stable than other AFm phases at room temperature and indirectly

stabilize ettringite [45]. Therefore, limestone filler improves accelerator reactivity in sprayed concrete applications, as indicated in [1,13].

Results suggest a synergistic effect between limestone filler and alkali-free accelerators, mainly for Al^{3+} additions above 0.163 mmol/g cement and for accelerators having Al_2O_3/SO_4^{2-} ratios above 0.60 employed at 7.0 % bcw. The acidic nature of alkali-free accelerators favors limestone dissolution, thereby enhancing Al^{3+} reaction, which is limited by gypsum dissolution in CEM I pastes. As hemihydrate is more soluble than gypsum, it inhibits calcium carbonate dissolution by the common ion (Ca^{2+}) effect, limiting its efficiency.

Limestone filler may also act as a nucleation site for the precipitation of aluminate hydrated phases formed by accelerator reaction, as observed by SEM imaging. Figure 4.13.a and 4.13.b present the microstructure of pastes OPC 96_G 4_F_AKF 0.60 7% and OPC 96_G 4_F_ALK 3% at 15 min of hydration, respectively. A limestone particle is indicated by an 'L' in each picture (identified by the EDS results 1 and 3).

^{1} Ca : Si : Al : S : Na = 100 : 3.2 : - : - : -
^{2} Ca : Si : Al : S : Na = 100 : 13.0 : 3.2 : 8.3 : - ^{3} Ca : Si : Al : S : Na = 100 : 9.1 : - : - : -
^{4} Ca : Si : Al : S : Na = 100 : 42.5 : 13.7 : 7.6 : 2.2

(a)   (b)
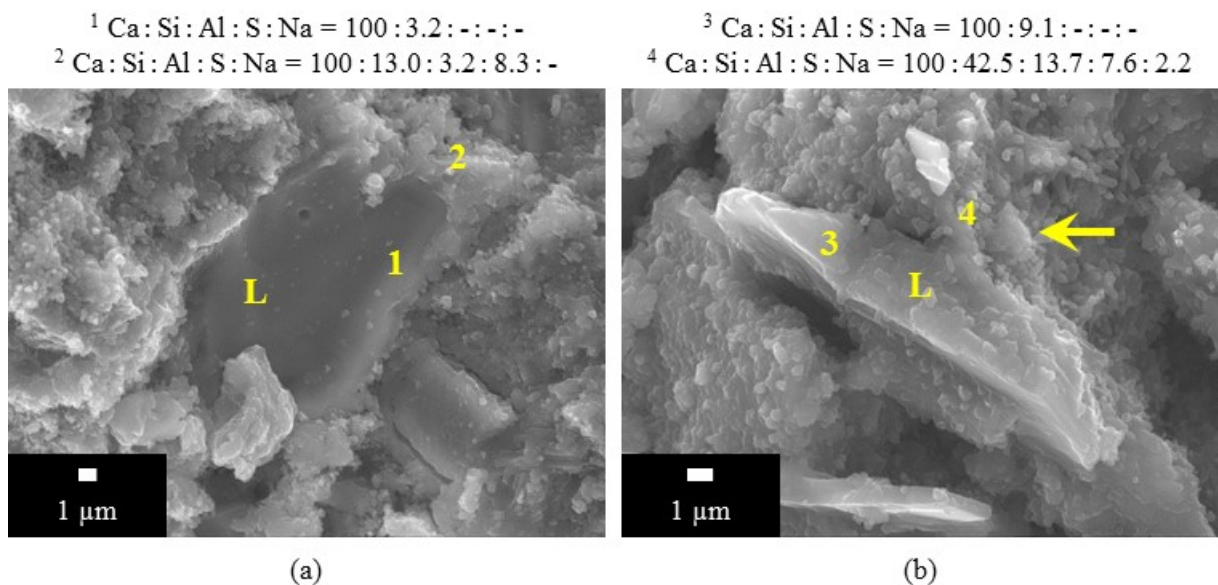
Figure 4.13 - Paste OPC 96_G 4_F_AKF 0.60 7% at 15 min (a) with corresponding EDS spectra 1 and 2 and paste OPC 96_G 4_F_ALK 3% at 15 min (b) with corresponding EDS spectra 3 and 4.

In figure 4.13.a, the limestone particle is embedded in the microstructure of the matrix. In the region corresponding to EDS 2, aluminate hydrates precipitated on the particle are composed mainly by AFt phases, since the Al/S ratio is 0.39 (below 0.667, which is the Al/S ratio of pure ettringite). This is expected, since the alkali-free accelerator contains sulfate ions and ettringite is the main hydrate formed by its reaction.

On the contrary, aluminate hydrates precipitated on the limestone surface when the alkaline accelerator is used (figure 4.13.b) present an Al/S ratio equal to 1.8 (EDS 4). Hence, they might be composed mainly by AFm phases (in pure monosulfoaluminate, the Al/S ratio is equal to 2). In addition, some hydrates surrounding the limestone particle are plate-like crystals (such as the region identified by an arrow), which are also characteristic of AFm phases [21,71].

Figure 4.14 shows the total energy released until 24 h in the pastes analyzed. Normalized results show the beneficial use of limestone filler on the overall cement hydration, mainly in pastes containing AKF 0.60 and AKF 0.74 (high Al^{3+} concentrations and high final C_3A/SO_3 ratios). Besides the physical effect of clinker dilution that increases the space for the precipitation of hydrates [64], limestone filler avoids accelerated undersulfated C_3A reactions and alite hydration may proceed normally. As a result, degrees of hydration at 24 h are around 6 % higher in pastes containing this addition.
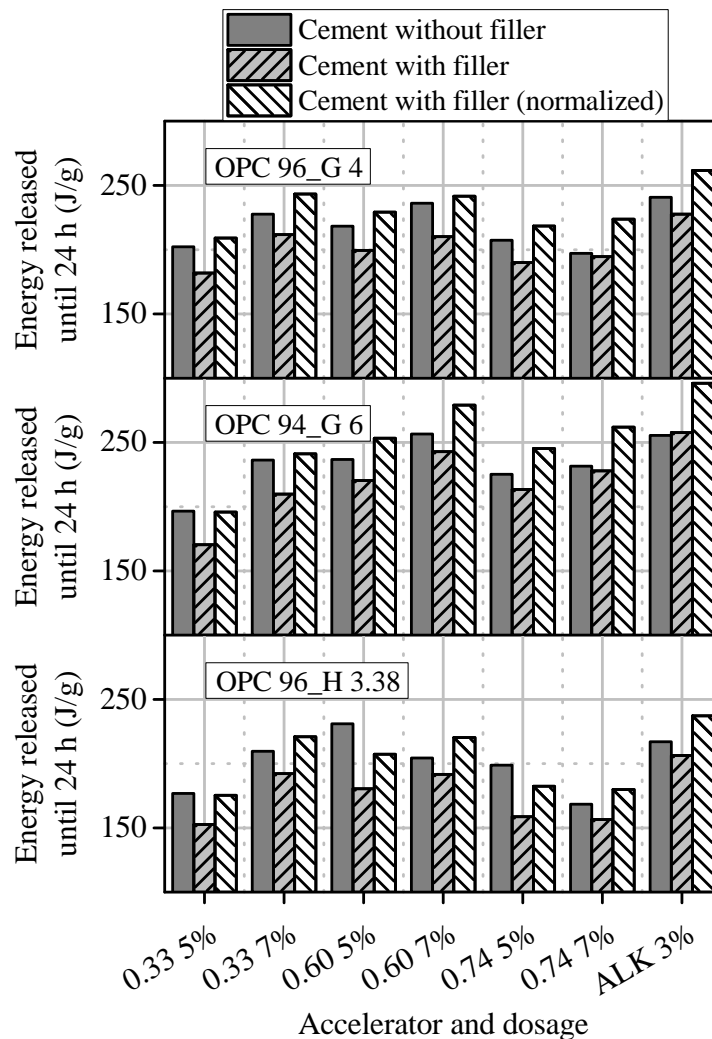
Figure 4.14 - Energy released until 24 h in pastes OPC 96_G 4, OPC 94_G 6 and OPC 96_H 3.38 with and without limestone filler.

The reactivity of the alkaline accelerator is slightly reduced by the use of limestone filler because this addition replaces part of the calcium sulfate contained in cement initially. As discussed in section 4.3.2.3, gypsum amount in cement is a key parameter to control the reaction of this accelerator. However, limestone filler compensates the fast sulfate depletion in alkaline accelerated pastes by controlling C_3A hydration, increasing their degree of hydration at 24 h.

4.3.2.7. Summary of results

Table 4.9 presents a summary of the parameters evaluated in this study and their influence on the overall hydration behavior of accelerated cement pastes. Ascending arrows indicate an increase in the parameter analyzed and descending arrows, a reduction.

Table 4.9 - Summary of the variables evaluated and their influence on hydration kinetics.

Parameter	Change	Refer to	Effect on hydration kinetics		
			Accelerator peak	Induction period	Main peak
Al^{3+} in accelerator or accelerator dosage	↑	Section: 4.3.2.1 Figure: 4.3	↑	Depends on Al_2O_3/SO_4^{2-} ratio and final C_3A/SO_3 ratio	Depends on Al_2O_3/SO_4^{2-} ratio and final C_3A/SO_3 ratio
Al_2O_3/SO_4^{2-} ratio of accelerator	↑ (above 0.60)	Section: 4.3.2.2 Figure: 4.4	-	Increase	
Gypsum amount	↑	Section: 4.3.2.3 Figures: 4.3, 4.7	↑	Increase	
Hemihydrate	↑	Section: 4.3.2.4 Figures: 4.8, 4.10	↑	Decrease	
C_3A content	↑	Section: 4.3.2.5 Figure: 4.11	↓	Decrease	
Limestone filler	↑	Section: 4.3.2.6 Figures: 4.12, 4.14	↑	Decrease	
Final C_3A/SO_3 ratio	↑	Section: 4.3.2.3 Figures: 4.5, 4.7	-	Increase	

4.4. Concluding remarks

Chapter 4 presented the evaluation of the influence of the chemical composition of cements and accelerators on the hydration behavior of accelerated cement pastes. The following conclusions may be drawn from the experimental results:

- Gypsum content in cement is a key parameter to balance sulfate consumption by accelerators and to control accelerator reactivity. Large gypsum amounts counterbalance high Al_2O_3/SO_4^{2-} ratios in accelerators and avoid uncontrolled C_3A reactions caused by sulfate depletion. As a result, alite hydrates properly and higher degrees of hydration are obtained until 24 h.

- The setting regulator type plays an important role in the overall hydration process. Calcium sulfate hemihydrate saturates the mixing water with calcium and sulfate ions faster than gypsum, which increases accelerator reactivity and leads to faster rates of precipitation of sulfoaluminate hydrates. The fast consumption of sulfate by accelerators results in accelerated C_3A reactions, with consequent formation of AFm phases. This process fills up the space available in the paste before the onset of the main hydration peak, decreasing the rate and extent of alite hydration. The combination of hemihydrate and accelerators with high Al_2O_3/SO_4^{2-} ratios is not adequate for proper cement hydration.

- A combination of gypsum and hemihydrate may be beneficious for cement hydration. Hemihydrate increases accelerator reactivity and sulfate left after accelerator reaction (in the form of gypsum) controls C_3A hydration. Therefore, initial strength gain rate should be faster and alite hydration could proceed normally, achieving higher degrees of hydration at 24 h.

- Cements containing low C_3A contents enhance accelerator reactivity because more sulfate is available for accelerator reaction. In pastes produced with SRC cements, the accelerated formation of AFm phases is avoided and alite dissolution is favored. On the other hand, induction periods are longer depending on accelerator type and the evolution of mechanical strength until 24 h may be compromised.

- Limestone filler improves accelerator reactivity when gypsum is the calcium sulfate source. Calcium carbonate reacts with Al^{3+} from accelerator, forming hemi and monocarboaluminate, and act as a nucleation site for the precipitation of sulfoaluminate

hydrated phases formed by accelerator reaction. Besides, it compensates the fast sulfate depletion caused by elevated accelerator dosages and avoids accelerated undersulfated C_3A reactions. As a result, alite hydration proceeds normally and higher degrees of hydration are achieved, when compared to CEM I pastes.

- Accelerators characterized by an Al_2O_3/SO_4^{2-} ratio equal to 0.33 (similar to ettringite) do not consume sulfate ions from the liquid phase and the initial C_3A/SO_3 ratio of cement is not altered. Therefore, unfavorable kinetics and mechanisms of cement hydration are avoided, increasing the rate and extension of alite hydration. However, ratios above 0.74 lead to a fast sulfate depletion and to accelerated undersulfated C_3A reactions. These processes limit the extension of alite hydration and may be detrimental for proper strength evolution.

- The final C_3A/SO_3 ratio of accelerated pastes may be used to predict the cement hydration behavior. This value should be kept between 0.67 and 0.90 in CEM I pastes containing gypsum and alkali-free accelerators to provide proper induction periods (below 4 h after accelerator addition) and alite hydration rates.

- As a recommendation, the selection of materials for an adequate compatibility between cement and accelerator should be based on the final C_3A/SO_3 ratio of the paste. Calcium sulfate amount in cement needs to be larger than 4.0 % and limestone filler should be employed. Al^{3+} supplied by accelerator should be in the range between 0.12 and 0.18 mmol/g cement, preferentially combining low Al^{3+} concentrations and high dosages of accelerator for a proper dispersion of these ions in the matrix. Finally, the Al_2O_3/SO_4^{2-} ratio of accelerator should be between 0.33 and 0.60.

- Summarizing, hydration of accelerated cementitious matrices is not a simple sum of the reactions of the isolated phases, but the resulting interaction among all hydrated and unhydrated phases during the whole process. Therefore, understanding the kinetics and mechanisms of hydration is extremely important in order to predict the behavior of the cementitious matrix during its service life.

5. Characterization of setting and hardening by ultrasound measurements

5.1. Introduction

Ultrasound (US) measurements are a versatile tool to characterize cementitious matrices. During the past years, several ultrasound techniques have been used to evaluate the setting process [119–121], mechanical strength [122,123], porosity [124–127], permeability [124–127] and durability [128,129] of pastes, mortars and concrete. The influence of different superplasticizers and additions on early strength development has also been evaluated [130–133].

Since ultrasound characterization is non-destructive, it is an important tool for quality control of conventional concrete mixes [134]. However, studies regarding sprayed concrete are limited due to the difficulty in following accelerated hydration reactions. Some studies have already been published about the subject [101,135] and the technique provided a continuous monitoring of the setting and hardening processes in accelerated cementitious matrices. It was more representative than Vicat, needle and pin penetration tests, since these standard methods are discontinuous and have a limited application range for sprayed concrete characterization [1].

Table 5.1 summarizes the most recent work conducted in the field of ultrasound measurements applied to cementitious matrices. Notice that the majority of the studies focuses on the characterization of conventional concrete by ultrasound propagation velocity and only a few also assesses the kinetics and mechanisms of hydration. None of them evaluates how accelerated chemical reactions and the resulting microstructure influence the propagation of ultrasound waves from a quantitative standpoint.

Table 5.1 - Summary of recent studies on ultrasound measurements applied to cementitious matrices.

Reference	Samples tested		Characterization			Quantitative relation between ultrasound and phase evolution
	Conventional	Accelerated	Ultrasound	Kinetics	Phase evolution	
[114,125, 127,128]	•		•	•		
[115–123, 126]	•		•			
[129]	•		•		•	
[101]		•	•	•		
[135]		•	•			
This study (Chapter 5)		•	•	•	•	•

The lack of such relations may compromise the characterization of accelerated cementitious matrices and the applicability of ultrasound measurements in practice. Therefore, it is fundamental to better comprehend how the chemical reactions occurring when accelerators are added and the resulting phase evolution influence the overall response to ultrasound propagation throughout the whole hydration process. By doing so, a more complete characterization of the evolution of mechanical properties of the matrix at early ages may be achieved, improving its design and quality control.

The objectives of the experimental campaign conducted in this chapter are:

- Characterize setting and hardening processes in accelerated cement pastes and mortars by ultrasound measurements.

- Identify the main properties and parameters that govern the propagation of ultrasound waves.

- Correlate chemical properties and phase composition with ultrasound propagation velocity.

In this part of the experimental program, tests were performed with cement pastes and mortars produced by mechanical mixing. The mix composition of the matrices was the same as the ones used in chapter 3. The experimental methodology consisted in monitoring the setting and hardening processes as well as the microstructure development by ultrasound propagation velocity. To complement this analysis, setting times were determined by the Vicat needle test and hydration kinetics were characterized by evolution of temperature. Results obtained by *in situ* XRD (presented in chapter 3) were used to explain the evolution of ultrasound propagation velocity.

Multivariate regression analyses were conducted to better comprehend how ultrasound velocity and the chemical properties of the matrix are related. Results indicate the main chemical parameters that influence microstructure development and ultrasound propagation velocity, explaining their origin. The correlations obtained are a simple useful tool to evaluate in a quantitative way how the ultrasound velocity is affected by the chemical characteristics of the matrix. Therefore, this study potentiates the use of this technique for characterization and control of matrices containing accelerators and for the evaluation of accelerator reactivity and compatibility with cement.

5.2. Experimental methodology

5.2.1. Materials

Cements, water, superplasticizer and accelerators employed in this section are the same as the ones used in chapter 3 (described in section 3.2.1). For the fabrication of mortars, standard silica sand following the requirements from UNE EN 196-1:2005 [136] was used.

5.2.2. Composition and preparation of cement pastes and mortars

5.2.2.1. Cement pastes

Cement pastes contained the same superplasticizer and accelerators dosages as pastes evaluated in chapter 3 (section 3.2.2) and present the composition shown in table 3.5. The amount of paste required for the determination of setting times and ultrasound propagation

velocity was approximately 700 g. Therefore, pastes could not be hand-mixed following the preparation method from chapter 3. Instead, they were mechanically mixed in a conventional mixer, adapting the procedures from UNE-EN 196-3:2005 [99], at 20 ºC and 50 % relative humidity. Accelerators were also added 1 h after cement and water had been mixed. The resulting paste was homogenized for 15 s at high speed. The molds for both tests were filled and consolidated manually right after accelerator homogenization.

Even though the preparation of pastes used for ultrasound measurements were not the same as for the tests performed in chapter 3, it does not limit the comparison of results. In each particular test, identical mixing procedures were employed for all the pastes. Therefore, the differences observed in their hydration behavior may be associated exclusively to the reactions occurring between cements and accelerators.

5.2.2.2. Mortars

Mortars were prepared using a sand/cement ratio equal to 2.0, w/c ratio equal to 0.45 and superplasticizer at 1.0 % bcw. Mortars contained the same accelerators dosages as cement pastes and also presented the composition shown in table 3.5. Batches containing 2330 g were prepared in a conventional mortar mixer, according to EN 196-1:2005 [136]. Accelerator addition and mold filling followed the same procedures as in cement pastes.

5.2.3. Test methods

Table 5.2 shows the tests performed with accelerated pastes and mortars. Their descriptions are presented subsequently. Setting times were determined with reference and accelerated pastes produced with CEM I and CEM II/A-L and accelerators AKF 0.38 7%, AKF 0.42 11%, AKF 0.61 5%, AKF 0.61 7% and ALK 3%. Ultrasound propagation velocity and evolution of temperature were obtained with reference and accelerated pastes and mortars, using the same mix composition as for the determination of setting times. Apart from these tests, results obtained with *in situ* XRD from section 3.3.3 will be used for discussion of results and regression analyses.

Table 5.2 - Tests performed with cement pastes and mortars.

Test	Sample	Age / period of time
Determination of setting times	Fresh paste	Until final setting time
Determination of US wave propagation velocity	Fresh paste and mortar	0 - 24 h
Evolution of temperature	Fresh paste and mortar	0 - 24 h

5.2.3.1. Determination of setting times

Setting times were determined using an automatic Vicat penetrometer. Although the standard UNE EN 196-3 (2005) [99] prescribes the use of a normal consistency paste, a w/c equal to 0.45 was adopted to facilitate handling and molding of the accelerated pastes and to use the same composition as the one employed for the other tests. Moreover, when low w/c ratios are used (0.27 - 0.32, for example), initial setting occurs approximately 2 min after accelerator addition, even when superplasticizers are used [5]. This would make the paste unworkable before the mold was filled, leading to inaccuracies in the results.

5.2.3.2. US wave propagation velocity and evolution of temperature

Longitudinal ultrasound wave (P-wave) propagation velocity was used to monitor the setting and hardening processes and the microstructure development in fresh accelerated cement pastes and mortars. The device used for this measurement is similar to the FreshCon system [137]. The container consists of 2 polymethacrylate walls and 4 spacers measuring 22 mm in length between them, where a U-shaped foam mold with an approximate volume of 140 mL is placed. On each exterior side of the container, a longitudinal wave transducer of 500 kHz of central frequency is attached.

Ultrasonic P-waves are generated by a wireless sensor network named WilTempUS, developed by the G-CARMA research group [134]. This system is composed by a base and a mote that monitor temperature, relative humidity (T/RH) and ultrasonic velocity at same time. Two channels coupled with commercial SHT15 sensors from Sensirion Company were employed to measure the temperature of the environment and the evolution of temperature of the hydrating sample. This experiment was performed during 24 h, with a recording interval of 10 s during the first 2 h and of 1 min after that.

Figure 5.1 shows the equipment used and the execution of the experiment. As tests were performed with accelerated cement matrices, shrinkage could cause the loss of contact between the matrix and the mold, interrupting the propagation of ultrasonic waves. To solve this problem, a coupling device formed by two springs pressing on the walls of the mold was used [138]. In addition, the equipment was placed inside a sealed plastic box with relative humidity above 95 % to avoid decoupling.
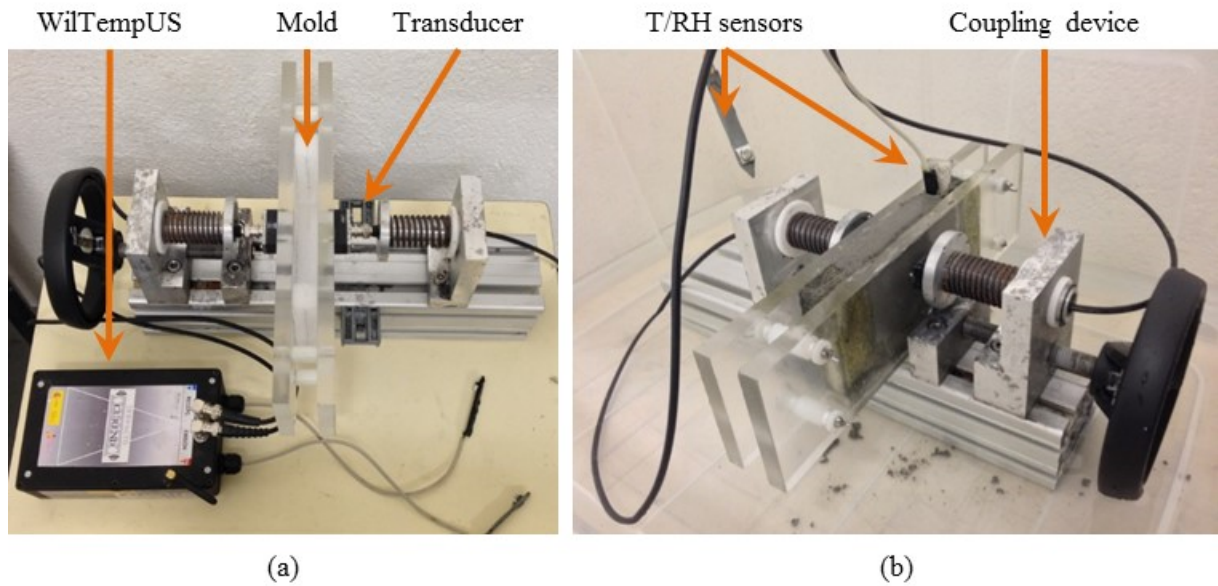
Figure 5.1 - Equipment for ultrasound measurements (a) and execution of the test (b).

Ultrasound measurements were performed in cement pastes and mortars. In cement pastes, kinetics and mechanisms of hydration are not influenced by aggregates and may provide a clearer evaluation of the chemical processes occurring during hydration. However, accelerated pastes are very reactive and shrinkage may limit the progression of the test. Therefore, accelerated mortars were also evaluated because aggregates provide more space for the precipitation of hydrated phases and reduce reaction rates. As a result, the negative effects of chemical shrinkage are minimized and a continuous monitoring of setting and hardening may be obtained.

5.3. Results and discussion

5.3.1. Setting times

Figure 5.2 presents setting times determined with cement pastes. Results obtained vary considerably in pastes with and without accelerators. Cement hydration in reference pastes is significantly retarded by the superplasticizer, increasing setting times.
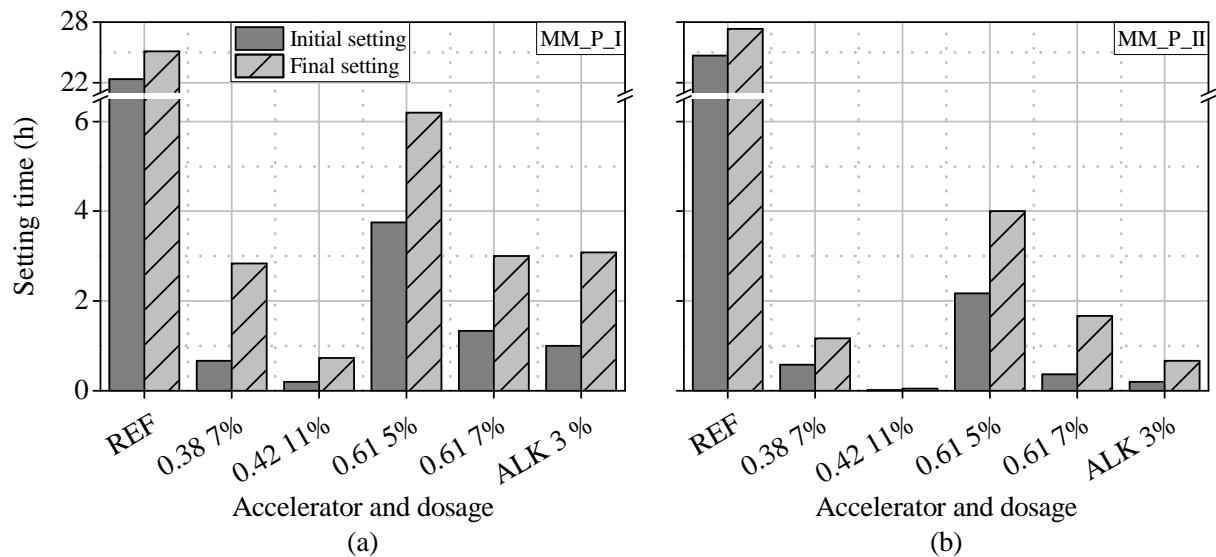
Figure 5.2 - Setting times determined with CEM I (a) and CEM II/A-L (b) mechanically mixed pastes.

Setting times are reduced in accelerated pastes and depend on cement type, accelerator type and dosage. Pastes produced with CEM II/A-L present shorter setting times than equivalent CEM I pastes. As discussed in section 4.3.2.6, limestone filler reacts with aluminum ions from accelerators, forming AFm phases [5]. Moreover, as cement is diluted by the filler addition, a larger space is available for the precipitation of hydrates [64]. Both processes contribute to reduce setting times.

As observed in *in situ* XRD (section 3.3.3), the amount of ettringite formed in accelerated pastes is directly proportional to Al^{3+} concentration in accelerators. Since ettringite is the main product that leads to initial mechanical strength in the matrices evaluated, the larger the amount of ettringite formed by accelerator reaction, the shorter the setting times of the pastes. Therefore, the ascending order of setting times is AKF 0.42 11% < ALK 3% < AKF 0.38 7% < AKF 0.61 7% < AKF 0.61 5% < REF.

5.3.2. US wave propagation velocity and evolution of temperature

5.3.2.1. Influence of phase evolution during hydration on ultrasound velocity

Figures 5.3 and 5.4 present the P-wave velocity, evolution of temperature and phase composition of pastes I_AKF 0.42 11% and II_AKF 0.61 5%, respectively. Theses pastes were selected because they presented the fastest and the slowest kinetics of hydration, respectively. The results of all the tests are presented altogether in order to recognize the main chemical processes that influence ultrasound propagation in the hydrating matrix. Five different stages, which are described subsequently, may be recognized in each picture.
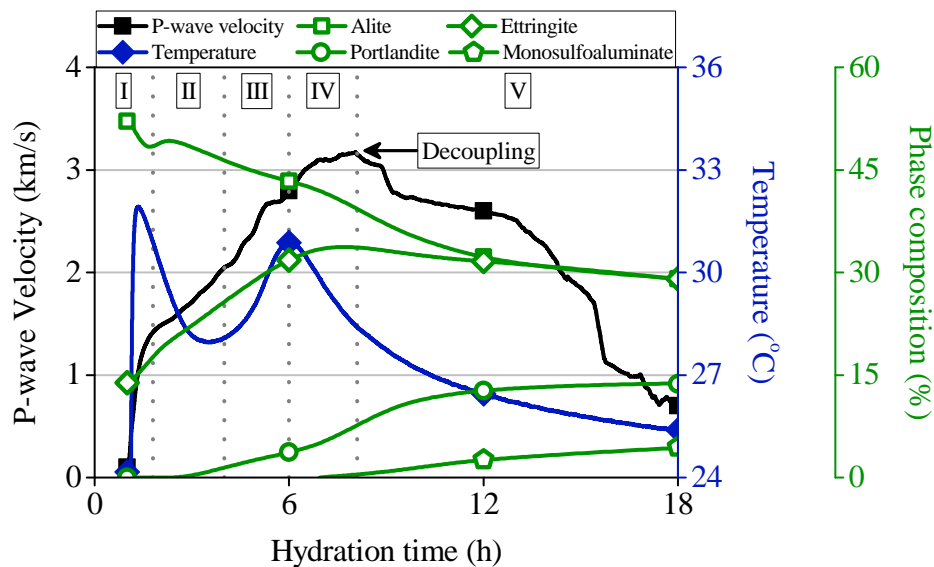
Figure 5.3 - Evolution of P-wave velocity, temperature and phase composition of paste MM_I_ALK 0.42 11%.
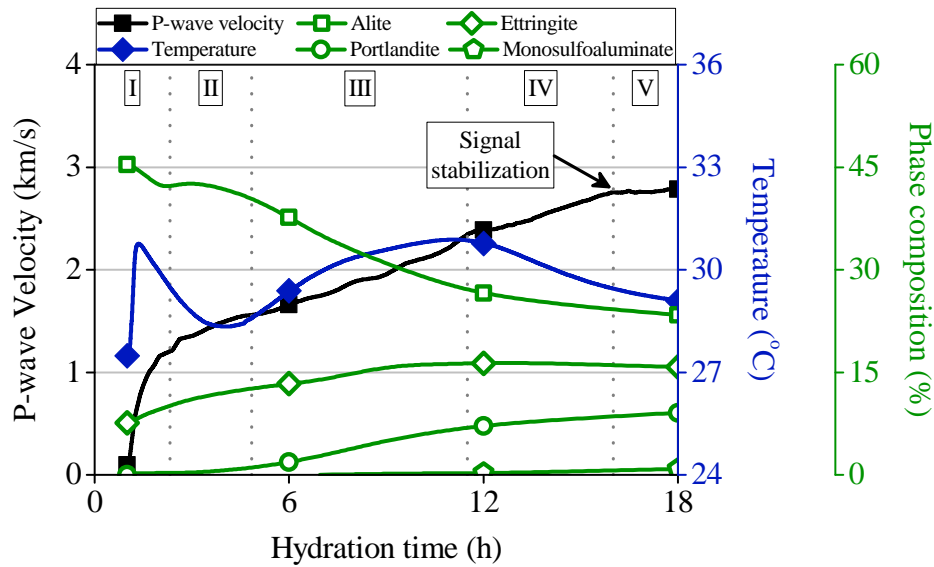
Figure 5.4 - Evolution of P-wave velocity, temperature and phase composition of paste MM_II_AKF 0.61 5%.

Stage I - accelerator reaction

Fast exothermic ettringite precipitation caused by accelerator reaction. This process increases the solid/liquid ratio of the matrix and improves the solid phase connectivity quickly. As a result, a sharp increase in ultrasound propagation velocity occurs, directly proportional to accelerator reactivity. Alite dissolution is minimal and does not contribute to increase P-wave velocity.

Stage II - induction period

The rate of ettringite formation decreases, consequently reducing the slope of ultrasound velocity curve at 1.8 and 2.3 h in pastes I_AKF 0.42 11% and II_AKF 0.61 5%, respectively. The temperature of the pastes also reduces due to low reaction rates. The extent of alite consumption and portlandite precipitation is low and does not influence propagation velocity.

Stage III - acceleration period

The onset of alite hydration occurs, with consequent precipitation of portlandite and C-S-H. C_3A hydration continues, as observed by the constant formation of ettringite. As hydration progresses and microstructure develops, the interconnectivity among solid particles improves

and the porosity of the matrix decreases. As a result, a constant increase in ultrasound propagation velocity is observed, which is directly proportional to the temperature rise of the matrix and to the rate of alite consumption.

Stage IV - deceleration period

Hydration rate starts to decelerate, leading to reductions in temperature and in the rate of increase of ultrasound propagation velocity.

Stage V - deceleration period

The transition from stage IV to stage V is accompanied by an inflection point in P-wave velocity. The test was interrupted in paste I_AKF 0.42 11% at around 8 h, due to the shrinkage of the paste and consequent decoupling of transducers. The loss of contact between the mold and the matrix coincides with the beginning of ettringite conversion to monosulfoaluminate. As ettringite has a relative low density and high molecular volume when compared to AFm phases [16,68], its consumption by C_3A and C_4AF hydrations leads to matrix shrinkage. This process happens mainly in CEM I pastes, due to its high C_3A content, and when accelerators containing high aluminum concentrations are employed, because large ettringite amounts are produced. In these cases, pore filling caused by C-S-H and portlandite formation does not compensate the shrinkage originated by ettringite consumption.

In paste II_AKF 0.61 5%, decoupling of transducers does not occur. Instead, ultrasound velocity stabilizes and remains constant after the beginning of stage V. As ettringite is indirectly stabilized by limestone filler [45] and its consumption occurs at a lower rate and extent than in paste I_AKF 0.42 11%, the reduction in the volume of aluminate hydrated phases is smaller. Therefore, shrinkage does not cause the loss of contact between mold walls and the matrix and ultrasound measurements continue.

5.3.2.2. General results of cement pastes and mortars

Figures 5.5 and 5.6 present the P-wave velocity and the evolution of temperature of cement pastes and mortars, respectively. Results obtained with CEM I are grouped on the left

and with CEM II/A-L are grouped on the right. Discussion is presented subsequently, organized by matrix type, cement type and accelerator type and dosage.
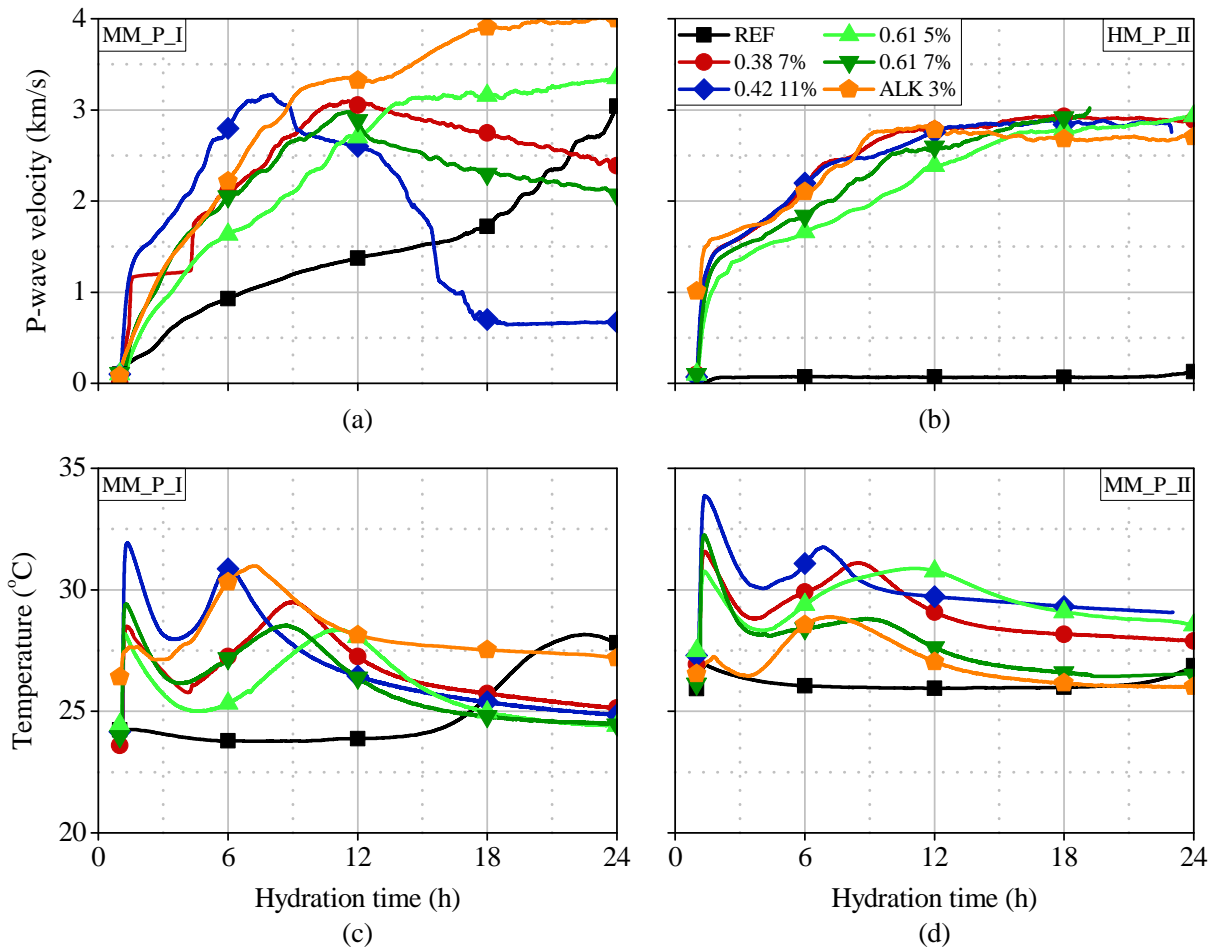
Figure 5.5 - Evolution of P-wave velocity (a and b) and temperature (c and d) in CEM I and CEM II/A-L mechanically mixed pastes from accelerator addition to 24 h.
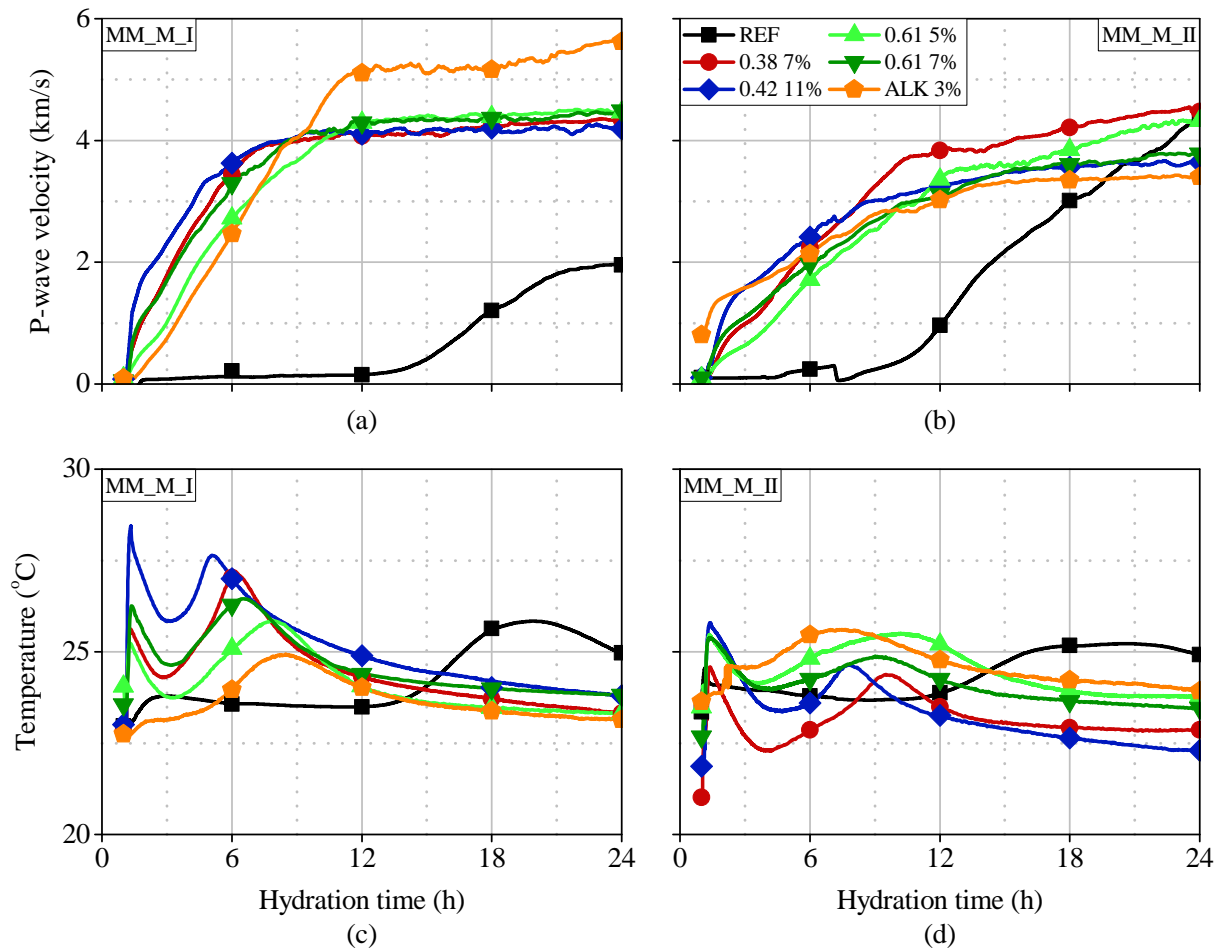
Figure 5.6 - Evolution of P-wave velocity (a and b) and temperature (c and d) in CEM I and CEM II/A-L mechanically mixed mortars from accelerator addition to 24 h.

Matrix type

Accelerator reactivity may be evaluated equally in either pastes or mortars. As pastes are constituted by more reactive systems, reaction kinetics are faster and a more resolved differentiation of the chemical processes occurring in the hydrating matrix is achieved. However, the shrinkage of pastes is more intense, which may lead to decoupling of transducers and interrupt the progression of the test when accelerators containing high Al^{3+} concentrations are used.

In mortars, aggregates dilute cement and accelerator and provide more space for hydration to occur. Therefore, shrinkage does not affect the progression of the test negatively and measurements are not interrupted. The development of microstructure derived from cement hydration and the reduction in porosity are clearer when mortars are employed. In reference

mortars, the main hydration process starts earlier than in reference cement pastes because aggregates increase the shearing during mixing and accelerate cement hydration [12].

Cement

Accelerator reactivity is improved in CEM II/A-L matrices. Since this cement contains 23 % less C_3A and 20 % more hemihydrate than CEM I (table 3.1), more sulfate is available to react with aluminum ions from accelerators and ettringite formation is favored. As discussed in section 4.3.2.6, limestone filler reacts with aluminum ions from accelerators [5] and provides a larger space for the precipitation of hydrates [64], increasing ultrasound propagation velocity. These processes also contribute to avoid the decoupling of transducers. As can be observed in figure 5.5.b, no decoupling occurred in CEM II/A-L pastes because the rate of ettringite conversion to AFm phases is lower than in equivalent CEM I pastes (according to figures 3.7.e and 3.7.f).

CEM I matrices present faster hydration kinetics because this cement contains more alite (table 3.1) and is finer than CEM II/A-L (table 3.3). Therefore, the rate of ultrasound velocity increase and the maximum velocity reached after the acceleration period are intensified. However, decoupling occurs more often due to the faster ettringite consumption by C_3A hydration (section 3.3.3). The ultrasound velocity curve in pastes I_AKF 0.38 7%, I_AKF 0.42 11% and I_AKF 0.61 7% were interrupted after the deceleration period.

Accelerator type and dosage

Hydration of pastes and mortars without accelerator is significantly retarded by the superplasticizer. Induction periods in these matrices are long and the main hydration process starts approximately at 14 h in mortars and after 18 h in pastes. The beginning of ultrasound velocity increase coincides with the onset of the main hydration peak in the curves of evolution of temperature.

In accelerated matrices, P-wave velocity depends on accelerator reactivity and is directly proportional to the amount of Al^{3+} added to the matrix. Matrices produced with AKF 0.42 11% present the highest values of ultrasound velocity in the first stage because this accelerator produces the largest amount of ettringite and, therefore, the largest interconnectivity

in the solid phase. On the contrary, pastes and mortars I_AKF 0.61 5% and II_AKF 0.61 5% present the lowest rate of ultrasound velocity increase, since AKF 0.61 used at 5.0 % bcw is the least reactive accelerator and provides the lowest amount of Al^{3+} ions. The descending order of ultrasound velocity in stage I is AKF 0.42 11% > AKF 0.38 7% > AKF 0.61 7% > AKF 0.61 5%, which is the reverse order observed in the determination of setting times.

During the acceleration period, the rate of ultrasound velocity increase is directly proportional to the degree of hydration of alite and C_3A and to the evolution of temperature of the matrix. In systems presenting low C_3A/SO_3 ratios (when accelerators AKF 0.38 and AKF 0.42 are employed) alite hydration is responsible for ultrasound velocity increase. Besides, the formation of AFm phases by accelerated C_3A reactions in matrices containing AKF 0.61 and ALK also contribute to increase P-wave velocity during the main hydration process.

Ultrasound velocity curves of mortars (figures 5.6.a and 5.6.b) indicate that accelerators that provide a sharp initial velocity increase tend to reduce the maximum velocity reached after the beginning of the deceleration period. On the contrary, accelerators containing low Al^{3+} concentrations lead to a low increase in ultrasound velocity due to accelerator reaction, but the maximum velocity reached after the main hydration peak is above the values of the other mortars. The first case is exemplified by mortars I_AKF 0.42 11% and II_AKF 0.42 11% and the second case occurs with mortars I_AKF 0.61 5% and II_AKF 0.61 5%. The ascending order of ultrasound velocity in stage V in CEM I mortars is AKF 0.42 11% < AKF 0.38 7% < AKF 0.61 7% < AKF 0.61 5%, which is the same order observed in the determination of setting times.

The main reason for this fact is that matrices produced with accelerators containing high Al^{3+} concentrations stiffen quickly and do not consolidate properly [1]. As a consequence, they present higher porosities, which decrease P-wave velocity. In contrast, setting times in matrices containing low reactive accelerators are longer, which leads to a better consolidation. Therefore, ultrasound propagation in the deceleration period is enhanced and its velocity increases.

In addition, since the elastic modulus of AFm phases is respectively 2 and 3.5 times higher than those of ettringite and C-S-H (E_{AFm} = 42.3 GPa [139], $E_{Ettringite}$ = 22.4 GPa [139], $E_{C\text{-}S\text{-}H}$ = 12.0 GPa [140]), undersulfated systems may lead to higher P-wave velocities during stage V. AFm phases formed by C_3A hydration increase the elastic modulus of the matrix [125] and, therefore, lead to increases in ultrasound velocity. This is the case of paste and mortar I_ALK 3% (C_3A/SO_3 ratio equal to 0.76, table 3.5).

Paste and mortar II_ALK 3% present a different behavior from the equivalent CEM I matrices. Since the alkaline accelerator does not contain any sulfate in its formulation, aluminate ions react with calcium ions and limestone filler, forming monosulfoaluminate and hemicarboaluminate (chemical equations 2.12 and 2.15 from table 2.5). These phases fill up the pores and increase the elastic modulus of the matrix quickly. Therefore, ultrasound velocity increases sharply, faster than in pastes and mortars containing alkali-free accelerators. However, as the early formation of AFm phases limits further alite hydration, pastes and mortars II_ALK 3% present the lowest increase in ultrasound velocity from the acceleration period on.

5.3.2.3. Comparison with final setting times

Table 5.3 presents the final setting times and the ultrasound velocity of accelerated cement pastes at the time of final set. The average ultrasound velocity for CEM I pastes is (1.54 ± 0.09) km/s and for CEM II/A-L pastes is (1.53 ± 0.05) km/s. These results indicate that final set occurs when ultrasound velocity reaches 1.5 km/s, approximately. Paste II_AKF 0.42 11% deviates from this behavior due to the high accelerator reactivity and consequent difficulties in molding operations (this paste was not used for the calculation of average results).

Table 5.3 - Comparison of final setting times and US velocity in mechanically mixed accelerated cement pastes.

Paste	Final setting time (h)	US velocity at final setting time (km/s)
I_AKF 0.38 7%	2.8	1.48
I_AKF 0.42 11%	0.73	1.39
I_AKF 0.61 5%	6.1	1.64
I_AKF 0.61 7%	3.0	1.59
I_ALK 3%	3.1	1.59
II_AKF 0.38 7%	1.2	1.49
II_AKF 0.42 11%	0.050	0.30
II_AKF 0.61 5%	4.0	1.57
II_AKF 0.61 7%	1.7	1.46
II_ALK 3%	0.67	1.58

The results shown in table 5.3 are in accordance with Reinhardt and Grosse [137], who reported that final set could be determined when ultrasound velocities reach 1.50 km/s. This value may also be adopted to determine final setting times in accelerated matrices.

Initial setting could not be correlated to ultrasound velocity because the equipment used in this research employs P-waves. Transversal waves (S-waves) should be used to characterize initial setting times [119].

5.4. Multivariate regression analyses

In this section, general models to predict ultrasound propagation velocity in accelerated matrices were developed based on multivariate regression analyses. P-wave velocities in mortars were selected as the standard dependent variables, because the results obtained with pastes were negatively affected by shrinkage and consequent decoupling of transducers. They were divided in three stages (accelerator reaction: from accelerator addition until 3 h; acceleration period: from 5 to 11 h; and deceleration period: from 13 h on) in order to provide a more meaningful analysis.

The independent variables correspond to the chemical properties of cement and accelerators and phase composition of pastes determined by *in situ* XRD (section 3.3.3). The most statistically significant independent variables were selected by analyses of variance (p-values below 0.05, confidence level above 95 %) and are shown in table 5.4. Although only two cement types were evaluated, limestone filler was adopted as an independent variable because it improves all the fitted models. These parameters are considered appropriate based on principles of accelerators, cement and hydration chemistry. Results are presented from sections 5.4.1 to 5.4.4.

Table 5.4 - Selection of statistically significant variables to model ultrasound velocity.

US velocity stage	Independent variables
Accelerator reaction	Time, ettringite content in paste, aluminum and sulfate contents in accelerator, filler content in cement
Acceleration period	Time, amorphous, ettringite and AFm contents in paste, filler content in cement
Deceleration period	Amorphous, ettringite and AFm contents in paste, filler content in cement, final C_3A/SO_3 ratio

5.4.1. Accelerator reaction (from accelerator addition until 3 h)

Table 5.5 presents the parameters used to model ultrasound velocity generated by accelerator reaction, their coefficients and p-values. Equation 5.1 represents the best-fit model obtained and figure 5.7 shows a plot of the ultrasound velocity determined experimentally versus the values predicted by the model.

Table 5.5 - Parameters adopted to model ultrasound velocity increase due to accelerator reaction.

Parameter	Abbreviation	Coefficient	P-value
Constant	-	- 1.53	< 0.001
Time (h)	t	0.826	0.001
(Time)^2	t^2	- 0.195	0.025
Ettringite content in paste (%)	E	0.0286	0.001
Aluminum content in accelerator (mmol/g cement)	Al	6.35	< 0.001
Sulfate content in accelerator (mmol/g cement)	$\bar{S}$	1.76	0.018
Filler content in cement (%)	F	0.101	< 0.001
Time·Sulfate content in accelerator	$t \cdot \bar{S}$	1.76	< 0.001
Time·Filler content in cement	$t \cdot F$	- 0.0199	0.017
Sulfate content in accelerator·Filler content in cement	$\bar{S} \cdot F$	- 0.695	< 0.001

$$V_{US} \text{ (km/s)} = \frac{-1.53 + 0.826 \cdot t - 0.195 \cdot t^2 + 0.0286 \cdot E + 6.35 \cdot Al + 1.76 \cdot \bar{S} +}{0.101 \cdot F + 1.76 \cdot t \cdot \bar{S} - 0.0199 \cdot t \cdot F - 0.695 \cdot \bar{S} \cdot F} \qquad \text{Equation 5.1}$$
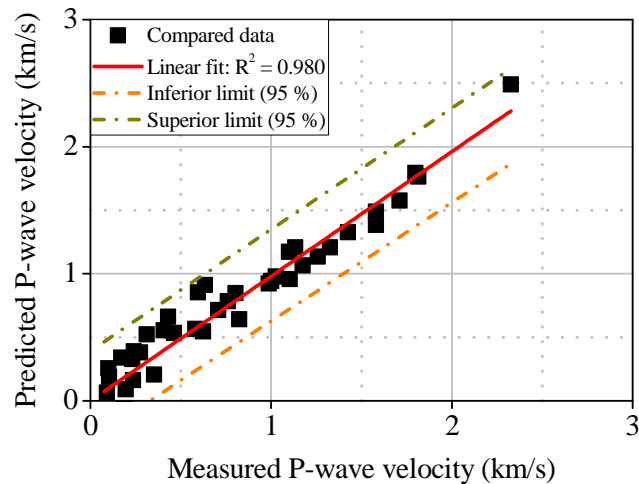
Figure 5.7 - Plot of measured versus predicted ultrasound propagation velocity due to accelerator reaction.

An overall R^2 value of 0.980 was achieved, demonstrating that the model proposed provides a statistically significant prediction of the measured results. It indicates that ultrasound velocity increases with time, depends majorly on accelerator reactivity and is influenced by limestone filler, in accordance with the discussion in section 5.3.2.

Furthermore, the model demonstrates that P-wave velocity is a function of ettringite amount produced by accelerator addition. Since ettringite is the main product that leads to the interconnectivity in the solid phase, the larger the amount of ettringite formed by accelerator reaction, the higher the ultrasound velocity in the matrix. The use of high dosages of accelerators and formulations containing high concentrations of aluminum and sulfate contribute to form ettringite, reducing setting times and increasing the rate of ultrasound velocity growth. Such situation is reflected in equation 5.1, since the ettringite content in paste and the aluminum and sulfate contents in accelerator appear with a positive sign.

5.4.2. Acceleration period (from 5 to 11 h)

Table 5.6 shows the parameters adopted to model ultrasound velocity during the acceleration period, their coefficients and p-values. Equation 5.2 presents the final model obtained and figure 5.8 represents a plot of the measured versus predicted ultrasound velocity.

Table 5.6 - Parameters selected to model ultrasound velocity increase during the acceleration period.

Parameter	Abbreviation	Coefficient	P-value
Constant	-	0.603	0.045
Time (h)	t	0.385	< 0.001
Amorphous phases content in paste (%)	Am	0.136	0.014
Ettringite content in paste (%)	E	0.0343	< 0.001
Filler content in cement (%)	F	- 0.0976	< 0.001
(AFm phases content in paste)^2 (%)	AFm^2	0.440	< 0.001
Time·Amorphous phases content in paste	t·Am	- 0.0214	0.009
Ettringite content in paste·AFm phases content in paste	E·AFm	- 0.0417	< 0.001

$$V_{US} \text{ (km/s)} = \frac{0.603 + 0.385 \cdot t + 0.136 \cdot Am + 0.0343 \cdot E - 0.0976 \cdot F +}{0.440 \cdot AFm^2 - 0.0214 \cdot t \cdot Am - 0.0417 \cdot E \cdot AFm} \quad \text{Equation 5.2}$$
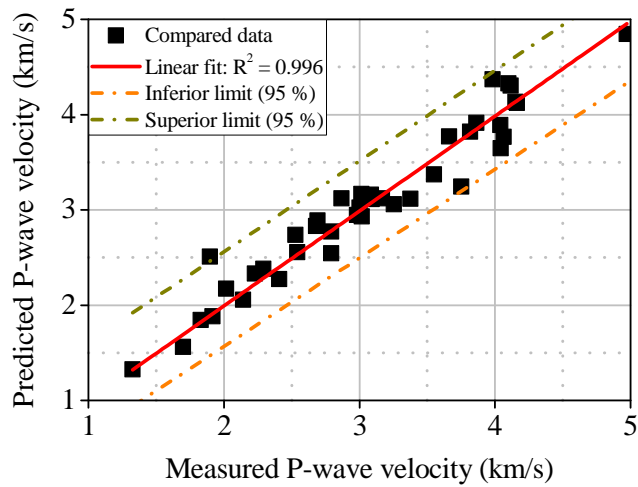
Figure 5.8 - Plot of measured versus predicted ultrasound propagation velocity during the acceleration period.

The fitted model presents R^2 equal to 0.996 and suggests a high correlation between measured and predicted ultrasound velocity during the acceleration period. It indicates that P-wave velocity depends on accelerator reaction, alite and C_3A hydrations.

P-wave velocity is directly proportional to C-S-H and ettringite contents in the matrix, because these phases determine the interconnectivity in the solid phase. Moreover, undersulfated systems present higher P-wave velocity, as AFm phases formed by C_3A hydration

increase the elastic modulus of the matrix (section 5.3.2). Since limestone filler postpones C_3A hydration, it contributes to reduce ultrasound velocity during the acceleration period.

5.4.3. Deceleration period and signal stabilization (from 13 h on)

Table 5.7 presents the parameters selected to model ultrasound velocity during the deceleration period, their coefficients and p-values. Equation 5.3 represents the final model obtained and figure 5.9 shows a plot of the ultrasound velocity determined experimentally versus the values predicted by the model.

Table 5.7 - Parameters adopted to model ultrasound velocity increase during the deceleration period.

Parameter	Abbreviation	Coefficient	P-value
Constant	-	4.81	< 0.001
Ettringite content in paste (%)	E	- 0.0540	< 0.001
AFm phases content in paste (%)	AFm	0.236	0.001
Filler content in cement (%)	F	0.132	< 0.001
(Final C_3A/SO_3 ratio)^2	$(C/\bar{S})^2$	2.07	0.001
Amorphous phases content in paste·AFm phases content in paste	Am·AFm	- 0.124	0.001
Filler content in cement·Final C_3A/SO_3 ratio	F·C/$\bar{S}$	- 0.433	< 0.001

$$V_{US} \text{ (km/s)} = \begin{array}{c} 4.81 - 0.0540 \cdot E + 0.236 \cdot AFm + 0.132 \cdot F + 2.07 \cdot (C/\bar{S})^2 - \\ 0.124 \cdot Am \cdot AFm - 0.433 \cdot F \cdot C/\bar{S} \end{array} \qquad \text{Equation 5.3}$$
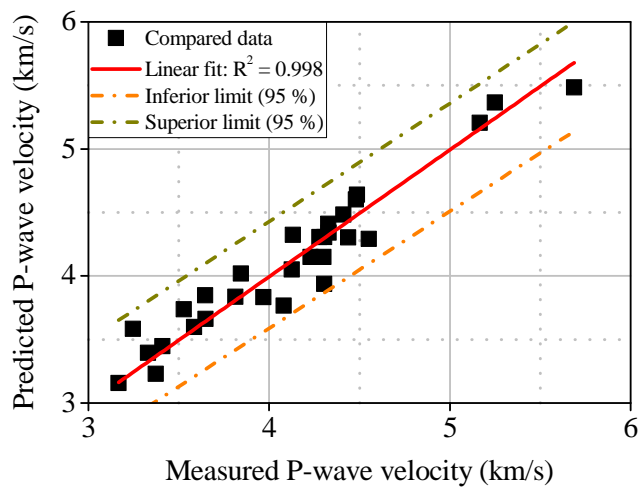
Figure 5.9 - Plot of measured versus predicted ultrasound propagation velocity during the deceleration period.

A high correlation between experimental and predicted data was obtained ($R^2 = 0.998$). This model indicates that undersulfated systems (high C_3A/SO_3 ratios) present higher ultrasound propagation velocities than properly sulfated matrices, due to their larger amounts of AFm phases and lower contents of ettringite and C-S-H (section 5.3.2). This corroborates the fact the accelerators ALK and AKF 0.61 lead to higher ultrasound propagation velocities than accelerators AKF 0.38 and 0.42. In addition, since limestone filler leads to the formation of hemi and monocarboaluminate, it also favors ultrasound propagation in the deceleration period.

5.4.4. Summary of results

Table 5.8 presents a summary of the parameters studied and their influence on the overall ultrasound wave propagation velocity. Ascending arrows indicate an increase in the parameter analyzed and descending arrows, a decrease. The number of arrows in each cell is directly proportional to the influence of the parameter analyzed, taking into account their coefficient obtained in each regression from sections 5.4.1 to 5.4.3.

Table 5.8 - Summary of the variables evaluated and their influence on ultrasound propagation velocity.

Parameter	Change	Effect on P-wave propagation velocity		
		Accelerator reaction	**Acceleration period**	**Deceleration period**
Al^{3+} in accelerator or accelerator dosage	↑	↑ ↑ ↑	-	-
SO_4^{2-} in accelerator	↑	↑	-	-
Ettringite amount formed by accelerator	↑	↑ ↑	↑	↓
Filler content in cement	↑	↑	↓	↑
Amorphous (C-S-H) content	↑	-	↑ ↑	↓
AFm content	↑	-	↑ ↑	↑ ↑ ↑
Final C_3A/SO_3 ratio	↑	-	-	↑ ↑

5.5. Concluding remarks

Chapter 5 presented the characterization of setting and hardening processes of accelerated cement pastes and mortars by ultrasound measurements. The following conclusions may be drawn from the experimental results:

- Ultrasound measurements provide a clear and continuous evaluation of setting, hardening and microstructure development during hydration of accelerated cement matrices. The technique employed was sensitive to cement composition, accelerator type and dosage and could distinguish hydration stages. It is an interesting tool for research and development of new accelerator formulations.

- Initial microstructure development is governed by accelerator reactivity. Ettringite formed by accelerator reaction increases the solid/liquid ratio of the matrix and improves the interconnectivity in the solid phase quickly. Consequently, ultrasound velocity increases sharply and is directly proportional to aluminum content in accelerators.

- Increase of P-wave velocity during the acceleration period is directly proportional to hydration rates. As alite and C_3A hydrate, forming respectively C-S-H and AFm phases, ultrasound velocity increases.

- When accelerators containing high aluminum contents are employed, the matrix stiffens quickly and does not consolidate properly. For that reason, the porosity of the matrix is high and P-wave velocity during the deceleration period is reduced.

- Undersulfated systems present higher ultrasound velocities during the deceleration period than properly sulfated matrices. C_3A hydration in the absence of sulfates leads to higher ultrasound velocities because the elastic modulus of AFm phases is 2 and 3.5 times higher than the elastic modulus of ettringite and C-S-H, respectively.

- Limestone filler decreases ultrasound velocity in the acceleration period because it retards C_3A hydration. However, P-wave velocity increases in the deceleration period in CEM II/A-L matrices because limestone leads to the formation of hemi and monocarboaluminate and provides a larger space for the precipitation of hydrates.

- Decoupling of transducers in cement pastes is associated with ettringite conversion to monosulfoaluminate. As AFm phases are denser than ettringite, their formation leads to matrix shrinkage and to the consequent loss of contact between the matrix and mold walls. Decoupling occurs mainly when cements contain large C_3A amounts and no limestone filler and when high Al^{3+} contents are added to the matrix.

- Final setting times in accelerated pastes may be determined when P-wave velocity reaches 1.5 km/s.

- Correlations between ultrasound propagation velocity in mortars and their chemical properties and phase composition were established. All regressions presented R^2 superior than 0.980, indicating that the models developed provide statistically significant predictions of the experimental results.

6. Influence of spraying on hydration[3]

6.1. Introduction

Sprayed concrete differs from conventional concrete due to the method of application and the use of accelerators to promote a rapid stiffening of the matrix right after mixing [1]. Accelerators are normally added to concrete at the nozzle, just before it is sprayed onto the substrate. As discussed in section 2.4.1, the method employed to fabricate accelerated cementitious matrices has a significant repercussion on their fresh and hardened properties.

The vast majority of studies on the compatibility and reactivity of accelerators with cement evaluates accelerated cement pastes produced by hand or mechanical mixing [4,10,17–20]. However, these mixing processes differ considerably from the one used in real applications of sprayed concrete. This is aggravated by the fact that nearly no study on the influence of spraying on the microstructure or on hydration kinetics of cementitious matrices containing accelerators may be found. Therefore, the evaluation of how spraying influences the hydration behavior of accelerated cementitious matrices is crucial to understand the performance of sprayed concrete.

The objectives of the experimental campaign conducted in this chapter are:

- Investigate the influence of spraying on accelerator reactivity and further cement hydration.

- Analyze the microstructure development and morphology of precipitated hydrates in pastes produced by spraying.

- Compare spraying with hand-mixing, highlighting the main properties affected by the mixing process.

In this part of the experimental program, tests were performed with cement pastes produced by spraying. Pastes were composed by the combination of 2 types of cement and 4 types of accelerator. Evolution of temperature, powder XRD, isothermal calorimetry, TGA and SEM analysis were performed to characterize the kinetics and mechanisms of hydration of accelerated sprayed pastes. The characterization of hand-mixed pastes presented in chapter 3 is used for comparison purposes. Results obtained explain important differences in hydration behavior caused by the mixing process and highlight in which situations the characterization of matrices produced by spraying might be necessary.

6.2. Experimental methodology

6.2.1. Materials

Cements, water, superplasticizer and accelerators employed in this section are the same as the ones used in chapter 3 (described in section 3.2.1).

6.2.2. Composition and preparation of sprayed cement pastes

Sprayed pastes contained the same superplasticizer and accelerators dosages as pastes evaluated in chapter 3 (section 3.2.2) and present the composition shown in table 3.5. However, the use of a w/c ratio equal to 0.45 was not feasible given the typical requirements of the spraying equipment. In fact, the use of such a high w/c ratio compromises the adequate setting of the paste right after accelerator addition and its stable adhesion to the surface of the substrate.

For this reason, pastes destined to spraying were produced using a w/c ratio equal to 0.32[4]. For future reference, all the pastes tested in this chapter will be referred to as *'sprayed pastes'*.

Batches containing 30 kg of paste were necessary to comply with the requirements of the spraying equipment (described in section 6.2.3) and to assure a homogeneous flow of paste through the pumping system. For this reason, cement pastes were prepared in a planetary mixer type 65/2 K-3, using 65 L containers. Paddle rotation and planetary speeds were 150 and 40 rpm, respectively.

Pastes were prepared under controlled conditions, at 20 °C and 50 % relative humidity. Cement and water were mixed for 240 s, followed by superplasticizer addition and additional 240 s of mixing. Accelerator was added to the paste by spraying 1 h after cement and water had been homogenized. The paste was kept in a climatic chamber at 20 °C before accelerator incorporation, in order to follow the procedures adopted in chapter 3 (section 3.2.2). Samples were destined to the tests right after accelerator homogenization.

6.2.3. Spraying process

The spraying process was conducted inside a thermally insulated climatic chamber at 20 °C and 50 % relative humidity, shown in figure 6.1. The equipment employed to produce sprayed pastes corresponds to a small-scale version of a concrete spraying system used in previous research [1] and is presented in figure 6.2. A helical screw pump type UP-Pictor was used and operated with the pressure of 6 bar, using a 3 HP air compressor. This type of pump is adequate for fluids like cement pastes and mortars, in contrast with piston pumps that are indicated to handle fluids with coarser particles [141]. It also assures a more constant flow of material, eliminating the pulsation effect.

---

[4] For comparison purposes, accelerated hand-mixed pastes were also produced with a w/c ratio of 0.32 and were analyzed by isothermal calorimetry. Results are presented in Appendix C.

Figure 6.1 - Climatic chamber used for spraying.
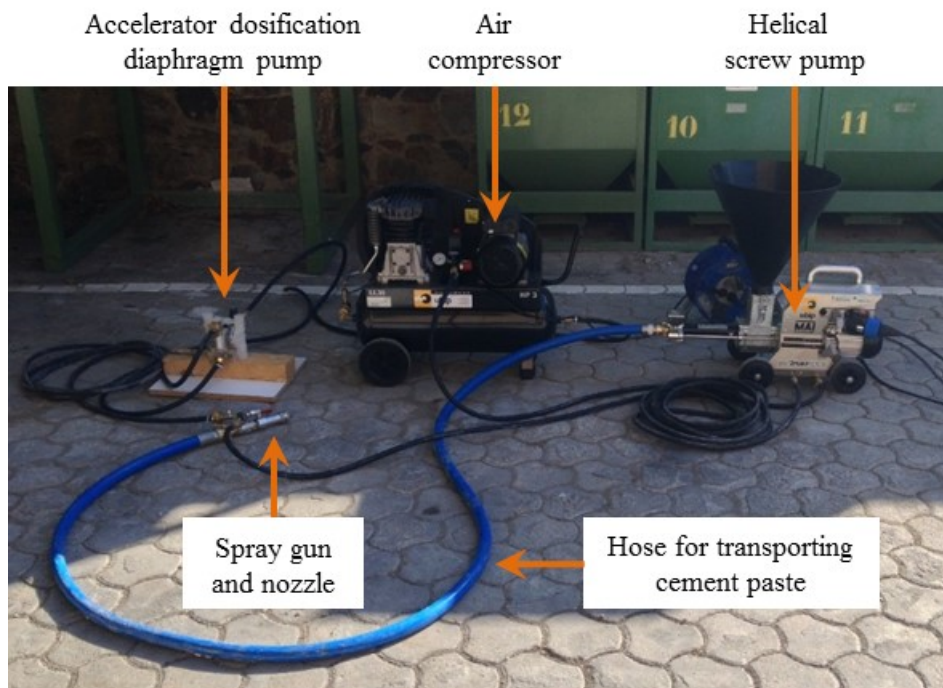
Figure 6.2 - Components of the spraying equipment for cement pastes.

Accelerators were dosed by an air-operated diaphragm pump type P.025. This type of pump presented a homogeneous suction for all the accelerators, since their viscosity varied according to their chemical composition. The flow of accelerators depended on their type and dosage and was calculated based on the optimal flow of cement paste (4.9 L/min).

The hose for transporting the fresh material measured 4 m in length and 40 mm in inner diameter. At its end, a spray gun, whose details are presented in figure 6.3, was connected. It contained three different inlets for the ingress of cement paste, accelerator and compressed air (figure 6.3.a). A nozzle, developed specifically for this study, was connected at the exit of the gun. It had a frustum shape with base diameter, top diameter and height equal to 14.0, 6.0 and 10.0 mm, respectively (figure 6.3.b). At the top part, an extension cylinder measuring 30.0 mm in length and 6.0 mm in inner diameter was installed in order to obtain a better homogenization of the sprayed mix. At its base, six 2 mm-holes for the inlet of accelerator and compressed air may be observed (see figure 6.3.c).
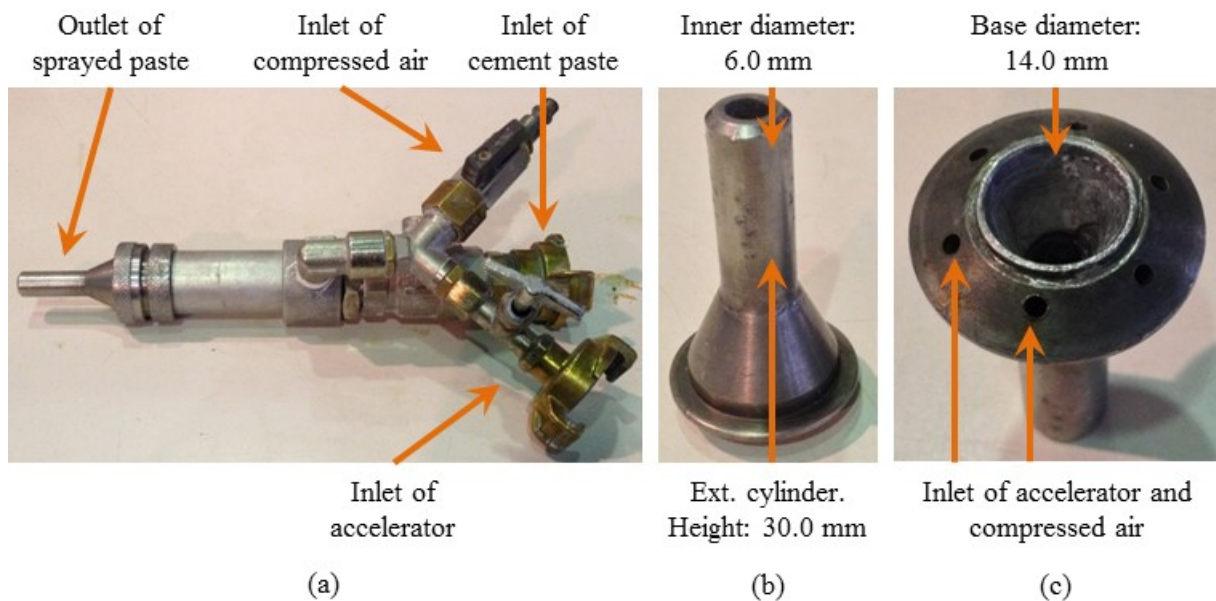
Figure 6.3 - Spray gun (a), nozzle for cement pastes (b) and base view of the nozzle, showing the holes for the inlet of accelerator and compressed air (c).

6.2.4. Test methods

Tests conducted with cement pastes are shown in table 6.1. Their descriptions are presented subsequently. Evolution of temperature and powder XRD were performed with sprayed pastes I_AKF 0.61 7%, II_AKF 0.61 7%, I_ALK 3% and II_ALK 3%. TGA and SEM were conducted with sprayed pastes I_AKF 0.61 7% and I_ALK 3%. Isothermal calorimetry was performed with reference sprayed pastes I_REF and II_REF and 10 different accelerated sprayed pastes, produced with CEM I and CEM II/A-L and accelerators AKF 0.38 7%, AKF 0.42 11%, AKF 0.61 5%, AKF 0.61 7% and ALK 3%.

Table 6.1 - Tests performed with sprayed pastes.

Test	Sample	Age / period of time
Evolution of temperature	Fresh paste	1 - 1.5 h
Powder XRD	Frozen and ground paste	15 min, 1, 3, 12 and 24 h after accelerator addition
Isothermal calorimetry	Fresh paste	0 - 24 h
TGA	Freeze-dried and ground paste	15 min, 3, 12 and 48 h after accelerator addition
SEM	Freeze-dried paste	15 min, 3 and 12 h after accelerator addition

6.2.4.1. Evolution of temperature

Evolution of temperature was measured in a semiadiabatic calorimeter with 300 g of cement paste, using thermocouples type K. This test started right after accelerator addition and was performed for 30 min. This period covers the accelerator reaction (accelerator peak in isothermal calorimetry).

6.2.4.2. Powder XRD, Isothermal calorimetry, TGA and SEM

Due to the logistics involved in the spraying process, it was not possible to perform *in situ* XRD with sprayed pastes. Instead, they were analyzed by powder XRD and analyzed by Rietveld refinement, following the procedures presented in section 3.2.3.3. Isothermal calorimetry, TGA and SEM were performed following the procedures described in sections 3.2.3.4, 3.2.3.5 and 3.2.3.6, respectively.

6.3. Results and discussion

6.3.1. Evolution of temperature

Evolution of temperature in hand-mixed and sprayed pastes is shown in figure 6.4. The temperature of the matrix during the accelerator peak in sprayed pastes is always higher than in hand-mixed pastes. Faster hydration kinetics caused by stronger shearing conditions during spraying contribute to increase the temperature of the pastes. Since the solubility of gypsum and hemihydrate decreases in temperatures above 30 °C [53] and C_3A reactivity is enhanced by

the increase in temperature [35], the spraying process may lead to the formation of AFm phases at the moment of accelerator addition. Larger amounts of gypsum in cement may be required to suppress the formation of AFm phases due to the increase in temperature caused by spraying.
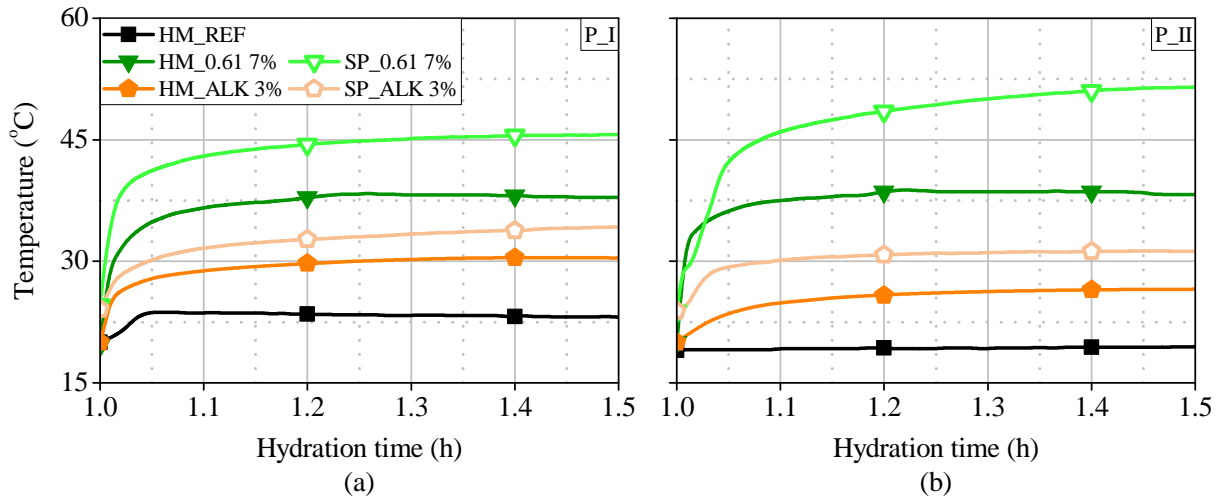
Figure 6.4 - Evolution of temperature in CEM I (a) and CEM II/A-L (b) pastes from 1 to 1.5 h.

6.3.2. Powder XRD

The evolution of phase composition (alite, portlandite and ettringite) of sprayed pastes I_AKF 0.61 7%, II_AKF 0.61 7%, I_ALK 3% and II_ALK 3% is presented in figure 6.5. Results obtained with CEM I pastes are grouped on the left and with CEM II/A-L are grouped on the right. Results regarding hand-mixed pastes are presented in figure 3.7 (section 3.3.3.2). With the purpose of simplifying the comprehension of the graphs and the analysis of results, the difference in alite, portlandite and ettringite contents from accelerator addition until 24 h in hand-mixed and sprayed pastes is summarized in table 6.2.
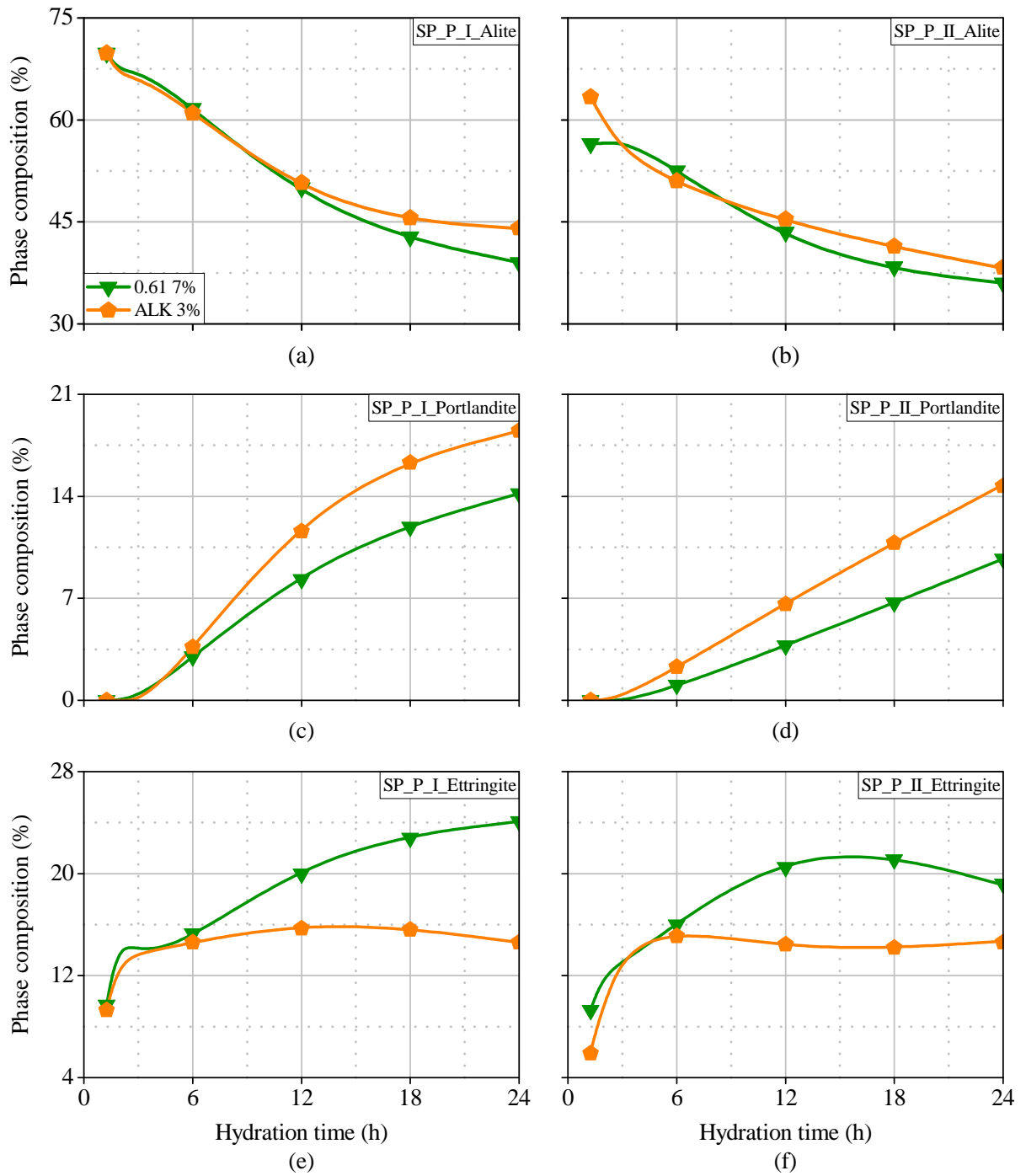
Figure 6.5 - Evolution of the contents of alite (a and b), portlandite (c and d) and ettringite (e and f) in CEM I and CEM II/A-L sprayed pastes from accelerator addition to 24 h.

Table 6.2 - Variation in the contents of alite, portlandite and ettringite during the first 24 h of hydration in accelerated pastes.

Variation in phase content	HM_I_ AKF 0.61 7%	HM_I_ ALK 3%	HM_II_ AKF 0.61 7%	HM_II_ ALK 3%	SP_I_ AKF 0.61 7%	SP_I_ ALK 3%	SP_II_ AKF 0.61 7%	SP_II_ ALK 3%
Alite consumed until 24 h (%)	31.1	25.5	26.3	26.5	30.8	25.8	20.5	25.2
Portlandite formed until 24 h (%)	19.1	19.4	16.6	20.2	14.2	18.5	9.7	14.8
Ettringite formed at 15 min (%)	9.9	13.3	13.9	14.8	9.7	9.3	9.3	6.0
Ettringite formed until 24 h (%)	24.7	17.0	26.7	22.5	24.1	14.6	19.1	14.7

The mixing procedure leads to major differences in the evolution of phase composition, although cement pastes produced by both processes have the same mix composition. In hand-mixed pastes, cement hydration proceeds at a larger extent and rate until 24 h, providing a higher consumption of alite and the consequent formation of larger amounts of portlandite. The differences in phase composition are more sensitive to accelerator type in sprayed pastes.

Ettringite is the main hydrate affected by the mixing process. As observed in table 6.2, variations in ettringite contents are more noticeable when accelerator ALK 3% is used, because its reaction depends on gypsum dissolution. Ettringite contents at 15 min in pastes HM_I_ALK 3% and HM_II_ALK 3% are 30 and 60 % higher than in the equivalent sprayed pastes, respectively. At 24 h, pastes HM_I_ALK 3% and HM_II_ALK 3% contain 24 and 35 % more ettringite than sprayed pastes with the same accelerator. Regarding pastes produced with AKF 0.61 7%, ettringite amounts in HM_I_AKF 0.61 7% and HM_II_AKF 0.61 7% are 2.0 and 33 % larger than the equivalent sprayed pastes at 15 min and 2.4 and 29 % larger at 24 h.

A possible explanation to this fact is that ettringite is formed too rapidly during spraying due to the high shearing conditions achieved in this case. The early-formed aluminate hydrates might present a low degree of crystallinity and be disposed in a gel-like structure. A similar outcome was already reported by [111], who observed a gel-like structure in ettringite precipitated at very early ages. Therefore, the lower crystallinity of ettringite in sprayed pastes may be expected, since a short time is available for the nucleation of crystals.

Furthermore, ettringite formed during the spraying process might not be suitably oriented for X-ray diffraction. In the case of needle-like structures, crystals disposed in a diffuse orientation cause the decrease of the intensities of diffracted X-ray beams. The result of the formation of precipitates in a disarranged microstructure is the quantification of lower amounts

of ettringite. As far as hydration progresses and once nucleation of ettringite occurs, crystal growth becomes rapid and the X-ray intensity due to ettringite strengthens up.

To evaluate the composition of aluminate hydrates precipitated in the first hour after accelerator addition, the evolution of C_3A and gypsum contents in hand-mixed and sprayed pastes is shown in table 6.3. In sprayed pastes, C_3A hydration is favored and less gypsum is consumed from 15 min to 1 h than in hand-mixed pastes. The C_3A/gypsum ratio of the hydrates formed from 15 min to 1 h, considering that all gypsum was consumed during C_3A hydration, is higher in sprayed pastes. This indicates that the formation of AFm phases is advanced and may take place during the accelerator peak, lowering ettringite contents in sprayed pastes. This process is more evident when accelerator ALK 3% is used and in the pastes containing CEM II/A-L.

Table 6.3 - Evolution of the contents of C_3A and gypsum in the first hour after accelerator addition in accelerated cement pastes.

Phase content	HM_I_ AKF 0.61 7%	HM_I_ ALK 3%	HM_II_ AKF 0.61 7%	HM_II_ ALK 3%	SP_I_ AKF 0.61 7%	SP_I_ ALK 3%	SP_II_ AKF 0.61 7%	SP_II_ ALK 3%
C_3A at 15 min (%)	2.3	2.1	1.5	1.8	2.8	3.0	3.1	3.1
C_3A at 1 h (%)	2.1	1.9	1.4	1.7	2.5	2.6	2.8	2.6
Gypsum at 15 min (%)	4.7	1.5	3.8	3.2	2.0	1.0	2.0	2.0
Gypsum at 1 h (%)	3.8	0.0	3.1	1.3	1.2	0.0	1.5	1.3
C_3A/gypsum ratio of hydrates formed from 15 min to 1h	0.22	0.13	0.14	0.05	0.38	0.40	0.60	0.71

6.3.3. Isothermal calorimetry

Heat of hydration curves of all sprayed pastes analyzed are presented in figure 6.6. Results obtained with CEM I pastes are presented on the left, whereas results from CEM II/A-L pastes are on the right. Figures 6.6.a and 6.6.b represent the curve from 0 to 24 h, while figures 6.6.c and 6.6.d present the heat flow generated in the accelerator peak. The characteristic points of the heat flow curves determined according to table 3.8 are summarized in table 6.4 and the conclusions derived from this analysis are presented subsequently.
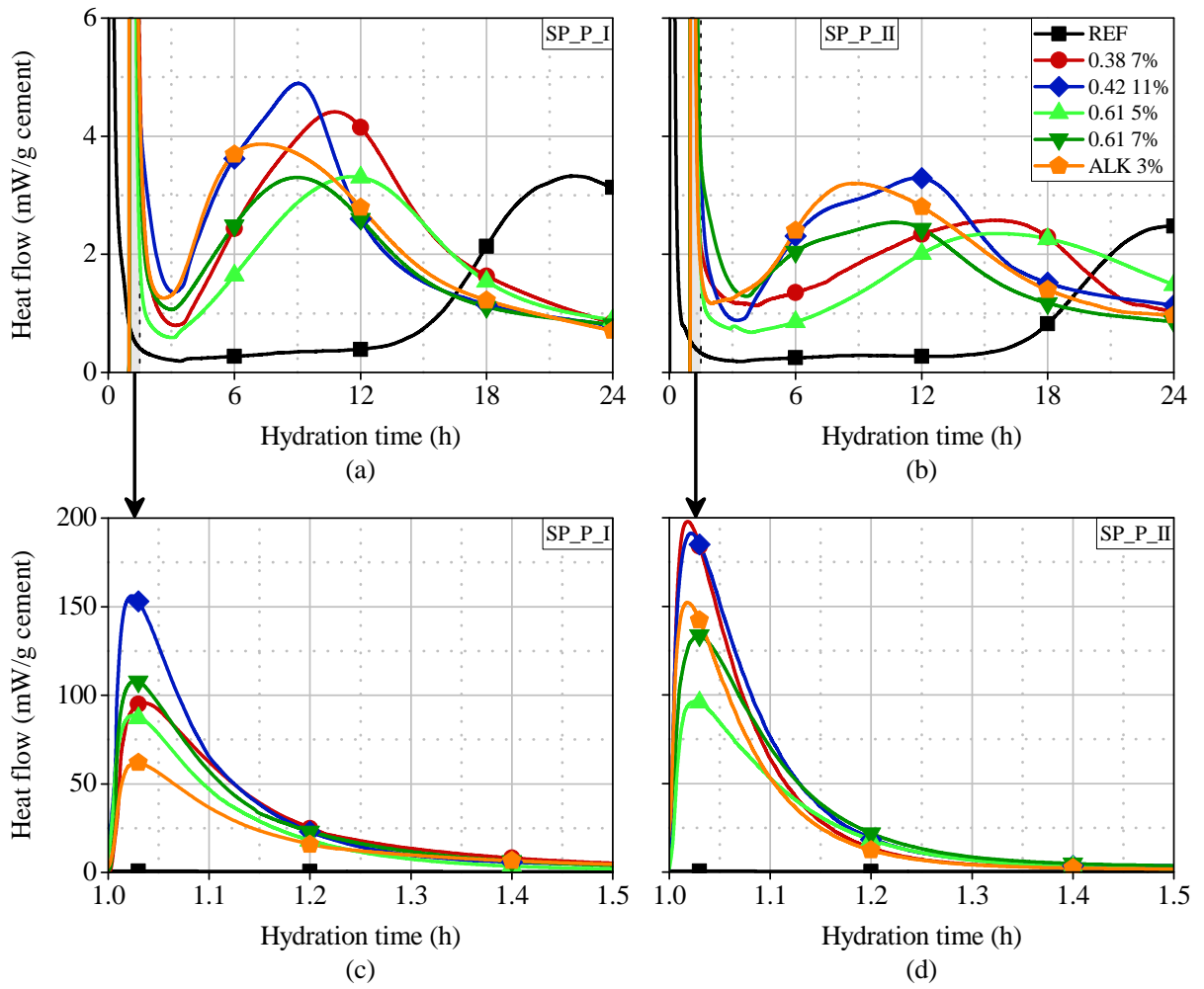
Figure 6.6 - Heat flow curves obtained with CEM I and CEM II/A-L sprayed pastes from 0 to 24 h (a and b) and from 1.0 to 1.5 h (c and d).

Table 6.4 - Analysis of the heat flow curves obtained with sprayed pastes.

Paste	Slope - accel. peak (mW/g.h)	Energy released - accel. peak (J/g)	Maximum heat flow - accel. peak (mW/g)	Induction period (h)	Slope acceleration - main peak (mW/g.h)	Energy released - main peak (J/g)	Maximum heat flow - main peak (mW/g)	Energy released until 24 h (J/g)
I_REF	-	-	-	13.35	0.50	151.2	3.32	116.1
I_AKF 0.38 7%	2818	51.58	88.8	2.10	0.66	174.1	4.37	192.3
I_AKF 0.42 11%	6424	63.38	156.6	1.91	1.02	156.2	4.90	184.2
I_AKF 0.61 5%	3187	43.22	91.7	1.77	0.40	141.8	3.32	153.4
I_AKF 0.61 7%	4644	53.07	108.3	1.76	0.52	125.0	3.30	148.7
I_ALK 3%	2434	35.40	62.1	1.66	1.02	152.7	3.87	174.1
II_REF	-	-	-	15.16	0.37	139.3	2.47	80.0
II_AKF 0.38 7%	10510	62.91	198.1	3.41	0.17	132.6	2.58	147.5
II_AKF 0.42 11%	4352	57.47	130.3	1.98	0.59	169.5	3.30	179.4
II_AKF 0.61 5%	3016	37.05	77.7	4.46	0.20	144.6	2.35	140.8
II_AKF 0.61 7%	3465	60.83	133.7	2.14	0.36	111.2	2.54	139.5
II_ALK 3%	8685	51.60	152.4	2.38	0.57	141.9	3.20	160.1

Results indicate that the rate of accelerator reaction (considered as the slope of the ascending part of the accelerator peak) is more than two times higher in sprayed pastes in comparison with hand-mixed pastes (see table 3.8 for the results of hand-mixed pastes). As this rate depends on the mixing procedure, it can be assumed that accelerator reaction is transport-controlled. In other words, the homogenization of the accelerator ions into the matrix is the limiting process of the reaction [19]. The stronger shearing conditions achieved through spraying turn the paste and the accelerator into small particles, as aerosols, and the reaction takes place faster due to a better homogenization.

A similar outcome is observed if the energy released and the maximum heat flow of the accelerator peak are analyzed. Again, sprayed pastes reach values considerably higher than the equivalent hand-mixed ones. The biggest difference is verified in pastes with CEM II/A-L, due to the presence of limestone filler and larger amounts of hemihydrate. Calcium carbonate from the filler may react with aluminate ions from accelerators and may also be partially dissolved

by the H$^+$ ions contained in alkali-free formulations, as discussed in section 4.3.2.6. Both processes contribute to increase the heat generated in the accelerator peak.

The rate of heat flow during the acceleration period, the energy released and the maximum heat flow obtained in the main hydration peak are also influenced by the mixing process (tables 3.9 and 6.4). Hand-mixed and sprayed pastes containing alkali-free accelerators present the same general mechanisms of hydration for both cements (see figures 3.9 and 6.6). However, the rate and extent of alite hydration in sprayed pastes is lower, as observed by the smaller slope, energy released and maximum heat flow obtained in the main peak.

In sprayed pastes with the alkaline accelerator (SP_I_ALK 3% and SP_II_ALK 3%), the main hydration peak is not dissociated into two thermal events, as in hand-mixed pastes (figure 3.9). A possible explanation to such difference is that the AFm formation might be advanced in time and occur during the accelerator peak due to the more efficient dispersion achieved with the spraying process. Consequently, the exothermic signals generated in ettringite and AFm formation are overlapped and cannot be distinguished. It may also be a consequence of the higher temperatures achieved during spraying (section 6.3.1) and is in total agreement with the results obtained from powder XRD (section 6.3.2).

This early formation of AFm phases is more pronounced in paste SP_II_ALK 3% due to the presence of limestone filler. The spraying process may favor the dissolution of calcium carbonate and its contact with aluminate ions, contributing to the formation of carbonated AFm phases, like hemi or monocarboaluminate. In addition, limestone filler controls C$_3$A hydration, indirectly stabilizing ettringite [45]. Since ettringite is the main product that provides initial mechanical strength when such accelerators are used, limestone filler improves their reactivity in sprayed concrete applications, as discussed in section 4.3.2.6.

The rate of reaction during the main hydration peak can also be observed in the energy release curves from figure 6.7. The curves corresponding to the sprayed pastes with alkali-free accelerators present a lower reaction rate (constant decrease in slope) from 12 h on, when compared to hand-mixed pastes (figure 3.10). As accelerator reaction occurs faster in sprayed pastes, aluminate hydrates fill up the pores more quickly, inhibiting the precipitation of silicate hydrates due to a lack of space [19]. This leads to lower degrees of hydration in sprayed pastes until 24 h. In other words, sprayed pastes tend to present higher reaction rates when the accelerator is added and lower hydration rates in the following hours.
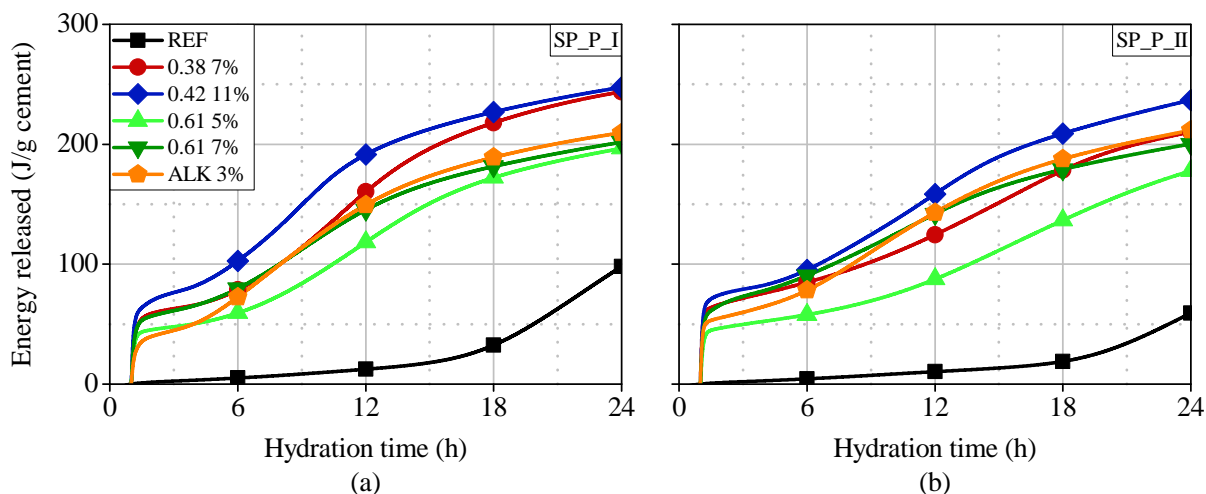
Figure 6.7 - Energy release curves obtained with CEM I (a) and CEM II/A-L (b) sprayed pastes from accelerator addition to 24 h.

The same behavior is observed in the pastes with the alkaline accelerator. In sprayed pastes, lower rates of hydration and lower maximum heat flows are observed. The accelerated C_3A reaction causes a delay in alite hydration, broadening the main hydration peak and lowering its intensity. In this case, alite solubility might be the limiting step of the hydration process, as also observed in [10].

The spraying process mainly influences systems with higher C_3A/SO_3 ratios, such as pastes with alkaline accelerators. The accelerated formation of AFm phases inhibits alite hydration. Since alkali-free accelerators also contain sulfates in their composition, the effect of spraying on cement hydration with this type of accelerator is not as significant as in alkaline accelerated pastes.

6.3.4. TGA

Results corresponding to the quantification of portlandite and chemically bound water by thermogravimetry are shown in table 6.5. A clear influence of the mixing process on the hydration behavior of cement pastes is observed. Sprayed pastes contain portlandite amounts between 5 and 15 % lower than the equivalent hand-mixed pastes at the same age (see table 3.10 for the results of hand-mixed pastes). This may be attributed to the inhibition in alite hydration caused by the massive precipitation of aluminate hydrates when accelerator is added. Such effect is more pronounced in sprayed pastes due to the better homogenization of cement and accelerator and becomes more evident as hydration proceeds.

Table 6.5 - Portlandite and chemically bound water quantified by thermogravimetry in sprayed pastes I_AKF 0.61 7% and I_ALK 3%.

Compound	Age	SP_I_AKF 0.61 7%	SP_I_ALK 3%
Portlandite (%)	15 min	2.28	1.65
	3 h	2.55	1.69
	12 h	9.39	10.76
	48 h	14.67	15.21
Chemically bound water (%)	15 min	3.72	2.79
	3 h	4.17	2.46
	12 h	9.74	8.82
	48 h	14.53	13.24

The same trend is observed regarding the quantification of chemically bound water. Sprayed pastes SP_I_AKF 0.61 7% and SP_I_ALK 3% present 10 and 18 % less chemical bound water at 15 min than the equivalent hand-mixed pastes. Those differences become respectively 21 and 10 % at 48 h and indicate that alite hydration proceeds slower in sprayed pastes and lower degrees of hydration are obtained during the period analyzed. These data corroborate the results obtained in powder XRD and isothermal calorimetry (sections 6.3.2 and 6.3.3).

For both types of accelerators, larger amounts of chemically bound water were expected in sprayed pastes at 15 min due to faster initial rates of reaction. However, accelerator reaction reaches its maximum 3 min after its addition (see figures 6.6.c and 6.6.d) and the difference between mixing processes may reduce in the course of the 12 min left to reach the first time interval analyzed. In addition, the temperature range between 50 and 200 °C comprehends the dehydration of ettringite, AFm phases, C-S-H, gypsum and hemihydrate and it is not possible to quantify how much water corresponds to each phase. Anyhow, it is possible to conclude that sprayed pastes have smaller amounts of C-S-H since they contain lower contents of portlandite in the periods evaluated.

Although AFm phases cannot be quantified properly by TGA, their presence in the sprayed paste with the alkaline accelerator (SP_I_ALK 3%) at 15 min of hydration may be detected. As observed in figure 6.8, the DTG curve presents two shoulders around 138 and 180 °C related to the formation of monosulfoaluminate, which was also observed by [142]. In

addition, the shoulder around 250 ºC corresponding to the water loss from the dehydroxylation of the aluminum hydroxide column in ettringite [97] is more pronounced in the hand-mixed paste.
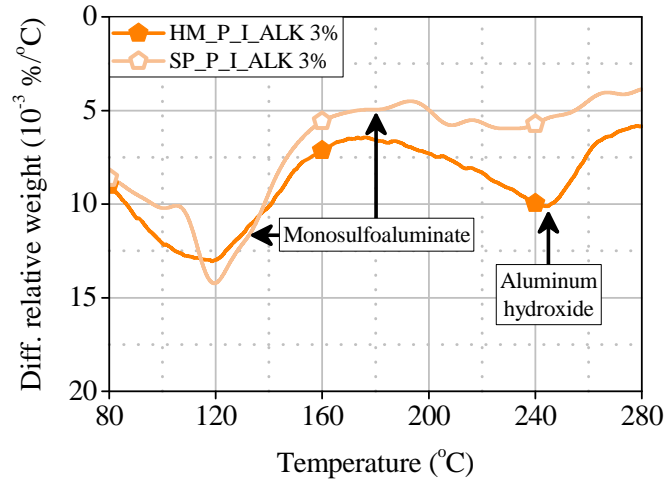
Figure 6.8 - DTG curves of pastes HM_I_ALK 3% and SP_I_ALK 3%, 15 min after accelerator addition.

These observations indicate that the high shearing conditions achieved during spraying induce the formation of AFm phases. They are associated with the enhanced aluminate reactivity and low sulfate availability in the paste with the alkaline accelerator (high final C_3A/SO_3 ratio). These processes validate the analysis of the accelerator peak in the calorimetric curves.

6.3.5. SEM and EDS microanalysis

SEM images obtained with sprayed pastes SP_I_AKF 0.61 7% and SP_I_ALK 3% are presented in figure 6.9 and 6.10, respectively. Both figures are organized as the hand-mixed pastes (figure 3.11 to 3.13, from section 3.3.6), containing two images of each paste freeze-dried at 15 min, 3 and 12 h of hydration.

[1] Ca : Si : Al : S : Na = 100 : 24.6 : 18.0 : 19.3 : 2.5
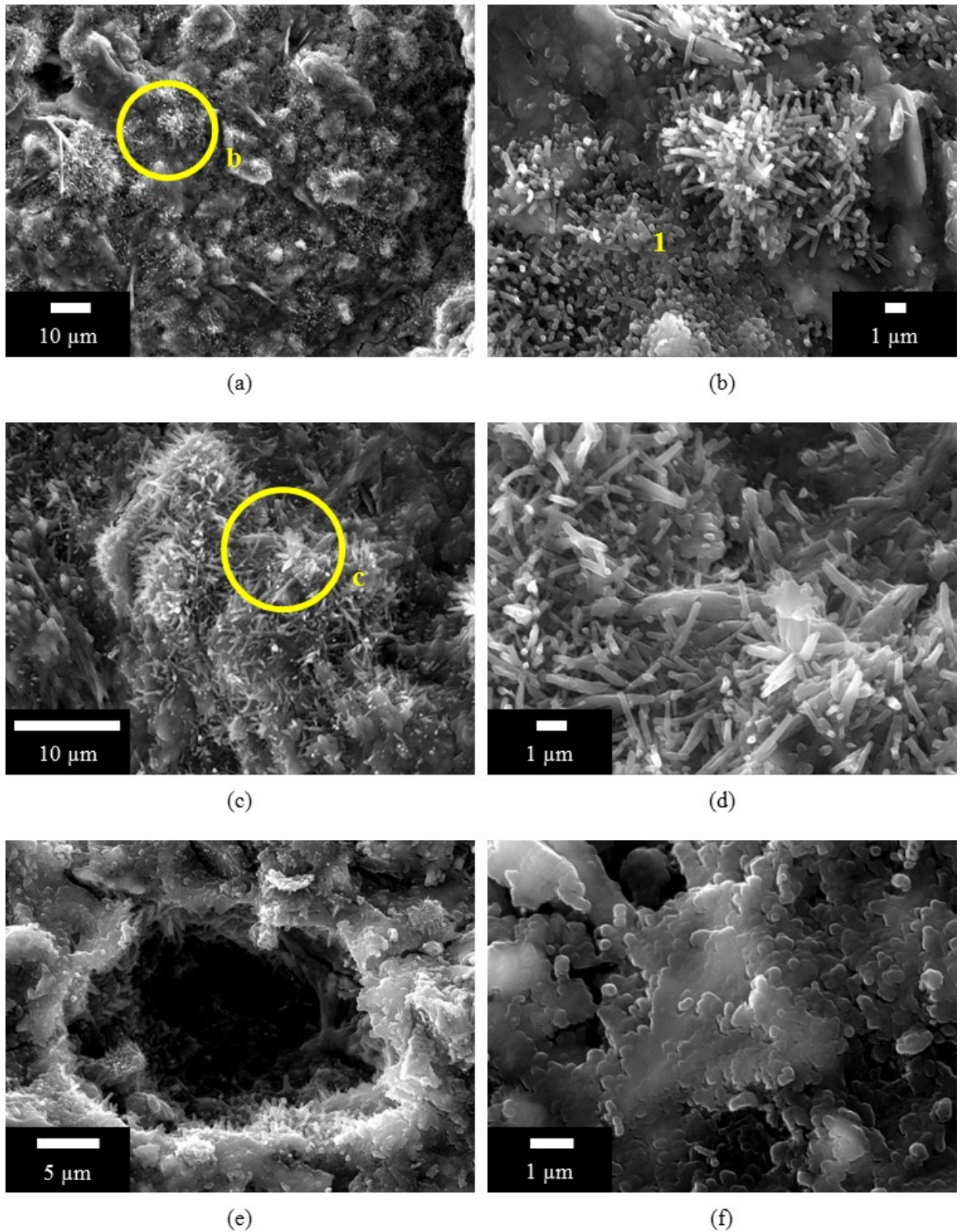
Figure 6.9 - SEM images of paste SP_I_AKF 0.61 7% at 15 min (a and b), 3 h (c and d) and 12 h (e and f).

^{1} Ca : Si : Al : S : Na = 100 : 18.5 : 15.0 : 11.1 : 2.0

^{2} Ca : Si : Al : S : Na = 100 : 24.4 : 43.0 : 6.1 : 10.9

^{3} Ca : Si : Al : S : Na = 100 : 33.4 : 45.3 : 23.2 : 7.3
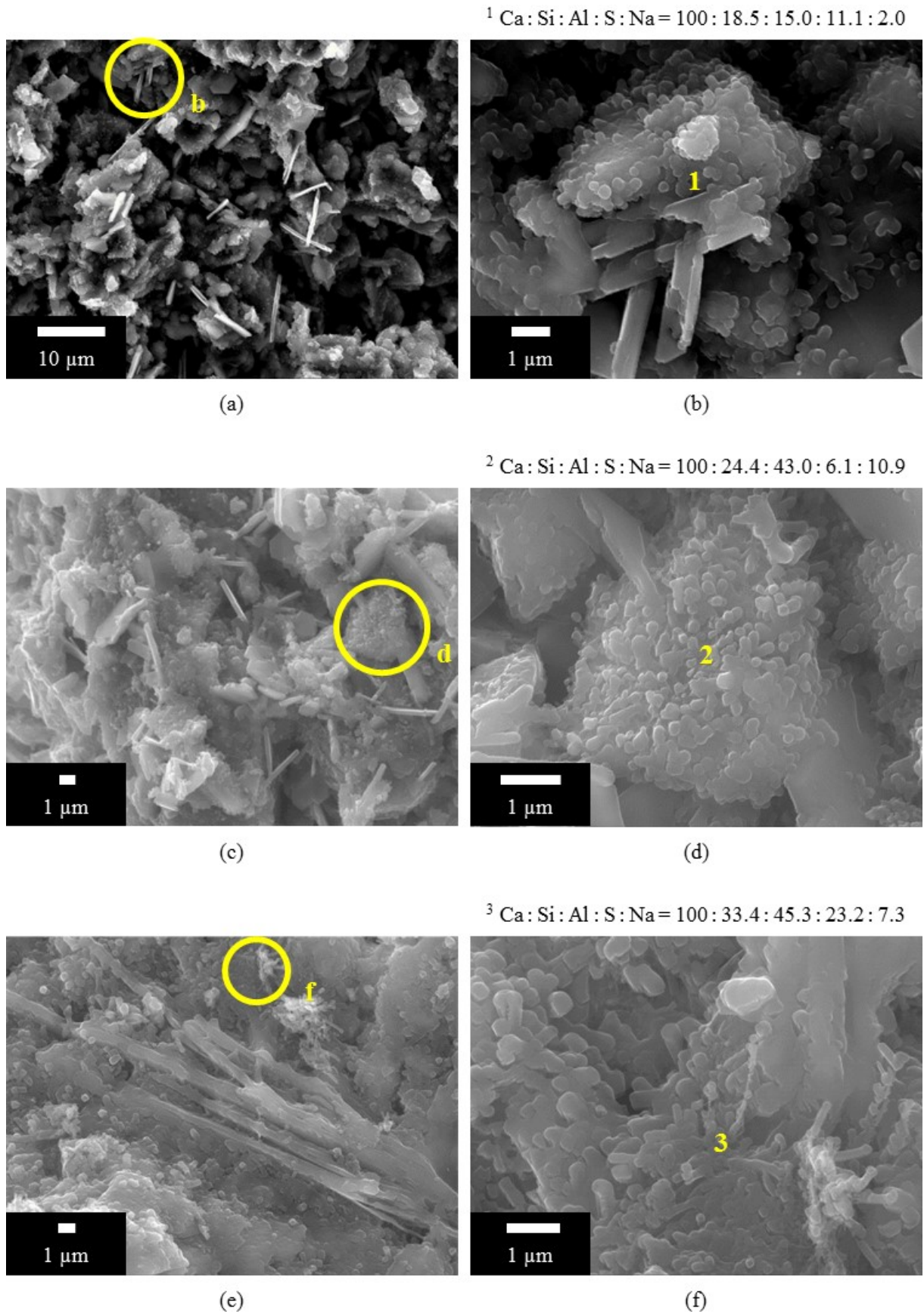
Figure 6.10 - SEM images of paste SP_I_ALK 3% at 15 min (a and b), 3 h (c and d) and 12 h (e and f).

The microstructure of the sprayed paste SP_I_AKF 0.61 7% at 15 min (figures 6.9.a and 6.9.b) is less organized than the equivalent hand-mixed paste at the same age (figures 3.12.a and 3.12.b). It is mainly composed by less-regularly-formed and highly dispersed aluminate hydrates. Ettringite needles present rounded terminations and measure approximately 1.5 µm (25 % shorter than the crystals formed in hand-mixed pastes at the same age). The difference in morphology is caused by the faster accelerator reaction during spraying. The region analyzed by EDS has an Al/S ratio equal to 0.93, which indicates the coexistence of AFt and AFm phases precipitated on a cement grain surface.

At 3 h of hydration (figures 6.9.c and 6.9.d), ettringite needles have grown and measure approximately 2 µm in length. In spite of that, their morphology does not present the same arrangement as in hand-mixed pastes (figures 3.12.c and 3.12.d), being still characterized by diffusely oriented needles. Such outcome corroborates the hypothesis described in section 6.3.2 and the data obtained in powder XRD (the disarranged microstructure leads to the quantification of smaller amounts of ettringite by XRD).

At 12 h of hydration, large pores are observed (diameter of 21 µm in figure 6.9.e). These large pores are formed because the fast setting matrix does not consolidate properly and entraps air during spraying and may lead to reductions in mechanical strength. Figure 6.9.f shows that cement grains present a large surface covered by hydrated phases. The formation of highly dispersed ettringite and other aluminate hydrates may decrease the rate of alite dissolution and limit further hydration due to space filling. That is a plausible explanation on why sprayed paste SP_I_AKF 0.61 7% presents a lower degree of hydration than the equivalent hand-mixed one. Such results are in line with the observations derived from the analysis of the energy release curves in isothermal calorimetry (see figures 3.10 and 6.7).

Regarding the sprayed paste with the alkaline accelerator at 15 min of hydration (SP_I_ALK 3% in figures 6.10.a and 6.10.b), the formation of aluminate hydrates over the surface of cement grains can be observed. These hydrates present an Al/S ratio equal to 1.35 and may be composed mainly by AFm phases. They are formed by the fast reaction of the accelerator with calcium ions in a medium with limited sulfate content.

At 3 h of hydration (figures 6.10.c and 6.10.d), hydrates formed in the sprayed paste SP_I_ALK 3% are hexagonal plates, presenting an Al/S ratio equal to 7.0 and an elevated sodium content. This aluminate hydrate may be the U-phase, also observed in hand-mixed pastes (figure 3.13.c and 3.13.d). Sodium concentration in the liquid phase in the sprayed paste

is 0.58 mol/L ([Na$^+$] equal to 0.184 mmol/g cement and w/c ratio equal to 0.32), which is also above the minimum for U-phase formation (0.40 mol/L, according to [115]).

The mixing procedure influences the morphology and the dispersion of this AFm phase significantly. This hydrate presents diameters varying from 12 to 40 µm and tends to agglomerate in hand-mixed pastes (figure 3.13.c). However, the average diameter in sprayed pastes is 3 µm and its dispersion is more homogeneous (figure 6.10.c). This difference in microstructure is caused by the high shearing conditions and better accelerator homogenization during spraying, similarly to the pastes with the alkali-free accelerator.

At 12 h of hydration (figures 6.10.e and 6.10.f), hydrates are more uniformly distributed in the whole matrix and present an Al/S ratio equal to 2.0, being composed by AFm phases. According to the discussion from section 3.3.3, AFm phases precipitated on the surface of a cement grain contribute to reduce the degree of hydration of alite in alkaline accelerated pastes. This fact justifies the smaller hydration degree measured at 24 h in sprayed pastes.

6.4. Considerations regarding sprayed concrete

The experimental campaign conducted in this chapter dealt with the chemical characterization of sprayed pastes in a laboratory scale. Cement pastes were employed to avoid the influence of aggregates on hydration kinetics and on the microstructure of the matrix. By doing so, results were based purely on the chemistry of cements and accelerators and on the mixing procedure.

The hydration behavior and the microstructure of sprayed concrete may differ from the results obtained with pastes, due to four main reasons:

- Equipment used for spraying concrete is more powerful than the small-scale equipment developed for this study. Then, shearing conditions are stronger, which may increase reaction rates [1].

- Aggregates also improve shearing conditions and accelerate cement hydration, as observed by [12]. They may also act as nucleation sites for the precipitation of hydrated phases, influencing the microstructure development.

- Aggregates dilute cement and accelerator and, therefore, concrete is a less reactive system than cement pastes. Therefore, the temperature reached during hydration is lower than in pastes and may alter the composition of the hydrated phases and the porosity of the matrix significantly [16].

- Coarse aggregates generate a high impact energy during spraying, which improves the consolidation of the matrix and alters its microstructure. In addition, coarse aggregates rebound during concrete spraying and produce a cement-rich layer between the substrate and the concrete, causing heterogeneities in the microstructure of the matrix [77].

6.5.   Concluding remarks

Chapter 6 presented the influence of the mixing procedure on the kinetics and mechanisms of hydration of cement pastes containing alkali-free and alkaline accelerators. The following conclusions may be drawn from the experimental results:

- As a general conclusion, spraying enhances accelerator reactivity and accelerates C_3A hydration. Consequently, it limits alite dissolution and further hydration, leading to lower degrees of reaction from 12 h on.

- The rate of accelerator reaction is transport-controlled. In sprayed pastes, aluminate ions from the accelerator react at a faster rate than in hand-mixed pastes. This is the result of the optimized diffusion and homogenization of the accelerator in the matrix.

- Spraying accelerates sulfate depletion from the liquid phase due to increased accelerator reactivity and to higher temperatures achieved during mixing. Therefore, the formation of AFm phases is advanced and may take place during accelerator reaction.

- Faster kinetics of accelerator and C_3A reactions generated by spraying suppress alite hydration. The early formed aluminate hydrates fill up the space available more quickly and decrease the extent and rate of alite hydration due to a lack of space. Consequently, this process diminishes the amount of portlandite formed and leads to lower degrees of hydration until 24 h in sprayed pastes.

- The mixing process influences the microstructure of the matrix significantly. In sprayed pastes, aluminate hydrated phases are more uniformly distributed throughout the whole

matrix. In addition, ettringite is found in a disarranged microstructure and is composed by shorter, less-regularly-formed and highly dispersed needle-like crystals. The difference in morphology is attributed to the high shearing conditions imposed by the spraying process, which cause a high diffusion of the accelerator and do not provide enough time for the crystals to nucleate and orientate properly. Since part of the ettringite crystals is not crystalline or not suitably oriented for X-ray diffraction, quantitative measurements using this technique provide lower ettringite contents.

- Spraying provides a higher sensitivity in the analysis of different accelerators and is recommended especially in the case of alkaline formulations, because their reactivity is limited by gypsum dissolution.

- As a recommendation, XRD, TGA and SEM should be preferentially conducted in sprayed pastes instead of in hand-mixed pastes. By doing so, a more representative quantification of the phases formed is obtained and variations in hydration mechanisms caused by the mixing process may be analyzed.

7. Mechanical characterization of sprayed mortars

7.1. Introduction

The performance of sprayed cementitious matrices containing accelerators is strongly related to their mechanical properties at short and long term. Mechanical strength development is the result of the combination of several factors related to mix composition, application method and microstructure of the matrix. In practice, this is the main parameter that governs the mix design and applicability of this type of matrix.

Substantial work has been conducted in the field of accelerated cementitious matrices [1,4–6,10,13,18,81,143–145]. Table 7.1 summarizes the most recent ones. Notice that the majority of studies focuses either on the chemical processes or on the mechanical properties of the matrices separately. No previous work addresses the correlation between them from a quantitative standpoint.

Table 7.1 - Summary of recent studies on accelerated cementitious matrices.

Reference	Samples tested		Characterization		Correlation between properties
	Sprayed	Hand-mixed	Chemical	Mechanical	
[4,5,10]		•	•		
[6,81,145]		•	•	•	
[1,18,143,144]	•			•	
[13]	•		•		
This study (Chapter 7)	•	•	•	•	•

Although some chemical reactions are known to influence empirically the properties of the matrix, it is not clear how, why and to what extent they are significant. Therefore, the influence of accelerated hydration reactions on the evolution of mechanical strength still needs to be evaluated. By doing so, the performance of sprayed materials may be better understood, providing tools to improve their design and quality control.

The objectives of the experimental campaign conducted in this chapter are:

- Analyze how accelerated hydration reactions influence the evolution of mechanical strength at early and late ages, elucidating the main mechanisms governing the mechanical performance of the matrix.

- Correlate chemical properties and phase composition of the matrix with its mechanical strength development, from a quantitative standpoint.

- Specify combinations of compatible materials to provide proper mechanical properties.

- Develop and adapt a small-scale testing for the characterization of sprayed matrices.

In this part of the experimental campaign, tests were performed with cement mortars produced by spraying. Mortars were composed by the same cements and accelerators as the ones used in chapter 3. Kinetics of hydration was evaluated by isothermal calorimetry and the results derived from *in situ* and powder XRD presented in chapter 3 were used in this evaluation. The evolution of mechanical strength was evaluated by needle and pin penetration resistance and compressive strength of extracted cores. To complement the analysis, water accessible porosity was also determined in extracted cores.

Multivariate regression analyses were conducted to correlate the chemical properties and phase evolution of the matrix with the development of mechanical strength at early and late ages. Results obtained may have a significant repercussion on the development of accelerators, showing which parameters of their composition may have a stronger influence on the resulting mechanical performance. It also provides valuable information for the selection of compatible cement-accelerator systems, shortening the trial and error procedure applied currently in practice for the definition of the composition of sprayed matrices.

7.2. Experimental methodology

7.2.1. Materials

Cements, water, superplasticizer and accelerators employed in this section are the same as the ones used in chapter 3 (described in section 3.2.1). For the fabrication of sprayed mortars, a calcareous sand with particle size distribution between 0 and 1 mm (figure 7.1) was employed. Its specific mass was 2.315 g/cm^3 and its water absorption was equal to 5.46 % by mass. This aggregate was selected in order to provide adequate rheology for the mix to be sprayed. In addition, aggregates with maximum diameter larger than 1.6 mm could not be employed in the spraying equipment used.
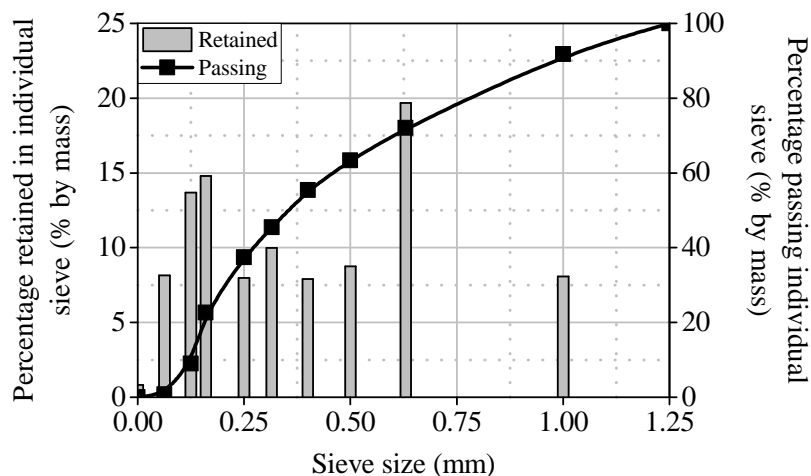
Figure 7.1 - Particle size distribution of the aggregate

7.2.2. Composition and preparation of mortars

Mortars contained the same accelerators dosages as cement pastes and also presented the composition shown in table 3.5. They had a sand/cement ratio of 1.7, w/c ratio equal to 0.51 and also contained superplasticizer at the dosage of 1.0 % bcw. This composition presented an adequate workability for pumping and spraying (spread diameter equal to 300 mm, with no bleeding, measured according to [146]).

Batches containing 96 kg of mortar were used, similarly to the procedure from chapter 6. This quantity was necessary to comply with the requirements of the spraying equipment, to assure a homogeneous flow of matrix through the pumping system and to provide enough material to fill up the panels for the tests. In this case, mortars were also prepared in a planetary mortar mixer type 65/2 K-3 (the same equipment used for cement pastes, described in section 6.2.2).

Mortars were prepared under controlled conditions, at 20 ºC and 50 % relative humidity. Cement and water were first mixed for 240 s. Superplasticizer was added and homogenized for additional 240 s. Then, aggregate was added and mixed for 300 s. After that, mortars were kept at 20 ºC until accelerator addition in order to follow the same procedure as in cement pastes and to avoid the influence of variations in temperature. Finally, mortars were sprayed with accelerators 1 h after cement and water had been mixed and were destined to the tests right after accelerator homogenization.

7.2.3. Spraying process

Sprayed mortars were fabricated using the same equipment and process as the ones used for the production of sprayed pastes (section 6.2.3). The only difference was the nozzle used for spraying mortars, which is shown in figure 7.2.a. It also had a frustum shape and height of 10.0 mm, similarly to the nozzle for spraying pastes (figure 6.3.b). However, the top diameter was larger (8.0 mm), to avoid obstructions due to the presence of aggregates. In addition, the extension cylinder was not necessary in this case because the amount of accelerators used was lower than in pastes (mortars contain less cement than pastes) and accelerator homogenization was considered adequate without its use.
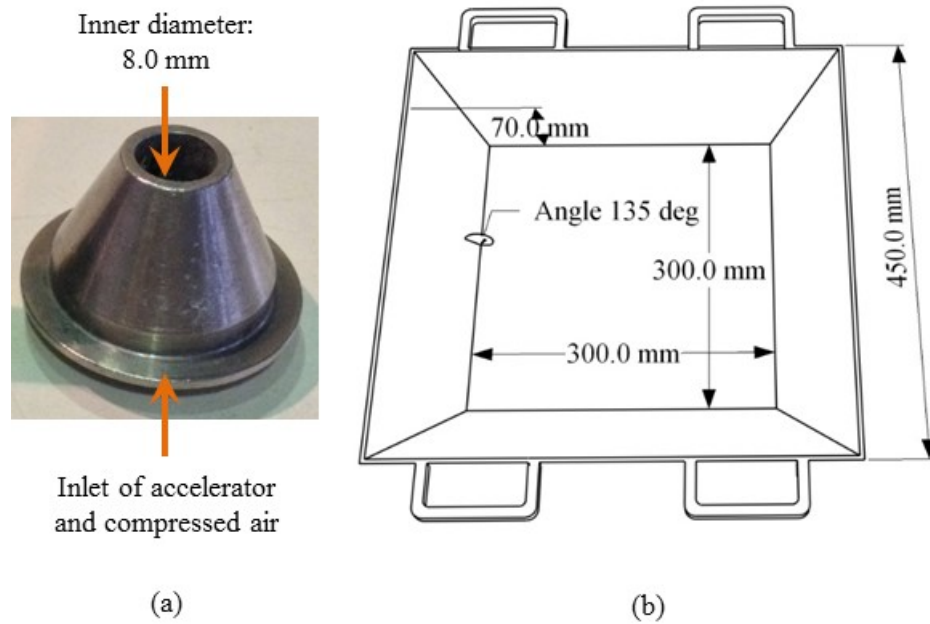
Figure 7.2 - Nozzle used for spraying mortars (a) and design of small-scale metal panels (b).

Metal panels were designed according to [90] and are depicted in figure 7.2.d. They were destined to the pin penetration test and to the extraction of cores for the determination of compressive strength and water accessible porosity. Metal panels were kept inside the chamber for 24 h after finishing spraying. After that, specimens were demolded, cores were extracted and cured by immersion in saturated calcium hydroxide solution at 20 ºC until the date of the test.

Rectangular wood molds measuring 300 mm x 150 mm x 70 mm were employed for the determination of penetration resistance. They were smaller than the metal panels due to limitations of space in the press used for the penetration test. Two metal panels and two wood panels were sprayed for each mix.

7.2.4. Test methods

Table 7.2 shows the tests performed with sprayed mortars. Their descriptions are presented subsequently. Needle and pin penetration tests were performed with accelerated sprayed mortars produced with CEM I and CEM II/A-L and accelerators AKF 0.38 7%, AKF 0.42 11%, AKF 0.61 5%, AKF 0.61 7% and ALK 3%. Isothermal calorimetry, compression and water accessible porosity were conducted with the same accelerated matrices and the reference mortars prepared with CEM I and CEM II/A-L. Apart from these tests, results

obtained with *in situ* and powder XRD from section 3.3.3 will be used for discussion of results and regression analyses.

Table 7.2 - Tests performed with sprayed mortars.

Test	Sample / specimen	Age / period of time
Isothermal calorimetry	Fresh mortar	0 - 24 h
Needle penetration test	Mortar panels	15, 30, 45, 60, 75, 90, 105 and 120 min after accelerator addition
Pin penetration test	Mortar panels	4, 6, 12 and 24 h after accelerator addition
Compression	Extracted cores	1, 3, 7, 28 and 98 days
Water accessible porosity[a]	Extracted cores	7 and 28 days

[a] Water accessible porosity was determined to obtain additional information for the evaluation of compressive strength.

7.2.4.1. Isothermal calorimetry

Isothermal calorimetry was performed following the procedures described in section 3.2.3.4.

7.2.4.2. Needle penetration test

Needle penetration test was performed to determine the penetration resistance (PR) of sprayed mortars until 2 h after accelerator addition. It is an adaptation of the procedure described in [100] and consists in mechanically introducing a cylindrical needle into the mortar at the velocity of 60 mm/min until the minimum penetration of 25 mm is reached (figure 7.3). The diameters of the needles were 4.5, 6.4, 9.0, 14.3, 20.28 and 28.66 mm and each needle was chosen according to matrix strength, so that the minimum penetration force at 25 mm was 100 N. The resulting force was divided by the sectional area of the needle to obtain the penetration resistance. Initial and final setting times were obtained when the penetration resistance reached 3.5 and 27.6 MPa, respectively. Five penetrations were performed at each age.
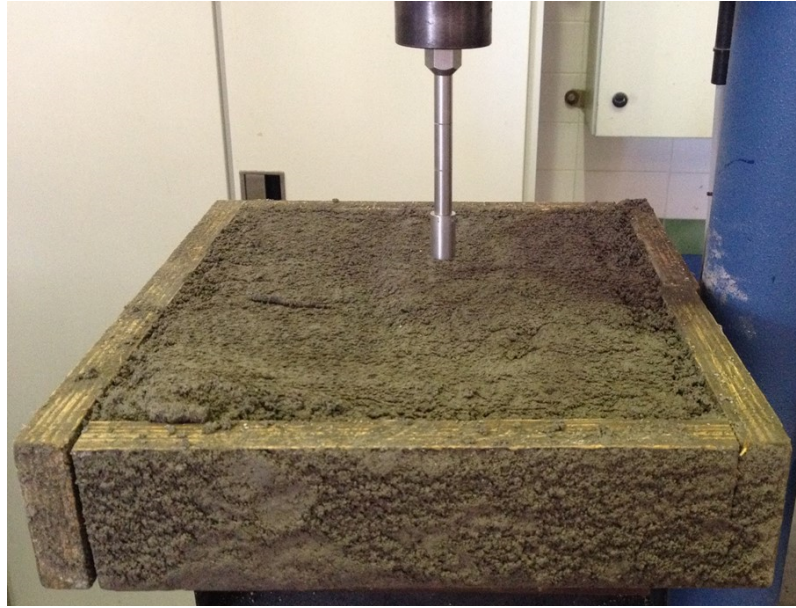
Figure 7.3 - Execution of the penetration test.

7.2.4.3. Pin penetration test

The goal of the pin penetration test was to determine an indirect compressive strength (If_c) of the matrix until 24 h. This test is an adaptation of the procedure described in [91] and consists in introducing a pin into the matrix using a Windsor® WP-2000 gun. The diameter and the length of the pin measure 3 and 30 mm, respectively. The depth of penetration is determined and the compressive strength is calculated based on a correlation table given in [147]. Five penetrations were performed at each age.

7.2.4.4. Compression

Compressive strength (f_c) was obtained from direct compression tests of cylindrical mortar cores measuring 25 mm in diameter and 50 mm in length. Cores were extracted from sprayed panels following the procedures from [90]. Tests were performed in a universal test machine at a pressure application rate equal to 0.45 MPa/min, according to [103]. Six specimens were tested at each age. Figure 7.4 shows the mortar specimens extracted from the sprayed panels and the execution of compression test.
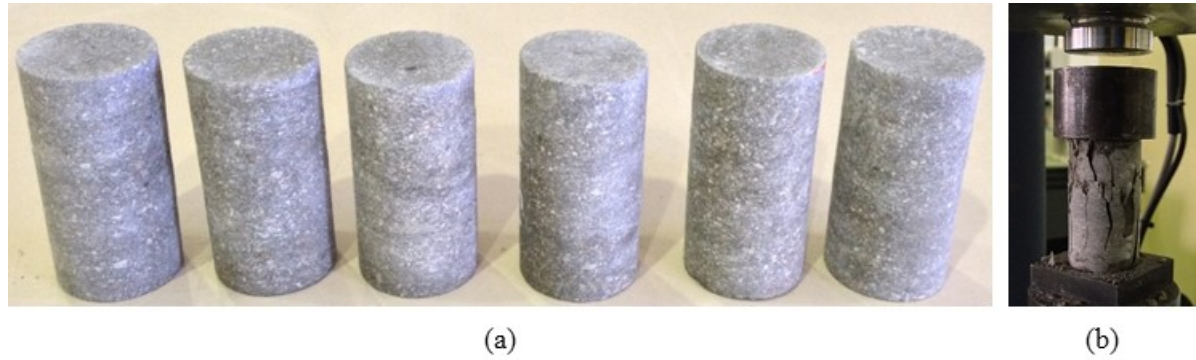
Figure 7.4 - Mortar cores extracted from the sprayed panels (a) and test specimen after compression test (b).

7.2.4.5. Water accessible porosity

Water accessible porosity (W_p) was determined according to [104]. Cores measuring 25 mm in diameter and 50 mm in length, extracted from sprayed panels, were used. Specimens were immersed in water during three days and their saturated weight (w_s) was measured after that. Then, specimens were dried at 60 ºC during five days and their dry weight (w_d) was determined. This temperature was used in order to avoid dehydration of C-S-H and ettringite and to obtain data about the capillary porosity. Water accessible porosity was calculated using equation 7.1. Three specimens were used at each age.

$$W_p \quad = \quad \frac{w_s - w_d}{w_d} \qquad \text{Equation 7.1}$$

7.3. Results and discussion

7.3.1. Isothermal calorimetry

Heat of hydration and energy release curves of all sprayed mortars analyzed are presented in figures 7.5 and 7.6, respectively. Results obtained with CEM I mortars are presented on the left, whereas results from CEM II/A-L mortars are on the right. Figures 7.5.a and 7.5.b represent the curve from 0 to 24 h, while figures 7.5.c and 7.5.d present the heat flow generated in the accelerator peak. The characteristic points of the heat flow curves determined according to table 3.8 are summarized in table 7.3.
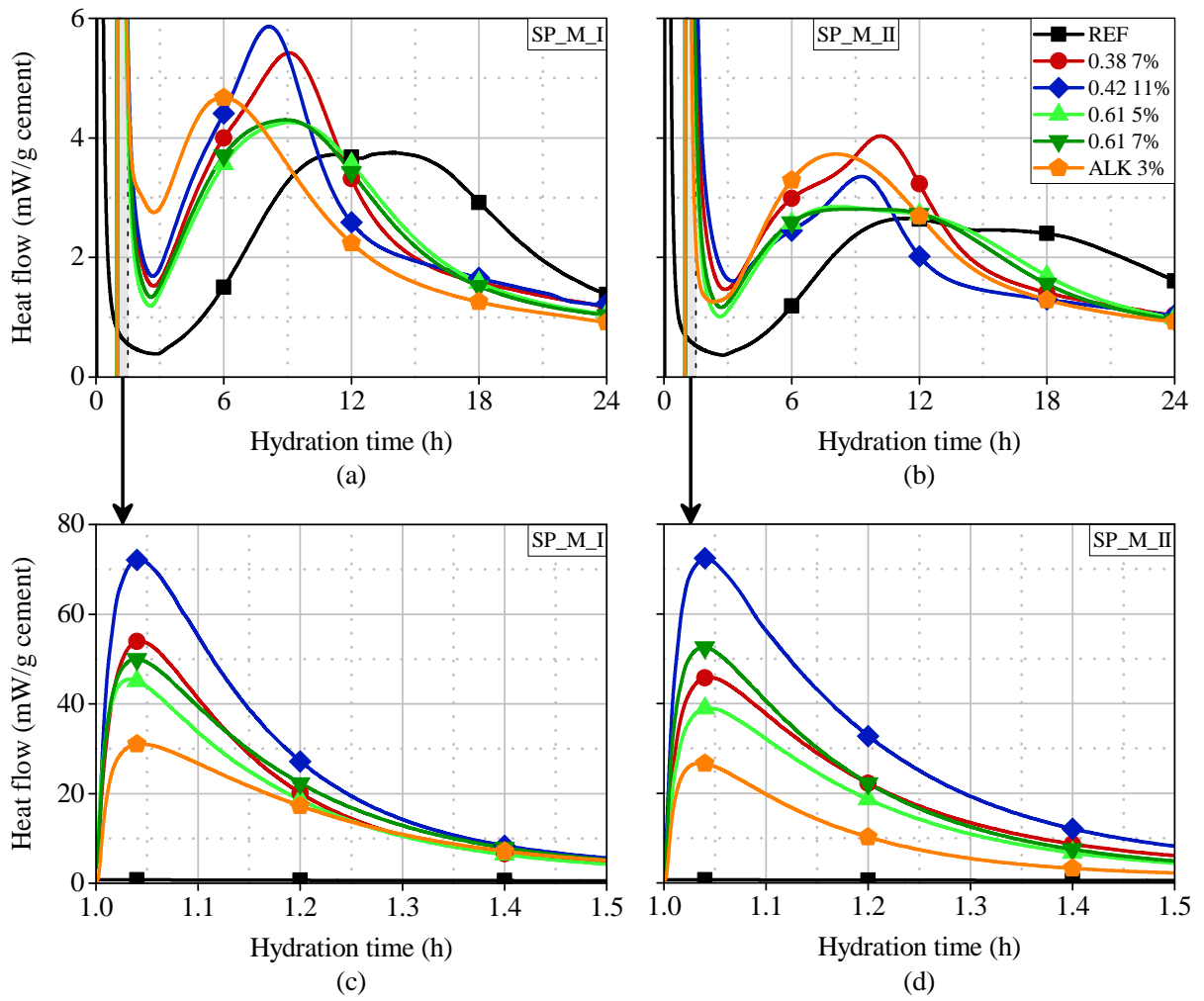
Figure 7.5 - Heat flow curves obtained with CEM I and CEM II/A-L sprayed mortars from 0 to 24 h (a and b) and from 1.0 to 1.5 h (c and d).
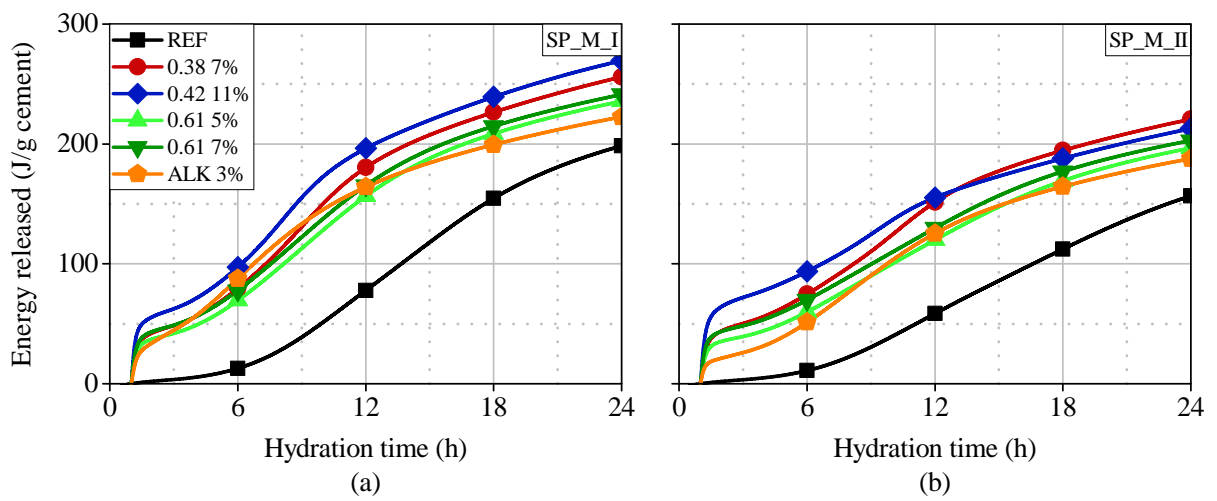
Figure 7.6 - Energy release curves obtained with CEM I (a) and CEM II/A-L (b) sprayed mortars from accelerator addition to 24 h.

Table 7.3 - Analysis of the heat flow curves obtained with sprayed mortars.

Mortar	Slope - accel. peak (mW/g.h)	Energy released - accel. peak (J/g)	Maximum heat flow - accel. peak (mW/g)	Induction period (h)	Slope acceleration - main peak (mW/g.h)	Energy released - main peak (J/g)	Maximum heat flow - main peak (mW/g)	Energy released until 24 h (J/g)
I_REF	-	-	-	4.16	0.56	207.7	3.72	244.1
I_AKF 0.38 7%	1168	37.14	54.0	1.43	0.87	220.5	5.42	244.4
I_AKF 0.42 11%	1574	49.10	72.1	1.45	0.99	225.8	5.86	246.1
I_AKF 0.61 5%	1115	32.65	45.5	1.26	0.76	199.0	4.26	228.7
I_AKF 0.61 7%	1113	37.90	50.0	1.30	0.78	196.2	4.30	229.0
I_ALK 3%	653	27.32	31.1	1.52	0.91	172.5	4.67	220.9
II_REF	-	-	-	4.07	0.40	173.7	2.66	185.3
II_AKF 0.38 7%	911	36.86	45.9	1.62	0.60	173.9	4.03	212.4
II_AKF 0.42 11%	1616	55.23	72.4	1.95	0.38	141.8	3.36	186.2
II_AKF 0.61 5%	793	30.76	39.0	1.34	0.54	157.1	2.85	194.5
II_AKF 0.61 7%	1185	38.38	52.5	1.41	0.53	152.4	2.81	193.1
II_ALK 3%	718	18.25	26.7	1.59	0.72	155.6	3.37	198.1

Results obtained by isothermal calorimetry of sprayed mortars are similar to the heat flow and energy release curves obtained with hand-mixed and sprayed pastes (figures 3.9 and 3.10 from section 3.3.4 and figures 6.6 and 6.7 from section 6.3.3). Because of that, the kinetics and mechanisms of hydration observed in pastes will be adopted in this section to explain the behavior of mortars, which will not be discussed further. The main difference in the behavior of pastes and mortars is the intensity from the accelerator peak, which is smaller in mortars due to the dilution of cement and accelerators caused by the aggregates.

7.3.2. Needle penetration resistance

Figure 7.7 presents the average results of needle penetration resistance from 15 to 120 min after accelerator addition in sprayed mortars. Reference mortars (without accelerator) were not evaluated because this period covers the induction period in these samples and no evolution of detectable penetration resistance was observed.
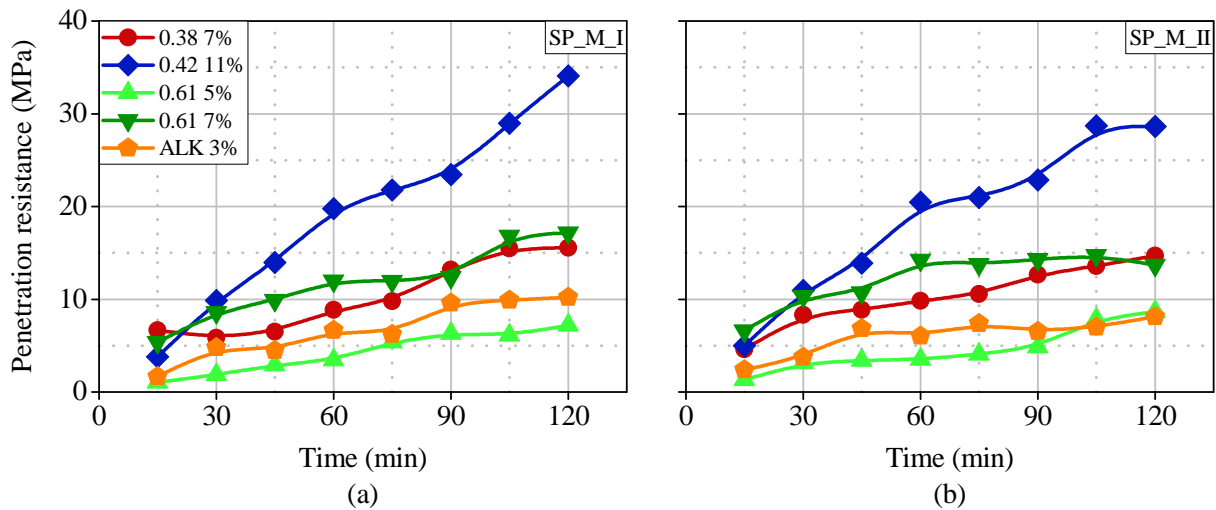
Figure 7.7 - Average values of needle penetration resistance obtained with CEM I (a) and CEM II/A-L (b) sprayed mortars from 15 to 120 min after accelerator addition.

The initial evolution of mechanical strength depends on accelerator type and dosage and is independent on cement type. As observed in *in situ* XRD (section 3.3.3) and isothermal calorimetry (sections 3.3.4, 6.3.3 and 7.3.1), the amount of ettringite formed in matrices produced with alkali-free accelerators is directly proportional to Al^{3+} content in the admixture. Such observation is corroborated by the penetration test, because increasing amounts of Al^{3+} added to the mortar provide higher initial strengths and higher rates of strength evolution. Therefore, mortars SP_I_AKF 0.42 11% and SP_II_AKF 0.42 11% present the highest values of penetration resistance, as accelerator AKF 0.42 11% is the most reactive. On the contrary, mortars SP_I_AKF 0.61 5% and SP_II_AKF 0.61 5% present the lowest mechanical strength since this accelerator used at 5.0 % bcw provides the lowest amount of Al^{3+} ions.

This may also be observed in the determination of initial and final setting times. Mortars containing AKF 0.38 7%, AKF 0.42 11% and AKF 0.61 7% presented initial setting times before 15 min, whereas initial setting times with matrices SP_I_AKF 0.61 5% and SP_II_AKF 0.61 5% were 56 and 60 min, respectively. Until the end of the test, final setting was only observed in mortars SP_I_AKF 0.42 11% and SP_II_AKF 0.42 11%, both at 100 min.

The penetration resistance of mortars SP_I_ALK 3% and SP_II_ALK 3% is only higher than the equivalent mortars produced with AKF 0.61 5%. They presented initial setting at 25 min. This difference is based on the aluminum content incorporated by these accelerators (table 3.5). As observed in *in situ* XRD and isothermal calorimetry, the rate of ettringite formation in alkaline accelerated pastes is the lowest because it is limited by gypsum dissolution. Therefore, initial mechanical strength evolution occurs at the lowest rate.

7.3.3. Indirect compressive strength

Figure 7.8 shows the average results of indirect compressive strength from 4 to 24 h after accelerator addition in sprayed mortars. Reference mortars were not evaluated because little evolution of mechanical strength was observed until 12 h of hydration due to the retarding effect of the superplasticizer. Compressive strength of mortar SP_II_ALK 3% at 4 h was below the detection limit of the equipment (1.2 MPa) and, therefore, is not shown.

Figure 7.8 - Average values of indirect compressive strength obtained with CEM I (a) and CEM II/A-L (b) sprayed mortars from 4 to 24 h after accelerator addition.

Results obtained depend on cement type. Mortars produced with CEM I present higher indirect compressive strengths than mortars containing CEM II/A-L, due to the higher alite content and fineness of the former (tables 3.1 and 3.3). From 4 to 12 h, CEM I mortars present a faster rate of strength evolution than CEM II/A-L mortars. After 12 h, the indirect compressive strength continues increasing in CEM I mortars, while a decrease in the rate of strength gain occurs in mortars produced with CEM II/A-L. These facts are related with higher slopes and energy released in the main hydration peak when CEM I is used (figure 7.5).

Besides, the evolution of mechanical strength during this period is also influenced by accelerator type and dosage and the compatibility between cement and accelerator. As a general rule, properly sulfated systems achieve faster rates of strength evolution than systems containing lower amounts of sulfate. Mortars with low final C_3A/SO_3 ratios (with AKF 0.38 and AKF 0.42, whose Al_2O_3/SO_4^{2-} ratios are similar to that of ettringite) present higher rates of strength evolution until 12 h of hydration. This is closely related with the reaction rate in the

acceleration period obtained with CEM I mortars (figure 7.5 and table 7.3). Mortars produced with AKF 0.61 5% and AKF 0.61 7% present a lower rate of strength evolution, as less sulfate is left to control C_3A hydration, decreasing the rate of alite consumption.

Results obtained with mortars containing the alkaline accelerator are also in agreement with the calorimetric curves. In mortar SP_I_ALK 3%, a fast rate of strength evolution is observed until 12 h, due to the elevated reaction rate in the main hydration peak. However, between 12 and 24 h, strength gain is minimal, as the degree of hydration in this mortar does not increase considerably during this period. As mortar SP_II_ALK 3% presents a wider main hydration peak than the equivalent CEM I mortar, a continuous evolution of mechanical strength until 24 h is achieved.

7.3.4. Compressive strength

In order to provide additional data for the discussion of the results of compressive strength, the water accessible porosity of sprayed mortars is analyzed initially. Figures 7.9.a and 7.9.b show the average results of water accessible porosity of CEM I and CEM II/A-L sprayed mortars, respectively, with cores extracted from sprayed panels tested at 7 and 28 days. Reference mortars were also evaluated.
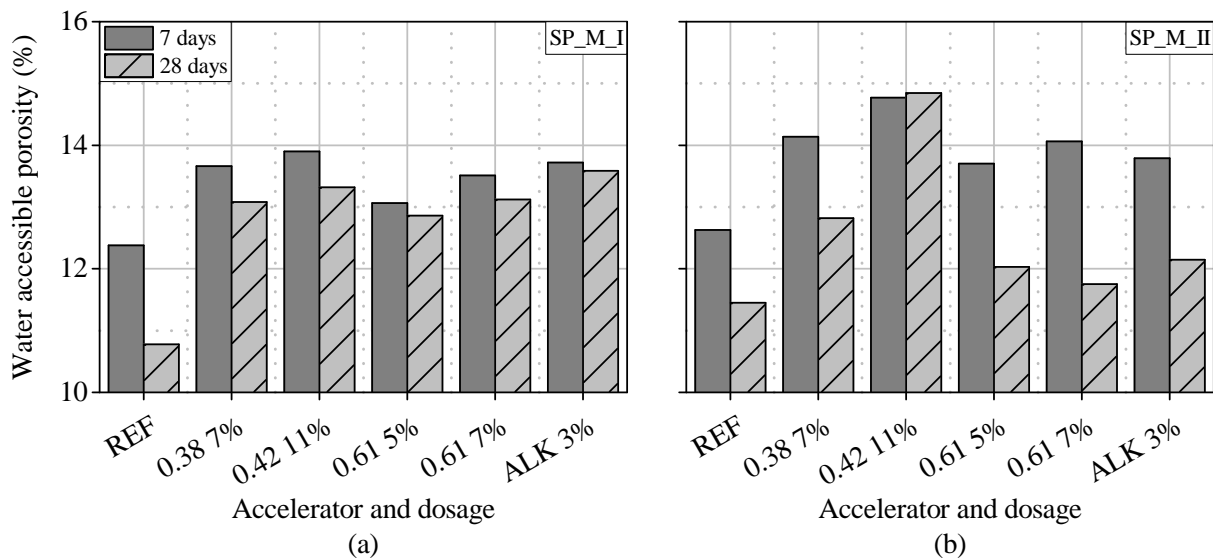
Figure 7.9 - Average values of water accessible porosity in CEM I (a) and CEM II/A-L (b) sprayed mortars at 7 and 28 days.

A significant difference in the values of water accessible porosity of reference and accelerated mortars is observed. Mortars I_REF and II_REF present the lowest values of water accessible porosity at both ages. Accelerated mortars have higher values of water accessible porosity due to the fast setting caused by accelerators and the inclusion of air during the spraying process. Fast setting does not allow enough time for the matrix to consolidate properly and eliminate the entrapped air, leading to higher porosities. As observed in figure 6.9.e, large pores are observed in sprayed pastes due to its poor consolidation.

Water accessible porosity depends on accelerator type and dosage in both cement types. As setting time is directly proportional to ettringite amount formed by accelerator reaction, the higher the accelerator reactivity and dosage, the higher the water accessible porosity of the matrix. The descending order of water accessible porosity is AKF 0.42 11% > AKF 0.38 7% > AKF 0.61 7% > ALK 3% > AKF 0.61 5% > REF.

The reduction in water accessible porosity from 7 to 28 days is more significant in reference mortars due to the lower amount of pores in the matrix. As alite hydration is inhibited in accelerated matrices (sections 3.3.4, 6.3.3 and 7.3.1), lower amounts of hydration products are formed. Because of that, the filling of pores occurs at a lower extent, leading to lower reductions in porosity.

Moreover, the reduction in water accessible porosity is lower in CEM I mortars, because the conversion of ettringite to monosulfoaluminate by C_3A and C_4AF hydrations is associated with increases in porosity (AFt has lower density and higher molecular volume than monosulfoaluminate [16,68]). In CEM II/A-L mortars, limestone filler controls C_3A hydration and leads to the formation of hemi and monocarboaluminate, which indirectly stabilize ettringite [45]. Consequently, larger reductions in porosity are obtained when limestone filler is employed.

Figure 7.10 presents the average compressive strength determined at 1, 3, 7, 28 and 98 days with reference and accelerated mortars. As observed in the evaluation of water accessible porosity, compressive strength varies significantly in mortars with and without accelerators. For a certain age, compressive strength of reference mortars are always higher than in accelerated mortars. Since compressive strength is inversely proportional to porosity [148], the use of accelerators causes a reduction in mechanical strength in part due to the poorer consolidation of the fast setting matrix and the inclusion of air during spraying. The faster the setting time (more reactive accelerators), the lower the compressive strength from 1 day on.
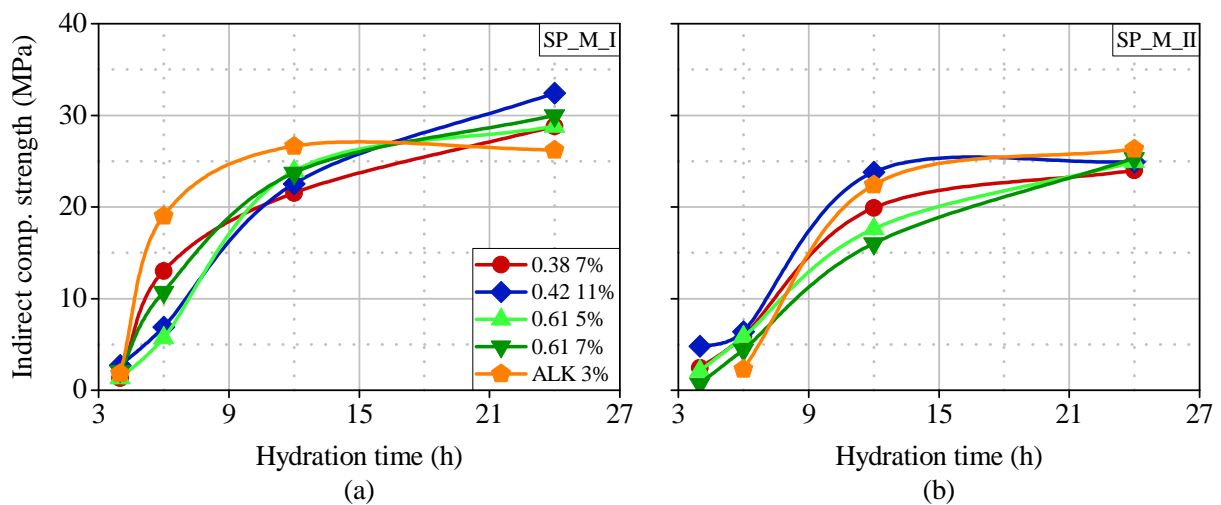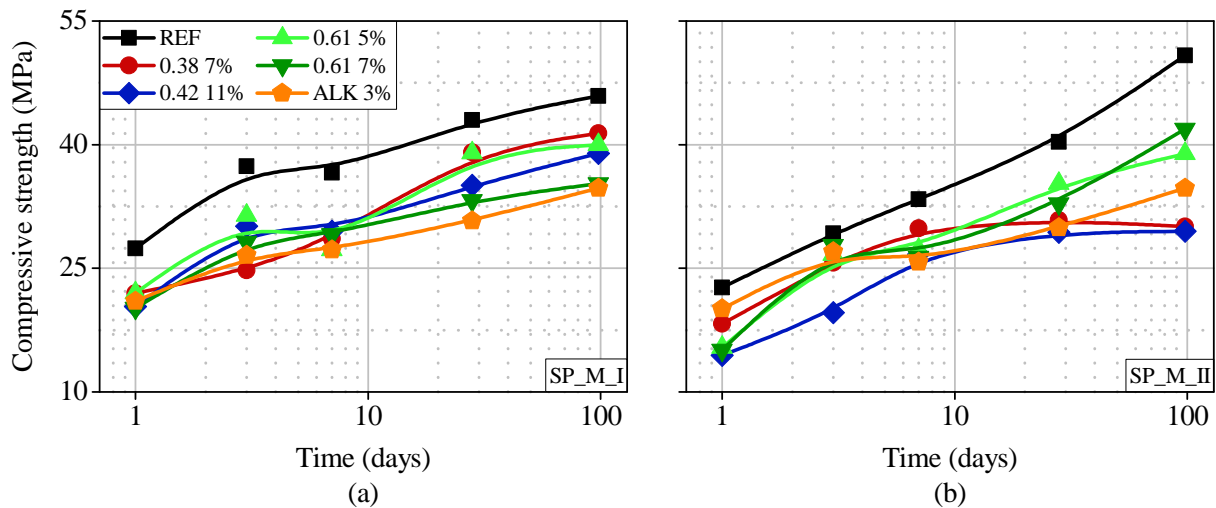
Figure 7.10 - Average values of compressive strength obtained with CEM I (a) and CEM II/A-L (b) sprayed mortars from 1 to 98 days.

Compressive strength at 1 day in mortars produced with alkali-free accelerators is inversely proportional to the final C_3A/SO_3 ratio of the matrix and follows the opposite order found for the evolution of penetration resistance (AKF 0.38 7% > AKF 0.61 5% > AKF 0.61 7% > AKF 0.42 11%), with the exception of AKF 0.42 11%. The higher amount of sulfate left after accelerator addition in mortar SP_I_AKF 0.38 7% controls C_3A reactions and alite hydration proceeds normally. Although AKF 0.42 has a low Al_2O_3/SO_4^{2-} ratio, it is the most reactive accelerator and produces the largest amount of ettringite. Therefore, it increases water accessible porosity and reduces compressive strength. This fact was also observed by [1] in experiments conducted with sprayed concrete.

Compressive strengths in CEM I mortars at 98 days present the same tendency as the results at 1 day. Mortar SP_I_AKF 0.38 7% presents the highest compressive strength among all accelerated mortars evaluated because alite hydration is not negatively affected by undersulfated C_3A reactions. Mortar SP_I_AKF 0.42 11% has the lowest compressive strength due to the elevated water accessible porosity.

A similar trend is observed with CEM II/A-L mortars at 1 day. However, at the age of 98 days, mortars SP_II_AKF 0.61 5% and SP_II_AKF 0.61 7% showed higher compressive strength than the equivalent CEM I mortars. Limestone filler contained in CEM II/A-L controls and retards C_3A reactions, avoiding the negative effects on silicate hydration and leading to higher degrees of hydration.

On the contrary, mortars SP_II_AKF 0.38 7% and SP_II_AKF 0.42 11% did not present the expected strength evolution, since compressive strength presents a low increase from 7 days on. As the conversion of ettringite to monosulfoaluminate occurs with a reduction in volume [16,68], this processes leads to increases in porosity. This increase in porosity may explain the low values of compressive strength in these matrices at 98 days, since the amounts of ettringite formed by AKF 0.38 and AKF 0.42 determined by *in situ* XRD (section 3.3.3.2) are the highest in the group of accelerators evaluated.

Regarding alkaline accelerated mortars, compressive strength of mortar SP_I_ALK 3% at 1 day is similar to mortars containing alkali-free accelerators, while SP_II_ALK 3% presents a higher value than the other accelerated matrices produced with CEM II/A-L. Since mortars produced with the alkaline accelerator have the highest C_3A/SO_3 ratios, C_3A hydration is advanced. This may be beneficious at early ages due to the densification of the matrix with aluminate hydrated products, resulting in improved compressive strengths at 1 day.

However, the early formation of AFm phases fills up the space available in the matrix quickly and the precipitation of these phases on the surface of cement grains reduces their solubility. Consequently, the rate and extent of alite hydration at later ages is reduced, resulting in lower ultimate compressive strengths. As presented in figure 3.7, pastes I_ALK 3% and II_ALK 3% have the highest content of unreacted alite at 98 days. Reductions in mechanical strength at late ages in sprayed concrete accelerated with sodium aluminate were also reported by [1].

7.4. Multivariate regression analyses

Multivariate regression analyses were performed to identify the relation between chemical processes occurring during hydration and the mechanical properties of the matrix. In this study, the mechanical properties (needle and pin penetration resistance and compressive strength) of the sprayed mortars were considered as dependent variables. As water accessible porosity influences mechanical strength, it was also considered as a dependent variable in the analysis. The independent variables correspond to the chemical properties of cement and accelerators and the phase composition of pastes determined by *in situ* and powder XRD.

In total, 29 parameters of each of the 12 mortars analyzed were evaluated (more than 10 different combinations for each regression). The most statistically significant independent

variables are shown in table 7.4. They were selected through analyses of variance adopting a confidence level equal to 95 % (only the independent variables that presented p-values below 0.05 were accepted). The influence of limestone filler was also analyzed, but results did not show a significant dependence on this variable.

Table 7.4 - Selection of statistically significant variables to model each test.

Dependent variable	Independent variables
Needle penetration resistance	Time, ettringite content in paste, aluminum content in accelerator
Pin penetration resistance	Alite, portlandite and amorphous phases contents in paste, final C_3A/SO_3 ratio, porosity
Compressive strength	Time, amorphous content in paste, aluminum content in accelerator, final C_3A/SO_3 ratio, porosity
Water accessible porosity	Time, maximum ettringite content, aluminum and sulfate contents in accelerator

Results are presented from sections 7.4.1 to 7.4.5. The correlations obtained are a simple useful tool to evaluate in a quantitative way how the mechanical behavior of the matrix is affected by the chemical characteristics of its starting materials. These correlations provide a reference for the selections of the components, depending on the application requirements. It is important to emphasize that these analyses are valid for the time interval studied here.

7.4.1. Needle penetration resistance (up to 2 h from casting)

Table 7.5 presents the parameters used to model the needle penetration resistance, their coefficients and p-values. Equation 7.2 represents the best-fit model and figure 7.11 shows a plot of the penetration resistance determined experimentally versus the values predicted by the model.

Table 7.5 - Parameters selected to model needle penetration resistance.

Parameter	Abbreviation	Coefficient	P-value
Time (min)	t	- 0.232	< 0.001
Ettringite content in paste (%)	E	0.283	< 0.001
Time·Aluminum content in accelerator (mmol/g cement)	t·Al	1.98	< 0.001

$$PR\ (MPa) \quad = \quad - 0.232 \cdot t + 0.283 \cdot E + 1.98 \cdot t \cdot Al \qquad \text{Equation 7.2}$$
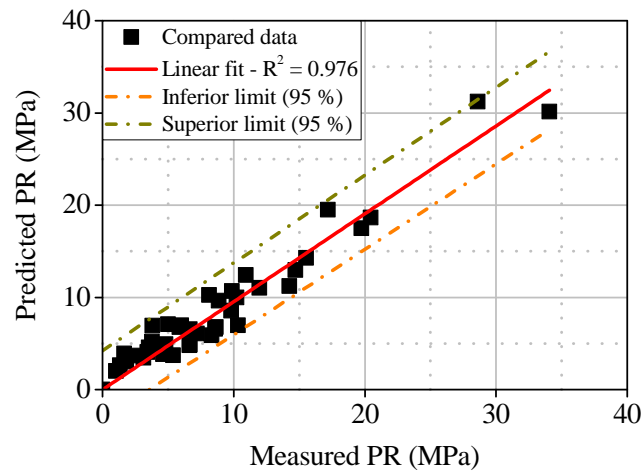
Figure 7.11 - Plot of measured versus predicted needle penetration resistance.

Despite the big difference in terms of the accelerators used, R^2 equal to 0.976 was achieved, demonstrating that the model proposed provides a statistically significant prediction of the measured results. It indicates that penetration resistance increases with time, depends majorly on accelerator reactivity and is not influenced by cement type, in accordance with the discussion in section 7.3.2.

Furthermore, the correlation demonstrates that penetration resistance is a function of the amount of ettringite produced by accelerator addition. Since ettringite is the main product that leads to initial mechanical strength in the sprayed mortars evaluated, the larger the amount of ettringite formed by accelerator addition, the higher the penetration resistance of the matrix. The use of high dosages of accelerators and formulations containing high concentrations of aluminum contribute to form ettringite, reducing setting times and increasing the rate of initial strength development.

7.4.2. Indirect compressive strength (from 4 to 24 h)

Table 7.6 summarizes the parameters adopted to model the indirect compressive strength determined by the pin penetration test, their coefficients and p-values. Equation 7.3 presents the final model obtained and figure 7.12 represents a plot of the measured versus the predicted indirect compressive strength.

Table 7.6 - Parameters adopted to model indirect compressive strength.

Parameter	Abbreviation	Coefficient	P-value
Constant	-	311.8	< 0.001
Alite content in paste (%)	C_3S	- 6.84	< 0.001
Portlandite content in paste (%)	CH	- 4.65	0.025
(Portlandite content in paste)^2	CH^2	- 0.128	< 0.001
Amorphous phases content in paste (%)	Am	0.810	0.012
Final C_3A/SO_3 ratio	$C/\bar{S}$	- 50.7	< 0.001
Porosity (%)	P	- 5.22	< 0.001
Alite content in paste·Porosity	$C_3S·P$	0.122	< 0.001
Portlandite content in paste·Final C_3A/SO_3 ratio	$CH·C/\bar{S}$	3.93	< 0.001
Portlandite content in paste·Porosity	CH·P	0.115	0.003

$$If_c \text{ (MPa)} = \begin{array}{l} 311.8 - 6.84·C_3S - 4.65·CH - 0.128·CH^2 + 0.810·Am - 50.7·C/\bar{S} \\ - 5.22·P + 0.122·C_3S·P + 3.93·CH·C/\bar{S} + 0.115·CH·P \end{array} \qquad \text{Equation 7.3}$$
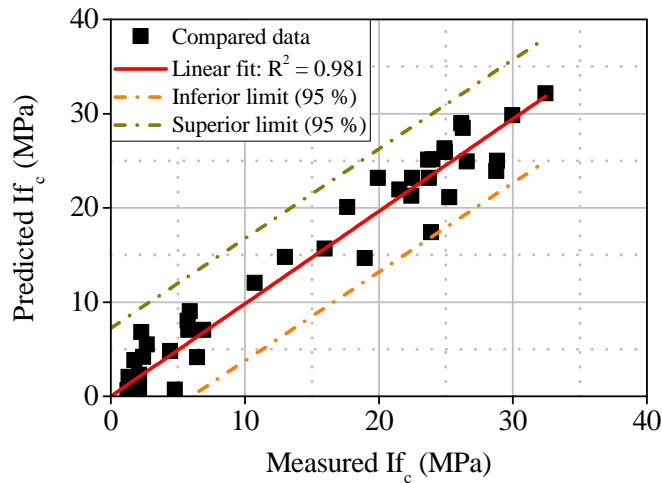
Figure 7.12 - Plot of measured versus predicted indirect compressive strength.

The fitted model presents R^2 equal to 0.981, suggesting a high correlation between measured and predicted indirect compressive strength. It indicates that pin penetration resistance depends on cement and accelerator types, as discussed in section 7.3.3.

According to the regression derived statistically, the indirect compressive strength is directly proportional to the degree of hydration of alite. As alite hydrates, forming portlandite

and C-S-H, compressive strength increases. The correlation also confirms that systems with high C_3A/SO_3 ratios tend to present reductions in the pin penetration resistance, because undersulfated C_3A reactions occur before the onset of the main hydration process. The precipitation of AFm phases on the surface of cement grains reduce their solubility and reactivity, suppressing alite hydration.

7.4.3. Compressive strength (from 24 h to 98 days)

Table 7.7 shows the parameters used to model the compressive strength, their coefficients and p-values. Equation 7.4 represents the best-fit model obtained and figure 7.13 shows a plot of the measured versus the predicted compressive strength.

Table 7.7 - Parameters adopted to model compressive strength.

Parameter	Abbreviation	Coefficient	P-value
Time (days)	t	0.0467	0.005
Amorphous phases content in paste (%)	Am	0.397	< 0.001
Aluminum content in accelerator (mmol/g cement)	Al	- 42.6	< 0.001
(Final C_3A/SO_3 ratio)^2	$(C/\bar{S})^2$	- 67.3	< 0.001
Final C_3A/SO_3 ratio·Porosity	$C/\bar{S}·P$	1.56	< 0.001

$$f_c \text{ (MPa)} \quad = \quad 0.0467·t + 0.397·Am - 42.6·Al - 67.3·(C/\bar{S})^2 + 1.56· C/\bar{S}·P \qquad \text{Equation 7.4}$$
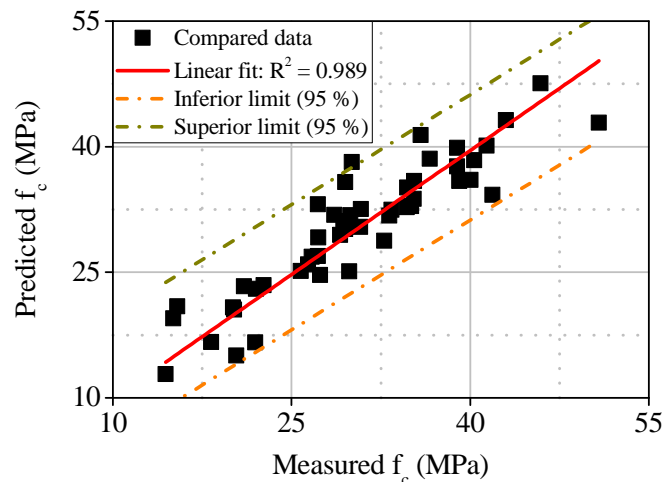
Figure 7.13 - Plot of measured versus predicted compressive strength.

The high coefficient of determination obtained (R^2 equal to 0.989) indicates that the model proposed predicts accurately the experimental results. Compressive strength increases with time and with the degree of hydration. The correlation confirms that the larger the content of amorphous phases, the higher the compressive strength of the matrix. This is consistent with the fact that C-S-H (indirectly quantified by the amorphous content) is the hydrated phase that presents the highest strength-contributing potential.

Furthermore, the use of high dosages of accelerator and formulations containing high aluminum concentrations tend to reduce the compressive strength, since the massive precipitation of ettringite leads to fast setting and to a poor consolidation of the matrix. As described in the previous section (section 7.4.2), systems characterized by elevated C_3A/SO_3 ratios contribute to the early formation of aluminate hydrates. This suppresses alite hydration, reduces the degree of hydration of the matrix and, consequently, reduces its ultimate compressive strength. Such situation is reflected in equation 7.4, since the final C_3A/SO_3 ratio and aluminum content in accelerator appear with a negative sign.

7.4.4. Water accessible porosity (from 7 to 28 days)

Table 7.8 presents the parameters selected to model water accessible porosity, their coefficients and p-values. Equation 7.5 represents the final model obtained and figure 7.14 shows a plot of the water accessible porosity determined experimentally versus the values predicted by the model.

Table 7.8 - Parameters used to model water accessible porosity.

Parameter	Abbreviation	Coefficient	P-value
Time (days)	t	- 0.0855	< 0.001
(Time)^2	t^2	0.000570	< 0.001
Maximum ettringite content (%)	E_{max}	1.88	< 0.001
(Maximum ettringite content)^2	E_{max}^2	- 0.0610	< 0.001
Sulfate content in accelerator (mmol/g cement)	$\bar{S}$	- 86.4	< 0.001
(Sulfate content in accelerator)^2	$\bar{S}^2$	- 194.4	< 0.001
Time·Aluminum content in accelerator (mmol/g cement)	t·Al	0.150	< 0.001
Maximum ettringite content·Sulfate content in accelerator	$E_{max}·\bar{S}$	6.40	< 0.001

$$W_p\,(\%) \;=\; \frac{-\,0.0855 \cdot t + 0.000570 \cdot t^2 + 1.88 \cdot E_{max} - 0.0610 \cdot E_{max}^2 - 86.4 \cdot \bar{S}}{-\,194.4 \cdot \bar{S}^2 + 0.150 \cdot t \cdot Al + 6.40 \cdot E_{max} \cdot \bar{S}}$$

Equation 7.5
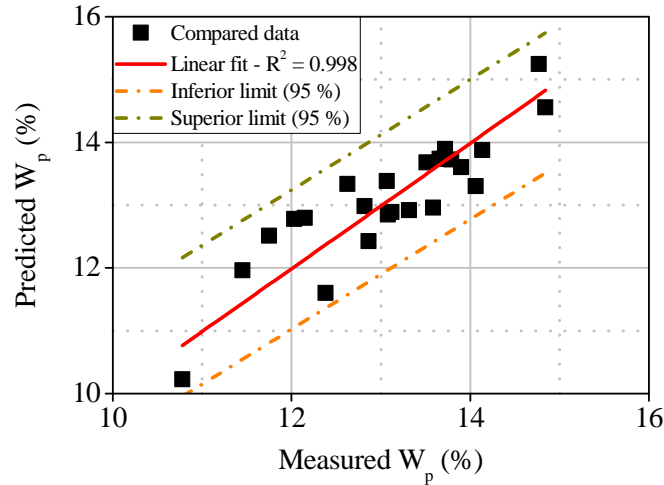
Figure 7.14 - Plot of measured versus predicted water accessible porosity.

Again, a high correlation between experimental and predicted data was obtained (R^2 equal to 0.998). The model indicates that water accessible porosity decreases with time, as expected. The degree of hydration of cement increases as time passes, filling up the pores with hydration products and reducing porosity.

As mentioned in sections 3.3.3 and 7.3.4, accelerators containing high aluminum concentrations tend to form large amounts of ettringite that compromise the consolidation and compaction during the spraying process, leading to increases in porosity. This is consistent with descending order of water accessible porosity presented in section 7.3.4 (AKF 0.42 11% > AKF 0.38 7% > AKF 0.61 7% > ALK 3% > AKF 0.61 5% > REF).

On the contrary, accelerators containing high amounts of sulfate contribute to reduce porosity because the conversion from ettringite to monosulfoaluminate, which occurs with reductions in volume, is reduced. In addition, the early formation of AFm phases is avoided. Therefore, alite hydration proceeds normally and pores are filled by the precipitation of C-S-H and portlandite. Both observations are present in equation 7.5 since the aluminum and sulfate contents in accelerators appear with positive and negative signs, respectively.

7.4.5. Summary of results

Table 7.9 presents a summary of the parameters studied and their influence on the development of properties of sprayed mortars. Ascending arrows indicate an increase in the parameter analyzed and descending arrows, a decrease. The number of arrows in each cell is directly proportional to the influence of the parameter analyzed, taking into account their coefficient obtained in each regression from sections 7.4.1 to 7.4.3.

Table 7.9 - Summary of the variables evaluated and their influence on mechanical strength.

Parameter	Change	Refer to	Effect on mechanical strength		
			0 - 2 h	4 - 24 h	24 h - 98 d
Al^{3+} in accelerator or accelerator dosage	↑	Section: 7.3.2 Figure: 7.7	↑ ↑ ↑	-	↓
Ettringite amount formed by accelerator	↑	Section: 7.3.2 Figure: 7.7	↑ ↑ ↑	-	↓
Alite consumption	↑	Sections: 7.3.3, 7.3.4 Figures: 7.8, 7.10	-	↑ ↑	↑
Amorphous (C-S-H) content	↑	Sections: 7.3.3, 7.3.4 Figures: 7.8, 7.10	-	↑	↑
Final C_3A/SO_3 ratio	↑	Sections: 7.3.3, 7.3.4 Figures: 7.8, 7.10	-	↓	↓ ↓
Porosity	↑	Sections: 7.3.3, 7.3.4 Figures: 7.8, 7.10	-	↓	↓ ↓

7.5. Concluding remarks

Chapter 7 presented the characterization of mechanical properties of accelerated sprayed mortars and their relation with the chemical processes occurring during hydration. The following conclusions may be drawn from the experimental results:

- The characterization of the hydration behavior of accelerated matrices by *in situ* and powder XRD and isothermal calorimetry explain the trends observed regarding the evolution of mechanical properties of sprayed matrices.

- Penetration resistance depends majorly on accelerator reactivity. High Al^{3+} contents incorporated in cement matrices will result in a fast and highly exothermic ettringite formation. This leads to fast setting and an elevated early strength gain. However, the large amounts of aluminate hydrated products formed by accelerator reaction suppresses alite hydration, reducing the mechanical strength at late ages.

- Strength development from 4 h on does not depend solely on porosity. Cement and accelerator types, the compatibility between them and the final C_3A/SO_3 ratio of the matrix play an important role on strength evolution.

- In properly sulfated systems (low final C_3A/SO_3 ratios), sulfate depletion occurs shortly after the acceleration period of the main hydration process. This retards C_3A reactions and avoids the early formation of AFm phases. Therefore, alite hydration proceeds normally, leading to higher degrees of hydration and higher compressive strength.

- In undersulfated systems (high final C_3A/SO_3 ratios), accelerated C_3A reactions occur before or during the acceleration period of silicate hydration. This process fills up the pores with aluminate hydrated products and reduce the solubility of cement phases. Consequently, it decreases the rate and extent of alite hydration and leads to lower degrees of hydration and mechanical strength at late ages.

- Water accessible porosity is mainly influenced by accelerator reactivity. When large ettringite amounts are formed, the matrix stiffens quickly due to the increase in its solid/liquid ratio, does not consolidate properly and entraps air during spraying. As a consequence, water accessible porosity increases in accelerated matrices, reducing compressive strength.

- Correlations between the mechanical strength evolution of mortars and their chemical properties and phase composition were established. All regressions were higher than 0.976, indicating that the models developed provide statistically significant predictions of the experimental results, despite the wide range of mixes evaluated.

- As a recommendation, the selection of materials for an adequate evolution of mechanical strength should be based on the chemical composition of cement and accelerators. In order to achieve a balance between short and long term properties, aluminum content added to the matrix, controlled by Al^{3+} concentration or accelerator dosage, should be the minimum necessary for an adequate spraying and consolidation consistency. Furthermore, its

Al_2O_3/SO_4^{2-} molar ratio should be similar to that of ettringite (0.33), so that sulfate balance of cement is not negatively altered. The most adequate final C_3A/SO_3 ratio of the accelerated matrix is the one to obtain properly sulfated systems.

- Finally, as a general analysis of the procedure employed, the small-scale spraying process is a good alternative to real sprayed concrete testing. It is better controlled, requires lower amount of material and is less expensive and labor intensive than field trials. It can be used successfully to evaluate accelerator reactivity, compatibility between cement and accelerator and the resulting mechanical properties of mortars.

8. Conclusions and future perspectives

8.1. General conclusions

As mentioned previously, sprayed concrete is a widely used technique that requires several further studies. The current work aimed at the characterization of hydration behavior, microstructure development and mechanical strength evolution of cementitious matrices produced with alkali-free and alkaline accelerators. This section presents the general conclusions obtained from each general objective defined in chapter 1.

Regarding the first general objective, kinetics and mechanisms of hydration and the microstructure development of accelerated cement pastes were characterized. This part focused on elucidating the main chemical processes occurring during accelerator reaction and further cement hydration. Accelerators alter mainly C_3A hydration, due to the consumption of sulfate ions from the liquid phase. The acceleration of C_3A reactions in undersulfated systems reduces the rate and extent of alite hydration and limits the development of mechanical strength of the matrix.

The second general objective comprised the parametrization of the early age hydration of accelerated cement pastes. The main chemical properties of cements and accelerators were evaluated and their influence on accelerator reactivity and further cement hydration was explained. Combinations of compatible materials for a proper hydration behavior were recommended.

Concerning the third general objective, ultrasound measurements were successfully employed to characterize the setting and hardening of cement pastes and mortars containing accelerators. A continuous evaluation of these processes was obtained and the main properties that influence microstructure development until 24 h were defined. Correlations between ultrasound propagation velocity and the chemical properties and phase composition of the matrix were obtained, providing a clear definition of the main parameters that influence US velocity.

The kinetics and mechanisms of hydration of sprayed pastes were characterized, according to the fourth general objective. The influence of the mixing process on accelerator reactivity and on further cement hydration was determined. Although several changes in hydration kinetics were observed when alkali-free accelerators were used, the fundamental reaction mechanisms did not change. However, when alkaline accelerators were employed, C_3A reactions were accelerated, affecting alite hydration negatively.

The last general objective, regarding the evaluation of the mechanical properties of accelerated cementitious matrices, was also accomplished. The main chemical processes influencing the evolution of mechanical strength at early and late ages were determined. Correlations between mechanical strength and the chemical properties and phase composition of the matrix were obtained. To finish, recommendations for the selection of materials for an adequate evolution of mechanical strength were given.

8.2. Specific conclusions

Chapter 1 outlines some specific objectives for each of the five general objectives proposed in this thesis. In each chapter corresponding to the experimental campaign, several results and conclusions were detailed. In order to provide a general idea of the results obtained, the main specific conclusions are presented subsequently.

Hydration and microstructure development of accelerated cementitious matrices

- Accelerator reactions lead to a fast formation of sulfoaluminate hydrates and their rate is directly proportional to the Al^{3+} content added to the matrix. When alkali-free accelerators are used, the main hydrate formed is ettringite, which precipitates as hexagonal needle-like

crystals with flat terminations in an ordered structure in hand-mixed pastes. However, in pastes accelerated with alkaline formulations, plate-like crystals of AFm phases are observed.

- The consumption of sulfate ions by accelerator reactions plays a major role on C_3A and alite hydrations. In properly sulfated systems, renewed C_3A hydration occurs after the acceleration period of alite hydration, which proceeds normally. However, in undersulfated systems, accelerated C_3A reactions occur, with consequent formation of AFm phases before the onset of alite hydration. This process limits the rate and extension of alite dissolution and further hydration.

- The early precipitation of aluminate hydrates formed by accelerator reaction fills up the space available in the matrix and suppresses alite hydration. This process is intensified when high dosages of accelerators are employed, since the Al^{3+} content added to the matrix is higher.

- Several parameters influence the early age hydration behavior of accelerated cement pastes. Regarding the chemical composition of cements, the rate of accelerator reaction increases when gypsum content is above 4 %, when hemihydrate is the setting regulator, if cements contain low C_3A contents and if limestone filler is used as an addition. Moreover, further cement hydration is enhanced when the final C_3A/SO_3 ratio of the matrix ranges between 0.67 and 0.90. In these systems, undersulfated C_3A reactions are avoided and alite hydration proceeds normally, achieving higher degrees of hydration until 24 h.

Characterization of setting and hardening by ultrasound measurements

- The setting and hardening processes of cement pastes and mortars containing accelerators were evaluated continuously by ultrasound propagation velocity. This technique is more precise than standard test methods (Vicat and penetration tests) commonly used to determine the mechanical strength of cementitious matrices at early ages. It is sensitive to changes in the mix composition, providing an interesting evaluation of the compatibility between cement and accelerators.

- Variations in kinetics of hydration may be analyzed by ultrasound measurements. The increase in ultrasound velocity during accelerator reaction is directly proportional to the

Al^{3+} content added to the matrix. The larger the ettringite amount formed by accelerators, the faster ultrasound waves will propagate through the matrix, due to the improvement in the interconnectivity in the solid phase.

- Ultrasound propagation during the acceleration period depends on the amount of C-S-H and AFm phases formed by alite and C_3A hydrations. Since the elastic modulus of AFm phases is 2 and 3.5 times higher than the elastic modulus of ettringite and C-S-H, respectively, undersulfated systems present higher ultrasound velocities during the deceleration period than properly sulfated ones. This is due to the larger amounts of AFm phases formed by accelerated C_3A hydration in matrices where low sulfate contents remain after accelerator reaction.

Influence of spraying on hydration

- Spraying increases the rate of accelerator reaction, which is transport-controlled, due to the optimized diffusion and homogenization of accelerators in the matrix. Due to this reason, sulfate consumption from the liquid phase is also accelerated, leading to faster C_3A reactions and the consequent precipitation of AFm phases before the onset of the main hydration process. Consequently, alite dissolution and further hydration are suppressed, reducing the degrees of hydration from 12 h on.

- The morphology of ettringite formed in sprayed pastes differs considerably from that in hand-mixed pastes. This hydrate is more uniformly distributed throughout the matrix, but the crystals precipitate in a disarranged microstructure and are characterized by shorter and less-regularly formed needles. The high shearing conditions achieved during spraying does not provide enough time for ettringite crystals to nucleate and orientate properly.

- Spraying provides a higher sensitivity in the analysis of different accelerators and is recommended especially in the case of alkaline formulations. However, the evaluation of different cementitious systems with the same accelerator by isothermal calorimetry may be performed effectively in hand-mixed pastes.

- XRD, TGA and SEM should be preferentially conducted in sprayed pastes in order to obtain a more representative quantification of the phases formed and to analyze variations in hydration mechanisms caused by the mixing process.

Mechanical behavior of accelerated cementitious matrices

- The mechanical strength evolution until 2 h of hydration depends majorly on accelerator reactivity and is directly proportional to the amount of Al^{3+} ions added to the matrix. The higher the amount of sulfoaluminate hydrates formed by accelerator reaction, the higher the strength of the matrix.

- The compatibility between cement and accelerator and the sulfate amount left after accelerator reaction play a major role on the development of mechanical properties from 4 h on. In properly sulfated systems, higher degrees of hydration and higher mechanical strength are obtained because uncontrolled C_3A reactions are avoided. However, the early formation of AFm phases in undersulfated systems decreases alite dissolution and leads to lower degrees of hydration and mechanical strength at late ages.

- When accelerators containing high Al^{3+} concentrations are used at high dosages, the matrix stiffens quickly due to the large amount of sulfoaluminate hydrates formed. Consequently, the matrix does not consolidate properly and entraps air during spraying, resulting in high porosities and low mechanical strength at late ages.

- Correlations between the chemical and mechanical properties of the matrix were established and the main chemical parameters affecting the development of mechanical strength and their relative importance were determined. All regressions presented R^2 higher than 0.976, indicating that the models developed provide statistically significant predictions of the experimental results, despite the wide range of mixes evaluated. The correlations obtained provide a simple and useful tool to predict the mechanical behavior of the matrix based on the chemical composition of cement and accelerators.

Small-scale spraying process

- The small-scale spraying process employed in chapters 6 and 7 may be used successfully to evaluate accelerator reactivity, compatibility between cement and accelerator and the resulting mechanical properties of mortars. It is a good alternative to real sprayed concrete testing, because it is easier to control, requires lower amount of material and is less expensive and labor intensive than field spray trials.

8.3. Future perspectives

Despite the contribution reported in the previous section, further research on the subjects addressed in this doctoral thesis is required. For that reason, several suggestions for future research and experimental programs are proposed below.

Chemistry of accelerator and cement hydration

- The addition of accelerators at different times should be evaluated because the ionic concentration in the liquid phase changes as hydration progresses. Therefore, different kinetics of hydration may be observed.

- The influence of temperature on accelerator reactivity and further cement hydration should be analyzed, since sprayed concrete is employed in diverse environmental conditions.

- The microstructure development of accelerated cement pastes should be analyzed *in situ* to avoid the influence of sample preparation on the morphology hydrated phases.

- The change in pH in the pore solution caused by different accelerators and its influence on hydration kinetics need to be further analyzed.

- Sprayed pastes should be prepared with different w/c ratios to analyze the effects on hydration kinetics.

- The compatibility of accelerators with other admixtures used to improve concrete performance, such as nanosilica, should be evaluated.

- Investigation on the influence of belite and ferrite phases on the early hydration of accelerated cementitious matrices should be considered.

- The hydration behavior and mechanical strength development of cementitious matrices accelerated with formulations containing fluoric acid should be analyzed. Nowadays, these formulations are common in countries from Asia in applications where the substrate for concrete spraying contains water infiltrations. As calcium fluoride presents a very low solubility, the precipitation of this phase on the surface of cement grains may limit alite hydration and the evolution of mechanical strength of the matrix.

Characterization of accelerated cementitious matrices

- The phase evolution of cement pastes containing accelerators should be characterized by high-resolution synchrotron X-ray powder diffraction. By using this technique, the radiation penetrates deeper in the sample and improves particle statistics, which increases the quality of the refinements. In addition, as an X-ray diagram is obtained in approximately 50 µs, a more detailed analysis of the evolution of aluminate hydrates generated by accelerator reaction may be obtained.

- A thermodynamic analysis of the hydration of accelerated cement pastes may be performed to obtain more information about the hydrate assemblage in these matrices. By using this tool, several formulations of accelerators may be analyzed theoretically, without numerous experimental tests. Furthermore, the hydration behavior of each mix may be predicted based on the chemical composition of cements and accelerators.

- Ultrasound measurements should be employed in sprayed matrices. In the equipment used in chapter 5, only hand-mixed matrices could be analyzed, due to the small size of the molds (140 mL). A special panel with transducers coupled to its base or the introduction of transducers on the surface of the sprayed material right after spraying may be feasible options for this evaluation. By doing so, an *in situ* characterization of setting and hardening in sprayed matrices could be assessed. In addition, this system could be employed in the construction site for the quality control of sprayed concrete, avoiding the use of penetration tests.

- The characterization of the pore size distribution of accelerated cementitious matrices by mercury intrusion porosimetry may provide valuable information about the compaction and consolidation of the matrix containing different accelerator types. This evaluation may help understand how the fast setting caused by reactive accelerators affects compressive strength.

- The durability of cementitious matrices containing different types of accelerators to external sulfate attack should be evaluated. As the sulfoaluminate hydrates formed by alkali-free and alkaline accelerators and further C_3A hydration depend on the sulfate balance of the matrix, the deleterious expansion reactions caused by the external sulfate attack may have different damaging effects depending on the accelerator used.

- The hydration behavior and microstructure of sprayed concrete should be evaluated because the stronger shearing conditions achieved by the equipment employed in concrete spraying may alter accelerator reactivity and hydration rates. In addition, coarse aggregates generate a high impact energy during spraying, which improves the consolidation of the matrix and alters the microstructure formed.

- Since the small-scale spraying process made use of cores measuring 25 mm in diameter and 50 mm in length, it is important to evaluate if cores of larger size are more adequate for the determination of compressive strength of sprayed mortar.

9. References

[1] I. Galobardes, Characterization and control of wet-mix sprayed concrete with accelerators. Ph.D. Thesis (2013).

[2] http://www.marketsandmarkets.com/Market-Reports/Sprayed-concrete-shotcrete-market-1116.html, Shotcrete/Sprayed Concr. Mark. by Process (Wet - Mix Dry - Mix. by Appl. (Undergr. Constr. Water Retaining Struct. Prot. Coatings, Repair Work. Others), by Syst. (Robotic Manual) by Reg. - Glob. Trends Forecas. (2015) 243. http://www.marketsandmarkets.com/Market-Reports/Sprayed-concrete-shotcrete-market-1116.html (accessed September 5, 2016).

[3] D. Lootens, B. Lindlar, R.J. Flatt, Some peculiar aspects of shotcrete accelerators, in: First international conference on microstructure related to durability of cementitious composites, Nanjing (China), 13-15 october, 2008: pp. 1255-1261.

[4] Q. Xu, J. Stark, Early hydration of ordinary Portland cement with an alkaline accelerator, Advances in Cement Research, 17 (2005) 1-8.

[5] R.P. Salvador, S.H.P. Cavalaro, A. Rueda, A.D. Figueiredo, Effect of cement composition on the reactivity of alkali-free accelerating admixtures for shotcrete. In: *7th International Symposium on Sprayed Concrete*. Sandefjord, Norway, June/2014: pp. 350-360.

[6] C. Maltese, C. Pistolesi, A. Bravo, F. Cella, T. Cerulli, D. Salvioni, Effects of an inorganic acid based alkali-free accelerator on the setting and compressive strength development, Cem. Concr. Res. 37 (2007) 528-536. doi:10.1016/j.cemconres.2007.01.002.

[7] L.R. Prudêncio, Accelerating admixtures for shotcrete. Cem. Concr. Comp. 20 (1998) 213-219.

[8] A.D. de Figueiredo, Early strength and physical properties in accelerated shotcrete in *Shotcrete for Underground Support VIII*, Campos do Jordão (Brazil), 11-15 April, 1999.

[9] M.M. Alonso, M. Palacios, F. Puertas, Compatibility between polycarboxylate-based admixtures and blended-cement pastes, Cem. Concr. Compos. 35 (2013) 151-162. doi:10.1016/j.cemconcomp.2012.08.020.

[10] R.P. Salvador, S.H.P. Cavalaro, I. Segura, A.D. Figueiredo, J. Pérez, Early age hydration of cement pastes with alkaline and alkali-free accelerators for sprayed concrete, Constr. Build. Mater. 111 (2016) 386-398. doi:10.1016/j.conbuildmat.2016.02.101.

[11] R.P. Salvador, S.H.P. Cavalaro, M.A. Cincotto, A.D. Figueiredo, Parameters controlling early age hydration of cement pastes containing accelerators for sprayed concrete, Cem. Concr. Res. 89 (2016) 230-248. doi:10.1016/j.conbuildmat.2016.02.101.

[12] P. Juilland, A. Kumar, E. Gallucci, R.J. Flatt, K.L. Scrivener, Effect of mixing on the early hydration of alite and OPC systems, Cem. Conc. Res. 42 (2012) 1175-1188. doi:10.1016/j.cemconres.2011.06.011.

[13] R.P. Salvador, S.H.P. Cavalaro, M. Cano, A.D. Figueiredo, Influence of spraying on the early hydration of accelerated cement pastes, Cem. Concr. Res. 88 (2016) 7-19. doi:10.1016/j.cemconres.2016.06.005.

[14] O.E. Kjellsen, K O, Detwiller, R J, Gjorv, K.O. Kjellsen, R.J. Detwiller, O.E. Gjorv, Development of microstructures in plain cement pastes hydrated at different temperatures, Cem. Conc. Res. 21 (1991) 179-189.

[15] B. Lothenbach, F. Winnefeld, C. Alder, E. Wieland, P. Lunk, Effect of temperature on the pore solution, microstructure and hydration products of Portland cement pastes, Cem. Conc. Res. 37 (2007) 483-491. doi:10.1016/j.cemconres.2006.11.016.

[16] B. Lothenbach, T. Matschei, G. Möschner, F.P. Glasser, Thermodynamic modelling of the effect of temperature on the hydration and porosity of Portland cement, Cem. Conc. Res. 38 (2008) 1-18. doi:10.1016/j.cemconres.2007.08.017.

[17] J.M. Martínez, Estudio de las variables en el proceso de producción de morteros con acelerante de fraguado. Master Thesis (2013).

[18] I. Galobardes, S.H. Cavalaro, A. Aguado, T. Garcia, Estimation of the modulus of elasticity for sprayed concrete, Constr. Build. Mater. 53 (2014) 48-58. doi:10.1016/j.conbuildmat.2013.11.046.

[19] P. Juilland, Early hydration of cementitious systems. Ph.D. Thesis (2009).

[20] T.P. DiNoia, P.J. Sandberg, Alkali-free shotcrete accelerator interactions with cement and admixtures in *Shotcrete: Engineering Developments*, 2004, 137-144.

[21] H.F.W. Taylor, Cement Chemistry. 2nd ed. Thomas Telford Publishing, 1997.

[22] M.A. Cincotto, Reações de hidratação e pozolânicas, in *Concreto: Ciência e tecnologia*, 2011, cap. 11.

[23] P.K. Mehta, P.J.M. Monteiro, Concrete: Microstructure, properties and materials, 2006. doi:10.1036/0071462899.

[24] AENOR. UNE-EN 197-1:2011. Cement. Part 1: Composition, specifications and conformity criteria for common cements, 2011.

[25] G. Sant, A. Kumar, C. Patapy, G.L. Saout, K. Scrivener, The influence of sodium and potassium hydroxide on volume changes in cementitious materials, Cem. Concr. Res. 42 (2012) 1447-1455. doi:10.1016/j.cemconres.2012.08.012.

[26] R. Siddique, M.I. Khan, Supplementary cementing materials, 2011. doi:10.1007/978-3-642-17866-5.

[27] M. Schneider, M. Romer, M. Tschudin, H. Bolio, Sustainable cement production-present and future, Cem. Concr. Res. 41 (2011) 642-650. doi:10.1016/j.cemconres.2011.03.019.

[28] C. Shi, A.F. Jiménez, A. Palomo, New cements for the 21st century: The pursuit of an alternative to Portland cement, Cem. Concr. Res. 41 (2011) 750-763. doi:10.1016/j.cemconres.2011.03.016.

[29] M. Antoni, J. Rossen, F. Martirena, K. Scrivener, Cement substitution by a combination of metakaolin and limestone, Cem. Concr. Res. 42 (2012) 1579-1589. doi:10.1016/j.cemconres.2012.09.006.

[30] M. Schneider, Process technology for efficient and sustainable cement production, Cem. Concr. Res. 78 (2015) 14-23. doi:10.1016/j.cemconres.2015.05.014.

[31] E. Gartner, H. Hirao, A review of alternative approaches to the reduction of CO_2 emissions associated with the manufacture of the binder phase in concrete, Cem. Concr. Res. 78 (2015) 126-142. doi:10.1016/j.cemconres.2015.04.012.

[32] F. Begarin, S. Garrault, A. Nonat, L. Nicoleau, Hydration of alite containing aluminium. 29th Cement and Concrete Science Congress, Sep. 2009, Leeds, United Kingdom. pp. 9-12, 2009. <hal-00452386>.

[33] P.C. Hewlett, Lea's chemistry of cement and concrete. 4th ed. Elsevier Science and Scientific Books, 2004.

[34] E.M. Gartner, J.F. Young, D.A. Damidot, I. Jawed, Hydration of Portland cement, in: P. Barnes, J. Bensted (Eds.), Struct. Perform. Cem., 2nd ed., Spon Press, London, 2002: pp. 57-113.

[35] A.P. Kirchheim, Aluminatos tricálcico cúbico e ortorrômbico: análise da hidratação *in situ* e produtos formados. Ph.D. Thesis (2008).

[36] C. Fischer, I. Kurganskaya, T. Schäfer, A. Lüttge, Variability of crystal surface reactivity: What do we know?, Appl. Geochemistry. 43 (2014) 132-157. doi:10.1016/j.apgeochem.2014.02.002.

[37] K.L. Scrivener, A. Nonat, Hydration of cementitious materials, present and future, Cem. Concr. Res. 41 (2011) 651-665. doi:10.1016/j.cemconres.2011.03.026.

[38] K.L. Scrivener, P. Juilland, P.J.M. Monteiro, Advances in understanding hydration of Portland cement, Cem. Concr. Res. 78 (2015) 38-56. doi:10.1016/j.cemconres.2015.05.025.

[39] S. Bishnoi, K.L. Scrivener, Studying nucleation and growth kinetics of alite hydration using μic, Cem. Concr. Res. 39 (2009) 849-860. doi:10.1016/j.cemconres.2009.07.004.

[40] V. Rheinheimer, I. Casanova, Hydration of C_3S thin films, Cem. Concr. Res. 42 (2012) 593-597. doi:10.1016/j.cemconres.2012.01.002.

[41] H. Minard, S. Garrault, L. Regnaud, A. Nonat, Mechanisms and parameters controlling the tricalcium aluminate reactivity in the presence of gypsum, Cem. Concr. Res. 37 (2007) 1418-1426. doi:10.1016/j.cemconres.2007.06.001.

[42] S. Pourchet, L. Regnaud, J.P. Perez, A. Nonat, Early C_3A hydration in the presence of different kinds of calcium sulfate, Cem. Concr. Res. 39 (2009) 989-996. doi:10.1016/j.cemconres.2009.07.019.

[43] A. Quennoz, Hydration of C_3A with calcium sulfate alone and in the presence of calcium silicate. Ph.D. Thesis (2011).

[44] G. Möschner, B. Lothenbach, R. Figi, R. Kretzschmar, Influence of citric acid on the hydration of Portland cement, Cem. Concr. Res. 39 (2009) 275-282. doi:10.1016/j.cemconres.2009.01.005.

[45] B. Lothenbach, G.L. Saout, E. Gallucci, K.L. Scrivener, Influence of limestone on the hydration of Portland cements, Cem. Concr. Res. 38 (2008) 848-860. doi:10.1016/j.cemconres.2008.01.002.

[46] P. Juilland, E. Gallucci, R. Flatt, K. Scrivener, Dissolution theory applied to the induction period in alite hydration, Cem. Concr. Res. 40 (2010) 831-844. doi:10.1016/j.cemconres.2010.01.012.

[47] J.W. Bullard, H.M. Jennings, R.A. Livingston, A. Nonat, G.W. Scherer, J.S. Schweitzer, et al., Mechanisms of cement hydration, Cem. Concr. Res. 41 (2011) 1208-1223. doi:10.1016/j.cemconres.2010.09.011.

[48] A. Bazzoni, M. Suhua, Q. Wang, X. Shen, M. Cantoni, K.L. Scrivener, The effect of magnesium and zinc ions on the hydration kinetics of C_3S, J. Am. Ceram. Soc. 97 (2014) 3684-3693. doi:10.1111/jace.13156.

[49] S. Bishnoi, K.L. Scrivener, μic: A new platform for modelling the hydration of cements, Cem. Concr. Res. 39 (2009) 266-274. doi:10.1016/j.cemconres.2008.12.002.

[50] A.J.M. Cuberos, A.G. de la Torre, M.C. Martín-Sedeño, L. Moreno-Real, M. Merlini, L.M. Ordónez, et al., Phase development in conventional and active belite cement pastes by Rietveld analysis and chemical constraints, Cem. Concr. Res. 39 (2009) 833-842. doi:10.1016/j.cemconres.2009.06.017.

[51] G. Álvarez-Pinazo, A. Cuesta, M. García-Maté, I. Santacruz, E.R. Losilla, S.G. Sanfélix, et al., In-situ early-age hydration study of sulfobelite cements by synchrotron powder diffraction, Cem. Concr. Res. 56 (2014) 12-19. doi:10.1016/j.cemconres.2013.10.009.

[52] A. Quennoz, K.L. Scrivener, Hydration of C_3A-gypsum systems, Cem. Concr. Res. 42 (2012) 1032-1041. doi:10.1016/j.cemconres.2012.04.005.

[53] J.A. Dean, Lange's handbook of chemistry. 15th ed. McGrawl-Hill Inc, 1999.

[54] A. Quennoz, K.L. Scrivener, Interactions between alite and C_3A-gypsum hydrations in model cements, Cem. Conc. Res. 44 (2013) 46-54. doi:10.1016/j.cemconres.2012.10.018.

[55] E. Koning, M. Gehlen, A.M. Flank, G. Calas, E. Epping, Rapid post-mortem incorporation of aluminum in diatom frustules: Evidence from chemical and structural analyses, Mar. Chem. 103 (2007) 208-222. doi:10.1016/j.marchem.2006.09.001.

[56] S. Dixit, P. Van Cappellen, Surface chemistry and reactivity of biogenic silica, Geochim. Cosmochim. Acta. 66 (2002) 2559-2568. doi:10.1016/S0016-7037(02)00854-2.

[57] B.R. Bickmore, K.L. Nagy, A.K. Gray, A.R. Brinkerhoff, The effect of Al(OH)$_4^-$ on the dissolution rate of quartz, Geochim. Cosmochim. Acta. 70 (2006) 290-305. doi:10.1016/j.gca.2005.09.017.

[58] T. Chappex, K.L. Scrivener, The influence of aluminium on the dissolution of amorphous silica and its relation to alkali silica reaction, Cem. Concr. Res. 42 (2012) 1645-1649. doi:10.1016/j.cemconres.2012.09.009.

[59] T. Chappex, K.L. Scrivener, The effect of aluminum in solution on the dissolution of amorphous silica and its relation to cementitious systems, J. Am. Ceram. Soc. 96 (2013) 592-597. doi:10.1111/jace.12098.

[60] A. Quennoz, E. Galucci, K.L. Scrivener, Calcium silicate - calcium aluminate interactions and their influence on cement early hydration. In: *13th International Congress on the Chemistry of Cement*. Madrid, Spain, July/2011: pp. 218.

[61] S. Garrault, A. Nonat, Y. Sallier, L. Nicolaeau, On the origin of the dormant period of cement hydration. In: *13th International Congress on the Chemistry of Cement*. Madrid, Spain, July/2011: pp. 240.

[62] X. Pardal, I. Pochard, A. Nonat, Experimental study of Si-Al substitution in calcium-silicate-hydrate (C-S-H) prepared under equilibrium conditions, Cem. Concr. Res. 39 (2009) 637-643. doi:10.1016/j.cemconres.2009.05.001.

[63] M. Daugaard Andersen, H.J. Jakobsen, Jø. Skibsted, Incorporation of aluminum in the calcium silicate hydrate (C-S-H) of hydrated Portland cements: A high-field ^{27}Al and ^{29}Si MAS NMR investigation, Inorg. Chem. 42 (2003) 2280-2287. doi:10.1021/ic020607b.

[64] E. Berodier, K. Scrivener, Understanding the filler effect on the nucleation and growth of C-S-H, J. Am. Ceram. Soc. 12 (2014) 3764-3773. doi:10.1111/jace.13177.

[65] M. Zajac, A. Rossberg, G. Le Saout, B. Lothenbach, Influence of limestone and anhydrite on the hydration of Portland cements, Cem. Concr. Compos. 46 (2014) 99-108. doi:10.1016/j.cemconcomp.2013.11.007.

[66] J. Bizzozero, K.L. Scrivener, Limestone reaction in calcium aluminate cement-calcium sulfate systems, Cem. Concr. Res. 76 (2015) 159-169. doi:10.1016/j.cemconres.2015.05.019.

[67] V. Rheinheimer, I. Casanova, An X-ray photoelectron spectroscopy study of the hydration of C_2S thin films, Cem. Concr. Res. 60 (2014) 83-90. doi:10.1016/j.cemconres.2014.03.005.

[68] T. Matschei, B. Lothenbach, F.P. Glasser, Thermodynamic properties of Portland cement hydrates in the system CaO-Al_2O_3-SiO_2-$CaSO_4$-$CaCO_3$-H_2O, Cem. Concr. Res. 37 (2007) 1379-1410. doi:10.1016/j.cemconres.2007.06.002.

[69] P. Barret, D. Bertrandie, Fundamental hydration kinetic features of the major cement constituents: Ca_3SiO_5 and β-Ca_2SiO_4, J. Chim. Phys. 83 (1986) 765-775.

[70] B. Lothenbach, L. Pelletier-chaignat, F. Winnefeld, Stability in the system CaO-Al_2O_3-H_2O, Cem. Concr. Res. 42 (2012) 1621-1634. doi:10.1016/j.cemconres.2012.09.002.

[71] T. Matschei, B. Lothenbach, F.P. Glasser, The AFm phase in Portland cement, Cem. Concr. Res. 37 (2007) 118-130. doi:10.1016/j.cemconres.2006.10.010.

[72] V. Kocaba, Development and evaluation of methods to follow microstructural development of cementitious systems including slags. Ph.D. Thesis (2009).

[73] K.L. Scrivener, The development of microstructure during the hydration of Portland cement. Ph.D. Thesis (1984).

[74] A. Nonat, J.C. Mutin, X. Lecoq, S.P. Jiang, Physico-chemical parameters determining hydration and particle interactions during the setting of silicate cements, Solid State Ionics. 101-103 (1997) 923-930.

[75] L.S. Castillo, A.A. de Cea, Bi-layer diaphragm walls: Evolution of concrete-to-concrete bond strength at early ages, Constr. Build. Mater. 31 (2012) 29-37. doi:10.1016/j.conbuildmat.2011.12.090.

[76] S. Austin, P. Robins, Y. Pan, Shear bond testing of concrete repairs, Cem. Concr. Res. 29 (1999) 1067-1076. doi:10.1016/S0008-8846(99)00088-5.

[77] C.I. Goodier, Wet-Process sprayed mortar and concrete for repair. Ph.D. Thesis (2000).

[78] EFNARC. European specification for sprayed concrete, 1996, pp. 30. ISBN 095224831X.

[79] N. Ginouse, M. Jolin, Investigation of spray pattern in shotcrete applications, Constr. Build. Mater. 93 (2015) 966-972. doi:10.1016/j.conbuildmat.2015.05.061.

[80] N. Ginouse, M. Jolin, Mechanisms of placement in sprayed concrete, Tunn. Undergr. Sp. Technol. 58 (2016) 177-185. doi:10.1016/j.tust.2016.05.005.

[81] C. Paglia, F. Wombacher, H. Böhni, The influence of alkali-free and alkaline shotcrete accelerators within cement systems: I. Characterization of the setting behavior, Cem. Concr. Res. 31 (2001) 913-918. doi:10.1016/S0008-8846(02)00967-5.

[82] Austrian Concrete Association, Sprayed concrete Guideline, 2013, pp. 94.

[83] C. Maltese, C. Pistolesi, A. Bravo, F. Cella, T. Cerulli, D. Salvioni, et al., Effects of alkali metal hydroxides on alkali-free accelerators, Adv. Cem. Res. 23 (2011) 277-288. doi:10.1680/adcr.2011.23.6.277.

[84] C. Maltese, C. Pistolesi, A. Bravo, T. Cerulli, D. Salvioni, M. Squinzi, Formation of nanocrystals of AFt phase during the reaction between alkali-free accelerators and hydrating cement: a key factor for sprayed concretes setting and hardening, RILEM Proc. F. Full J. TitleRILEM Proc. PRO 45 (2005) 329-338.

[85] C. Maltese, C. Pistolesi, A. Bravo, F. Cella, T. Cerulli, D. Salvioni, Effects of setting regulators on the efficiency of an inorganic acid based alkali-free accelerator reacting with a Portland cement, Cem. Concr. Res. 37 (2007) 528-536. doi:10.1016/j.cemconres.2007.01.002.

[86] C. Maltese, C. Pistolesi, A. Bravo, F. Cella, T. Cerulli, D. Salvioni, A case history: Effect of moisture on the setting behaviour of a Portland cement reacting with an alkali-free accelerator, 37 (2007) 856-865. doi:10.1016/j.cemconres.2007.02.020.

[87] B. Lagerblad, L.E. Bryne, Texture and bond at the interfacial between hard rock and sprayed concrete at early age hardening time. In: *7th International Symposium on Sprayed Concrete*. Sandefjord, Norway, June/2014: pp. 255-265.

[88] AENOR, UNE-EN 14487-1. Sprayed concrete. Part 1: Definitions, specifications and conformity, 2008.

[89] AENOR, UNE-EN 14487-2. Sprayed concrete. Part 2: Execution, 2008.

[90] AENOR. UNE-EN 14488-1:2006. Testing sprayed concrete. Part 1: Sampling fresh and hardened concrete, 2006.

[91] AENOR. UNE-EN 14488-2:2007. Testing sprayed concrete. Part 2: Compressive strength of young sprayed concrete, 2007.

[92]   AENOR, UNE-EN 14488-4. Testing sprayed concrete. Part 4: Bond strength of cores by direct tension, 2008.

[93]   AENOR, UNE-EN 14488-6. Testing sprayed concrete. Part 6: Thickness of concrete on a substrate, 2007.

[94]   L. Wadsö, F. Winnefeld, K. Riding, P. Sandberg, Calorimetry, in: A Pract. Guid. to Microstruct. Anal. Cem. Mater., CRC Press, 2015: pp. 37-74. doi:doi:10.1201/b19074-3.

[95]   P.J. Sandberg, W. Walsh, Use of calorimetry to select materials for shotcrete, in: *Shotcrete: Elements of a System*, CRC Press, 2010: pp. 255-259. doi:doi:10.1201/b10545-30.

[96]   R. Snellings, X-ray powder diffraction applied to cement, in: A Pract. Guid. to Microstruct. Anal. Cem. Mater., CRC Press, 2015: pp. 107-176. doi:doi:10.1201/b19074-5.

[97] B. Lothenbach, P. Durdzinski, K.D.E. Weerdt, Thermogravimetric analysis, in: A Pract. Guid. to Microstruct. Anal. Cem. Mater., CRC Press, 2015: pp. 177-212. doi:doi:10.1201/b19074-6.

[98] K. Scrivener, A. Bazzoni, B. Mota, J. Rossen, Electron microscopy, in: A Pract. Guid. to Microstruct. Anal. Cem. Mater., CRC Press, 2015: pp. 351-418. doi:doi:10.1201/b19074-9.

[99] AENOR, UNE-EN 196-3. Methods of testing cement. Part 3: Determination of setting times and soundness, 2009.

[100] ASTM C 403/C 403M-08. Standard test method for time of setting of concrete mixtures by penetration resistance, 2008. doi:10.1520/E0336-11.the.

[101] N. De Belie, C.U. Grosse, J. Kurz, H. Reinhardt, Ultrasound monitoring of the influence of different accelerating admixtures and cement types for shotcrete on setting and hardening behaviour, 35 (2005) 2087-2094. doi:10.1016/j.cemconres.2005.03.011.

[102] H.A.G. Díaz, Caracterización de aditivos acelerantes de fraguado mediante ultrasonidos. Master Thesis (2014).

[103] AENOR, UNE-EN 12390-3. Testing hardened concrete. Part 3: Compressive strength of test specimens, 2009.

[104]   AENOR, UNE 83980. Concrete durability. Test methods. Determination of the water absorption, density and accessible porosity for water in concrete, 2014.

[105]   AENOR, UNE-EN 196-2. Methods of testing cement. Part 2: Chemical analysis of cement, 2006.

[106] M.M. Alonso, F. Puertas, Adsorption of PCE and PNS superplasticisers on cubic and orthorhombic C3A. Effect of sulfate, Constr. Build. Mater. 78 (2015) 324-332. doi:10.1016/j.conbuildmat.2014.12.050.

[107] I.C. Madsen, N.V.Y. Scarlett, A. Kern, Description and survey of methodologies for the determination of amorphous content via X-ray powder diffraction, Zeitschrift Für Krist. 226 (12) (2011) 944-955. doi:10.1524/zkri.2011.1437.

[108] J. Zhang, G.W. Scherer, Comparison of methods for arresting hydration of cement, Cem. Conc. Res. 41 (2011) 1024-1036. doi:10.1016/j.cemconres.2011.06.003.

[109] L.J. Parrot, Modelling the development of microstructure, Proc Research on the manufacture and use of cements, Henniker NH, Engineering Foundation, New York, 1986, p. 47-73.

[110] I. Pane, W. Hansen, Investigation of blended cement hydration by isothermal calorimetry and thermal analysis, Cem. Conc. Res. 35 (2005) 1155-1164. doi:10.1016/j.cemconres.2004.10.027.

[111] F.P. Glasser, The stability of ettringite In: International RILEM TC 186-ISA Workshop on internal sulfate attack and delayed ettringite formation. Villars, Switzerland, September/2002.

[112] A. Kumar, G. Sant, C. Patapy, C. Gianocca, K.L. Scrivener, The influence of sodium and potassium hydroxide on alite hydration: Experiments and simulations, Cem. Conc. Res. 42 (2012) 1513-1523.

[113] E. Gallucci, P. Mathur, K. Scrivener, Microstructural development of early age hydration shells around cement grains, Cem. Concr. Res. 40 (2010) 4-13. doi:10.1016/j.cemconres.2009.09.015.

[114] J.M. Makar, G.W. Chan, by High-Resolution Scanning Electron Microscopy, 1299 (2008) 1292-1299. doi:10.1111/j.1551-2916.2008.02304.x.

[115] G. Li, P. Le Bescop, The U phase formation in cement-based systems containing high amounts of Na_2SO_4, Cem. Concr. Res. 26 (1996) 27-33.

[116] M.J. Sánchez-Herrero, A. Fernández-Jiménez, A. Palomo, $C_4A_3\check{S}$ hydration in different alkaline media, Cem. Concr. Res. 46 (2013) 41-49.

[117] W. Lukas, Substitution of Si in the lattice of ettringite, Cem. Conc. Res. 6 (1976) 225-234.

[118] D.P. Bentz, E.J. Garboczi, C.J. Haecker, O.M. Jensen, Effects of cement particle size distribution on performance properties of Portland cement-based materials, Cem. Concr. Res. 29 (1999) 1663-1671. doi:10.1016/S0008-8846(99)00163-5.

[119] J. Carette, S. Staquet, Monitoring the setting process of mortars by ultrasonic P and S-wave transmission velocity measurement, Constr. Build. Mater. 94 (2015) 196-208. doi:10.1016/j.conbuildmat.2015.06.054.

[120] G. Trtnik, M.I. Valic, G. Turk, Measurement of setting process of cement pastes using non-destructive ultrasonic shear wave reflection technique, NDT&E Int. 56 (2013) 65-75. doi:10.1016/j.ndteint.2013.02.004.

[121] N. Robeyst, C.U. Grosse, N. De Belie, Monitoring fresh concrete by ultrasonic transmission measurements: Exploratory multi-way analysis of the spectral information, Chemom. Intell. Lab. Syst. 95 (2009) 64-73. doi:10.1016/j.chemolab.2008.08.005.

[122] T. Voigt, G. Ye, Z. Sun, S.P. Shah, K. Van Breugel, Early age microstructure of Portland cement mortar investigated by ultrasonic shear waves and numerical simulation, Cem. Concr. Res. 35 (2005) 858-866. doi:10.1016/j.cemconres.2004.09.004.

[123] T. Voigt, Y. Akkaya, S.P. Shah, Determination of early age mortar and concrete strength by ultrasonic wave reflections, ASCE J. Mater. Civ. Eng. 15 (2003) 247-254. doi:10.1061/(ASCE)0899-1561(2003)15:3(247).

[124] M. Molero, I. Segura, M.G. Hernández, M.A.G. Izquierdo, J.J. Anaya, Characterization of mortar samples using ultrasonic scattering attenuation, Phys. Procedia. 3 (2010) 839-845. doi:10.1016/j.phpro.2010.01.108.

[125] Z. Lafhaj, M. Goueygou, A. Djerbi, M. Kaczmarek, Correlation between porosity, permeability and ultrasonic parameters of mortar with variable water/cement ratio and water content, Cem. Concr. Res. 36 (2006) 625-633. doi:10.1016/j.cemconres.2005.11.009.

[126] F.J. Juanes, L.G. Ullate, J.J. Anaya, NDE ultrasonic methods to characterize the porosity of mortar, NDT&E Int. 34 (2001) 557-562. doi:10.1016/S0963-8695(01)00020-2.

[127] M.G. Hernández, J.J. Anaya, T. Sanchez, I. Segura, Porosity estimation of aged mortar using a micromechanical model, Ultrasonics. 44 (2006) e1007-e1011. doi:10.1016/j.ultras.2006.05.195.

[128] M. Molero, S. Aparicio, G. Al-Assadi, M.J. Casati , M.G. Hernández, J.J. Anaya, Evaluation of freeze-thaw damage in concrete by ultrasonic imaging, NDT&E Int. 52 (2012) 86-94. doi:10.1016/j.ndteint.2012.05.004.

[129] I. Segura, M. Molero, S. Aparicio, J.J. Anaya, A. Moragues, Decalcification of cement mortars: Characterization and modelling, Cem. Concr. Compos. 35 (2013) 136-150. doi:10.1016/j.cemconcomp.2012.08.015.

[130] H. Von Daake, D. Stephan, Setting of cement with controlled superplasticizer addition monitored by ultrasonic measurements and calorimetry, Cem. Concr. Compos. 66 (2016) 24-37. doi:10.1016/j.cemconcomp.2015.11.004.

[131] H.K. Lee, K.M. Lee, Y.H. Kim, H. Yim, D.B. Bae, Ultrasonic in-situ monitoring of setting process of high-performance concrete, Cem. Concr. Res. 34 (2004) 631-640. doi:10.1016/j.cemconres.2003.10.012.

[132] N. Robeyst, E. Gruyaert, C.U. Grosse, N. De Belie, Monitoring the setting of concrete containing blast-furnace slag by measuring the ultrasonic p-wave velocity, Cem. Concr. Compos. 38 (2008) 1169-1176. doi:10.1016/j.cemconres.2008.04.006.

[133] G. Trtnik, G. Turk, Influence of superplasticizers on the evolution of ultrasonic P-wave velocity through cement pastes at early age, Cem. Concr. Res. 51 (2013) 22-31. doi:10.1016/j.cemconres.2013.04.007.

[134] S. Aparicio, J. Ranz, R. Fernández, V. Albert, J. V Fuente, M.G. Hernández, Non-destructive monitoring of curing process in precast concrete, IOP Conf. Ser. Mater. Sci. Eng. 42 (2012) 12050.

[135] D. Lootens, M. Hansson, L. Oblak, B. Lindlar, Ultrasonic wave propagation for strength measurements: applications in shotcrete. In: *7th International Symposium on Sprayed Concrete*. Sandefjord, Norway, June/2014.

[136] AENOR, UNE-EN 196-1:2005. Method of testing cement. Part 1: Determination of strength, 2005.

[137] H.W. Reinhardt, C.U. Grosse, Continuous monitoring of setting and hardening of mortar and concrete, Constr. Build. Mater. 18 (2004) 145-154. doi:10.1016/j.conbuildmat.2003.10.002.

[138] J.R. García, Caracterización no destructiva del proceso de curado en materiales cementicios. Ph.D. Thesis (2015).

[139] S. Kamali, M. Moranville, E. Garboczi, S. Prené, B. Gerard, Hydrate dissolution influence on the Young's modulus of cement pastes, in: Proc. 5th Int. Conf. Fract. Mech. Concr. Concr. Struct. Vail, USA, 2004, 631-638.

[140] G. Constantinides, F.-J. Ulm, The effect of two types of C-S-H on the elasticity of cement-based materials: Results from nanoindentation and micromechanical modeling, Cem. Concr. Res. 34 (2004) 67-80. doi:10.1016/S0008-8846(03)00230-8.

[141] J. Woodward, An introduction to geotechnical processes. 1st ed. Spon Press, 2005.

[142] L. Pelletier-chaignat, F. Winnefeld, B. Lothenbach, C. Jörg, Beneficial use of limestone filler with calcium sulphoaluminate cement, Constr. Build. Mater. 26 (2012) 619-627. doi:10.1016/j.conbuildmat.2011.06.065.

[143] S.A. Austin, P.J. Robins, C.I. Goddier, The hardened performance of wet process sprayed mortars, Chem. Eng. (2009) 33. doi:10.1080/0042311YYxxxxxxxx.

[144] C.I. Goodier, S.A. Austin, P.J. Robins, Low-volume wet-process sprayed concrete: hardened properties. Mat. and Struc. 41 (2000) 99-111.

[145] C.S.B. Paglia, F.J. Wombacher, H.K. Böhni, Influence of alkali-free and alkaline shotcrete accelerators within cement systems: hydration, microstructure and strength Development, (2005) 353-357.

[146] AENOR, UNE-EN 1015-3. Methods of test for mortar for masonry. Part 3: Determination of consistency of fresh mortar (by flow table), 2000.

[147] Windsor pin system WP-2000. Instruction manual, 2010, pp. 25.

[148] C. Lian, Y. Zhuge, S. Beecham, The relationship between porosity and strength for porous concrete, Constr. Build. Mater. 25 (2011) 4294-4298. doi:10.1016/j.conbuildmat.2011.05.005.

[149] A.G. de la Torre, S. Bruque, J. Campo, M.A.G. Aranda, The superstructure of C_3S from synchrotron and neutron powder diffraction and its role in quantitative analysis, Cem. Conc. Res. 32 (2002) 1347-1356.

[150] T. Tsurumi, Y. Hirano, H. Kato, T. Kamiya, M. Daimon, Crystal structure and hydration of belite, Ceramic Transactions 40 (1994) 19-25.

[151] W.G. Mumme, R.J. Hill, G. Bushnell-Wye, E.R. Segnit, Rietveld crystal structure refinements, crystal chemistry and calculated powder diffraction data for the polymorphs of dicalcium silicate and related phases, N. Jb. Miner. Abh. 169 (1995) 35-68.

[152] P. Mondal, J.W. Jeffery, The crystal structure of tricalcium aluminate, $Ca_3Al_2O_6$. Acta Cryst. B31 (1975) 689-697.

[153] F. Nishi, Y. Takeuchi, The Al_6O_{18} rings of tetrahedral in the structure of $Ca_{8.5}NaAl_6O_{18}$, Acta Cryst. B 31 (1975) 1169-1173.

[154] A.A. Colville, S. Geller, The crystal structure of brownmillerite, Ca_2FeAlO_5. Acta Cryst, B27 (1971) 2311-2315.

[155] Q. Huang, O. Chmaissem, J.J. Caponi, C. Chaillout, M. Marezio, J.L. Tholence, A. Santoro, Neutron powder diffraction study of the crystal structure of $HgBa_2Ca_4Cu_5O_{12+\delta}$ at room temperature and at 10 K, Phys. C 227 (1994) 1-9.

[156] H.E. Petch, The hydrogen positions in portlandite, $Ca(OH)_2$, as indicated by the electron distribution, Acta Cryst. 14 (1961) 950-957.

[157] R. Wartchow, Datensammlung nach der "learnt profile"-methode(LP) für calcit und vergleich mit der "background peak background"-methode (BPB), Zeit. Kristall. 186 (1989) 300-302.

[158] D. Taylor, Thermal expansion data. I. binary oxides with the sodium chloride and wurtzite structure, M O, Trans. J. Brit. Ceram. Soc. 83 (1984) 5-9.

[159] H. Effenberger, A. Kirfel, G. Will, Studies of the electron density distribution of dolomite, $CaMg(CO_3)_2$, Mineral. Petrol. 31 (1983) 151-164.

[160] A.G. de la Torre, M.G. Lopez-Olmo, C. Alvarez-Rua, S.G. Granda, M.A.G. Aranda, Structure and microstructure of gypsum and its relevance to Rietveld quantitative phase analyses, Powder Diffraction 19 (2004) 240-246.

[161] H. Weiss, M.F. Bräu, How much water does calcined gypsum contain? Angew. Chem. Int. Ed. 48 (2009) 3520-3524.

[162] J.A. McGinnety, Redetermination of the structures of potassium sulphate and potassium chromate: the effect of electrostatic crystal forces upon observed bond lengths, Acta Cryst. B 28 (1972) 2845-2852.

[163] A.G. Nord, Refinement of the crystal structure of thenardite, Na_2SO_4 (V), Acta Chem. Scand. 27 (1973) 814-822.

[164] P. Ballirano, G. Belardi, A. Maras, Refinement of the structure of synthetic syngenite $K_2Ca(SO_4)_2·H_2O$ from X-ray powder diffraction data, Neues Jb Mineral. 182 (2005) 15-21.

[165] F. Goetz-Neunhoeffer, J. Neubauer, Refined ettringite structure for quantitative X-ray diffraction analysis, Powder Diffraction 21 (2006) 4-11.

[166] R. Allmann, Die Doppelschichtstruktur der plaettchenfoermigen Calcium-Aluminium-Hydroxysalze am Beispiel des $(CaO)_3.Al_2O_3.CaSO_4(H_2O)_{12}$, Neues Jahrbuch fuer Mineralogie Monatshefte (1968) 140-144.

[167] T. Runcevski, R.E. Dinnebier, O.V. Magdysyuk, H. Pöllmann, Crystal structures of calcium hemicarboaluminate and carbonated calcium hemicarboaluminate from synchrotron powder diffraction data, Acta Cryst. B68 (2012) 493-500.

[168] M. François, G. Renaudin, O. Evrard, A cementitious compound with composition $3CaO.Al_2O_3.CaCO_3.11H_2O$, Acta Crystallographica, Section C: Crystal Structure Communications 54 (1998) 1214-1217.

[169] E.P. Flint, H.F. McMurdie, L.S. Wells, Hydrothermal and X-Ray studies of the garnet-hydrogarnet series and the relationship of the series to hydration products of Portland cement. Journal of Research of the National Bureau of Standards, 26 (1941) 13-33.

[170] E. N. Maslen, V. A. Streltsov, N. R. Streltsova, N. Ishizawa, Y. Satow, Synchrotron X-ray study of the electron density in alpha-Al_2O_3, Acta Cryst. B49 (1993) 973-980. doi:10.1107/S0108768193006901.

[171] L.A. Gobbo, Aplicação da difração de raios-X e método de Rietveld no estudo do cimento Portland. Ph.D. Thesis (2009).

Appendix A

The structure models used for Rietveld refinement of X-ray diagrams obtained with anhydrous clinkers, cements and pastes are presented in table A.1.

Table A.1 - References of phase structures used for Rietveld refinement.

Phase	Formula	Crystal system	PDF number	ICSD codes	Reference
Alite[a,b]	Ca_3SiO_5	Monoclinic	01-070-8632	94742	[149]
Belite[a,b]	Ca_2SiO_{4m}	Monoclinic	01-083-0460	79550	[150]
Belite[a]	Ca_2SiO_{4o}	Orthorhombic	01-086-0399	81097	[151]
Calcium aluminate[a,b]	$Ca_3Al_2O_{6c}$	Cubic	00-038-1429	1841	[152]
Calcium aluminate[a]	$Ca_3Al_2O_{6o}$	Orthorhombic	00-032-0150	1880	[153]
Ferrite[a,b]	Ca_2AlFeO_5	Orthorhombic	01-071-0667	9197	[154]
Lime[a]	CaO	Cubic	00-043-1001	75785	[155]
Portlandite[a,b]	$Ca(OH)_2$	Rhombohedral	01-072-0156	15741	[156]
Calcite[a,b]	$CaCO_3$	Rhombohedral	01-083-0577	79673	[157]
Periclase[a]	MgO	Cubic	00-045-0946	104844	[158]
Dolomite[a]	$CaMg(CO_3)_2$	Trigonal	01-075-1761	31335	[159]
Gypsum[a,b]	$CaSO_4 \cdot 2H_2O$	Monoclinic	00-033-0311	151692	[160]

Table A.1 - References of phase structures used for Rietveld refinement (*continued*).

Phase	Formula	Crystal system	PDF number	ICSD codes	Reference
Hemihydrate[a]	$CaSO_4 \cdot 0.5H_2O$	Monoclinic	00-041-0224	380286	[161]
Arcanite[a]	K_2SO_4	Orthorhombic	01-070-1488	2827	[162]
Thenardite[a]	Na_2SO_4	Orthorhombic	01-070-1541	2895	[163]
Syngenite[a]	$K_2Ca(SO_4)_2 \cdot H_2O$	Monoclinic	00-028-0739	157072	[164]
Ettringite[b]	$Ca_6Al_2(SO_4)_3 \cdot (OH)_{12} \cdot 26H_2O$	Hexagonal	00-041-1451	155395	[165]
Monosulfoaluminate[b]	$Ca_4Al_2(OH)_{12} \cdot SO_4 \cdot 6H_2O$	Rhombohedral	-	24461	[166]
Hemicarboaluminate[b]	$Ca_4Al_2(OH)_{12} \cdot OH \cdot 0.5CO_3 \cdot 4H_2O$	Rhombohedral	00-041-0221	263124	[167]
Monocarboaluminate[b]	$Ca_4Al_2(OH)_{12} \cdot CO_3 \cdot 5H_2O$	Triclinic	01-087-0493	59327	[168]
Hydrogarnet[b]	$Ca_3Al_2O_6 \cdot 6H_2O$	Cubic	01-077-0240	38279	[169]
Alumina (standard)[a,b]	Al_2O_3	Rhombohedral	01-081-2267	73725	[170]

[a] Used for the quantification of anhydrous clinkers and cements.

[b] Used for the quantification of cement pastes.

The strategy for Rietveld refinement was based on [171] and is presented subsequently.

a) Background adjustment, due to the use of Kapton® film, for *in situ* measurements.

b) Scale factor of all the phases.

c) Flat background.

d) Zero shift.

e) Polinomial background (second and fourth order polynomials for *in situ* and powder measurements, respectively).

f) Unit cell parameters (a, b, c and β) of all the phases to a maximum variation of ± 1 % of the standard values.

g) Peak full width at half maximum (W) when phase content is above 5 %.

h) Preferred orientation of alite, gypsum, calcite, ettringite and portlandite ([-1 0 1], [0 2 0], [1 0 4], [1 0 0] and [0 0 1], respectively).

i) Peak shape (η) and Caglioti parameters (U and V) of alite when its content is above 40 % and only peak shape when it is below 40 %.

j) Peak shape of portlandite when its content is above 10 %.

k) Atomic coordinates were not refined.

Appendix B

Heat flow curves of all the pastes evaluated by isothermal calorimetry in chapter 4 (discussions from section 4.3.2.1 to 4.3.2.6) are shown from figure B.1 to B.8, grouped by cement type. Figures identified by 'a' represent the curve from 0 to 24 h and figures identified by 'b' show a zoom of the heat of hydration curve from 1.0 to 1.5 h, corresponding to the accelerator peak. The characteristic points of the heat flow curves are summarized in table B.1.

Figure B.1 - Heat flow curves obtained with pastes OPC 98_G 2 from 0 to 24 h (a) and from 1.0 to 1.5 h (b).

Figure B.2 - Heat flow curves obtained with pastes OPC 96_G 4 from 0 to 24 h (a) and from 1.0 to 1.5 h (b).
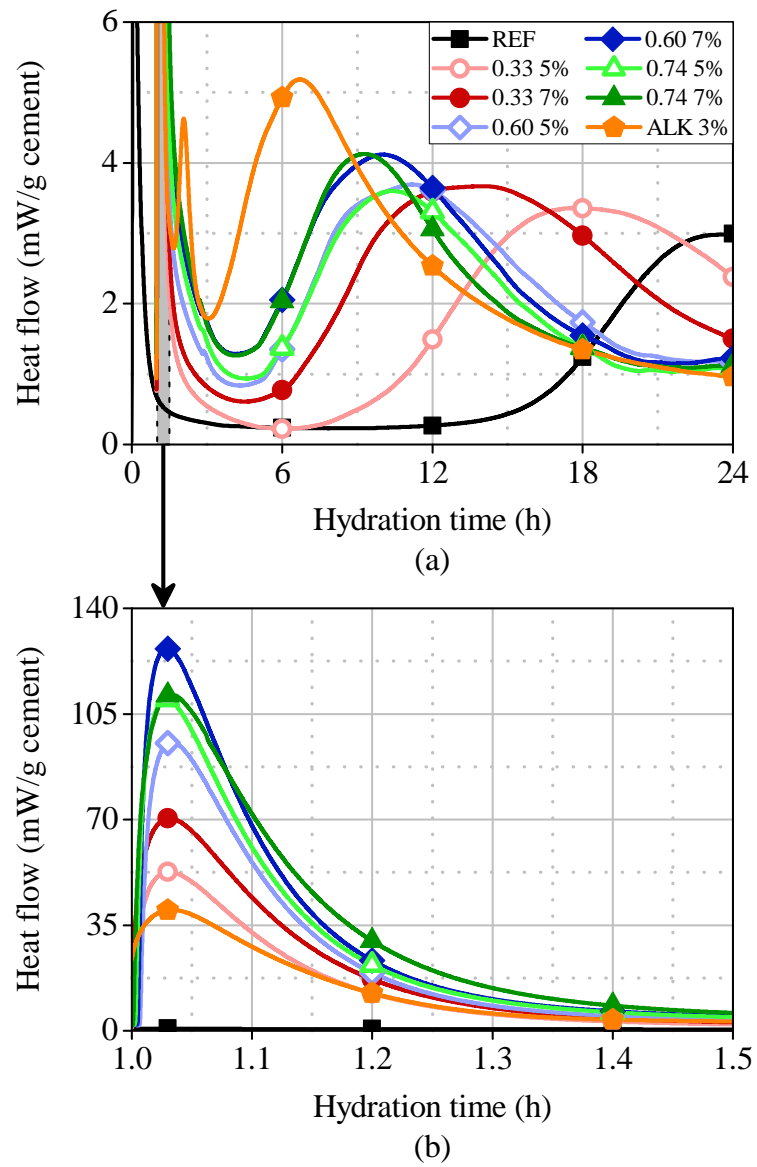
Figure B.3 - Heat flow curves obtained with pastes OPC 94_G 6 from 0 to 24 h (a) and from 1.0 to 1.5 h (b).
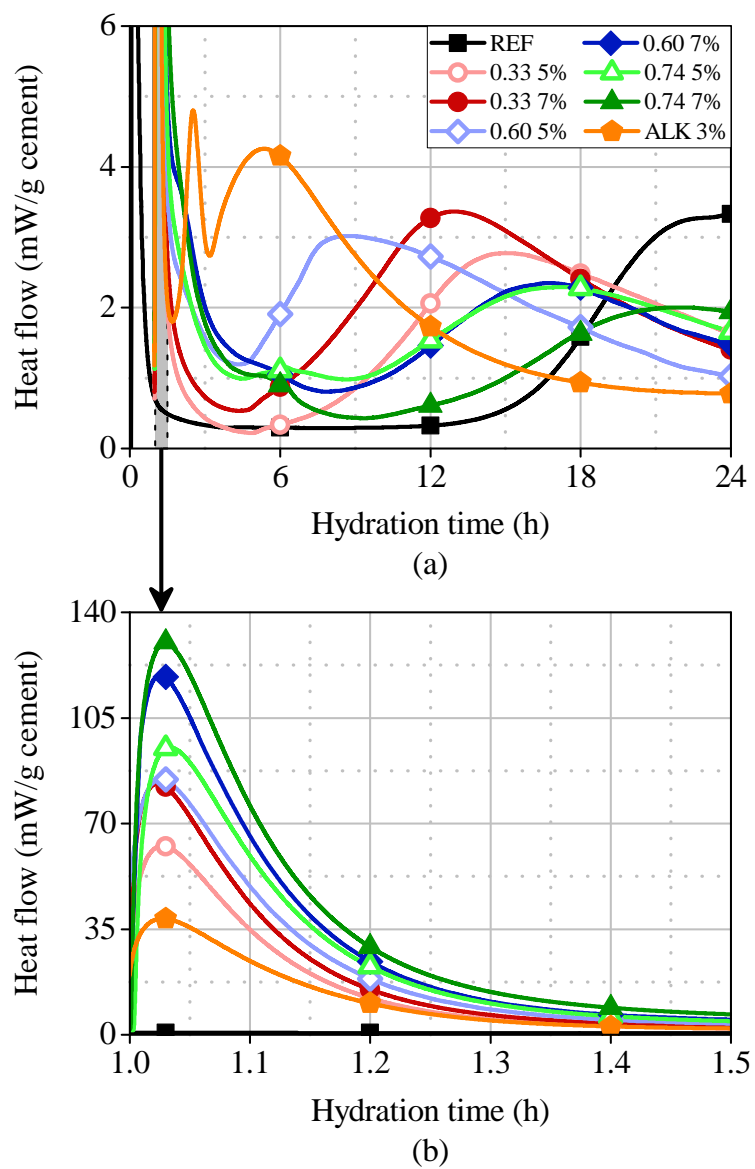
Figure B.4 - Heat flow curves obtained with pastes OPC 96_H 3.38 from 0 to 24 h (a) and from 1.0 to 1.5 h (b).
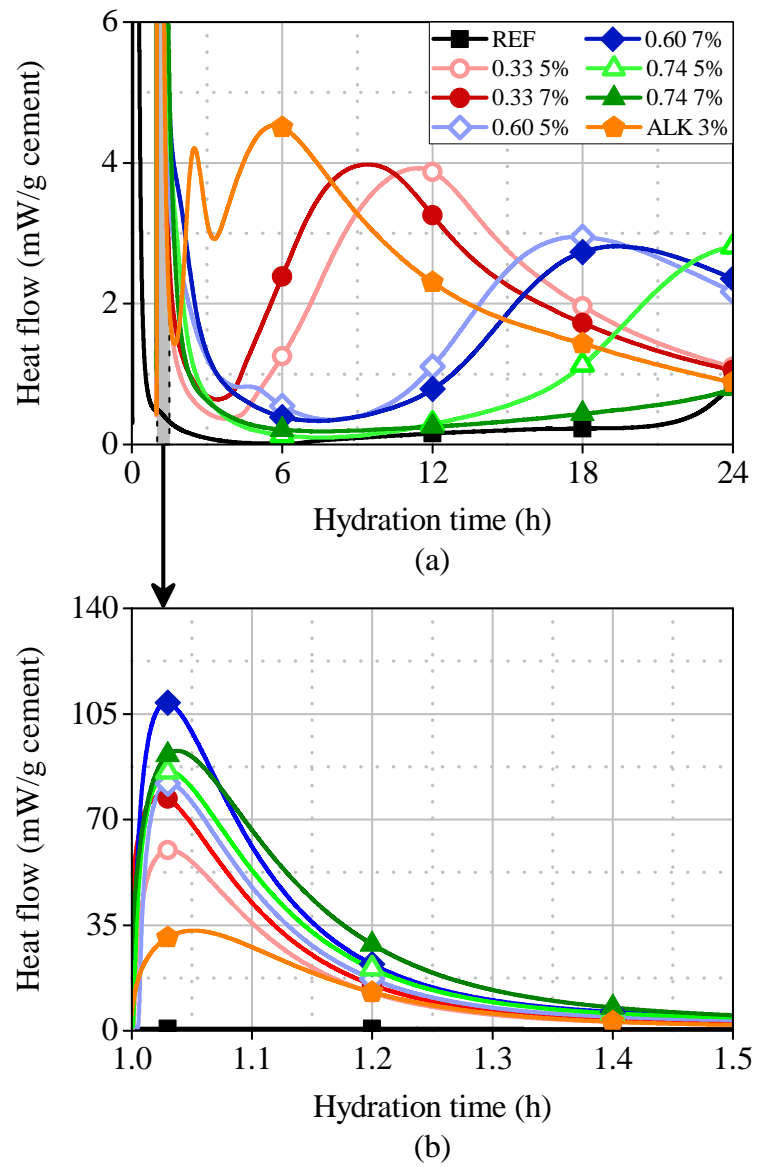
Figure B.5 - Heat flow curves obtained with pastes OPC 96_G 4_F from 0 to 24 h (a) and from 1.0 to 1.5 h (b).

Figure B.6 - Heat flow curves obtained with pastes OPC 94_G 6_F from 0 to 24 h (a) and from 1.0 to 1.5 h (b).
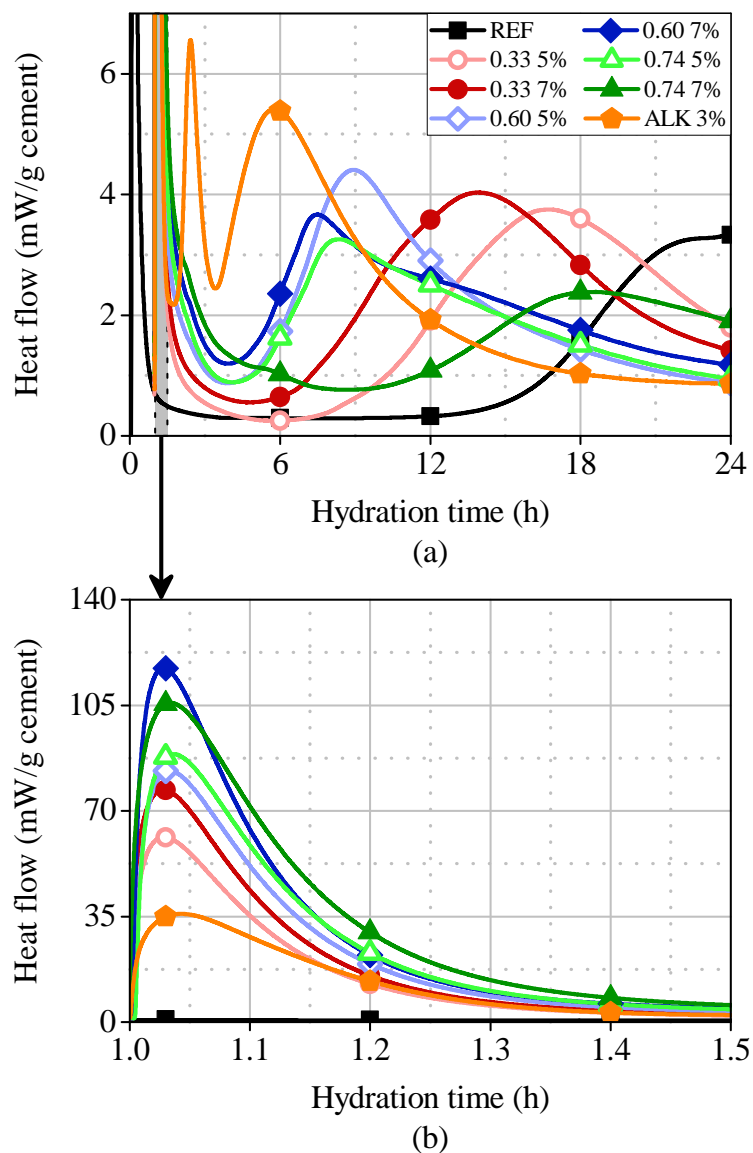
Figure B.7 - Heat flow curves obtained with pastes OPC 96_H 3.38_F from 0 to 24 h (a) and from 1.0 to 1.5 h (b).

Figure B.8 - Heat flow curves obtained with pastes SRC 96_G 4 from 0 to 24 h (a) and from 1.0 to 1.5 h (b).
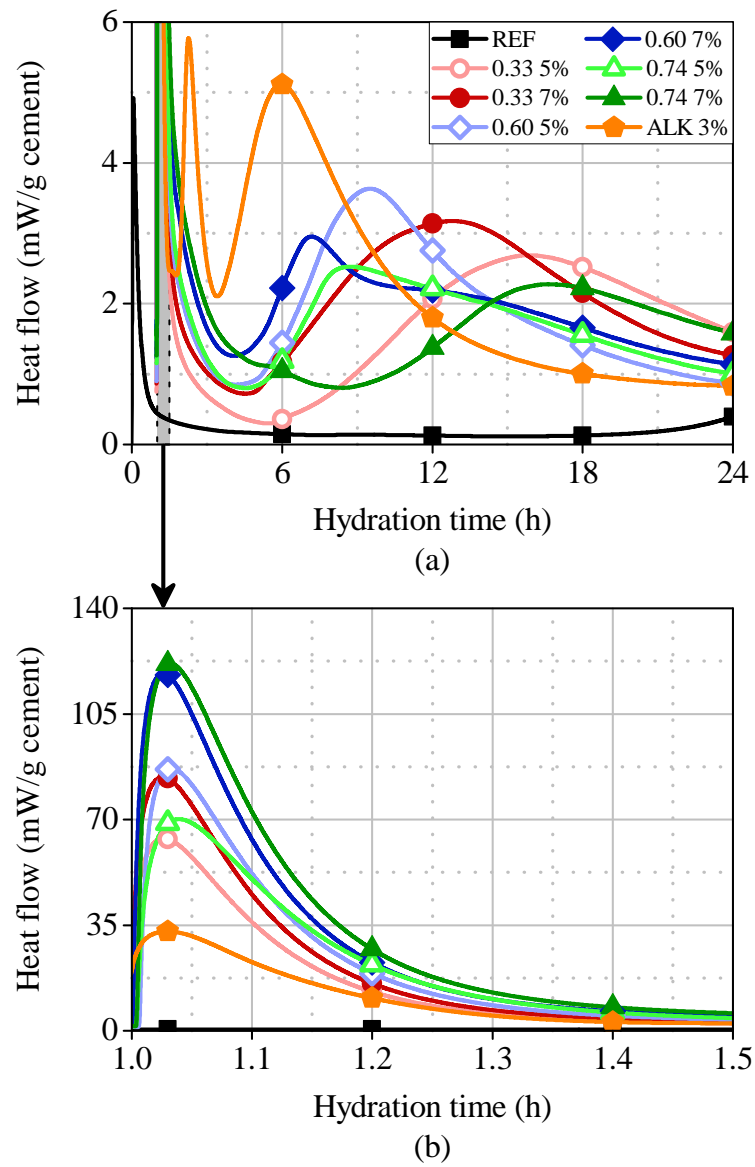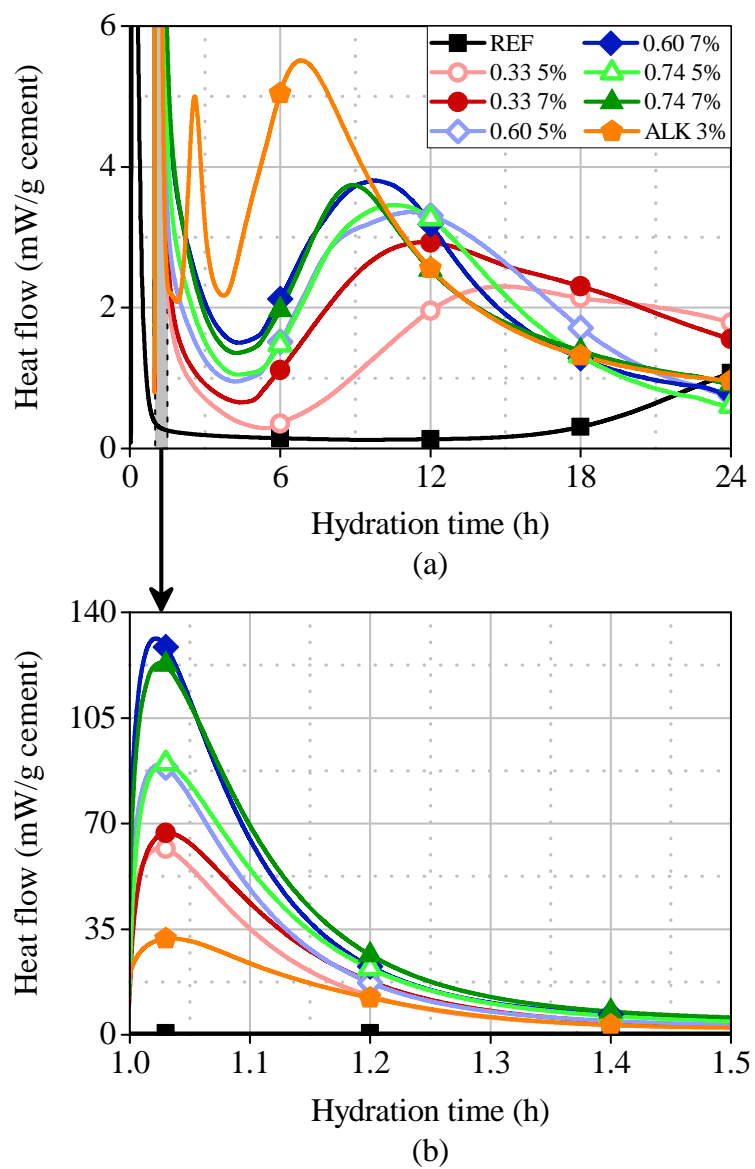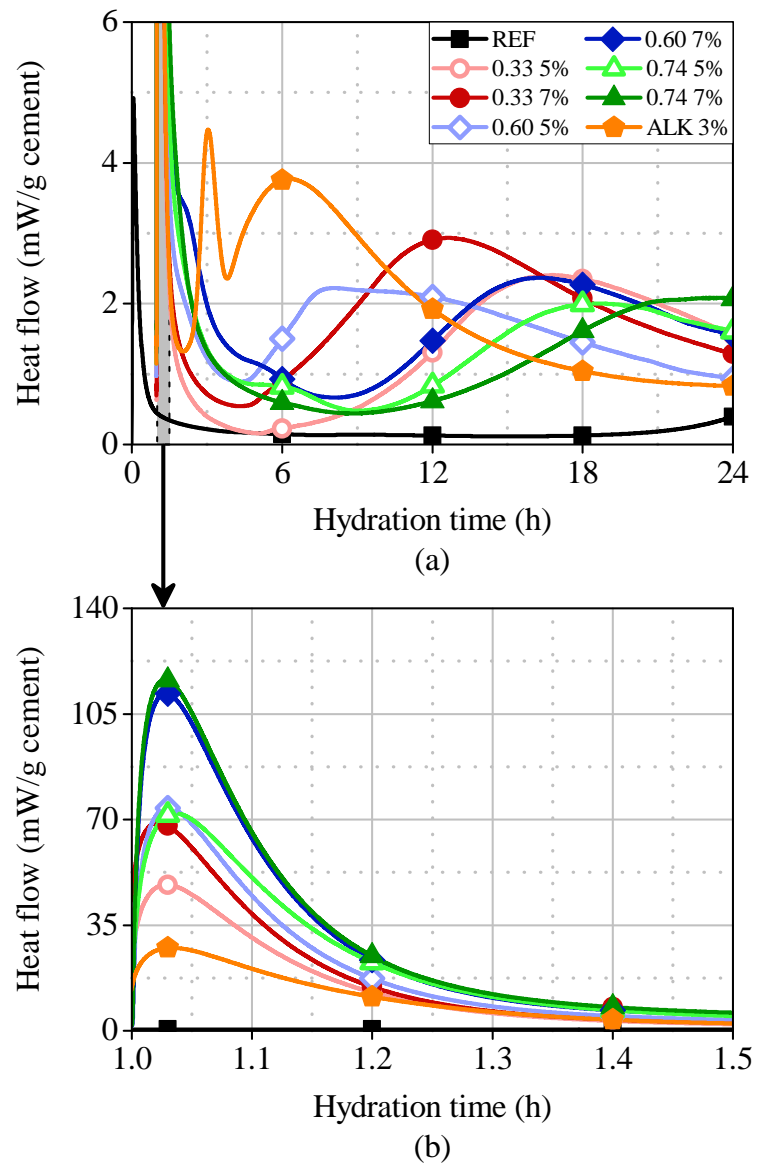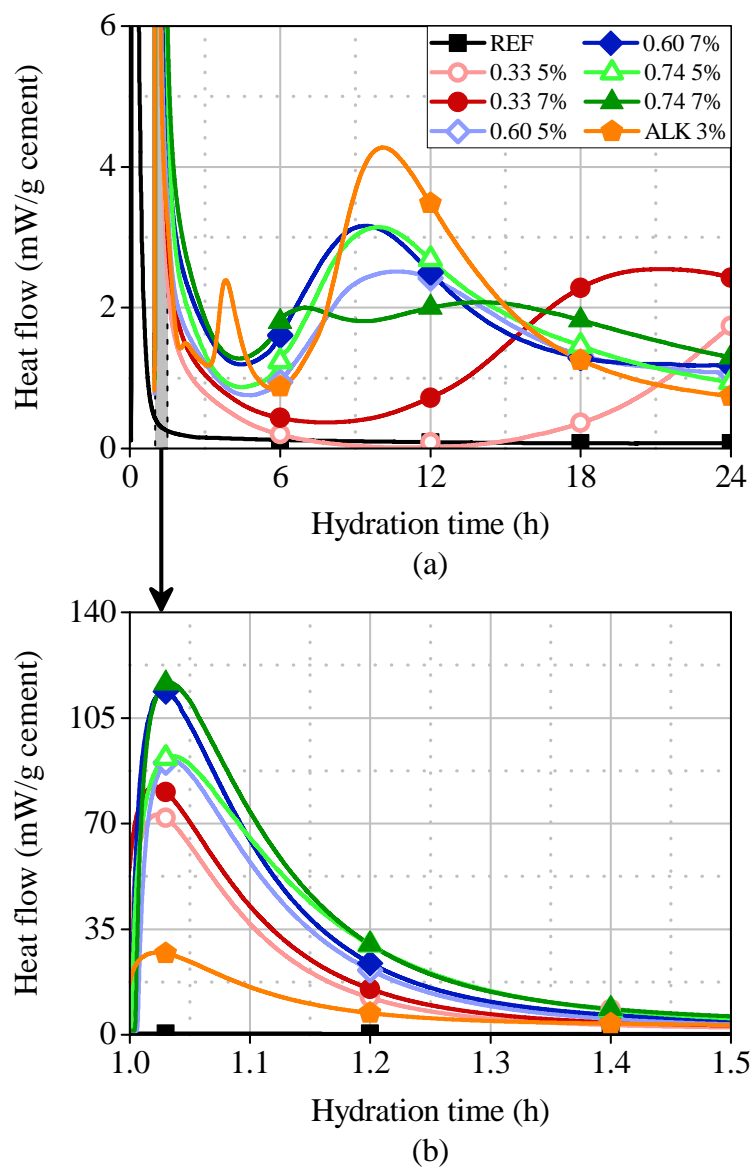
Table B.1 - Analysis of the heat flow curves obtained with accelerated pastes.

Paste	Final C_3A/SO_3 molar ratio	Slope - accelerator peak (mW/g.h)	Energy released - accelerator peak (J/g)	Induction period (h)	Slope acceleration - main peak (mW/g.h)	Energy released - main peak (J/g)	Energy released until 24 h (J/g)
OPC 98_G 2_ AKF 0.33 5%	0.85	1544	18.25	3.00	0.66	154.7	210.3
OPC 98_G 2_ AKF 0.33 7%	0.85	2072	27.10	2.45	0.84	156.7	217.0
OPC 98_G 2_ AKF 0.60 5%	1.35	2437	28.57	8.74	0.42	152.0	187.2
OPC 98_G 2_ AKF 0.60 7%	1.77	2887	42.64	9.65	0.36	153.9	180.9
OPC 98_G 2_ AKF 0.74 5%	1.95	2131	34.67	13.54	0.30	161.3	123.6
OPC 98_G 2_ AKF 0.74 7%	4.03	1721	46.02	20.54	0.17	157.7	86.2
OPC 98_G 2_ ALK 3%	7.57	469	10.75	1.93	1.02	154.5	233.0
OPC 96_G 4_ AKF 0.33 5%	0.56	1702	18.79	7.61	0.51	154.8	202.3
OPC 96_G 4_ AKF 0.33 7%	0.56	2087	26.49	5.26	0.59	168.7	227.6
OPC 96_G 4_ AKF 0.60 5%	0.75	2134	31.78	3.70	1.05	128.4	218.3
OPC 96_G 4_ AKF 0.60 7%	0.87	3550	44.55	3.35	1.00	142.9	236.1
OPC 96_G 4_ AKF 0.74 5%	0.91	2078	37.13	3.61	0.82	115.4	207.4
OPC 96_G 4_ AKF 0.74 7%	1.21	2302	50.93	9.24	0.25	124.7	197.2
OPC 96_G 4_ ALK 3%	1.41	577	12.11	2.02	1.87	131.4	240.7
OPC 94_G 6_ AKF 0.33 5%	0.42	1294	16.14	7.86	0.46	166.3	196.5
OPC 94_G 6_ AKF 0.33 7%	0.42	1613	26.54	4.69	0.63	180.9	236.3
OPC 94_G 6_ AKF 0.60 5%	0.51	2766	34.28	3.85	0.77	136.9	236.8
OPC 94_G 6_ AKF 0.60 7%	0.57	5112	47.28	3.49	0.82	144.4	256.5
OPC 94_G 6_ AKF 0.74 5%	0.59	3930	41.78	4.02	0.72	116.7	225.2
OPC 94_G 6_ AKF 0.74 7%	0.70	3185	51.59	3.67	0.86	127.6	231.6
OPC 94_G 6_ ALK 3%	0.76	717	13.56	1.98	1.40	160.3	255.5

Table B.1 - Analysis of the heat flow curves obtained with accelerated pastes (*continued*).

Paste	Final C_3A/SO_3 molar ratio	Slope - accelerator peak (mW/g.h)	Energy released - accelerator peak (J/g)	Induction period (h)	Slope acceleration - main peak (mW/g.h)	Energy released - main peak (J/g)	Energy released until 24 h (J/g)
OPC 96_H 3.38_ AKF 0.33 5%	0.56	1738	18.95	6.16	0.38	132.6	176.8
OPC 96_H 3.38_ AKF 0.33 7%	0.56	2603	27.73	4.17	0.42	154.7	209.5
OPC 96_H 3.38_ AKF 0.60 5%	0.75	2679	33.25	3.26	0.61	131.0	231.0
OPC 96_H 3.38_ AKF 0.60 7%	0.87	4498	47.40	7.97	0.26	120.6	204.4
OPC 96_H 3.38_ AKF 0.74 5%	0.91	2445	38.83	7.87	0.22	124.2	198.8
OPC 96_H 3.38_ AKF 0.74 7%	1.21	3819	56.75	10.64	0.19	129.7	168.4
OPC 96_H 3.38_ ALK 3%	1.41	891	10.33	1.72	1.16	112.0	217.0
OPC 96_G 4_ F_ AKF 0.33 5%	0.56	1693	20.27	5.22	0.32	133.1	181.8
OPC 96_G 4_ F_ AKF 0.33 7%	0.56	2511	28.75	3.44	0.44	148.3	211.7
OPC 96_G 4_ F_ AKF 0.60 5%	0.79	2551	31.76	3.85	0.79	113.6	199.4
OPC 96_G 4_ F_ AKF 0.60 7%	0.95	3660	45.62	3.38	0.82	121.7	210.2
OPC 96_G 4_ F_ AKF 0.74 5%	1.00	1522	30.90	3.93	0.63	102.7	190.0
OPC 96_G 4_ F_ AKF 0.74 7%	1.46	3428	51.05	8.28	0.26	107.9	194.6
OPC 96_G 4_ F_ALK 3%	1.82	655	9.18	2.10	1.64	119.0	227.6
OPC 94_G 6_ F_ AKF 0.33 5%	0.42	1532	20.03	4.82	0.29	136.6	170.4
OPC 94_G 6_ F_ AKF 0.33 7%	0.42	1484	26.25	3.41	0.45	164.4	209.8
OPC 94_G 6_ F_ AKF 0.60 5%	0.53	2523	32.45	3.61	0.66	131.4	220.4
OPC 94_G 6_ F_ AKF 0.60 7%	0.60	4275	50.14	3.56	0.67	121.6	242.8
OPC 94_G 6_ F_ AKF 0.74 5%	0.62	2324	37.77	3.76	0.66	115.0	213.4
OPC 94_G 6_ F_ AKF 0.74 7%	0.78	3979	52.42	3.61	0.73	116.5	227.9
OPC 94_G 6_ F_ALK 3%	0.87	544	10.21	2.28	1.37	158.8	257.6

Table B.1 - Analysis of the heat flow curves obtained with accelerated pastes (*continued*).

Paste	Final C₃A/SO₃ molar ratio	Slope - accelerator peak (mW/g.h)	Energy released - accelerator peak (J/g)	Induction period (h)	Slope acceleration - main peak (mW/g.h)	Energy released - main peak (J/g)	Energy released until 24 h (J/g)
OPC 96_H 3.38_ F_ AKF 0.33 5%	0.56	1118	15.67	6.88	0.30	108.1	152.6
OPC 96_H 3.38_ F_ AKF 0.33 7%	0.56	1897	23.97	3.41	0.37	136.9	192.2
OPC 96_H 3.38_ F_ AKF 0.60 5%	0.79	1913	27.63	3.18	0.49	97.1	180.4
OPC 96_H 3.38_ F_ AKF 0.60 7%	0.95	3049	45.22	7.87	0.31	110.5	191.7
OPC 96_H 3.38_ F_ AKF 0.74 5%	1.00	1458	33.51	9.09	0.24	92.9	158.7
OPC 96_H 3.38_ F_ AKF 0.74 7%	1.46	3303	48.25	9.87	0.17	98.7	156.5
OPC 96_H 3.38_ F_ALK 3%	1.82	512	8.08	2.35	1.03	107.5	206.4
SRC 96_G 4_ AKF 0.33 5%	0.17	2264	21.83	16.17	0.24	131.1	83.0
SRC 96_G 4_ AKF 0.33 7%	0.17	2339	28.61	9.78	0.27	145.0	159.0
SRC 96_G 4_ AKF 0.60 5%	0.24	2460	35.39	3.85	0.49	86.8	181.5
SRC 96_G 4_ AKF 0.60 7%	0.28	3858	45.58	3.85	0.61	99.1	207.0
SRC 96_G 4_ AKF 0.74 5%	0.30	1954	46.0	3.99	0.65	107.1	201.8
SRC 96_G 4_ AKF 0.74 7%	0.41	3736	52.40	3.44	0.43	123.0	204.9
SRC 96_G 4_ ALK 3%	0.49	716	4.66	5.59	1.31	104.5	197.8

Appendix C

In order to compare how the w/c ratio influences the hydration of accelerated hand-mixed pastes, heat flow curves of pastes containing w/c ratios of 0.45 and 0.32 are compared in figure C.1. All the materials used and admixtures dosages are described in section 3.2.1.
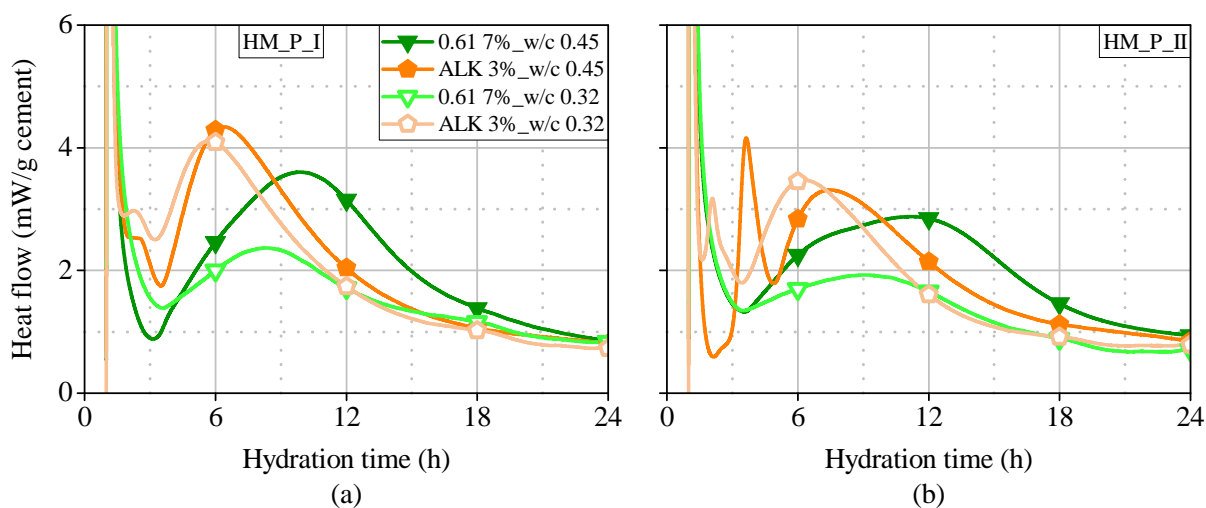

Figure C.1 - Heat flow curves obtained with hand-mixed pastes using w/c ratios of 0.32 and 0.45 with CEM I (a) and CEM II/A-L (b).

Pastes produced with the w/c equal to 0.32 present a small reduction in induction periods and in the maximum intensity of the main hydration peak for both types of cement and accelerators. However, no difference in hydration mechanisms were observed. For this reason, the differences in hydration behavior seen in sprayed and hand-mixed pastes may be associated

exclusively to the mixing process, disregarding the effect of the lower w/c ratio of sprayed pastes.

Publication

The publication developed during the PhD period is presented subsequently.

<u>**Communication in conferences**</u>

<u>R.P. Salvador</u>, S.H.P. Cavalaro, A. Rueda, A.D. Figueiredo, Effect of cement composition on the reactivity of alkali-free accelerating admixtures for shotcrete. In: *7th International Symposium on Sprayed Concrete*. Sandefjord, Norway, June/2014: pp. 350-360.

I. Galobardes, <u>R.P. Salvador</u>, A.D. Figueiredo, S.H.P. Cavalaro, A. Rueda, Wet-mix sprayed concrete set accelerating admixtures: Comparison between traditional aluminate based accelerators and new formulations of alkali free accelerators. In: *56º Congresso Brasileiro do Concreto - IBRACON*. Natal, Brasil, October/2014.

<u>R.P. Salvador</u>, S.H.P. Cavalaro, A. Rueda, A.D. Figueiredo, Hydration and microstructure development in accelerated cement pastes produced by spraying for the evaluation of sprayed concrete. *In: 14th International congress on the chemistry of cement (ICCC 2015)*. Beijing, China, October/2015.

Articles published in indexed Journals

R.P. Salvador, S.H.P. Cavalaro, I. Segura, A.D. Figueiredo, J. Pérez, Early age hydration of cement pastes with alkaline and alkali-free accelerators for sprayed concrete, *Construction and Building Materials*, 111 (2016) 386-398. doi:10.1016/j.conbuildmat.2016.02.101.

R.P. Salvador, S.H.P. Cavalaro, M. Cano, A.D. Figueiredo, Influence of spraying on the early hydration of accelerated cement pastes, *Cement and Concrete Research*, 88 (2016) 7-19. doi:10.1016/j.cemconres.2016.06.005.

R.P. Salvador, S.H.P. Cavalaro, M.A. Cincotto, A.D. Figueiredo, Parameters controlling early age hydration of cement pastes containing accelerators for sprayed concrete. *Cement and Concrete Research*, 89 (2016) 230-248. doi: 10.1016/j.cemconres.2016.09.002.

Articles submitted to indexed Journals

R.P. Salvador, S.H.P. Cavalaro, R. Monte, A.D. Figueiredo, Relation between chemical processes and mechanical properties of sprayed cementitious matrices containing accelerators (submitted - under review).

R.P. Salvador, S.H.P. Cavalaro, I. Segura, M.G. Hernández, J. Ranz, A.D. Figueiredo, Relation between ultrasound measurements and phase evolution in accelerated cementitious matrices (submitted - under review).